Network Approaches to Understanding The Functional Effects of Focal Brain Lesions

Michael Gavin Hart

Corpus Christi

March 2018

This dissertation is submitted for the degree of Doctor of Philosophy.

UNIVERSITY OF CAMBRIDGE

Network Approaches to Understanding the Functional Effects of Focal Brain Lesions

Michael Gavin Hart

Complex network models of functional connectivity have emerged as a paradigm shift in brain mapping over the past decade. Despite significant attention within the neuroimaging and cognitive neuroscience communities, these approaches have hitherto not been extensively explored in neurosurgery. The aim of this thesis is to investigate how the field of connectomics can contribute to understanding the effects of focal brain lesions and to functional brain mapping in neurosurgery.

This datasets for this thesis include a clinical population with focal brain tumours and a cohort focused on healthy adolescent brain development. Multiple network analyses of increasing complexity are performed based upon resting state functional MRI.

In patients with focal brain tumours, the full complement of resting state networks were apparent, while also suggesting putative patterns of network plasticity. Connectome analysis was able to identify potential signatures of node robustness and connections at risk that could be used to individually plan surgery. Focal lesions induced the formation of new hubs while down regulating previously established hubs. Overall these data are consistent with a dynamic rather than a static response to the presence of focal lesions.

Adolescent brain development demonstrated discrete dynamics with distinct gender specific and age-gender interactions. Network architecture also became more robust, particularly to random removal of nodes and edges. Overall these data provide evidence for the early vulnerability rather than enhanced plasticity of brain networks.

In summary, this thesis presents a combined analysis of pathological and healthy development datasets focused on understanding the functional effects of focal brain lesions at a network level. The coda serves as an introduction to a forthcoming study, known as Connectomics and Electrical Stimulation for Augmenting Resection (CAESAR), which is an evolution of the results and methods herein.

This thesis is dedicated to my family – my parents, sister, wife Jennifer, and my sons Lucas and Nathan.

University of Cambridge
2018

CONTENTS

PREFACE 1

ACKNOWLEDGEMENTS 2

LIST OF PUBLICATIONS 3

PRIZES 4

1. INTRODUCTION 5

2. GENERAL METHODOLOGY

2.1. MALTINGS 49

2.2. NSPN 55

2.3. NETWORK ANALYSIS 63

RESULTS

3. RESTING STATE NETWORKS AND BRAIN TUMOURS 67

4. BRAIN MAPPING WITH THE FUNCTIONAL CONNECTOME 83

5. NETWORK HUB PLASTICITY DUE TO FOCAL BRAIN TUMOURS 108

6. DEVELOPMENTAL PLASTICITY IN RESTING STATE NETWORKS 131

7. NETWORK TOPOLOGY & ROBUSTNESS DURING ADOLESCENCE 158

8. GENERAL DISCUSSION

8.1. SUMMARY 187

8.2. LIMITATIONS 191

8.3. FUTURE WORK AND CAESAR PROJECT 194

9. REFERENCES 200

PREFACE

This dissertation is the result of my own work and includes nothing which is the outcome of work done in collaboration except as declared in the Preface and specified in the text.

It is not substantially the same as any that I have submitted, or, is being concurrently submitted for a degree or diploma or other qualification at the University of Cambridge or any other University or similar institution except as declared in the Preface and specified in the text. I further state that no substantial part of my dissertation has already been submitted, or, is being concurrently submitted for any such degree, diploma or other qualification at the University of Cambridge or any other University or similar institution except as declared in the Preface and specified in the text.

It does not exceed the word limit of sixty thousand words, including tables, footnotes, bibliography and appendices, set out by the Faculty of Clinical Medicine and Clinical Veterinary Medicine.

ACKNOWLEDGMENTS

Firstly, I would like to acknowledge the role of my funders - the Neuroscience in Psychiatry Network (NSPN) and Wellcome Trust Biomedical Research Centre - for making this work possible.

Additionally I am grateful to the neurosurgery department in Addenbrooke's hospital for allowing me the time out of my training programme to enter in the world of research for 3 years.

Finally, my PhD experience and this thesis would not have been the same had it not have been for the confidence, ambition, and knowledge that my supervisor – Professor John Suckling – instilled in me.

PUBLICATIONS

This thesis is comprised of the following journal publications:

1.) Hart MG, Ypma RY, Romero-Garcia R, Price SJ, Suckling J. Graph theory analysis of complex brain networks: new concepts in brain mapping applied to neurosurgery. Journal of Neurosurgery 2016;124(6):1665-1678 doi: 10.3171/2015.4.JNS142683

2.) Hart MG, Price SJ, Suckling J. Functional connectivity networks for pre-operative brain mapping. Journal of Neurosurgery, published online August 26, 2016; doi: 10.3171/2016.6.JNS1662

3.) Hart MG, Price SJ, Suckling J. Pre-operative brain mapping with the functional connectome. British Journal of Neurosurgery 2016;30(5):506-17 doi: 10.1080/02688697.2016.1208809.

PRIZES

The following prizes were awarded for work relating to this thesis:

1.) ‘Connectome analysis for pre-operative brain mapping in neurosurgery’
Sir Hugh Cairns Prize, Society of British Neurological Surgeons (SBNS), April 2016

2.) ‘Network Guided Neurosurgery: the trial of Connectomics and Electrical Stimulation for Augmenting Resection (CAESAR)’
Cambridge Society for the Application of Research (CSAR), March 2017.

CHAPTER 1: INTRODUCTION

Graph theory analysis of complex brain networks: new concepts in brain mapping applied to neurosurgery

The current chapter is based on the following publication:

Hart MG, Ypma RY, Romero-Garcia R, Price SJ, Suckling J. Graph theory analysis of complex brain networks: new concepts in brain mapping applied to neurosurgery. Journal of Neurosurgery 2016;124(6):1665-1678 doi: 10.3171/2015.4.JNS142683

The brain as a complex network

"To make the delicate, awesome, and fateful work of the neurosurgeon more accurate, gentle and safe." This statement by Professor Al Rhoton, one of the 20th Century's most famous neurosurgeons and anatomists, encapsulates the objectives of both neurosurgical management and research. Achieving this goal for many fields of neurosurgery requires preserving or improving a patient's brain function. Thus, understanding functional neuroanatomy is fundamental to the advancement of surgical techniques and subsequent therapeutic strategies.

The human brain is the most complex system yet discovered, and understanding its form and function remains as one of the greatest scientific challenges. The digital age has produced the necessary technologies and concepts to begin to make sense of the bewildering complexity of this most mysterious organ. Recently, ideas of the brain as a network of unceasing communication have emerged by comparison to other, common, natural and manmade systems that share key organisational principles (Bullmore & Sporns, 2009. A combination of *in-vivo* imaging, statistical modeling, and graph theoretical analysis has allowed the development of increasingly realistic models with explanatory and predictive properties. A paradigm shift has subsequently arisen describing brain function as a consequence of information exchange between its components rather than information processing within individual components (Sporns 2012).

Here the aim is to introduce complex brain networks and graph theory to the neurosurgical community. To begin, how the brain can be viewed as a complex network and how graph theory can be used to explore the network's properties is described. With these ideas established new avenues that have been created in understanding functional neuroanatomy, the brain's response to injury, and the effects of focal lesions are discussed. Following this, the potential role for investigating healthy development to improve our understanding of brain plasticity and exploring how age-dependent evolution of network architecture affects the response to *in silico* brain injury is highlighted. Finally, early results of complex network analyses and graph theory applied to 'real world' scenarios in neurosurgery are described.

Development of the network based approach: a historical perspective

The brain at rest

Non-invasive, tomographic, *in-vivo* functional neuroimaging began with the discovery of Blood Oxygenation-Level Dependent (BOLD) endogenous contrast (Ogawa et al., 1992) where neuronal activity produces local blood oxygenation changes detectable by magnetic resonance imaging (MRI). The cognitive neuroscience community was an early adopter of this technology with a burgeoning in discoveries that certain brain functions are localised to anatomical regions, previously only surmised through lesioning or electrophysiological studies (Varela, Lachaux, & Rodriguez, 2001), with significant contributions from neurosurgery (Greeblatt, Dagi, & Epstein, 1997; Penfield & Rasmussen, 1950).

However, it was soon discovered, using positron emission tomography (PET), that task-induced activity accounts for only 1-5% of the total energy budget of the brain, the most energetically expensive human organ. The great majority of brain metabolism is consumed continually, even in the absence of a cognitive stimulus when it is at "rest" (Raichle & Mintun, 2006).

Changing the focus from task-based experiments to analysing spontaneous activity while participants were resting revealed synchronous low frequency (<0.1Hz) fluctuations in the BOLD signal that formed coherent networks of neural activity (Biswal, Yetkin, Haughton, & Hyde, 1995). Central to this frame-shift in thinking was

the discovery of the so-called default mode network (DMN), a synchronous set of dispersed brain regions continuously active at rest, but reduced in activity during cognitively effortful tasks (Fox & Raichle, 2007; Fox et al., 2014; van den Heuvel & Pol, 2010). The close relationship of the DMN and other resting state networks to task based activation patterns (Smith et al., 2009) implies an inter-connectedness between brain networks and the underlying structural connectivity and has led to the paradigm that resting state architecture reflects task based activity (Damoiseaux & Greicius, 2009; Honey, Thivierge, & Sporns, 2010). Consequently, the brain at rest is now viewed as constantly oscillating through a variety of functional domain specific architectures that can subsequently be selected during task performance as appropriate.

Resting state fMRI

Synonymous with this rise in networks and connectivity has been the emergence of resting state functional (f)MRI. Resting state fMRI involves acquiring multiple 3D volumes with echo planar imaging sensitive to blood oxygen level dependent (BOLD) contrast in the absence of a direct task or stimulus. During the image acquisition participants are instructed to either keep their eyes open (with or without fixing on an object) or closed but not to fall asleep. With these data each voxel has a time series of BOLD contrast (one time point per 3D volume) over the duration of the experiment. The statistical dependencies (e.g. Pearson correlations) between these time series are the fundamental properties underlying functional connectivity based research.

Related resting state imaging modalities

In addition to resting state fMRI many important contributions in brain connectivity research have come from a variety of neuroimaging modalities (Table 1.1) including: electroencephalography (EEG) (Micheloyannis et al., 2006); magnetoencephalography (MEG) (Stam, 2004); positron emission tomography (PET) (Di, 2012; Sanabria-Diaz, Martinez-Montes, & Melie-Garcia, 2013); structural MRI (He, Chen, & Evans, 2007); and diffusion based imaging (Hagmann et al., 2007; 2008). Many of these modalities have complimentary strengths and weaknesses e.g. MEG has excellent temporal resolution in the order of milliseconds but coarse spatial resolution compared to resting state fMRI. Experiments can be designed to use combinations of modalities to best compliment the strengths of each approach, for

example simultaneous resting state fMRI and EEG to enable high temporal and spatial resolution. Taken together, there is now a large movement in neuroimaging studies, using a variety of methods, towards viewing the functional integration or connectivity, superseding functional segregation and the localisationist viewpoint (Friston, 2011).

Network analysis methods

Describing the organizational characteristics and evolution of networks in both space and time has been the subject of many mathematical approaches (for example dynamic casual modeling (DCM) (Beckmann, DeLuca, Devlin, & Smith, 2005), computational modeling with neural mass models (Deco et al., 2014), independent component analysis (ICA) (Beckmann et al., 2005), and graph theory (Bullmore & Sporns, 2009)). While a network approach to brain function is not a new idea (Catani, 2005; Hebb, 1942; Mesulam, 1990; Sporns, 2012), recent focus on brain connectivity as the underlying principle of the brain has gained eminence in the past decade, culminating in the search for the connectome, or the brains 'wiring diagram'.

Connectomics

The final evolutionary step in the connectivity perspective is to model whole brain connectivity. The term connectome was used to describe this 'wiring diagram' and was simultaneously coined by Patrick Hagmann in his PhD thesis (Hagmann, 2005) and by Olaf Sporns, Guilio Tononi and Rolf Kotter in a review paper in 2005 (Sporns, Tononi, & Kotter, 2005). This paradigm is based on the premise that to understand the function of the whole system one must not only understand the features of the individual elements independently, but also their interactions. The authors argue that if cognition is to be understood in terms of dynamic structure-function relationships one needs a detailed structural model of neuronal units and connections. To do this, one will require co-ordinated multi-disciplinary efforts with resultant publicly available databases. Already significant progress has been made in the field with the flagship freely available '1000 connectome' project (Biswal et al., 2010) and Human Connectome Project (Friston et al., 2013), among others.

Technique	Acquisition	Application to brain networks	Strengths	Weaknesses
Structural MRI	Single 3D volume of the brain (e.g. T1 mprage)	Analyses structural covariance of morphological measures (e.g. cortical thickness or volume) between brain regions (high correlation implies a network link).	Simple to acquire and not limited by artefacts to the same degree as other MRI based sequences	Limited by degree of inference one can deduce based on cortical measures
Diffusion MRI	Specific sequence using gradients to measure the free water diffusion as a surrogate measure of white matter tracts	Reconstruction of tracts can be used to imply structural connectivity between brain regions	Suggests a clear correlation with underlying structural connectivity and the brains 'wiring diagram'	Variations in sequences and algorithms can significantly affect the network parameters
Resting FMRI	Specific 4D sequence sensitive to BOLD contrast reflecting the haemodynamic response of neuronal activity	Analyses statistical dependencies between parcellated brain regions. Often performed in the 'resting' state.	Reasonably high temporal and good spatial resolution	Indirect measure of neuronal activity. Significant artefacts require careful pre-processing.
Electro-encephalography (EEG)	Uses electrodes to directly measure electrical signals in the brain	Measures statistical dependency between pairwise combinations of channels, often in multiple frequency bands	Best temporal resolution and direct measure of (extracellular) neuronal currents	Significant spatial limitations and distortion due to the skull and scalp
Magneto-encephalography (MEG)	Uses a magnetometer to measure magnetic field alterations due to neuronal electrical activity	Measures statistical dependency between all pairwise combinations of channels	Exceptionally high temporal resolution but limited spatial resolution (particularly subcortical)	Difficulties with localizing signal spatially and accounting for poor signal to noise ratio
Positron Emission Tomography (PET)	Injection of a radiosotope followed by detection of gamma rays	Covariance in glucose metabolism between regions	Direct metabolic data and is a good biomarker for certain diseases e.g. Alzheimer's	Radiation, limited repeatability, potentially lower spatial resolution unless combined with MRI

Table 1.1: neuroimaging methods for complex network analyses

What is a complex network?

Graph theory was originally devised to solve real world problems by viewing the system as an abstract network (Figure 1.1), which allowed its properties to be analyzed mathematically (Fornito, Zalesky, Breakspear, 2013). A network consists of point-like components, nodes or vertices, V, and the relationships between them, links or edges, E. For example, when characterizing social relationships nodes are individual people and the presence or absence of an edge between two nodes indicates whether the corresponding people are friends or not. Together, the sets of nodes and edges form a binary 'friendship' graph: G={V,E}. Further information can be encoded, for example the strength of the friendship can be represented by assigning a value, or weight to the edges. Weighted or binary graphs can be directed, if an edge has an associated direction, say if each person were independently asked about their relationships with others in the network, or undirected in which case no directionality in the relationships is implied. The strength of graph theory is that once a graph has been constructed, the same analyses can therefore be applied to graphs originating from a wide spectrum of real-world networks.

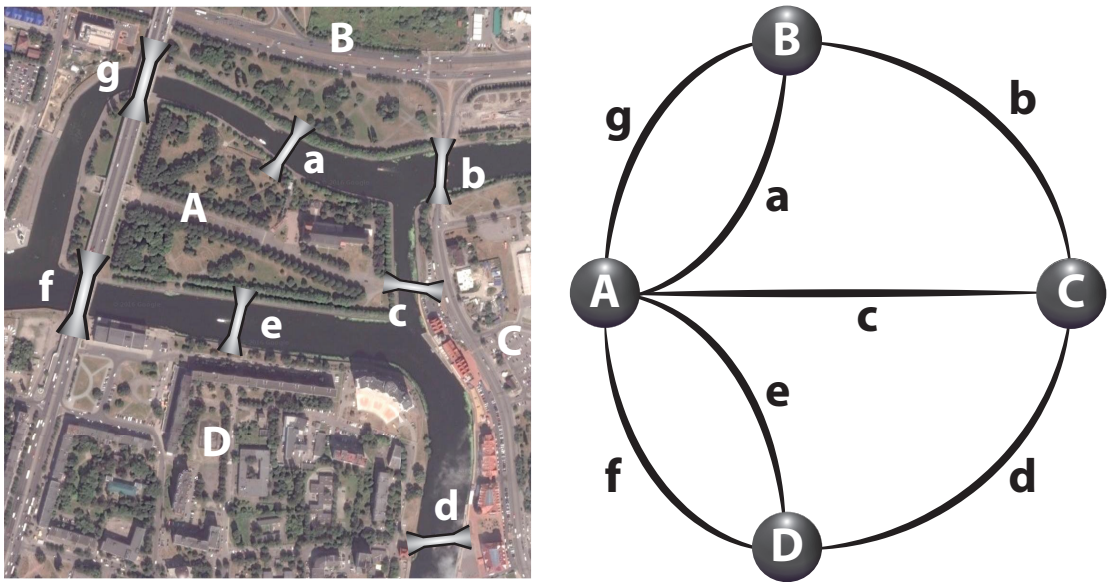

Figure 1.1: The Konigsberg bridge problem

The city of Konigsberg in Prussia (now Kaliningrad in Russia) was set on the river Pregel incorporating several islands connected by seven bridges. The problem involved was finding a way to walk through the city such that every bridge would be

crossed once and only once. In 1735, Leonard Euler (1707-1783) mapped the problem out in terms of a simple graph, which allowed him to analyze the problem with mathematical rigor and generate a formal proof. It was shown that there was no solution, as for it to be true the graph needed less than two nodes of odd degree. The general term for traversing a network by passing each edge once and only once is now termed an 'Eulerian walk'.

Network measures

Once the network is formed, the properties of it (and therefore the real-life network it represents) can be captured mathematically with graph theory (Figure 1.2 & Table 1.2). In a binary graph the simplest property is the degree of a node – the number of connections or links that it has – which is a measure of how well the node is connected. The degree distribution is the histogram of node degrees for the overall network and is an important network property (Amaral, Scala, Barthelemy, & Stanley, 2000) that can be used to distinguish between networks (described below). The total number of connections in a network can also be regarded as an estimate of the cost in establishing a particular configuration (Achard & Bullmore, 2007).

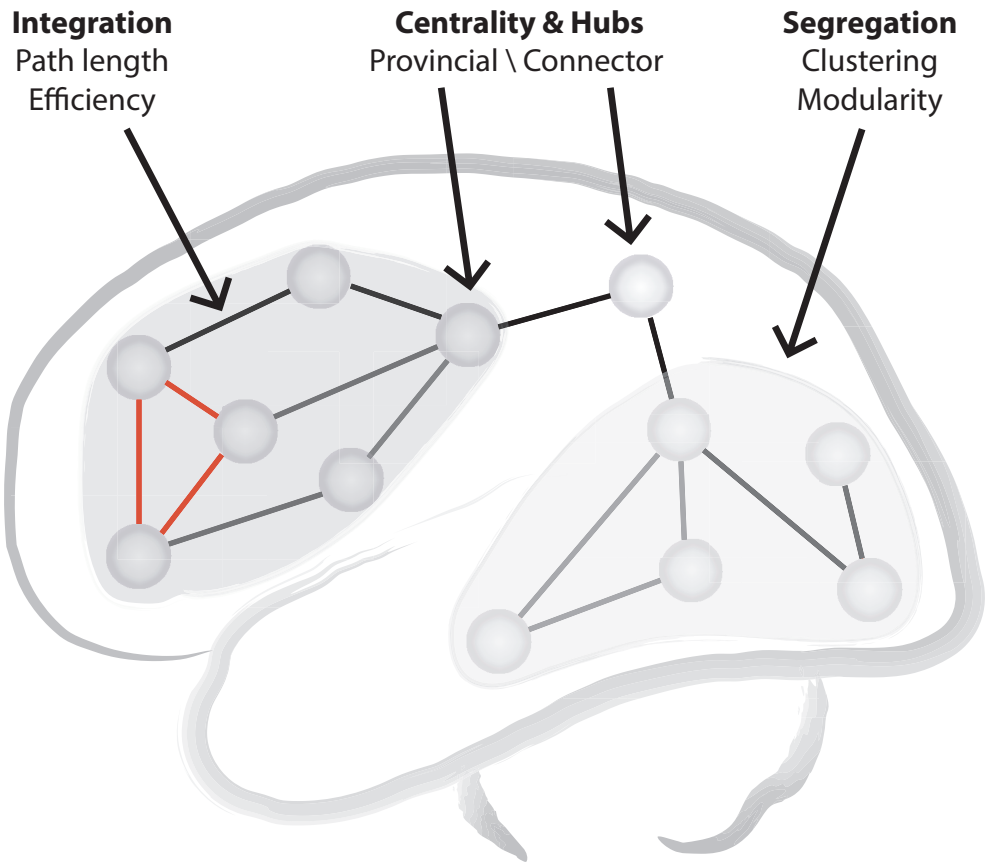

Figure 1.2: Network measures

The main network measures and their classification are summarised in a hypothetical network illustration. Measures of segregation focus on community structure either in the form of small triangles (clustering) or larger groups of related components (modules). Measures of integration are based on the number of steps (edges) between individual nodes (known as the path length). The final main class of network measures are hubs, which can be defined in a variety of ways, depending either on how many links they have (degree), or how many paths.

Measure	Definition
Adjacency matrix	A means of displaying the nodes of a network and the edges or relationship between each pair of nodes.
Centrality	A measure that describes how critical a given nodes features are to the overall network. Many variations of centrality are available reflecting whether they refer to the number of edges or paths that pass through a region, for example.
Clustering	A measure of segregation defined as the number of neighbours of a node that are also neighbours of each other (and hence form a triangle). Usually displayed as a coefficient based on the maximum possible number of clusters.
Complex network	A network with non-trivial features, usually taken to refer to small-world or scale-free topology
Connectome	A term originally coined approximately 10 years ago to describe the structural architecture of the brain that guides the functional connections.
Cost	A measure of the connection density of a network. Usually displayed as a percentage of the maximum number of connections in a network. Theoretically related to the wiring length cost involved in forming connections between nodes.
Degree	The number of connections a node has with other nodes in the network
Degree distribution	The histogram of the degrees of all nodes for the network
Efficiency	The inverse of path length. Often more accurate than path length when used in sparsely connected graphs such as the brain.
Hub	A feature of a node that makes it pertinent to the networks overall characteristics. Can be defined in a variety of ways such as on centrality or degree of a node.
Module	A conglomeration of nodes that are more strongly connected to each other than nodes outside the module. Often defined using hierarchical clustering algorithms.
Path length	A measure of integration that describes the number of discrete steps between nodes (or edges) required to move from one node to another.
Parcellation	Partition of the brain into distinct regions or clusters
Percolation theory	A branch of mathematics that considers the connectivity of a graph, and is often used to model the effects of disrupting the network in terms of how connected the majority of its components are
Resting state	Refers to the brains activity when not engaging in a task
Rich club	A group of nodes with highly central features (and often key hubs) that are also highly connected to each other (i.e. have high assortativity)
Robustness	The ability of a network to sustain its characteristic features when either nodes or edges are removed

Table 1.2: glossary of network terminology

Network segregation relates to how well the network can be separated into constituent communities of nodes (Tononi, Sporns, & Edelman, 1994). A standard measure for determining segregation is the clustering co-efficient, which can be thought of as the tendency of nodes that share neighbors to be connected (e.g. are your friends each other's friends?). In a binary network a triangle is formed when two neighbours of a node are also neighbours of each other, which is then scaled by the total number of

possible connections available to that node i.e. it is the proportion of total triangles versus possible closed triangles for a node.

The weighted clustering is somewhat different in that it reflects the average intensity (geometric mean) of its constituent edges, known as sub-graph intensity (Onnela et al., 2005). To account for potentially disproportionate effects of edge weights they are most appropriate when scaled in the unit interval and approximated to a normal distribution. While the weighted clustering co-efficient is often treated as a measure of network segregation, it essentially characterises triadic sub-graphs and their potential for integration; therefore it does not necessarily reflect the dynamics between the constituent components (unlike the binary version).

A related term is nodal or local efficiency, which is the inverse harmonic mean of path lengths for the local sub-network of a node that are its immediate neighbours (Latora & Marchiori, 2001). In essence this captures the degree to which any node is integrated within its local community, thereby incorporating elements of the clustering co-efficient together with path length.

Another alternative to the clustering co-efficient for capturing network segregation is transitivity (Rubinov & Sporns, 2010). This estimates the probability that any two nodes that are connected to a third are also joined together at a global level. This is subtly different from the global clustering co-efficient that tells us the average number of closed triangles around a node.

Network integration measures the connectedness of distinct regions. One way of defining this is by the number of edges required to move from any one node to a target node, and when taken as an average across all nodes in the network is known as the average path length (Watts & Strogatz, 1998). The characteristic path length is the average across the whole network. Typically path length is computed with Dijkstra's algorithm (Dijkstra, 1959) or one of its variations e.g. Prim's for a minimum spanning tree or Johnson's for negative weight distances.

A related measure is global efficiency, which is the inverse of harmonic mean of its path lengths (Latora & Marchiori, 2001). Global efficiency is believed to represent information exchange in a parallel system and therefore may be a better characterisation of integration in the connectome when compared to mean path length, which is a better measure of information exchange in a sequential system. By taking the harmonic mean, global efficiency also avoids issues with network fragmentation and resultant infinite paths, and more generally reduces the weightings of nodes with a very long path length that might represent outliers (Achard & Bullmore, 2007).

In order to perform analysis of these methods of network integration one must first transform a connectivity matrix of node closeness, formed from Pearson correlations for example, to one of node distances, known as the distance matrix. Typically a higher correlation is viewed as a closer distance and therefore the transformation is some form of an inverse of the connectivity matrix. Using a simple inverse however creates a skewed distribution of edge weights. A more mathematically principled method involves using the Dombi t-norm from Fuzzy Logic to approximate distance as (Simas & Amaral, 2014):

$$D = \left(\frac{1}{A}\right) - 1$$

(Eq. 1.1)

where A is measure of statistical dependency or closeness between any given pair of nodes (e.g. Pearson or wavelet correlation).

Network models

An alternative to computing a network's metrics, which are mainly descriptive, is to propose models of graph architecture that explain the measured properties [Albert & Barabasi, 2001]. Historically, two simple models, both amenable to mathematical formulism, have been studied (Figure 1.3). A lattice graph is a regular array of nodes with connections solely between adjacent nodes. As all connections are local, lattices show a high clustering coefficient, but also a high path length (as getting from one edge of the graph to another requires traversing a large number of nodes). On the

other end of the spectrum is a random graph, where nodes are connected at random. As this leads to few local connections, random graphs have low clustering, but short path lengths. Neither lattices nor random graphs represent accurate models of real world networks.

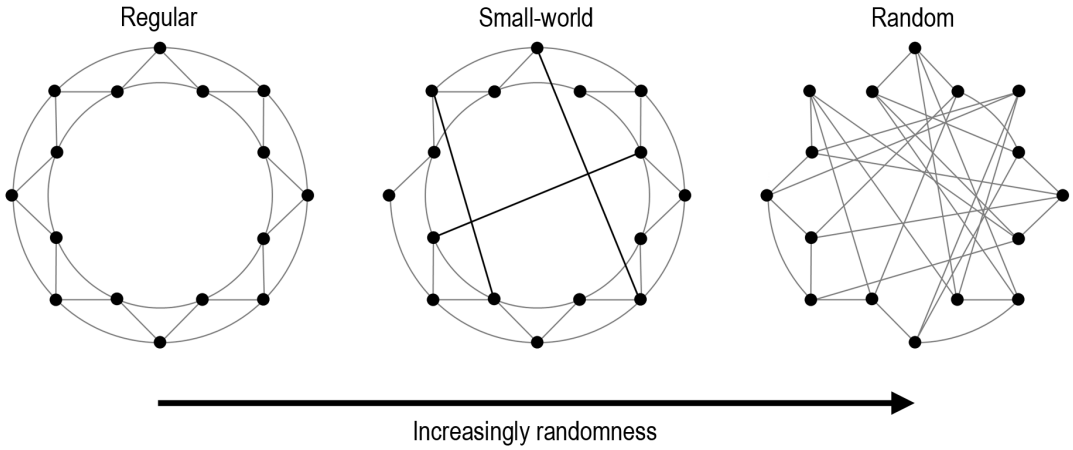

Figure 1.3: Network types and the "small world"

The two traditional classes of network models (lattice and random graphs) are shown on either end of a spectrum with small world graphs lying in the middle. By re-wiring a few of the short range connections in the lattice to any other node with a fixed probability, the small world graph maintains high clustering (a key feature of the lattice) but dramatically reduces its path length (in keeping with a random graph), thereby parsimoniously balancing the features of segregation and integration. When the lattice has become completely rewired randomly, it has become a random graph.

Graph theory experienced a quantum leap in the late 1990s when two seminal papers showed a range of real world networks were well approximated by two elegant network models. The first of these created graphs by 're-wiring' lattices (Figure 1.3): converting some of the short-range connections into long-range connections (or 'short cuts') (Watts & Strogatz, 1998). It was found that after only a few re-wirings the graphs showed a strongly reduced average path length, while maintaining high clustering. This property, where most interactions are local (high segregation) but where it is still possible to reach any part of the graph in a few steps (high

integration), was dubbed the ‘small world’ property. It was found to be a ubiquitous property of seemingly disparate complex networks including the Internet, Hollywood actor collaborations, power grid organization, and neural networks.

To formalize the small world definition one typically compares the clustering and path lengths with those from randomised controlled networks, leading to normalised clustering (γ) and path lengths (λ). A small world can be quantified as one where the clustering co-efficient is higher than the comparable random graph but the path length is similar:

$$\delta = \frac{\gamma}{\lambda}$$

(Eq. 1.2)

Alternative definitions of small world characteristics have been described. One could take a comparable lattice network as a more appropriate null model for clustering, which would be the theoretically maximally clustered network architecture, while still comparing this over the ratio of path length for a randomised network, which represents the theoretically minimal path length (Telesford, Joyce, Hayasaka, Burdette, & Laurienti, 2011):

$$\delta = \frac{L_{rand}}{L} - \frac{C}{C_{lat}}$$

(Eq.1.3)

where L is path length and C is clustering. In this instance a positive value will suggest a randomised network, negative values a lattice, and values around zero a small world.

Concurrent with the formulation of small world networks, another feature found to be common in many real world networks is the existence of a small number of highly connected nodes (called ‘hubs’) (Barabasi & Albert, 1999). The degree distribution of random networks follows a Poisson distribution whereby most nodes have similar degree (or number of connections). However, this is a poor fit to the degree

distribution in many real world networks where most nodes have relatively low degree but there are a few with disproportionately high degree. If one plots this on a log-log scale the fit is approximately linear and therefore the resulting degree distribution follows a power law distribution with the exponent its degree exponent. Such networks are known as scale-free networks because they lack an internal scale consequent on the wide degree distribution. For example, if we randomly select a node, the degree of the node in question could be very small to arbitrarily large.

Many real world networks have been found to exhibit this property, although often the distribution is capped due to physical restraints (e.g. the finite size of a brain or number of links in a transportation network), in which case an exponentially truncated power law degree distribution is appropriate (Achard, Salvador, Whitcher, Suckling, & Bullmore, 2006). However, even if the degree distribution is not a true power law fit, it is most often a form of heavy tailed distribution (fat-tailed, long-tailed, sub-exponential). These asymmetric degree distributions still vary from the Poisson distribution of random graphs by predicting a higher proportion of low degree nodes and the existence of a minority of nodes with a disproportionately high degree distribution known as hubs. One can test this by showing the variance in degree distribution is significantly larger than the mean degree. Formally, one says the second moment (variance), and all higher moments, of the degree distribution in the $N \to \infty$ limit diverges and tends to infinity when the degree exponent is between 2 and 3 (Barabasi, 2016).

In addition to describing scale-free networks, a generative model was also proposed to form such networks using a simple process of sequentially adding nodes to a graph and preferentially attaching them to nodes that already had many connections (e.g. everyone wants to be friends with the popular person, or in an actor network it is most likely that new actors work with established actors with many connections rather than other new actors). A consequence of this model is that the most central hubs in this network are never the newest actors but those that have been there among the longest duration. This phenomenon is colloquially known as the ‘rich get richer’ (Barabasi & Albert, 1999).

Despite the elegant simplicity of the Barabasi-Albert model, it predicts a rigid degree distribution exponent and doesn't capture other processes important in real networks, such as aging in the actor network or self-links in the internet. An evolution of the Barabasi-Albert model is the Bianconi-Barabasi model of network fitness (Bianconi, Barabasi, 2001), whereby each node also has a fitness parameter that governs its potential to add new connections, and which allows newer nodes to grow quickly and also become hubs if they have high fitness. Other models have been proposed, including those capturing node ageing (Amaral, Scala, Barthelemy, & Stanley, 2000) and internal links (Barabasi et al., 2002), both of which predict scale free degree distributions.

Since the 1990s, small world networks and scale-free degree distributions have been the defining properties of complex networks with non-trivial topological features, contrasting with random graphs and lattices. Conservation of network properties over a wide range of fields has facilitated trans-disciplinary sharing of rules for growth, evolution, and robustness between networks. The realization that these rules could model the behavior of real networks has led to the establishment and blossoming of network science over the past two decades and the application of complex networks to the central nervous systems of vertebrates and invertebrates, including humans.

How are brain networks abstracted from empirical data?

Resting state networks

Functional connectivity analysis of resting state fMRI data began with the finding that the BOLD contrast time series data of one sensorimotor region was statistically similar to that of the contralateral homologous region, resulting in the first resting state network, the sensorimotor network (Biswal, Yetkin, Haughton, & Hyde, 1995. This approach of generating functional connectivity maps based on the time series of an *a priori* defined seed is termed seed connectivity analysis. Extending this work to different seed locations allowed identification of several canonical resting state networks based on primary and association cortices with both local and distributed connectivity clusters. In theory any location can be used as a seed although typically locations are chosen to correspond to pre-existing canonical network locations, prior task based activation localisations, or regions hypothesised to be of

pathophysiological significance. Seed connectivity analysis is therefore model based and the most direct way of visualizing the connectivity of any given region using a mass univariate manner, potentially allowing relatively straightforward inference. However, more complex multivariate relationships involving whole brain connectivity are not captured, and the results can vary depending the seed location and threshold for connectivity.

Model-free methods for analyzing resting state fMRI data are also available, most prominently involving independent component analysis (ICA). Here the underlying whole brain time series data is modeled as a linear mixture of independent sources that can be separated in a statistically principled manner (Beckman et al., 2005). However, ICA has unique artifacts of its own, the analysis itself can be more demanding, and occasionally the inference can be more challenging due to the higher level of abstraction applied to the data during processing (van den Heuvel & Pol, 2010). Nevertheless, whatever means of analysis is chosen, resting state networks are consistently extractable and show a high degree of concordance regardless of the chosen method of analysis, suggesting they are a universal underlying feature of the brains functional architecture.

Connectomics

Methods of constructing graphs from diverse neuroimaging modalities share many similar concepts (Figure 1.4), but with subtle differences that depend on the nature of the data (Bullmore & Sporns, 2009; Fornito, Zalesky, & Breakspear, 2013). Multiple spatial scales of data can be accommodated ranging from microscales (e.g. light microscopy, typically ~10 μm) through mesoscales (e.g. viral tracers, typically ~0.1 mm) to macroscales (e.g. MRI, typically ~1 mm) (Sporns, 2010). Depending on the data that is input and the planned inference of that data defines the consequent network as either: structural, if anatomical data is used (e.g. diffusion imaging or cortical morphology); functional, if temporally varying data is the basis (e.g. resting fMRI, EEG, MEG, or PET); or effective, if the data is attempting to suggest causal influences between regions (i.e. a directed graph).

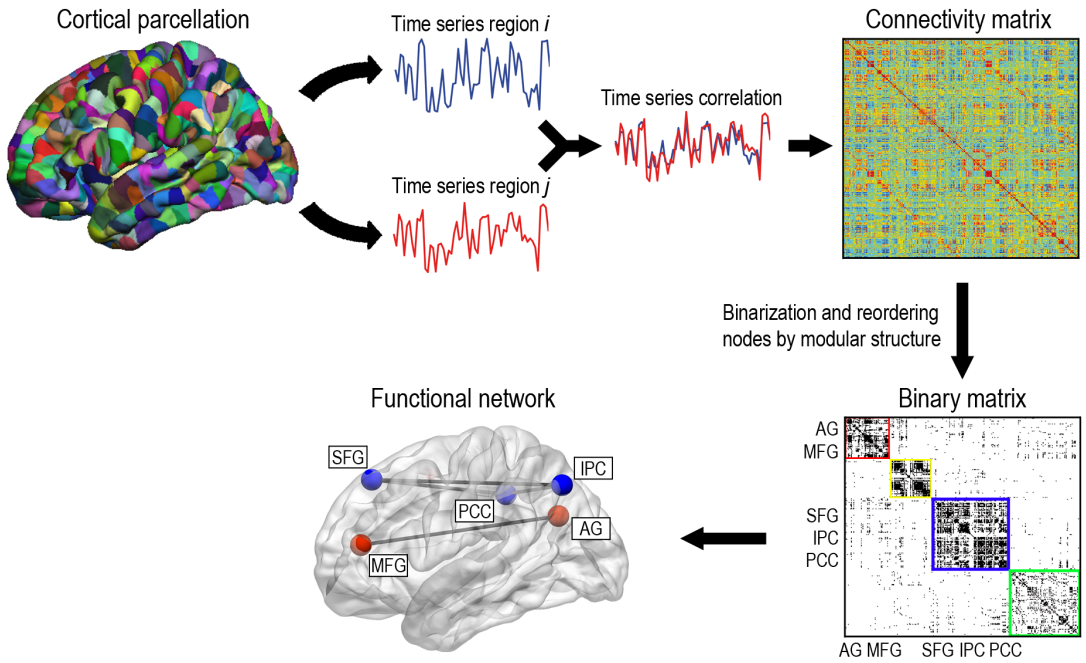

Figure 1.4: Constructing a graph from resting state fMRI data

Firstly, the brain is parcellated into discrete regions (known as nodes). In this case, a random parcellation is chosen based on an anatomical atlas but keeping the surface area constant. Subsequently, the mean time series of the 4D resting state fMRI data is extracted for each parcel, and the relationship between each pair of these is calculated (known as an edge, or a link). Usually this relationship is the Pearson correlation, although it can also be other measures, but it is essentially a form of statistical dependency. Once this has been done for each pair of parcels, the data is displayed in terms of an adjacency matrix that highlights the connectivity between each region. In the matrix, rows and columns represent parcels (or nodes), and the relationships (or edges) are the entries in the matrix. The matrix can then be thresholded, binarised, or arranged in a hierarchical fashion. Finally, the connectivity data is translated back into anatomical space for display purpose. In this case it is overlaid with a translucent brain with lines to reflect significant links between regions, and the colors represent the module that the node belongs to.

Recalling that both vertices and edges are required to construct a network, the first stage is to define the nodes. This may be straightforward, for example the positions of

EEG or MEG electrodes, or require division of tomographic brain imaging data by some arbitrary, although principled method, known as parcellation. Multiple options exist but currently there is no agreed upon standard at a group or individual level (Zalesky et al., 2010). The earliest parcellations tended to be anatomical and based on either gyral and sulcal landmarks (e.g. Desikan-Killany) or histological architecture (Eickoff-Zilles). While these parcellations are intuitive they are less than ideal for graph theory given the inhomogeneous parcel size (which can potentially bias connectivity estimates) and they are typically of low resolution (60-120 nodes) limiting the applicability of complex network analysis. Higher resolution parcellations with equal parcellation surface areas or volumes can be created through either randomization (Whitaker et al., 2015), clustering of voxel wise time series data (Craddock et al., 2011), or sub-division of anatomical parcellations (Zalesky et al., 2010). While these are theoretically technically better for graph theory, there are issues with the accuracy of registration of randomized networks to individual anatomy, where template boundaries may cross sulcal and gyral landmarks, and also with choosing the appropriate resolution. Finally, voxel based parcellation methods have been proposed (Erguiluz et al., 2005; van den Heuvel et al., 2008), and while offering the highest resolution, they can be computationally burdensome in practice and can have issues with statistical validity in terms of spatial and temporal degrees of freedom, particularly when the parcellation resolution exceeds the number of time points in the data. In the future, individual parcellation schemes may become more achievable, based on for example concordance of multi-modal imaging data (Glasser et al., 2016), or independent component analysis (Smith et al., 2015). Until then, a principled approach to parcellation should involve choosing a template that best matches the goals of a study (e.g. study specific clustering for an atypical population, or a low resolution anatomical template when one wishes for an intuitive visualization of nodes) or use different templates to determine consistency of effects across parcellation schemes.

Once nodes have been established, edges need to be defined. For data collected over time, such as EEG, MEG or resting fMRI, the strength of a connection between two nodes is frequently estimated by the statistical dependencies between their time-series, most often measured with Pearson's correlation. Despite its ubiquity, there are issues with using simple correlations (Fornito, Zalesky, & Bullmore., 2016). For

example, it only quantifies linear relationships, can produce 'false positive' connections that are a product of indirect connectivity, it averages connectivity dynamics over the entire time series window, and produces a scalar summary of both phase and amplitude coupling. Another difficulty is that it can produce negative correlations, particularly if used with global mean signal regression in pre-statistical processing of resting state fMRI data, which can make inference challenging to resolve at a biological level. Partial correlations can be used to reduce the effects of indirect connections but can lead to different artifacts such as increased clustering co-efficient and reduced long-range connectivity (Zalesky et al., 2010)). These effects can be partially reduced by using regularized (e.g. ridge, lasso, or elastic) methods of partial correlation (Varoquaux, Gramfort, Poline, & Thiron, 2010) but currently the choice of appropriate hyper-parameters is unprincipled. Information measures such as mutual information of spectral frequency data can be used to capture non-linear relationships (Salvador et al., 2005).

For data without temporal information such as estimates of brain structure from MRI (cortical thickness, grey matter volume, and cortical surface), edge strengths are the covariance of observations between-individuals and thus represent averages within a group or population sample (He, Chen, & Evans, 2007). Diffusion MRI uses a slightly different method whereby the number of tracts (calculated from a tractography algorithm) are calculated between parcels (Hagmann et al., 2007; 2008). This requires creation of a whole brain 'fibre cloud' (or tractogram) whereby tractography is created at multiple seeds in the brain. These locations can be chosen to be in the white matter immediately adjacent to a cortical parcel, or can be deeper in the white matter in random locations. Difficulties with tractography include resolving crossing-fibres – particularly in the centrum semi-ovale and intersection of the internal capsule (projection fibres) and corpus callosum (commissural fibres) – and modeling inter-hemispheric connections (Craddock et al., 2013). These issues are the subject of extensive research including novel scanner sequences (diffusion spectrum and kurtosis imaging) and tensor modeling (e.g. Q-ball or ball-and-sticks models). More general issues with diffusion imaging based techniques include determining the functional significance of each tract and how to weight its connectivity (i.e. number of streamlines, normalized streamlines, or mean FA or MD of a tract).

Once these calculations are complete the data are organized into a two-dimensional adjacency matrix where nodes are represented by rows and columns, and edge weights are indicated by the matrix entries. Subsequently the methods of analysis are shared irrespective of the original data or the final objective of the analysis (Kaiser, 2011). Once the graph has been created its properties can be characterized using a range of graph theory measures. Open source toolboxes have been developed with optimized coding to provide efficient, reliable, and standardized computation of measures and methods for statistical testing (Rubinov & Sporns, 2010).

One of the most appealing aspects of networks is their representation or visualization that renders them in a manner which makes interpretation possible (Margulies, Böttger, Watanabe, & Gorgolewski, 2013). However, currently there is no standardized way in which to do this, and the choice of technique depends on the data and planned inferences (Figure 1.5). Traditionally, visualizing neuroimaging data, particularly that for task based fMRI, has emphasized anatomical accuracy and clarity. However, for connectivity and graph theory analyses, the emphasis changes to the pattern of interactions between any two nodes.

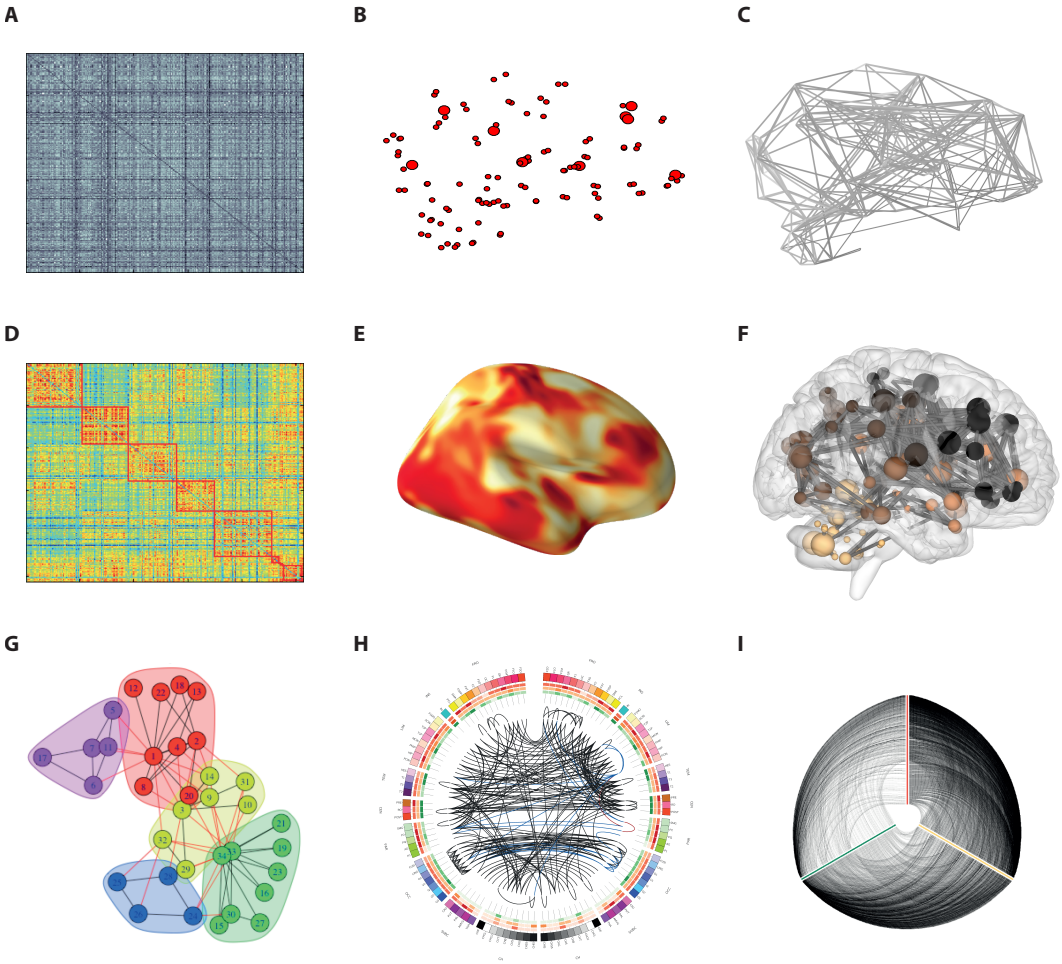

Figure 1.5: Network visualization

In the simplest form, connectivity data can be represented in terms of a two-dimensional adjacency matrix, although this does not take into account any spatial information. Translating connectivity patterns to physical space was originally performed in a two-dimensional plane (B & C) where circles and lines were used to denote nodes and connections between nodes in physical space (Achard, Salvador, Whitcher, Suckling, & Bullmore, 2006; Salvador, Suckling, Schwarzbauer, & Bullmore, 2005). These steps can be evolved, for example to include modular and coloured display of matrix information (D). A weakness of this approach was that it often wasn't reconcilable with recognizable anatomy, a concern that can be allayed by rendering the parcellation (E) or wiring diagram (F) on a surface reconstruction. The latter renditions can also display the functional properties of individual nodes by varying node size or color can help illustrate their properties without requiring edges to be displayed; this can be of use when characterizing hubs and their associated 'rich clubs' for example. A limitation of displaying heavily connected and detailed graphs

is line clutter, whereby the graph appears to represent a lattice, and extracting information from the figure becomes impractical. Techniques borrowed from other complex network displays such as hierarchical edge bundling spring embedding algorithms (e.g. Kamada-Kawai, G) can be used to clarify the display of such information. Finally, more abstract renditions of connectivity data can be performed, whereby the display is detached almost completely from traditional anatomical localization, and instead emphasizes complexity and multivariate display of data using either spring-force embedding diagrams to do away with the physical properties of the network and emphasise its intrinsic properties (H), circular representations (Irimia, Chambers, Torgerson, & Van Horn, 2012a; Irimia et al., 2012b; McGonigle, Malizia, & Mirehdi, 2011), or Hive plots (I) where a regular but abstract physical structure is given to the network and useful for comparing properties visually between different networks or analysis pipelines. Animated representations have also been proposed to demonstrate dynamics in graph evolution.

The brain's small world: insights from graph theory into anatomical models

A fundamental property of brain networks – either structural or functional – is that they demonstrate clear small world characteristics; that is, they are simultaneously segregated (high clustering coefficient) and integrated (short path lengths) (Bassett & Bullmore, 2006; Sporns, Chialvo, Kaiser, & Hilgetag, 2004; Watts & Strogatz, 1998). In this manner they parsimoniously balance the needs of localised specialisation and global efficiency. This highly non-random pattern of connections is also remarkably sparse, in that the overall number of binary connections is a small proportion (~5-10%) of the maximum number possible, emphasizing the highly organized nature of brain networks (Young, 1992). Small world characteristics and sparse networks are complimentary features in that they demonstrate how simultaneous segregation and integration can be achieved at a low cost of connections. Sparse small world attributes are robust in that they are reproducible across imaging modalities (diffusion MRI (Hagmann et al., 2007; 2008), resting fMRI (Achard et al., 2006; Salvador et al., 2005; Wang, Zuo, & He, 2010), structural MRI (He et al., 2007), EEG ("Small-World Networks and Functional Connectivity in Alzheimer's Disease," 2006), MEG (Stam, 2004), and PET(Di, 2012; Sanabria-Diaz, Martínez-Montes, & Melie-Garcia, 2013)),

disease states, and species e.g. cat, macaque, and nematode *caenorhabditis elegans* (E. Bullmore & Sporns, 2012).

Technological advancements in mesoscale connectomics with viral tract tracing in animal models have recently challenged this notion of universal small world organization and sparsity of connections (Oh et al, 2014). A key difference in this study was the high connection density (66%) most likely due to the increased discovery rate of previously undiscovered connections matched with a low-resolution template, making it more likely that any two parcels have at least one connection. With such a connection density, network randomisation algorithms produce less variance in the resulting networks, and hence normalised ratios of clustering and path length are approximately equivalent. However, advances in graph theoretical analyses of high density mesoscale networks using weighted networks and metrics has found evidence that the small world property is still prevalent (Rubinov, Ypma, Watson & Bullmore, 2015).

Hubs

The degree distribution of brain networks is difficult to accurately reproduce due to the small number of overall connections using common anatomical parcellations (Kaiser, Martin, Andras, & Young, 2007). However, while it appears that brain networks do not demonstrate scale-free properties in their degree distribution, they do have a heavy tailed distribution best approximated by an exponentially truncated power law (Achard et al., 2006). This deviance from true scale-free architecture is not entirely unexpected given the space constraints involved. In other words, it would be difficult to imagine having sufficient room for a brain growing inside a closed space like the skull to accommodate super-connected regions that would reside in the extreme tail of the degree distribution (Amaral, Scala, Barthelemy, & Stanley, 2000). Other topologically constrained networks such as transportation networks and internet routers face similar issues (Barabási & Albert, 1999).

A consequence of the heavy tailed degree distribution is the existence of highly connected nodes known as hubs (van den Heuvel & Sporns, 2013). These hubs are believed to play a key role in facilitating the flow of information in the network, particularly in the connectivity between distributed higher order association cortices.

It is believed that hubs play a key role in linking higher order association cortices that are involved in more sophisticated cognitive processing such as executive function, memory and salience. Therefore while it is unlikely that hubs are eloquent *per se,* in the sense that removal or stimulation of a hub will lead to a direct clinical manifestation in a specific domain, it could be that hubs resemble a form of cognitive eloquence analogous to that of the primary cortices (Sporns, Honey, & Kotter, 2007).

While degree and strength can be used to identify hubs, there are multiple measures available to capture the influence of a node in overall network function, known as centrality measures. Each measure aims to capture a specific feature believed to be important in defining a given nodes influence on the entire network. Hence, with multiple features and measures available, a diverse range of hub nodes can be identified (Fornito, Zalesky, & Bullmore, 2016). For example, closeness centrality is the mean distance from one node to all others in a network. Betweenness centrality is the fraction of shortest paths in a network that pass through a node (Freeman, 1977). Eigenvector centrality is a mathematical approach that captures the number of connections to other nodes as well as the quality of the connections from these neighbours. Modular decomposition can be used define the role of hubs (Guimera & Ameral, 2005). Participation co-efficient identifies hubs that integrate different modules. Within-module degree z-score captures the centrality of a node within a given module and known as provincial hubs.

Given the myriad methods to define hubs it is unsurprising that their location varies between studies and with the chosen centrality measure. One way to handle this issue would be to define the specific measure of influence hypothesized to be of interest within the network *pre-hoc*. An alternative is to look at consensus hubs, that is, hubs that score highly over a variety of features and thereby encapsulate centrality as a key characteristic of the node independent of the actual centrality measurement. This method was applied when scoring the top 20% of nodes by degree, betweenness, closeness, and their inverse clustering co-efficient (which is negatively correlated with centrality). Using this approach hub regions were identified bilaterally in the caudate nucleus, superior frontal gyrus, and putamen, and on the right in the cingulate gyrus and precuneus, and the left thalamus (van den Heuvel & Sporns, 2010).

Rich club

Related to hubs is the so-called 'rich club' phenomena, whereby the distribution of connections between such hubs is often found to be significantly non-random, with highly connected hubs strongly connected to each other(van den Heuvel & Sporns, 2011). Evidence for rich club organization is available for a wide range of different networks including those of transportation, Hollywood actors, and scientific citations.

Analysis of rich club organization differs depending on whether binary or weighted measures are used (Colizza et al., 2006; Opsahl et al., 2008). In both however a cluster of nodes is defined as identified as being part of the rich club, most commonly by ranking nodes in order of a centrality measure like strength or degree, then using a threshold to create the rich club component. For binary analysis, the number of edges or density within this rich club is compared with the density in the entire network. In a weighted analysis the putative rich club component is identified and the sum of its edge weights is computed then compared with that from the same number of highest edge weights in the whole network. Both binary and weighted measures are compared with those from comparable randomized networks in order to create normalized rich club co-efficients.

Within the brain, rich club hubs tend to belong to multiple modules and have similar topological overlap in their connectivity with each other. The rich club plays a critical role in network dynamics (Misic et al., 2008), demonstrated by the disproportionate reduction in network integration upon their simulated removal. Formation of a rich club comes at a high network cost however, with many of the connections within the rich club being longer distance than those on average within the network (van den Heuvel et al., 2012; Fulcher & Fornito, 2016).

Modularity

Community detection is performed by grouping nodes into communities or modules such that they are more strongly connected to nodes within their own module than to those in other modules (Newman, 2004). Modules derived from a graph theoretical treatment are consistent with those identified using other means of assessing brain connectivity and resting state networks, such as SCA and ICA (van den Heuvel & Pol, 2010). These modules can be further broken down into sub-modules in a

hierarchical manner (Smith et al., 2009). Within these modules, highly connected hubs have been identified which are further sub-classified as either connector hubs if they link modules, or provincial hubs if they mainly integrate nodes within a module (Guimera & Amaral, 2005; Sporns, Honey, & Kötter, 2007). Together these two extremes of module hubs may function to simultaneously balance network segregation and integration.

Modularity by itself reflects local specialization and is a marker of network segregation, but also allows cost effective network integration through simply adding a few long-range connections between modules (Fornito, Zalesky, Bullmore, 2016). Furthermore, while modular networks are small worlds, the converse is not true. For example, the original lattice re-wiring model for creating small world networks does not recapitulate hierarchical modularity features. Therefore it is possible that the functional advantages of a small world topology may be a consequence of their modular organization.

The significance of a hierarchical modular organization is multifaceted (Bassett et al., 2010; Meunier et al., 2011). Network disruption and cascading failures of individual elements can be contained within individual modules thereby limiting the global impact of such events. This feature that may be relevant to the propagation of seizures where it has been shown that a reduction in modularity is associated with increasingly synchronized network dynamics analogous to patterns seen during seizures (Kaiser et al., 2007). Hierarchical modularity is also necessary for self-organised critical dynamics and neuronal complexity (Kitchbichler et al., 2009). Modules tend to be associated with distinct functions or groups of functions suggesting task specialization, particularly in the primary cortices involved in movement, vision, and hearing (Smith et al., 2009). However a break down in modularity with consequently increased network integration is also important particularly in higher order cognitive tasks. This is consistent with network integration being more predictive of better performance in intelligence tests than network segregation.

Network formation & generative models

Rules for neural network growth have been developed that try to accurately predict the behavior of real brain networks. For instance, when new nodes are connected

preferentially to a highly connected ‘rich club’, the degree distribution matches that of other real world networks, a scenario known as the ‘rich get richer’ (Barabási & Albert, 1999). Other models include the ageing of vertices, whereby a certain number of nodes disappears over time, a process that replicates scale-free degree distributions (Amaral et al., 2000). Clarifying the constraints and stimuli for network growth may allow insights into brain repair or adaptation after injury.

It should now be apparent that network models of brain structure and function aim to describe how the simultaneous demands of functional segregation and integration are met. In this new perspective, the focus changes from a localization approach, in which particular cognitive functions takes place in specified brain regions, to an integrative or connectomics based approach that emphasizes information flow across the entire network. Additionally, the vocabulary that accompanies graph theory offers a new way of expressing the exploration of the brain. A prominent structural and functional core can be defined based on specific hubs, modules, and efficiency, which can be used to re-explore classical models of brain activity. Whether differences in network parameters can be identified with enough reliability to encompass individual variability, dynamic reconfiguration, and evolutionary changes remains to be seen.

Applications of graph theory to neurosurgery: new concepts in brain mapping

While graph theory analysis of complex networks has allowed significant advances in our understanding of normal brain structure and function, to be clinically relevant it must also make neurosurgery “more accurate, gentle, and safe”. We now discuss how graph theory can be applied to brain mapping, and in doing so give a new perspective that sees function from a connectivity-based perspective, rather than purely localized. Supplementing traditional methods of brain mapping (such as intra-operative cortical stimulation), graph theory also allows prediction of dynamic changes (possibly in a reparative manner), as well predicting how the brain can adapt (or not) to the presence of focal lesions, including those purposefully induced by surgery. Finally we highlight the potential of developmental models to providing insight into network plasticity and robustness that could prove useful for understanding the effects of brain injury in neurosurgery.

Network models of brain function

Graph theory has characterized brain functional organization as a highly efficient, small world network. Understanding how this network architecture affects intellectual function may enable the abstract concepts and measures of graph theory to develop clinically relevant meaning. For example, network features may be able to reflect an individual's performance, learning, or impairment in performing a specific neurocognitive task.

To understand the relationship between function and individual networks, comparison with statistical techniques such as ICA have been particularly insightful. Networks identified through ICA of fMRI data in the absence of an external stimulus were compared spatially to those derived during experiments that required cognitive engagement (Smith et al., 2009). A close correspondence was found between behavioral domains in the corresponding task-based fMRI and resting fMRI networks, suggesting at baseline the brain is already organized along functional boundaries. Furthermore, when the ICA network decomposition was performed at a higher resolution (70 components), a hierarchical organization of functional modules was apparent. That is, within a specific functional domain or module, smaller sub-modules were now present that reflected more discrete yet still related functional components. It can then be hypothesized that such modules (and hierarchical sub-modules) represent a repertoire of functional networks that can be called upon for task-directed activities.

Experiments examining intelligence and network topology found a higher intelligence quotient (IQ) was negatively correlated with path length but not with clustering or overall connectivity (van den Heuvel, Stam, Kahn, & Hulshoff Pol, 2009). As a longer path length is inversely proportional to efficiency, this suggests that network efficiency is a key factor for cognitive function. Furthermore, the medial prefrontal cortex and precuneus (among other regions) were identified as having the greatest effect on network organization and global network efficiency. Notably, this study is a demonstration of how task performance patterns are reflected in functional connectivity at rest.

This critical role of path length and it's inverse, efficiency, has been corroborated in a study examining brain structural networks (Li et al., 2009). High intelligence corresponds to higher global efficiency in both weighted and binary graphs. During the performance of a task, a more prominent small world architecture was found in those without higher education than in those with a University education, suggesting that more efficient network communication was required in the former group in order to complete the task (Micheloyannis et al., 2006). In support of this hypothesis, studies on modularity have found that higher cognitive function leads to a break down of network segregation to facilitate integration, which in turn leads to a reduced small world co-efficient. Higher education may therefore reflect the ability of the brain to decompose its modular and small world architecture in support of greater integration required to perform specific cognitive tasks.

Resting state connectivity can also reflect post-task learning (Muraskin et al., 2016). After performing a Go/No-Go task seed connectivity analysis found increased connectivity between the right SMA and left insula among those who improved their performance the most. There was a suggestion, albeit failing to survive multiple comparison testing, that this functional connectivity difference was reflected by increased structural connectivity measured with DTI. Another study used cognitive training to improve working memory and found increased connectivity with fronto-parietal attention networks (Caeyenberghs, Matzler-Baddeley). Specifically, it was the integration or efficiency within this attention network that was most reflective of improvements in memory during the training programme.

Application of complex network analysis to predict cognitive impairment has been performed in a cohort of survivors of childhood leukaemia (Kesler, Huston-Warren, & Watson, 2016). Here it was hypothesized that chemotherapy during childhood would leak to white matter injury and later life cognitive decline. Small worldness was impaired as was clustering in the frontal, parietal, occipital, and limbic lobes. Furthermore, a random forest model was able to correctly classify those having cognitive impairment with 89% accuracy. Therefore, complex networks do not only predict function in healthy participants, but are also sensitive to pathological functional impairment.

In conclusion, network integration and efficiency appears to be the key determinant of intellectual function and higher cognitive functions. While markers of network segregation, such as local efficiency or module hierarchy, may be important for discrete specialized task performance, these hypotheses have not been born out with the experimental data. Analysing brain function with complex network analyses also allows insights into learning, task based performance, and predicting pathological cognitive impairment. Relating network topology to specific neuropsychological tasks and to the effects of cortical stimulation findings will be critical to translating graph theoretical measures to predicting clinically meaningful phenotypes.

Network robustness and percolation theory

Connectomics can be used to model the network effects of focal brain injury through application of percolation theory (Barabasi, 2016). A selective 'synthetic' lesion can be created by either removing an individual node (and all of its connections) or by removing an individual connection from the network. Note that the actual pathophysiological disease mechanism on the individual nodes or edges isn't necessarily directly modelled: rather, the aim is to capture the consequences of this focal disruption on global network function and architecture.

In graph theory, the study of network disruption is typically treated as an inverse percolation problem. Percolation theory is a mathematical concept prominent in statistical physics for its role in offering analytically treatable examples of phase transitions and critical phenomena (Bollobas & Riordan, 2006). A typical example is modelling fluid flow through a lattice, whereby percolation of the fluid through the lattice occurs when there is a path of connected links (referred to as bonds in this context) from one side of the lattice to the other. An inverse percolation problem is therefore how removal of specific links affects global network properties, such as the ability of fluid to pass through the lattice (figure 1.6).

In graph theory, percolation has been used to model how graphs fragment upon cumulative vertex or edge removal, or how graphs coalesce into a connected cluster upon adding links (Albert, Jeong, & Barabasi, 2000). This transition between states (connected or fragmented) is not gradual but typically occurs at a critical percolating threshold. In random graphs this phenomena has been formally studied and the

conditions upon which a connected component exists have been established, namely when each node has at least one connection on average (Erdos, 1959).

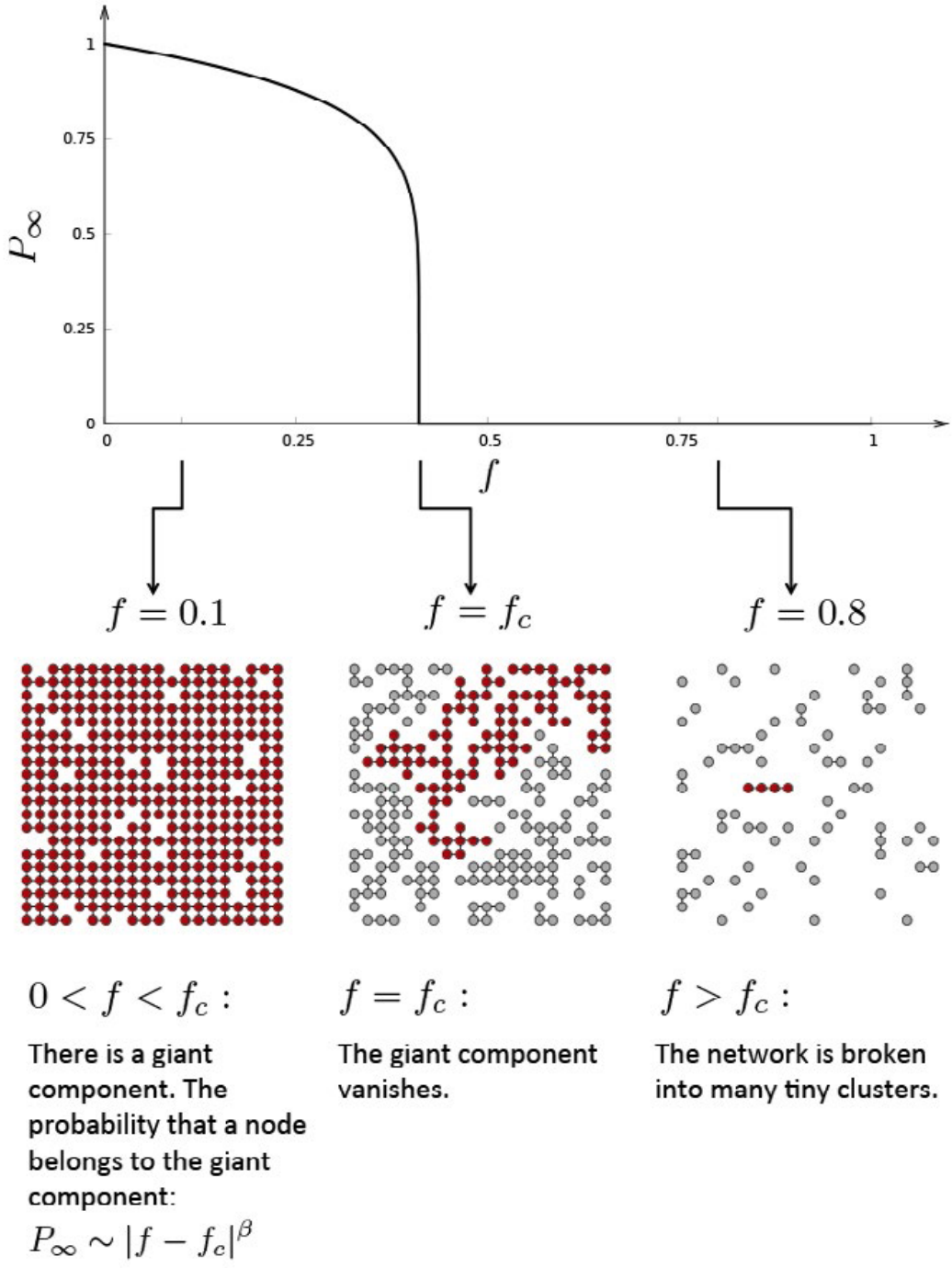

Figure 1.6: Percolation on lattices

The consequences of node removal can be treated as an inverse percolation problem. As nodes are removed the network becomes fragmented, a transition that can be captured by describing the size of the giant component and it's features (corresponding graphs underneath). From [Barabasi, 2016].

The response of a network to percolation is dependent on its degree distribution. In a scale free network, the majority of nodes have low degree, therefore randomly removing a node will most likely involve a low degree node and have little consequence. However, focused removal of a hub node will have a disproportionate impact on the network, suggesting increased vulnerability. In contrast, a random graph (with a binomial degree distribution) has little variation in node degree, and therefore when compared to a scale free network will have a higher vulnerability to random error but less so to focused attack. Heavy tailed distributions (i.e. fat tailed, long tailed, and sub-exponential) lie somewhere between these two extremes.

While random graphs (with a Poisson degree distribution) are not an accurate model of many real world networks, the concept of percolation thresholds has been extended to graphs of natural systems with diverse degree distributions. Here, percolation of networks consecutively removes nodes in either a random manner ('random error'), or in order of some specific network measure ('focused attack'). A pervasive feature of real world networks – including the internet, world wide web (WWW), power grid and actor network – is enhanced resistance to random error but increased vulnerability to focused attack when compared with comparative random graphs (Albert, Heong, & Barabasi, 2000).

Percolation has also been applied to brain networks where it was found that the resilience to random error was lower than a scale free network but higher than a random graph while the converse was true for focused attack; this data was used as evidence to argue for a broad tail degree distribution in brain networks constructed from empirical data. This analysis used a relatively low resolution network (116 nodes), while a higher resolution voxel-wise network (~10,000 nodes) suggested a power law degree distribution (Eguiliz 2005, Fraiman 2009, van den Hueval 2008c). However, this approach assumes each voxel is independent in time and space. It is also unlikely that the physical space of the brain is sufficient to allow such a wide variation in node degree distribution (i.e. for hub nodes in the far tail). Overall it appears that the brain develops selective robustness for random error but at the cost of increased vulnerability to focused attack. Rather than brain development selecting for such robustness, it is more likely that it is a by-product of the formation of developing

efficient processing (for example through a rich-club organizational topology)(Kaiser et al., 2007).

In conclusion, percolation offers an analytically tractable *in silico* model that allows networks to be defined on their response to simulated injury. Robustness refers to a network that can maintain its original function upon perturbation while resilience refers to an adaption or recovery of function. Related concepts include degeneracy, whereby unrelated network elements can adopt the roles of the missing network elements, and redundancy, whereby there are many components that can substitute for the perturbed elements (Tononi, Sporns, & Edelman, 1999). Applying percolation theory to simulate clinical brain injury allows a unique opportunity to explore pathophysiology *in silico* and represents a relatively unexplored niche that draws on the strengths of diverse fields including statistical physics, graph theory, and connectomics.

Synthetic brain lesioning

Analysis of the effects of lesions on brain function has a long tradition of providing insight into functional localization (Rorden & Karnath, 2004), which has been complimented by high-resolution neuroimaging (Bates et al, 2003). However, understanding brain function from a localization perspective is limited in its ability to account for dynamic changes, individual variability, and neurocognitive processes that require distributed rather than discrete processing. Network based analysis of lesion effects offers a complimentary consideration of system-wide functional disturbance. In addition, models can be readily created to virtually examine the effects of postulated lesions.

Robustness of individual nodes to lesioning can be performed by removing a node then quantifying the change by comparing the ratio of general network measures before and after. This concept is closely related to delta centrality (Latora & Marchiori, 2003), whereby nodes with a disproportionate effect on global network measures upon their removal, and can be used to quantify the so-called ‘Achille’s heel’ of a network. This approach can be extended to individual or groups of edges to identify a core white matter scaffold maintaining global network integrity (Irmia & van Horn, 2014). Similar to other centrality measures, the overall outcome is sensitive

to the feature and therefore the measure of interest. For example, using a cumulative score (comprising of assortativity, characteristic path length, density and transitivity) this core scaffold was found to be distinct from rich club connections, in contrast to the belief that rich club organisation is critical to complex functional dynamics. However, a subsequent analysis using different global measures (Estrada's communicability and Tononi's integration) found that removal of rich club edges tended to produce the largest changes (de Reus & van den Heuvel, 2014).

Modeling the effect of larger, potentially more realistic cortical lesions was performed on a structural connectivity data set with simulated neural dynamics (Alstott, Breakspear, Hagmann, Cammoun, & Sporns, 2009). Networks were robust to random node deletion or targeted removal of nodes based on their degree or strength, but vulnerable to targeted removal of highly central 'hub' nodes. Simulated dynamic effects of lesions varied in size and spatial pattern depending on the lesion location, with lesions in the midline as well as those involving temporo-parietal junction and superior frontal gyrus tending to have the greatest effect on neural dynamics. In general, lesions reduced functional connectivity, with effects most pronounced in the ipsilateral hemisphere, but also extending in a non-local manner to the contra-lateral hemisphere. Finally, the extent that alterations of the structural network produced dynamic consequences was most accurately predicted by injury to the DMN rather than, for instance, the degree or strength of connections directly incorporated by the lesion. How these simulated lesions and corresponding network disruption relate to actual neuropsychological findings in patients will have to await clinical confirmation. However, it is likely that the relationship between simulated and *in-vivo* lesions is considerably more complex, non-linear, and incorporates dynamic reparative mechanisms such as synaptic plasticity.

White matter or structural disconnectivity and its effects on function networks have been studied in a model of structural networks created from empirical data followed by a computer simulation of resting-state BOLD signals using the network as a substrate. Randomly removing links or decreasing the global coupling strength resulted in characteristic patterns of increased hierarchy, efficiency, and robustness, but reduced small worldness, clustering and generated a narrower degree distribution (Cabral, Hugues, Kringelbach, & Deco, 2012). This pattern of altered network

dynamics was found to be similar to that found in patients with schizophrenia, suggesting that altered structural connectivity could be responsible for dynamic and phenotypic changes. However, the effects of focal lesions are unlikely to be explained purely in terms of alterations to structural connectivity, and will most likely require a model combining structural and functional factors.

A theoretical study of the dynamic effects of lesions has been performed using models of oscillatory cortical activity superimposed on a structural connectivity backbone (Honey & Sporns, 2008). Lesion effects extended beyond the individual locale and were influenced by the clustering patterns within the network. While these effects were consistent for all lesion locations, the effects were most prominent for lesions in frontal and parietal association cortices. A similar study design has been used to assess the effects of lesions on network synchrony and metastability (Vasa et al., 2015). Consequences of lesions in the adjacent neighbourhood were predictable based on a variety of structural measures, whereas global changes were most affected by removal of hubs, defined on the basis of high eigenvector centrality or between module participation co-efficient.

Extending synthetic lesioning studies to clinical populations and cognitive outcome has reveals that high network robustness is correlated with high intelligence quotient (Santarnecchi et al., 2015). This robustness is supported by integration between distributed fronto-parietal networks involved in language and memory. While this is in concordance with the theory of cognitive reserve, whereby higher intelligence is protective against the clinical effects of neurodegeneration, it is somewhat discordant with the view that hubs play an integrative role critical for higher cognition but also represent the networks 'Achille's heel'. Potential explanations could be that the hubs collectively form a rich club that can compensate for removal of any one component, that the dynamics of hub function are altering over time, or that the results are specific to the individual cognitive outcomes and network metrics of the study.

The sole study relating network robustness to empirical lesions focused on the relationship between hubs and cognitive outcome (Warren et al., 2015). Consequences of a variety of focal brain lesions were dependent on the centrality measures used to define hubs, with more severe cognitive deficits apparent in lesions

to hubs defined on system density and between-module participation co-efficient than those defined on degree. This work is suggestive of hubs reflecting cognitive eloquence. It was not explored whether individual performance on a task was reflected by increased robustness, whereby highly functioning individuals would be less affected by removal of a hub node. Furthermore, the role of hub definition and lesion effects is still relatively unexplored, and the cross-sectional design requires that associative findings will require prospective validation.

A network approach has revealed key features in terms of the robustness and resilience to lesioning of the brain. Application of theory from other complex systems in response to, for example, the re-routing of traffic after road closures (Csányi & Kertész, 1995), or percolation theory and the degree to which networks can be impaired ('slowed down') before critical function is affected (as opposed to directly removing a node) (Callaway, Newman, Strogatz, & Watts, 2000) offer potential to understanding the subtleties of changes in information flow due to lesions. Network models of lesion effects could also be elaborated to encompass dynamic changes and potential neurocognitive functional consequences. Cognitive deficits could then be predicted based on the vulnerability of a network to attack and its potential for repair.

Speculatively, accurate lesion modeling could be utilized in intra-operative brain mapping to define the extent of resection or the effects of a surgical intervention. One can envision classifying brain regions into those that are highly vulnerable, serve critical function, or have limited potential for recovery, and thus need to be preserved. On the other hand, regions may be highly resilient, have limited functional importance, or have significant dynamic potential for re-organization. In this case a safer resection could be predicted with little functional consequence.

Understanding brain injury through networks of healthy development

Characterising plasticity

Brain networks are not static, but are dynamic over a wide range of time scales: from seconds to years. Normal development offers an ideal opportunity to measure the long-term evolution of their properties. In terms of neurosurgical relevance, characteristic patterns of network dynamics could be used as a proxy for plasticity and to explain recovery from focal neurological disorders.

Prior to adolescence neural connectivity consists predominantly of diffuse short-range connections. During adolescence this pattern evolves with an increase in long-range connections and decrease in short-range connections, reflecting a changes from anatomical to functional coupling (Fair et al., 2007). By adulthood networks had also developed an increased hierarchy and the inter-regional connectivity patterns had changed to form stronger cortico-cortical, but weaker subcortical-cortical connections (Fair et al., 2010; Supekar et al., 2009). This is analogous to processes occurring at cellular scales where over-connectivity is refined through selective pruning. Overall this results in an increased pattern of functional integration in the brain.

Alterations in connectivity strengths are reflected by an increasingly modular organization. In children, the DMN is sparsely connected within itself and tended to only include anatomical (i.e. local) patterns of connections, whereas in adults, the DNM had developed into a more densely connected network encompassing the characteristic distributed DMN regions (Fair et al., 2009). This pattern of increasing modular prominence is mirrored in the salience (Uddin et al., 2011) and fronto-thalamic networks (Fair et al., 2010). Module formation varies with age, with more sophisticated higher cognitive modules such as the paralimbic module maturing later than the lower order sensorimotor network (Khundrakpam et al., 2010). Following modular trajectories during later life reveals that those modules that form the latest are also the first to degenerate, consistent with the ‘last-in first-out’ theory of cognitive decline (Douaud et al., 2014). At a neuronal level this could reflect Hebbian learning (Hebb, 1942) whereby increased co-activation in specific cognitive domains results in increased functional connectivity and the formation of distinct modules.

Developmental changes in functional connectivity are sufficiently robust to allow machine learning algorithms to predict brain maturation patterns with 92% accuracy (Dosenbach, Nardos, Cohen, & Fair, 2010). Consistent with previous studies the main weights driving this model were weakening of short-range functional connections, confirming the importance of connection pruning to overall development. Analysing the location of these weight changes revealed that they were mainly between functionally distinct modules. A complimentary strengthening of long-range between major brain functional modules was also apparent and overall these changes resulted in an increasingly segregated, modular architecture. Overall this produced modules that were more segregated from each other, but more densely connected within themselves, thereby producing a link between modular evolution and functional integration.

Determining how the corresponding network changes relate to cognition has revealed increasing local and global efficiency during adolescence is related to increased intelligence, similar to that found in adult populations (Rubia et al., 2013). Modular evolution has also been found to be a critical driver in the emergence of cognitive function (Gu et al., 2015). Using within and between module connectivity, the functional role of each module could be translated to a space defined as either provincial versus connector and cohesive versus incohesive. Using these definitions it could be shown that different systems roles demonstrated different developmental trajectories during development. Sensorimotor systems tended to be cohesive provincial systems but became increasingly segregated. Subcortical and cerebellar networks were incohesive provincial systems and this role became more defined during development. The default mode was unique in being a cohesive connector network that became both increasingly cohesive within itself and increasingly connected to others during development.

Hub connectivity and rich club formation are key features of the adult brain networks and their maturational trajectories have been investigated with diffusion tensor based structural connectomes (Baker et al., 2015). Previously the structural connectome had been shown to be static in its development trajectory during adolescence (Hwang, Hallquist, & Luna, 2013), and this was reflected here by minimal increases and decreases in connectivity. However, these connectivity changes reached the majority

of the brains nodes, and hub regions were preferentially involved in forming new connections with each other. Hub locations also changed over time with subcortical hubs decreasing and fronto-subcortical and fronto-parietal hub networks gaining prominence.

A caveat to these developmental changes is the effect of head motion and its reduction with increasing age (Power et al., 2012). Essentially motion adds nuisance variance that is more homogenous in adjacent voxels resulting in a distance-dependent effect on the time series. In graph theory analysis this will result in stronger local connectivity and weaker long-distance connectivity, therefore clearly compounding the argument that similar changes could be due to functional development. Robust correction of motion-related artifacts attenuated some developmental effects but similar changes were still apparent (Satterthwaite et al., 2012). Furthermore, motion artifacts tended to obscure within module connectivity, and therefore allowed increased sensitivity to detecting segregation of functional modules.

These findings suggest that networks demonstrate characteristic patterns of dynamics over the two or more decades of brain development, converging to a more cohesive, efficient, and modular topology (Dennis & Thompson, 2013; Lenroot & Giedd, 2006). Overall it appears that whole brain integration evolves with increased long-range connectivity, modules emerge and become more segregated from each other, corresponding to improved cognitive maturity, with network hubs playing a key role in driving the process. Network models of development appear complimentary to traditional models, for example Hebbian learning, whereby repeated stimulation of one cell by another leads to increased synaptic efficiency (Vértes, Alexander-Bloch, & Bullmore, 2014). Determining the rules behind these network dynamics will require understanding of how they relate to neuro-cognitive traits, learning, and evolution.

From a neurosurgical perspective, lesions (either pathological or surgically induced) could trigger mechanisms that normally occur during development in order to repair the network. Using these principles, a description of how a brain network reconnects following attenuation or removal of specific nodes and edges could lead to an

explanation of adaptation and reconstituted function. Potentially rehabilitation could be tailored to the expected dynamic cascade of effects, or lack thereof.

Linking network architecture and robustness

Modelling developmental changes in brain network architecture and how it affects the response to injury has not, as far as I am aware, previously been performed. Studies of the connectome in healthy development have already been described while studies in brain robustness have tended to focus on static network architectures and inference on the network degree distribution or architectural features. Linking these two analysis themes in connectomics potentially opens up a new niche within network analysis and consequently the potential for novel findings.

While the developmental response to brain injury has not been subject to connectome analysis, it has previously enjoyed considerable attention within the neuropsychology literature (Dennis, 2010). Two distinct hypotheses on the effects of focal brain injury have developed in parallel. One proposes a negative relationship existed between age at brain injury and functional outcome, and has been coined the Kenard principle. Another proposes early brain vulnerability, whereby the brain is more vulnerable earlier on in its development, and with age the brain develops increased robustness to injury. While connectome approaches to understanding the age-dependent response to brain injury is an undeveloped niche, the developmental neuropsychology literature provides a rich background with which to explore network approaches to brain injury. In general the field has been in relative quiescence in recent decades, possibly due to the decline in use of animal experiments. However, important unresolved questions remain about non-linear effects of age and brain injury, the relative contributions of network robustness and resilience mediated through plasticity to overall outcome, and the impact of lesions in non-primary (e.g. association) cortices and even outside the cortex.

Empirical applications of complex networks in neuro-oncology

A fundamental goal in the resection of intrinsic brain lesions is to maximize the extent of resection for oncological gain (Stummer et al., 2012; 2006) while preserving brain function (McGirt et al., 2009) and ensuring a good quality of life. Current surgical

methods in neuro-oncology including awake surgery (Sanai, Mirzadeh, & Berger, 2008), cortical mapping (De Benedictis et al., 2010), and neurophysiological techniques (Bello et al., 2007), have led to significant advancements in patient outcome and the emergence of supra-marginal resections whereby tumor resections are extended to functional boundaries (Ius, Angelini, de Schotten, Mandonnet, & Duffau, 2011). Brain mapping has played a key role in the field since the pioneering days of Penfield (Penfield & Rasmussen, 1950) and identification of the sensory-motor homunculus. Further advances have included numerous well known patients with specific lesions associated with distinct neurocognitive profiles. However only more recently have studies began to investigating more complex functional topologies, for example suggesting hierarchical topology is involved in restoring function after lesions (Duffau, 2012).

Network science and graph theory offers a new language with which to progress our understanding of functional organization and plasticity in response to brain tumours. An abnormal signature of brain connectivity has been identified in patients with brain tumours (Bartolomei, Bosma, Klein, Baayen, Reijneveld, Postma, Heimans, van Dijk, de Munck, de Jongh, Cover, & Stam, 2006a; 2006b; Xu et al., 2013). In general, brain networks in patients with tumours have been found to be more random and less organised, not just locally but in a diffuse manner. Specific findings include reduced efficiency in patients with tumours in the frontal and temporal but not parietal lobes. Also, network hubs were also re-organised, with the right insula being a hub in controls but not patients. A follow-up study focusing on frontal lobe tumour confirmed reduced local efficiency but increased global efficiency, and reduced clustering (Huang et al., 2014). Whether these global network dynamics reflect compensatory mechanisms or possible non-local effects of the tumour awaits clarification.

For graph theory measures to have clinical relevance it is necessary to relate network disruption to the patient's symptoms and function. The degree to which network features are perturbed has been correlated with neuropsychological deficits involving both local and diffuse brain regions with reduced global efficiency, and small worldness correlated with lower intelligence quotient scores (Bosma et al., 2008; 2009; Xu et al., 2013). Applying graph theory measures to identify the

neuropsychological function of a network allows a novel means to map out a functional resection boundary depending on the anticipated cognitive consequences.

Surgical effects on networks and how this corresponds to clinical outcomes has been studied (Guggisberg et al., 2008; Huang et al., 2014). Networks were found to be restored to a more organized state post-surgery from a more disorganized state pre-operatively. Additionally, a specific pattern of network disruption pre-operatively was able to predict neurocognitive outcome (Guggisberg et al., 2008). Regions that showed decreased coherence could be resected without new deficits appearing, while increased connectivity was associated with eloquent tissue. Seizure outcome has also been correlated with improvement in network characteristics (Douw et al., 2008). In this case there was a trend for patients without seizures to have a larger decrease in inter-hemispheric connectivity in the theta band. Modeling the effects of surgery and the predicted network effects may thus offer a new avenue in pre-operative surgical planning. For example, surgery could be tailored to produce a predicted network effect that prevents new neuropsychological deficits or optimizes seizure outcome.

Recovery of sensorimotor function after supplementary motor area (SMA) tumour resection has been studied with a sub-graph analysis involving the pre-central, post-central, and SMA in a longitudinal manner before and after surgery (Vassal et al., 2016). Initially there was a decline in ipsilateral intra and inter-hemispheric connectivity post-op but both recovered to normal and supranormal levels at follow-up. Inter-hemispheric connectivity was also correlated with pre-operative symptoms and post-operative recovery, suggesting if may function as a biomarker of repair or potential for injury. Finally, the clinical hypothesis that the contralateral SMA sub-serves the function of the resected SMA was corroborated through increased connectivity between the ipsilateral pre-central gyrus and contralateral SMA.

Non-local effects of tumours can be assessed with graph theory too. In a cohort of patients with brain tumours outside the sensorimotor network, motor weakness was associated with reduced connectivity in the sensorimotor network, particularly involving interhemispheric connections (Otten et al., 2012). Concordantly, recovery from a motor deficit was associated with increased functional connectivity, while a lack of recovery was not. Furthermore, connectivity of the premotor area was

associated with motor speed regardless of the presence of overt weakness suggesting connectivity can be a biomarker of performance even without overt clinical deficits.

These preliminary studies demonstrate the potential of using network measures to assess clinical function and the effects of surgery in patients with brain tumors. Modeling the effects of lesions (and surgery) on networks offers a way to analyse the predicted effects of surgery on a network which in turn could be used to tailor the extent of resection based on the anticipated functional consequences and potential for network re-organisation. This final concept will involve unification of concepts of function, plasticity, and network robustness in understanding the consequences of brain injury.

THESIS STRUCTURE

Basic science research into functional brain mapping has aligned itself along a path that considers the brain as a product of its connections rather than isolated functional locations: integrating these advancements into clinical brain mapping will therefore be at the forefront of making neurosurgery "more accurate, gentle, and safe".

This thesis develops these concepts in a series of distinct yet related chapters considering the utility of specific network analysis approaches (highlighted in bold italics below) and study designs to addressing clinically meaningful hypotheses related to the effects of focal brain injury, namely:

- Chapter 3: Canonical ***resting state networks*** remain identifiable in the presence of focal brain tumours and demonstrate the requisite sensitivity for detecting putative plasticity or recovery- related changes in response to focal brain tumours

- Chapter 4: ***Connectomics*** offers potential to understand global rather than just local effects of focal tumours, and can be used and visualized in an intuitive and surgically relevant manner for pre-surgical planning

- Chapter 5: Focal tumours stimulate re-organisation and ***network hub plasticity*** to enable the brain to adapt in a parsimonious and utilitarian manner, thereby preserving function

- Chapter 6: Synaptic refinement, used as a proxy for potential plasticity and resilience to brain injury, can be captured as age-dependent changes in ***functional connectivity*** during adolescence, but demonstrates distinct gender, age, and age-gender interaction effects reflecting the external phenotypic differences observed in cognitive, emotional, and social behavioural terms

- Chapter 7: Brain network architecture controls the consequences of focal brain injury, and evolution of complex topology during adolescence serves to improve robustness to injury; both of these effects can be studied through ***percolation theory analysis***, which offers a tractable approach to studying *in silico* brain injury.

In answering these hypotheses the aim is to determine what each methodology offers neurosurgery. Each methodology is deemed to be complimentary in nature, and therefore the approach is not of a comparison between different methodologies; rather, the aim is to determine the strength and weaknesses of each methodology and what specific clinical and neuroscientific hypotheses and be appropriately addressed.

CHAPTER 2: METHODOLOGY

This thesis draws upon two independent datasets, the first of which is Markers of Aggressive Local Therapy In Newly Diagnosed Glioblastomas (MALTINGS). This study was primarily designed to investigate tumour invasiveness but also included pilot data testing the applicability of resting state fMRI and related analyses in patients with brain tumours. The second dataset is Understanding and Characterising Healthy Adolescent-to-Adult Neurodevelopmental Growth Effects (UChange) which is a constituent study of the Neuroscience in Psychiatry Network (NSPN). This is a large dataset of healthy adolescents that seeks to identify normal developmental trajectories. Combining these two datasets provides a complimentary approach to studying individual network effects at in patients with brain tumours, while additionally allowing characterisation of pervasive network plasticity rules that can subsequently be tested at in clinical populations.

2.1. MALTINGS

2.1.1. Study design

The study was approved by the Local Regional Ethics Committee (protocol number NIHR/CS/009/011) and all participants provided written informed consent. Inclusion criteria were the MRI appearance of a tumour consistent with a glioblastoma, specifically inviting patients with tumours in the right temporo-parieto-occipital region to provide a homogenous sample. Participants were deemed suitable for surgical resection or biopsy based on the consensus of the neuro-oncology multi-disciplinary team.

We selected a cohort of the initially 5 participants that formed the pilot or discovery dataset, then subsequently recruited 6 more participants as a validation dataset, all between April and June 2014. Basic demographic information is summarized in **table 2.1**. All subjects had a confirmed high grade glioma at local histological review according to WHO criteria (Louis et al., 2007). Compete resection was defined as no contrast enhancing component on MRI within 72 hours of surgery (Wen et al., 2010). Tumour locations are displayed in **figure 2.1.**

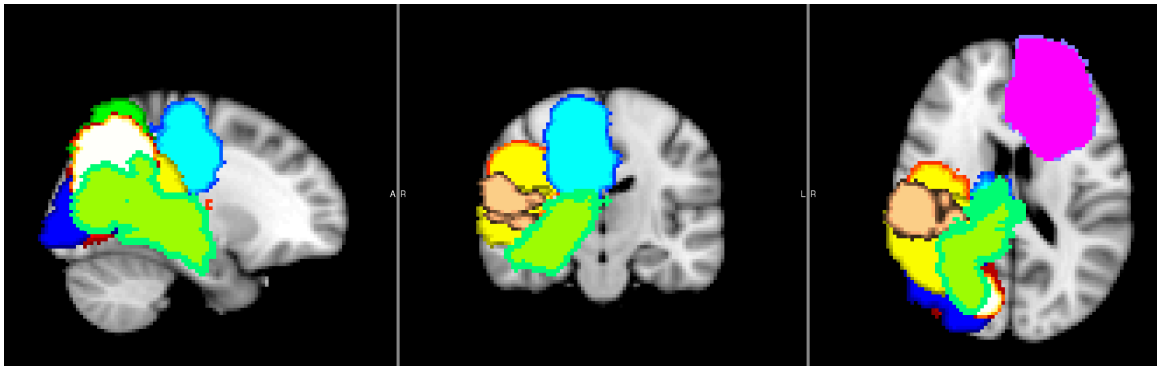

Figure 2.1: tumour locations

A binary mask of each participant's tumour is drawn in structural space then transformed to the template space of the Montreal Neurological Institute (MNI).

Age	Sex	Seizures	Pre-op exam	Post-op exam	Pathology	Surgery	Tumour location	Molecular markers	Survival (months)
64	F	Pre-op	Left pronator drift	Homonymous hemianopia	Glioblastoma	No residual disease	Right superior parietal lobule	-ve / 85%	23
73	F	No	Intact	Homonymous hemianopia	Glioblastoma	No residual disease	Right inferior parietal lobule to occipital pole	-ve / MIB 32%	13
79	M	No	Hemianopia	No change	Glioblastoma	No residual disease	Right inferior occipital lobe	-ve / MIB 28%	17
76	M	Pre-op	Left hemiparesis	Contralateral motor paresis deterioration	Glioblastoma	Biopsy	Right superior para-central lobule	-ve / MIB 18%	Unavailable
36	M	Post-op	Left hemiparesis	No change	Anaplastic astrocytoma	No residual disease	Right post-central gyrus and supramarginal gyrus	-ve / MIB 30%	
62	M	No	Hemianopia	No change	Glioblastoma	Biopsy	Right thalamic to temporo-parietal-occipital region	-ve / MIB 12.5%	14*
52	M	No	Left	No change	Glioblastom	Complet	Right	-ve / MIB	15*

			hemiparesis		a	e resection	supramarginal gyrus	25%	
57	M	No	Memory & language	No change	Glioblastoma	Complete resection	Left superior frontal gyrus	-ve / MIB 26.1%	16*
36	M	No	Hemianopia	No change	Glioblastoma	Complete resection	Right parieto-occipital	-ve / MIB 8.3%	18*
44	M	Pre-op	Nil	No change	Glioblastoma	Biopsy	Left caudate	+ve / MIB 38%	12*
50	M	No	Hemianopia	No change	Glioblastoma	Complete resection	Right supramarginal gyrus / occipital lobe	-ve / MIB 45%	8

Table 2.1: MALTINGS study participant demographics (Discovery | Validation) Tumour centre co-ordinates are in MNI152 2mm space. Molecular markers includes IDH-1 and MGMT status. *censored data (i.e. patient still alive at time of data collection).

2.1.2. Imaging parameters

2.1.2.1. Structural

Anatomical images were acquired using a T1-weighted magnetization prepared rapid gradient echo (MPRAGE) sequence (FOV 256mm x 240mm x 176mm; matrix 256x240x176; voxel size 1mm isotropic; TR 2300ms; TE 2.98ms; flip angle 9 degrees).

2.1.2.2. Resting state functional MRI

Resting-state fMRI data were acquired using a multi-echo echo planar imaging sequence with online reconstruction [30]: repetition time (TR) 2.42 seconds; GRAPPA with acceleration factor of 2; flip angle of 90 degrees; matrix size. 64 by 64 by 34; FOV of 240 x 240 mm; in-plane resolution of 3.75 x 3.75 mm; slice thickness of 3.75 mm with 10% gap; alternating sequential slice acquisition; 34 oblique slices; bandwidth of 2368 Hz/pixel; and echo times (TE) of 13, 30.55 and 48.1ms.

2.1.3. Image processing

An overview of the imaging analysis pipeline is presented in **figure 2.2**.

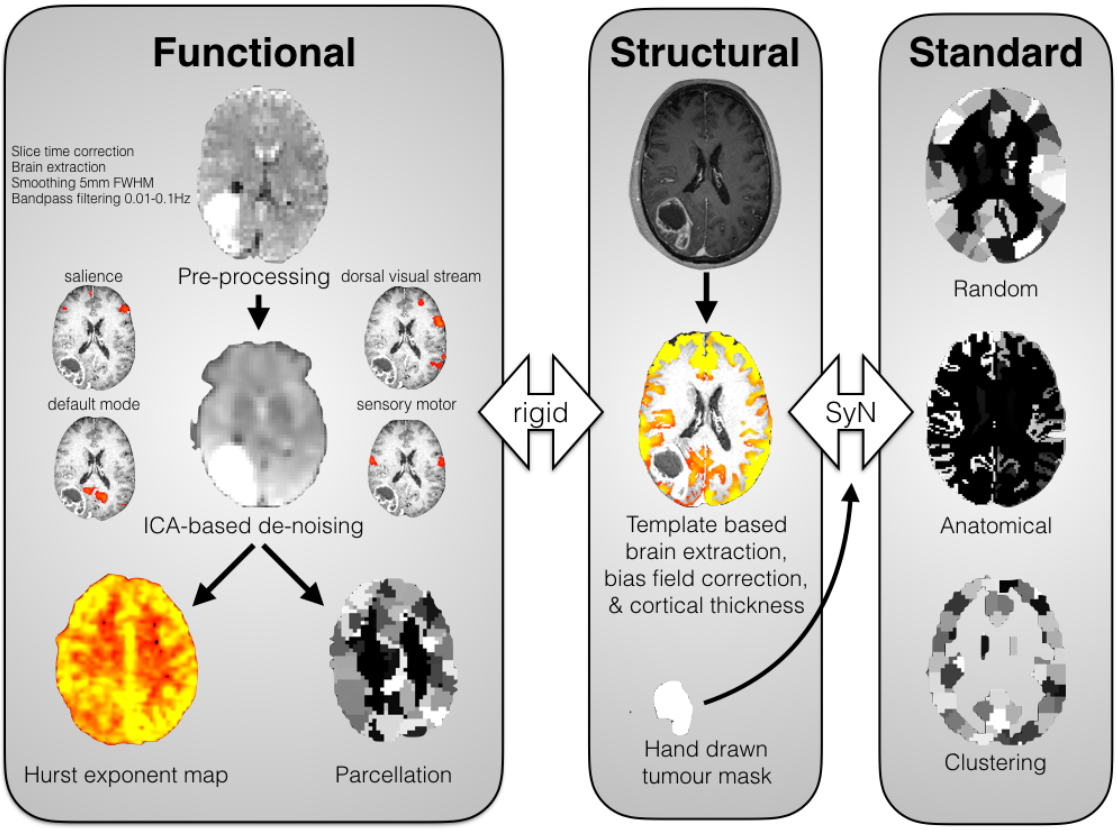

Figure 2.2: overview of image processing pipeline

Functional images underwent multi-echo ICA-based de-noising and selected pre-statistical processing in functional space. Anatomical images underwent brain extraction, bias field correction, and tissue segmentation (including hand drawn masks of the tumour contrast-enhancing volume). Standard space is used to define parcellation templates which are then transformed to functional space for time series extraction or for display of resting state networks and comparison with canonical networks. SyN = symmetrical diffeomorphic normalisation, FWHM = fixed width at half maximum.

2.1.3.1. Structural

Advanced Normalization Tools (ANTS) cortical thickness pipeline (Avants, Tustison, & Song, 2009; Das et al, 2008; Tustison, Avants, & Cook, 2013) was used to perform automated volume based cortical thickness estimation workflow including: initial bias

correction on input anatomical MRI; brain extraction using a hybrid segmentation/template-based strategy; alternating between prior-based segmentation and white matter posterior probability weighted bias correction; and cortical thickness estimation in native space. A hand drawn tumour mask was used as an additional prior for segmentation. Finally non-linear warps to MNI space were computed using symmetrical diffeomorphic registration with a binary mask of the tumour to exclude it from the cost-function weighting.

2.1.3.2. resting state functional MRI

Data pre-processing was performed using AFNI (Cox, 1996) (http://afni.nimh.nih.gov/afni/). The first 15 seconds of image data were discarded to allow for magnetization to reach steady state. Subsequent steps included: slice time correction; rigid-body motion correction; de-spiking; and functional imaging brain extraction.

For de-noising we used multi-echo independent component analysis (ME-ICA) (Kundu, Inati, Evans, Luh, & Bandettini, 2012; Kundu et al, 2013). This is a method for resting state fMRI analysis and de-noising in a data-driven and physically principled manner based on the T2* decay of BOLD signals (**figure 2.3**). As TE is varied, physiologically relevant BOLD contrast is expected to vary while non-physiologically relevant contrast or noise (e.g. head movement or cardio-respiratory signal) remains stable. The behaviors of these two signals can be modeled with a pseudo-F statistic resulting in two curves with distinct changes in gradient with BOLD contrast (κ) and noise (ρ). Multi-echo fMRI time series are first concatenated then decomposed into independent components (ICs) using FastICA following which each IC is categorized as either BOLD signal (high κ:ρ ratio) and retained or noise (low κ:ρ ratio) and regressed out.

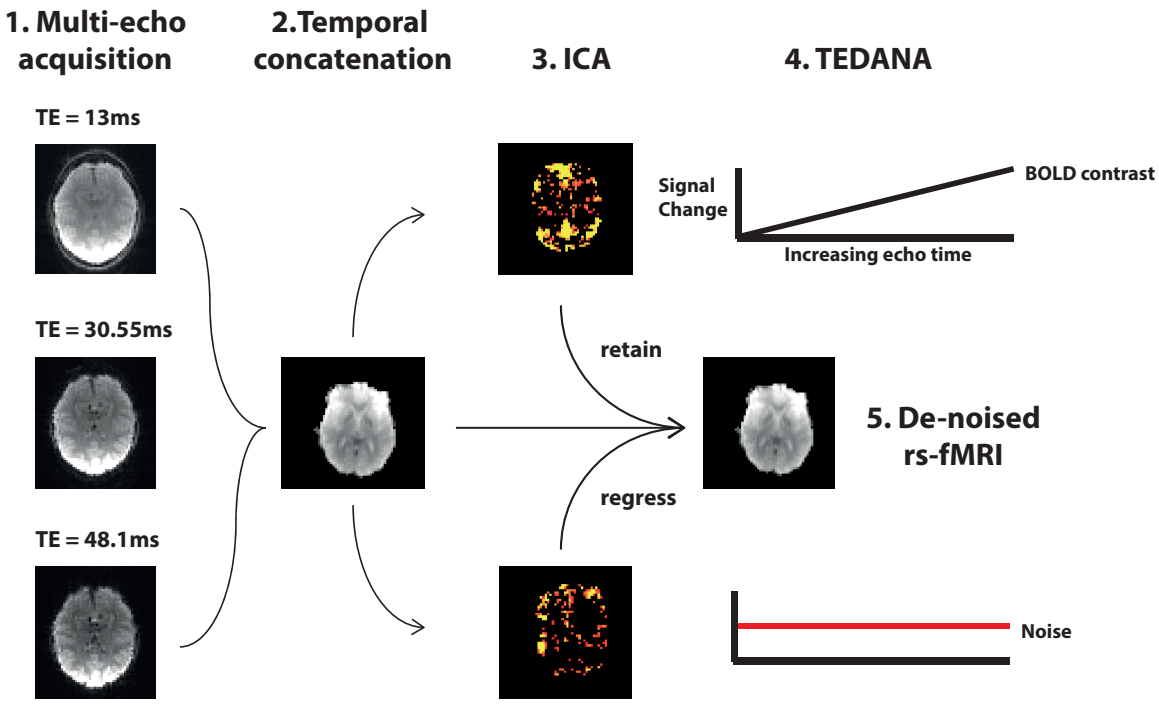

Figure 2.3: multi-echo independent component analysis

Initially resting state gradient echo echo-planar imaging data is acquired at multiple different echo times. These undergo rigid-body alignment and concatenation into a single 4D volume prior to subsequent independent component analysis (ICA). The resultant ICA networks are subjected to Time Echo Dependent Analysis (TEDANA). Here components that scale positively with increasing echo time are classified as related to BOLD contrast while those ICA components that do not scale with echo time are classified as noise. Here the ICA components represent the default mode network (BOLD contrast) or head motion (noise, represented by the typical extra-cerebral peripheral rim of contrast). The bad components are then regressed out of the original temporally concatenated 4D data with ordinary least squares in a fully automated process.

2.2. Neuroscience in Psychiatry Network (NSPN)

2.2.1. Study Design

Understanding and Characterising Healthy Adolescent-to-Adult Neurodevelopmental Growth Effects (UChange) is a constituent study of the Neuroscience in Psychiatry Network (NSPN). The study enrolled 2135 participants from schools, colleges, NHS primary care services and direct advertisements in north London and Cambridgeshire. This primary cohort was stratified into 5 age-defined strata in 2-year epochs from 14 to 24 years inclusive. Recruitment within each stratum was evenly balanced for sex and ethnicity with the proportion of subjects ascribing their ethnicity as 'white' matched to within 10% of that in the local populations. Inclusion criteria were: age between 14 and 24 years inclusive; able to understand written and spoken English; willing and able to give informed consent for recruitment into the study cohort and consent to be re-contacted directly for possible participation in future studies within the consortium. Exclusion criteria were participation in a clinical trial of an investigational medical product within the past 12 months. Participants completed questionnaire assessments of socio-demographic status, family and educational or occupational environments, and sub-clinical psychopathology.

Of the complete UChange cohort, 300 participants were invited for MRI assessments; this thesis is based on a 100 participant interim subsample of this dataset. Additional exclusion criteria for this study were: current treatment for a psychiatric disorder or for drug or alcohol dependence; current or past history of neurological disorders or trauma including epilepsy or head injury causing loss of consciousness; learning disability requiring specialist educational support and/or medical treatment; or had a safety contraindication to MRI scanning. An overview of the MRI analysis pipeline is in **figure 2.4**.

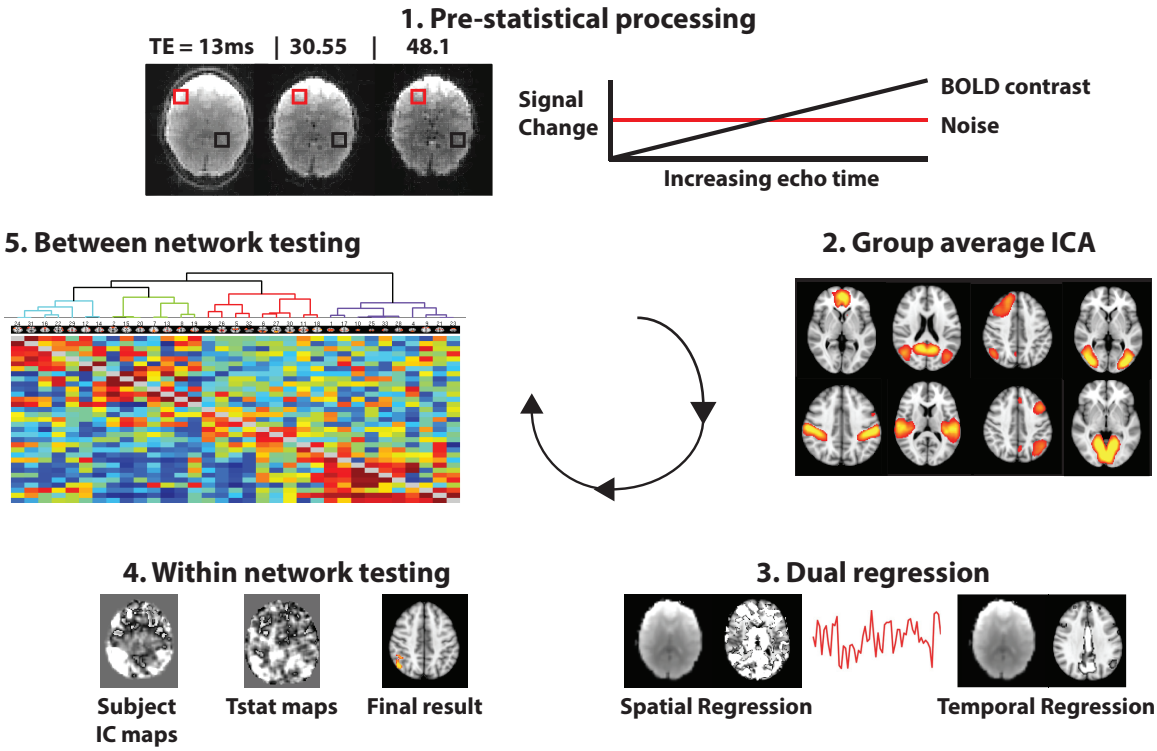

Figure 2.4: NSPN MRI analysis pipeline

Resting state functional MRI data is acquired and processed with multi-echo independent component analysis (ME-ICA). Subsequently a group independent component analysis is performed to identify group average ICA networks. Individual representations of these group ICA networks are computed with dual regression. Subject specific ICA networks can then be converted to t-stat maps and tested for within network changes. Between network testing can be performed by computing the statistical dependencies between subject specific IC maps, for example with Pearson product moment correlation, forming a connectivity or adjacency matrix.

Number of participants	100
Location	Cambridge: 61%, London: 39%
Gender	Female: 50%
Age (years)	18.59 (16.6 – 21.3)
Intelligence quotient (IQ)	111.5 (103.8 – 121)
Handedness	Right handed: 76.2%
Index of multiple deprivation (IMD)	10.9 (5.4 – 21.2)
Ethnicity	White 83% Asian 5% Black 2% Mixed 6% Other 4% Declined to comment 0%

Figure 2.2: NSPN UChange study participant characteristics
For continuous measures (age, IQ, index of multiple deprivation) data represents median (interquartile range) unless otherwise stated. Adapted form Whitaker et al, 2015.

2.2.2. Imaging parameters

2.2.2.1. Structural

All scans were acquired using the multi-parametric mapping (MPM) sequence (Weiskopf et al, 2011) implemented on three identical 3T whole-body MRI systems (Magnetom TIM Trio; VB17 software version; Siemens Healthcare): two located in Cambridge and one located in London. Between-site reliability and tolerability of all MRI procedures were satisfactorily assessed by a pilot study of five healthy volunteers each scanned for ~25 min at each site (Weiskopf et al, 2011). The between-site bias was less than 3% and the between-site coefficient of variation was less than 8% for both longitudinal relaxation rate (R1) and MT parameters (Weiskopf et al, 2011).

Quantitative R1 maps were determined from the apparent R1 maps by correcting for local RF transmit field inhomogeneities and imperfect RF spoiling (Preibisch & Deichmann, 2009), which was adapted to the current FLASH acquisition parameters. Subsequent calculation of RF transmit field maps from the 3D EPI acquisition and correction for off-resonance effects was performed (Lutti et al, 2010].

2.2.2.2. Resting state functional MRI

Resting state fMRI data were acquired using the same sequence parameters as those used for the MALTINGS study in **section 2.1.**

2.2.3. Image processing

2.2.3.1. Structural

The Advanced Normalization Tools (ANTS) cortical thickness pipelines was used to specifically perform initial bias correction on input anatomical MRI and brain extraction using a hybrid segmentation/template-based strategy. Affine (12 degrees of freedom) registration between structural space and the standard space defined by the MNI152 brain at 2mm resolution was performed with FLIRT (Jenkinson & Smith, 2001; Jenkinson, Bannister, Brady, & Smith, 2002) by FSL [(http://fsl.fmrib.ox.ac.uk/fsl/fslwiki/)].

2.2.4.2. Functional

Pre-processing of resting state fMRI data was performed as described for the MALTINGS study in **section 2.1.** Registration from functional to structural space was performed with boundary based registration (Greve & Fischl, 2009).

2.2.4. Group Independent Component Analysis (ICA)

Analysis was carried out using Probabilistic Independent Component Analysis (Beckmann & Smith, 2004) as implemented in MELODIC (Multivariate Exploratory Linear Decomposition into Independent Components) Version 5.01 (Jenkinson, Beckmann, Behrens, Woolrich, & Smith, 2012). Independent Component Analysis

(ICA) is a powerful statistical technique for data reduction without relying on a prior hypothesis (**figure 2.5**). In terms of resting state fMRI data the original 4D time series is decomposed into a finite subspace of statistically independent spatial maps each of which often define functional domains, hierarchical components of functional systems, or non-physiological noise-related signal (e.g. head movement or cardio-respiratory effects).

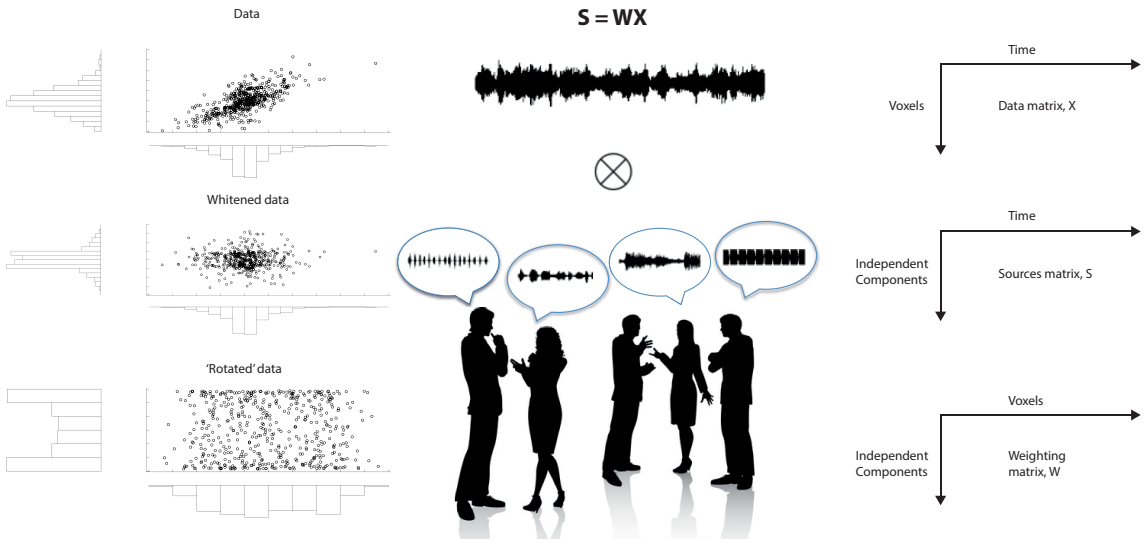

Figure 2.5: principles of independent component analysis

Independent component analysis (ICA) is an example of a blind-source separation algorithm, otherwise known as a solution to the cocktail party problem of identifying signal sources from an input of mixed signals (in this example referring to individual conversations and background noise). Signal (S) is viewed as a linear combination of the data (X) and unmixing matrix (W). Initially the data (top left) is whitened (middle left) then rotated (lower left) to maximize the negative entropy / Gausiannity (or mutual information) of the data (displayed on the axis histograms). Mathematically, one takes the original data matrix (X, voxels by time) to construct the sources (S, independent components by time) by matrix multiplication with the unmixing matrix (W, independent components by voxels).

Processing commenced with masking and discarding all non-brain voxels, followed by voxel-wise de-meaning of the data, and normalisation of the voxel-wise variance. These data were then whitened and projected into an N-dimensional subspace using

probabilistic Principal Component Analysis (PCA), where the number (N) of dimensions was estimated using either manually or using the Laplace approximation to the Bayesian evidence of the model order (Beckmann & Smith, 2004; Minka, 2000).

The whitened observations were decomposed into sets of vectors that describe signal variation across the temporal domain (time-courses) and across the spatial domain (maps) by optimising for non-Gaussian spatial source distributions using a fixed-point iteration technique [otherwise known as FAST-ICA]. Estimated independent component (IC) maps were divided by the standard deviation of the residual noise and thresholded at a posterior probability threshold of $P > 0.5$ by using an alternative hypothesis-testing approach based on the fit of a Gaussian / Gamma mixture model to the histogram of intensity values in each map (Beckmann & Smith, 2004).

By default ICA will estimate one independent components for each row (or time point) in the data matrix. However, this behavior estimates more components than the plausible number of underlying sources (Majeed & Avison, 2014). Because the underlying data contains white noise it is still typically a full rank matrix estimation of the independent components directly from original data matrix risks over-fitting noise sources. Therefore it is necessary to reduce the dimensionality of the data. Dimensionality reduction can be achieved either manually, or by using principal component analysis (PCA) in the spatial domain to decompose the data into a set of orthogonal images, ranked according to their contribution to the total variance in the data, then fitting a Laplacian approximation to the Bayseian probability of the model order.

Each IC was then manually inspected to identify if it was related to instrumental or biological noise or signal based on its topology and presence of a 1/f power spectrum (Griffanti et al., 2014; Salimi-Khorshidi et al, 2014). Individual ICA networks were classified as good or bad depending on their spatial and temporal features. For example, spatial locations outside the grey matter and a lack of 1/f power spectra indicative of the component being composed of signal of BOLD-contrast origin and regressed out from the initial time series (Griffanti et al, 2014; Salim-Khorshidi et al, 2014). Characterisation of group level ICA networks was performed by spatial cross-

correlation with canonical template networks (Smith et al, 2009). Finally, all group level ICA networks believed to be related to noise rather than BOLD contrast were removed and regressed (using ordinary least squares) out from the original time series. Correspondence of each individual network representation with that of the original canonical network template was performed with spatial cross correlation with canonical networks defined using a publicly available online template of ten well-characterized canonical networks [Smith et al, 2009] (**figure 2.6 & table 2.3**) (http://fsl.fmrib.ox.ac.uk/analysis/brainmap+rsns/).

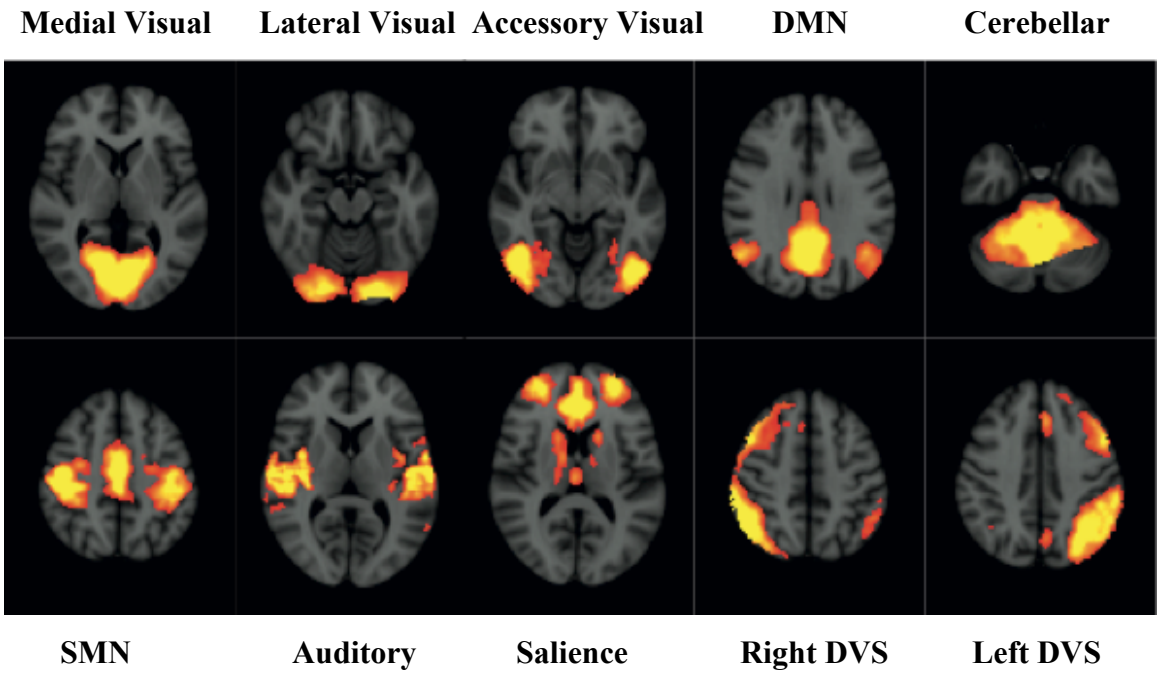

Figure 2.6: canonical ICA networks

From left to right, top to bottom. Medial visual, lateral visual, accessory visual, default mode network (DMN), cerebellum / pons, sensorimotor / supplementary motor area (SMN), auditory, salience, right dorsal visual stream (DVS), left dorsal visual stream (DVS).

Name	Location	Function
Medial visual	Adjacent to calcarine sulcus / V1	Primary visual cortex
Lateral visual	Posterior occipital hemisphere	Visual association cortex
Accessory visual	Lingual & fusiform gyri	Visual association cortex. Also fusiform face area.
Default mode	Precuneus, medial prefrontal, lateral parietal	Task negative / internal reflection
Cerebellum	Pons, middle cerebellar peduncle, cerebellar hemispheres bilaterally	Also putative role in cerebellar cognitive-affective network.
Sensorimotor	Pre & post-central gyri	Primary motor & sensory cortex
Auditory	Heschl gyrus	Primary auditory cortex
Salience	Anterior cingulate, insula (bilateral)	Internal reflection / processing
Left dorsal visual stream	Lateral frontal & parietal cortex	Memory / attention / language
Right dorsal visual stream	Lateral frontal & parietal cortex	Memory / attention

Table 2.3: canonical ICA network features

Network names and locations refer to those from **figure 2.6**.

2.2.5. Dual Regression

The set of spatial maps from these canonical networks was used to generate subject-specific versions of the spatial maps, and associated time series, using dual regression (Beckmann et al, 2009; Filippini et al, 2009). First, for each subject, the un-thresholded group IC spatial maps were regressed (as spatial regressors in a multiple regression) into each participants pre-processed 4D space-time data. This produces in

a set of subject-specific time series, one per group-level spatial map. Next, these time series are regressed (as temporal regressors in a multiple regression) into the same 4D data, resulting in a set of subject-specific spatial maps, one per group-level spatial map.

2.3. NETWORK ANALYSIS

2.3.1. Connectivity matrix construction

Between ICA network modelling was carried out using FSLNets (beta) version 0.6 (fsl.fmrib.ox.ac.uk/fsl/fslwiki/FSLNets). Subject specific network time series were cleaned by removing nodes related to imaging artifact and regression out artifact-related time series, defined on the basis of inspection of ICA network topology or the spectral decomposition / power spectrum (identifying those without a 1/f time course suggestive of predominant high frequency signal likely to be related to noise (Griffanti et al, 2014; Salimi-Khorshidi et al, 2014).

For each subject, the N-node time series were fed into network modelling, creating a NxN node matrix of connectivity estimates. Network matrixes were calculated using full correlation (normalised covariances), partial correlation, L1 regularised (lasso) partial correlation (rho = 10), and L2 regularised (ridge, or Tikhonov) regression (rho = 0.5). Values were subsequently Guassianised into Z-stats.

Cluster analysis, also called segmentation analysis or taxonomy analysis, partitions sample data into groups or clusters. Clusters are formed such that objects in the same cluster are very similar, and objects in different clusters are very distinct. Hierarchical clustering groups components into a multilevel tree or dendrogram (Smith et al, 2009). The algorithm uses a measure of similarity or dissimilarity between the elements – in our case IC networks – which we defined as the corresponding Pearson correlation between the paired independent component time series. Distance between correlations is computed using Ward's linkage, which takes the incremental sum of squares; that is, the increase in the total within-cluster sum of squares as a result of joining two clusters. The within-cluster sum of squares is defined as the sum of the

squares of the distances between all objects in the cluster and the centroid of the cluster. Next, the IC networks are linked in a binary fashion based on their similarity (corresponding in our case to a high Pearson correlation value). These pairs of independent components form a new binary cluster and this process is repeated until all newly formed clusters are linked together in a global (whole brain) hierarchical tree. In the dendrogram the ICA networks are ordered along the base and links are represented by inverted U-shaped lines with height corresponding to the distance (differences in correlation coefficients) between clusters.

2.3.2. Graph theory measures

The following global graph theory measures were used for network analysis in this thesis: transitivity (Newman, 2003); assortativity (Leung & Chau, 2007); global efficiency (Latora & Marchiori, 2007); modularity (Newman, 2004). Nodal graph theory measures included: mean strength (Rubinov & Sporns, 2010); clustering (Onnela et al, 2005); local efficiency (Latora & Marchiori, 2001); path length (Rubinov & Sporns, 2010).

Hub measures

Measures of centrality can be used to identify hubs, or nodes that have a disproportionate role in some general aspect of overall network function or topology. Different classes of hubs can be defined based on the methods used for their identification, or by comparing centrality across multiple measures 'hubness' can be viewed as a generic feature in itself beyond that of a single measure. Hub measures included: closeness centrality (Freeman, 1978): betweenness centrality (Freeman, 1978); within module degree z-score (Guimera & Amaral, 2005); participation co-efficient (Guimera & Amaral, 2005); eigenvector centrality (Bonacich, 1972).

Delta centrality measures

Delta centrality measures refer to the percentage change in global network measures upon removal of the node and all of its connections from the network (Latora & Marchiori, 2007). Measures used in delta centrality originally included global

efficiency, but could be generalised to any global graph theory measure (e.g. transitivity, assortativity, or modularity 'Q' score).

Small world architecture

In addition to global and nodal graph theory measures, over-arching small world architecture measures have been defined in a number of ways. The original Humphries small world model is based on clustering (C) and path length (L) as ratios over the corresponding randomized networks (Maslov & Sneppen, 2002) to create normalised mean clustering (γ) and characteristic path lengths (λ). According to this definition a small world network will have similar characteristic path length but increased clustering, resulting in a score >1:

$$\sigma = \frac{\gamma}{\lambda} = \frac{C/C_{rand}}{L/L_{rand}}$$

(Eq 2.1)

The Latora small world model is based on similar principle of the ratio of clustering to path length, but obviates the use of randomised comparison networks and instead uses local (E_{loc}) and global (E_{glob}) efficiency as markers of the clustering co-efficient and characteristic path length, respectively:

$$\sigma = \frac{E_{loc}}{E_{glob}}$$

(Eq 2.2)

Finally, the Taylor small world model considers characteristic path length normalized by that of comparable randomized networks, but instead considers clustering normalized by that of corresponding lattice networks as a more appropriate network for normalisation. Consequently a value of 0 is small world, <0 is lattice like, and >0 is random:

$$\sigma = \frac{L_{rand}}{L} - \frac{C}{C_{latt}}$$

(Eq 2.3)

Definitions are specific to weighted and undirected networks. All measures except modularity were performed for non-negatively weighted networks after transformation of connectivity estimates to the unit interval. Conversion of proximity

measures to distances typically involves some sort of connectivity weight inversion, whereby a higher connectivity is translated to a shorter distance. In this thesis this conversion is refined by application of t-norms from fuzzy logic (Simas & Rocha, 2012; Simas & Rocha, 2015; Simas et al, 2015).

Semi-metricity

Semi-metricity refers to violation of the triangle inequality in distance space; that is, for correlations between A, B, C once converted to distances, can only form a connected triplet if the space is distorted – or semi-metric. Distances between nodes in graphs are typically considered geodesic and computed using an all-pairs shortest-paths (APSP) algorithm e.g. Dijkstra's or Johnson's algorithms. In geometry, the shortest distance between two nodes in a three node triangle is the direct link i.e. a single geodesic step. In functional connectome networks, the shortest path is taken to be the statistical dependency between regions e.g. Pearson product moment correlation, ρ. If the indirect connection (a two node step) is shorter, determined by the summed weights in the APSP distance, then the distance is semi-metric. Semi-metricity therefore defines the ratio of direct versus indirect paths for each node or the whole network:

$$SMP = \frac{\rho}{APSP^{W}} \qquad \text{(Eq 2.4)}$$

A semi-metric ratio >1 reflects an indirect connection, and a SMP of 1 reflects a direct connection; that is, the APSP weight is the same as the Pearson correlation (i.e. the APSP distance is a single step). A semi-metric percentage for a node represents its direct to indirect connection ratio.

CHAPTER 3: RESTING STATE NETWORKS AND BRAIN TUMOURS

The next section is based on the results from the following publication:

Hart MG, Price SJ, Suckling J. Functional connectivity networks for pre-operative brain mapping in neurosurgery. Journal of Neurosurgery, published online August 26, 2016 doi: 10.3171/2016.6.JNS1662

PRECIS

This thesis begins by focusing on functional connectivity analysis and resting state networks. These data form the foundations of connectomics and higher order network modeling, therefore it is importance to resolve potential issues with image processing and ensure the validity of the underlying data. Once these principles have been established themes of plasticity and network responses to brain lesions are then developed in subsequent chapters.

INTRODUCTION

Neurosurgical management of focal brain lesions is based on the tenet that a more accurate and extensive resection is often closely correlated with successful outcome, but only if resection can be achieved while preserving (or even improving) brain function (McGirt et al, 2009; Stummer et al., 2006; 2012). Function therefore constrains resection and ultimately the success of much of what is attempted in neurosurgery. Accordingly, understanding functional neuroanatomy is fundamental to the advancement of neurosurgery.

Functional brain mapping has a rich history involving many modalities (Catani, 2005; Finger, 2001; Mesulam, 2005) and has been aided by significant contributions from the neurosurgical community (Greenblatt, Dagi, & Epstein, 1997). Perspectives on brain mapping were originally directed toward a localization approach – whereby distinct functions are sub-served by activities in distinct brain regions – which has proven successful, particularly in identifying the functions of the primary cortices. A

more recent construct has viewed the brain as a set of interlocking, distributed processing networks. Synonymous with this approach has been the adoption of "resting-state" (that is, when there is no external stimulus or specific cognitive task) BOLD-sensitive functional MRI (fMRI). Here, a key result has been the observation of networks that self-organize at 'rest' (Damoiseaux & Greicius, 2009; Fox & Raichle, 2007; van den Heuvel & Pol, 2010), supporting the idea that metabolic increases associated with task activity are only a few percent of the total energy consumption of the brain (Raichle & Mintun, 2006). Over the past two decades the network based approach, spurred on by findings particularly from resting-state fMRI but also other modalities (Biswal, Yetkin, Haughton, & Hyde, 1995; Raichle, 2011; Zhang & Raichle, 2010), has gained precedence to the extent that the literature focusing on functional integration now exceeds that on localization (Friston, 2011).

One of the potential uses of resting state fMRI is the mapping of functional connectivity networks, also known as resting state networks. One method for identifying these networks is seed-based connectivity analysis (SCA), which involves extracting a time series from a selected seed region and then measuring its correlation with all other voxels in the brain in a mass univariate approach (**Figure 3.1**). A summary of canonical functional connectivity networks commonly described in the literature is presented in **Table 3.1** and **Figure 3.2**. Adoption of resting state fMRI in the neurosurgical patient population is attractive for many reasons, including rapid whole brain mapping rather than regional constraint by a single task or set of tasks; identification of higher-order networks and non-focal processes in addition to primary cortices; compliance independence, facilitating use in populations not able to adequately perform tasks (e.g. due to motor or language deficits); and applicability to populations not typically suited for task-based experiments, such as children and anesthetised participants (Shimony et al, 2009; Zhang & Raichle, 2010).

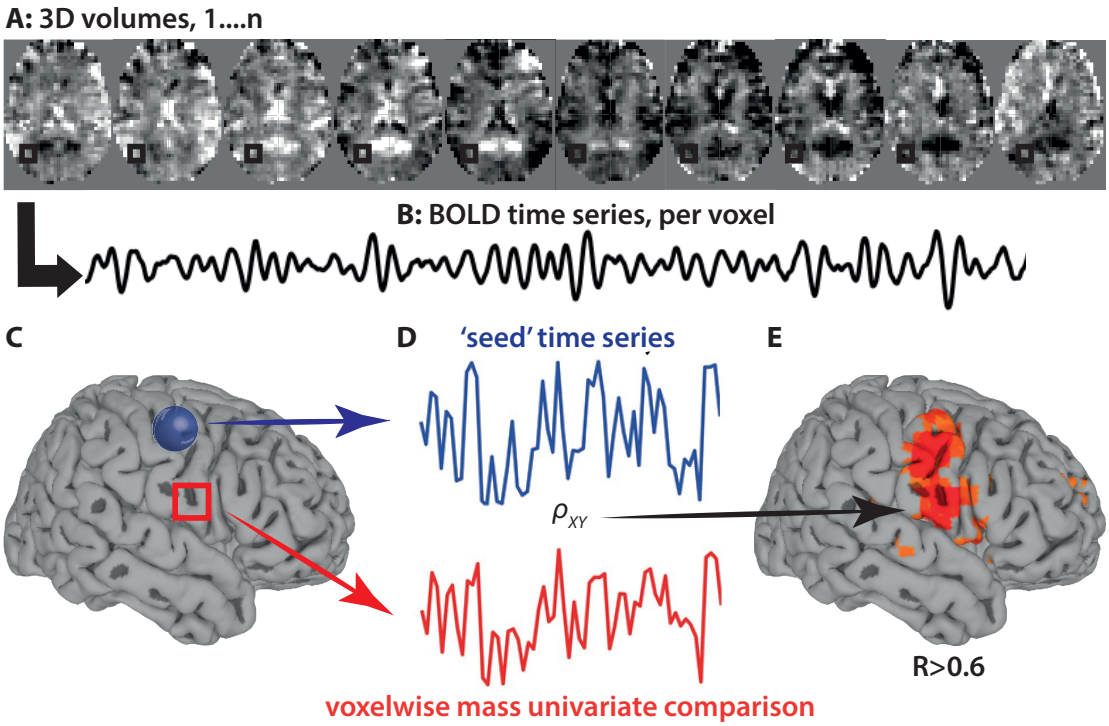

Figure 3.1: SCA methods

A: A resting state fMRI sequence (in the present study, ME-ICA) acquired 269 whole-brain 3D volumes over the scanning period (1 volume in 2.42 sec [the TR], total acquisition time10 min 51 sec). The black box illustrates how the BOLD contrast changed over time. B: Each voxel therefore has a signal contrast change over time or the time series, which is shown here, with the time series of the region highlighted by the black box. C: A seed (in blue) is chosen depending on, for example, previous literature findings, a scientific hypothesis, or task-based activation. We selected a seed in the middle pre-central gyrus and used a red box to highlight a region in the inferior pre-central gyrus. The cortical reconstruction was performed with SUMA (http://afni.nimh.nih.gov/afni/suma). D: The time series of this seed (in blue) is then compared with the time series of all other voxels, involving a measure of statistical dependency, most commonly Pearson correlation. Here, we used the area in the red box to show how the time series were compared. For SCA, however, all voxels were compared in a mass-univariate comparison independent of the seed time series. E: The voxel-wise correlation coefficients are rendered on the same cortical surface and thresholded to display those with a specified correlation (e.g., R > 0.5) Note, important preprocessing steps for both the resting state fMRI scans and structural images need to be carried out before SCA.

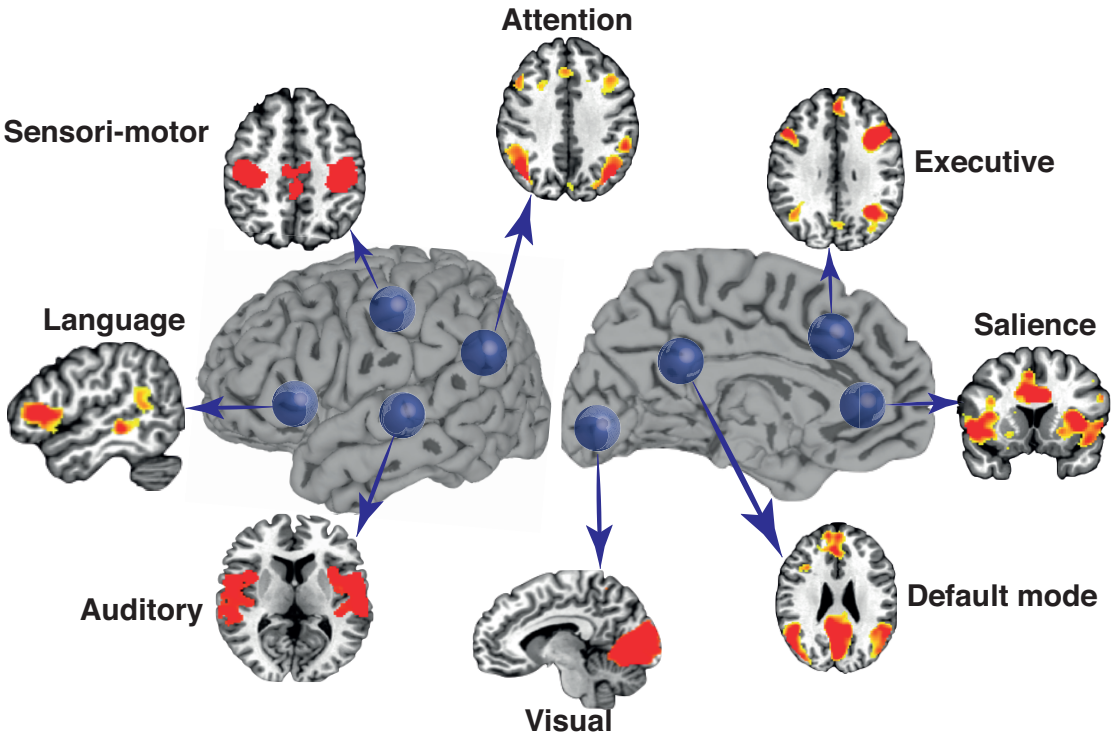

Figure 3.2: Functional connectivity and resting-state networks

The 7 most commonly described canonical functional connectivity networks are displayed along with the corresponding seed locations that are used to build the networks (see **Figure 3.1**). Also included was a putative language network derived from a seed in the left inferior frontal gyrus (Broca's region) because of the significance of this network for neurosurgical planning.

Network	Seed location	Regions	Proposed function
Default mode	Precuneus	Precuneus/posterior cingulate area, lateral parietal, medial pre-frontal	Task negative network with complex and ambiguous function potentially related in internal reflection and self-reference
Visual	Calcarine sulcus	Medial striate and extrastriate regions	Vision (including dorsal and ventral streams)
Sensori-motor	Central sulcus	Central sulcus and adjacent gyri bilaterally	Penfield homunculus. Fine motor and cortical sensory function
Auditory	Heschl gyrus	Heschl gyrus bilaterally	Cortical auditory function
Executive	Medial prefrontal	Frontal eye field, intra-parietal sulcus, middle temporal area	Typical task positive network involved in working memory and focused attention
Salience	Anterior cingulate	Anterior cingulate and bilateral insular cortices	Integration of processed sensory data with internal cues to guide behaviour
Attention (dorsal)	Posterior lateral parietal	Lateral pre-frontal and dorsal parietal	Visuo-spatial control
Language	Broca's region	Broca-Wernicke-Geschwind circuit	Expressive, receptive and repetitive language

Table 3.1: resting state networks

Study	N	Pathology	Tumour locations	Resting state fMRI analysis method	Network of interest	Comments
Sair et al., 2015[36]	49	WHO II (20), III (12), IV (10), other (7)	Left hemisphere (38): not otherwise specified	ICA with manually selected 'best match'	Language	Variability in individual correspondence with task fMRI
Rosazza et al., 2014[39]	13	Meningioma (1), Metastasis (2), benign (3), HGG (4), LGG (2), lymphoma (1)	Sensori-motor region and pre-motor, right (8)	ICA ('best match' selection) & SCA (anatomical and task based seeds)	SMN	Comparison with task fMRI and cortical stimulation
Mitchell et al., 2013[35]	7	Glioma WHO II (5), IV (1), no surgery (1)	Frontal (2), fronto-parietal (2), fronto-temporal (1), parietal (1), temporal (1)	MLP algorithm (artificial neural network)	Visual, dorsal and ventral attention, fronto-parietal, DMN,	Agreement with ECS Distorted SMN in 3 of 7

					SMN, language	
Harris et al., 2013[20]	68	WHO II (21), III (14), IV (33)	Not specified	Default mode network template based 'SCA'	DMN	Pseudo-resting state fMRI
Manglore et al., 2013[31]	6	'brain tumour'	Motor cortex (6)	SCA	SMN	Comparison with task fMRI Reduced connectivity ipsilateral to tumour
Bottger et al., 2011[6]	8	Glioma WHO I-IV & metastasis	Frontal (4), central (3), parietal (1)	Seed correlation ('LIPSIA')	SMN, language, DMN, dorsal attention	Assessed clinical usability of a seed-based network tool
Zhang et al., 2009[56]	4	HGG (3), metastasis (1)	Fronto-parietal (4)	SCA (4) & SCA/ICA (1) based on anatomical co-ordinates	SMN	Correlation with task fMRI & CS SMN only
Liu et al., 2009[28]	6	Glioma WHO 1-2 (3), non-tumour (3)	Central region (5), occipital (1). Right (3), left (2), bilateral (1)	SCA and manually identified anatomical seeds	SMN	Comparison with task fMRI SMN only
Kokkonen et al., 2009[25]	8	Meningioma (3), cavernoma (2), Glioma WHO 1 (2) & 3 (1)	Frontal, temporal, parietal and occipital tumours and their combinations (side not stated)	ICA and spatial cross correlation template matching	SMN	Comparison with task fMRI SMN only
Quigley et al., 2001[37]	12	Tumour, cyst, AVM, agenesis of the corpus callosum	Numbers of each pathology, location, or hemisphere not specified	SCA with task fMRI seed locations	SMN, auditory, language	Network comparison with task fMRI activation maps

Table 3.2: summary of resting FMRI studies in neuro-oncology patients

AVM: arterio-venous malformation, CS: cortical stimulation, ICA: independent component analysis, HGG: high grade glioma, LGG: low grade glioma, MLP: multi-layer perceptron, SCA: seed connectivity analysis, SMN: sensori-motor network, WHO: World Health Organisation.

Resting state fMRI studies in neuro-oncology patients have been previously performed but have typically focused on the accuracy of mapping primary cortices using comparison with results from studies using cortical stimulation to corroborate the findings (**Table 3.2**) [Bottger et al, 2011; Harris et al, 2013; Kokkonen et al, 2009; Liu et al, 2009; Manglore et al, 2013; Mitchell et al, 2013; Quigley et al, 2001; Rosazza et al, 2014; Sair et al, 2015; Zhang et al, 2009]. However one of the main advantages of resting state fMRI is the potential for mapping out higher-order functional connectivity networks that are less amenable to cortical stimulation. It should be noted that fMRI studies should not be expected to agree perfectly with studies involving cortical stimulation, as these approaches map the brain with different biological processes (blood oxygenation status rather than neural activity), different physical signals (nuclear magnetic resonance rather than electrical impedance), and distinct experimental designs (naturalistic observations rather than direct experimental manipulation). Therefore, mapping of functional connectivity networks should be considered complementary to, rather than a replacement for, more traditional methods of brain activity mapping.

Given the potential academic and clinical advantages of resting state fMRI, we set out to test if it could be applied to neurosurgical patients in a more extended fashion than has been explored previously. Specifically, we sought to use SCA to:

1. Explore whether the functional connectivity networks most commonly identified in healthy populations could also be identified in a cohort with intrinsic brain tumors,
2. Assess whether functional connectivity networks could be used in a preoperative brain mapping scenario requiring rapid and robust acquisition with a minimum of user intervention, and
3. Identify patterns of networks perturbed by the tumour to assess if the technique has the requisite sensitivity for detecting putative plasticity or recovery-related changes.

METHODS

Study characteristics, participant demographics, MRI sequence parameters, and initial image processing methods are described in **chapter 2.**

Seed Connectivity Analysis (SCA)

Correlation maps were created with the AFNI package InstaCorr (Cox, 2012). The parameters set included automatic cortical masking, band pass filtering of 0.01–0.1 Hz, smoothing to 6-mm full width at half maximum, and seed defined as spheres of 10 mm diameter. The selection of seed locations was based on the literature on the most common and well-characterised resting-state networks (**Table 3.1 and Figure 3.1.2**) (Raichle, 2011; Zhang & Raichle, 2010). In addition, a putative language network was also sought with a seed in Broca's area in the left inferior frontal gyrus. Once a seed was selected, Pearson correlations between the mean time series of the seed-region voxels and all other voxels were calculated (**Figure 3.1**). For consistency, we thresholded the correlation maps at R = 0.6 for all participants and networks.

We initially used the seed locations shown in **Figure 3.2**, with a sphere having a radius of 10 mm. When a seed could be in either hemisphere (e.g., a central sulcus seed for the sensorimotor network [SMN]), we placed our seed in the left hemisphere (contralateral to the tumor). However, basing seed locations on coordinates may not be optimal given individual differences in anatomy, standard-space registration, and functional connectivity (Margulies et al, 2009). One of the significant advances of InstaCorr is that it allows flexible movement of the seed location while displaying the corresponding network in real time. Although the network produced is sensitive to seed location (Margulies et al, 2009), we constrained this flexibility by allowing our seeds to vary only within 10 mm of each other (corresponding to the radius of our seed) to create comparable networks across the participants with seeds that overlapped each other. Our aim was to balance homogeneous seed location with individual flexibility in seed location (**Figure 3.3**).

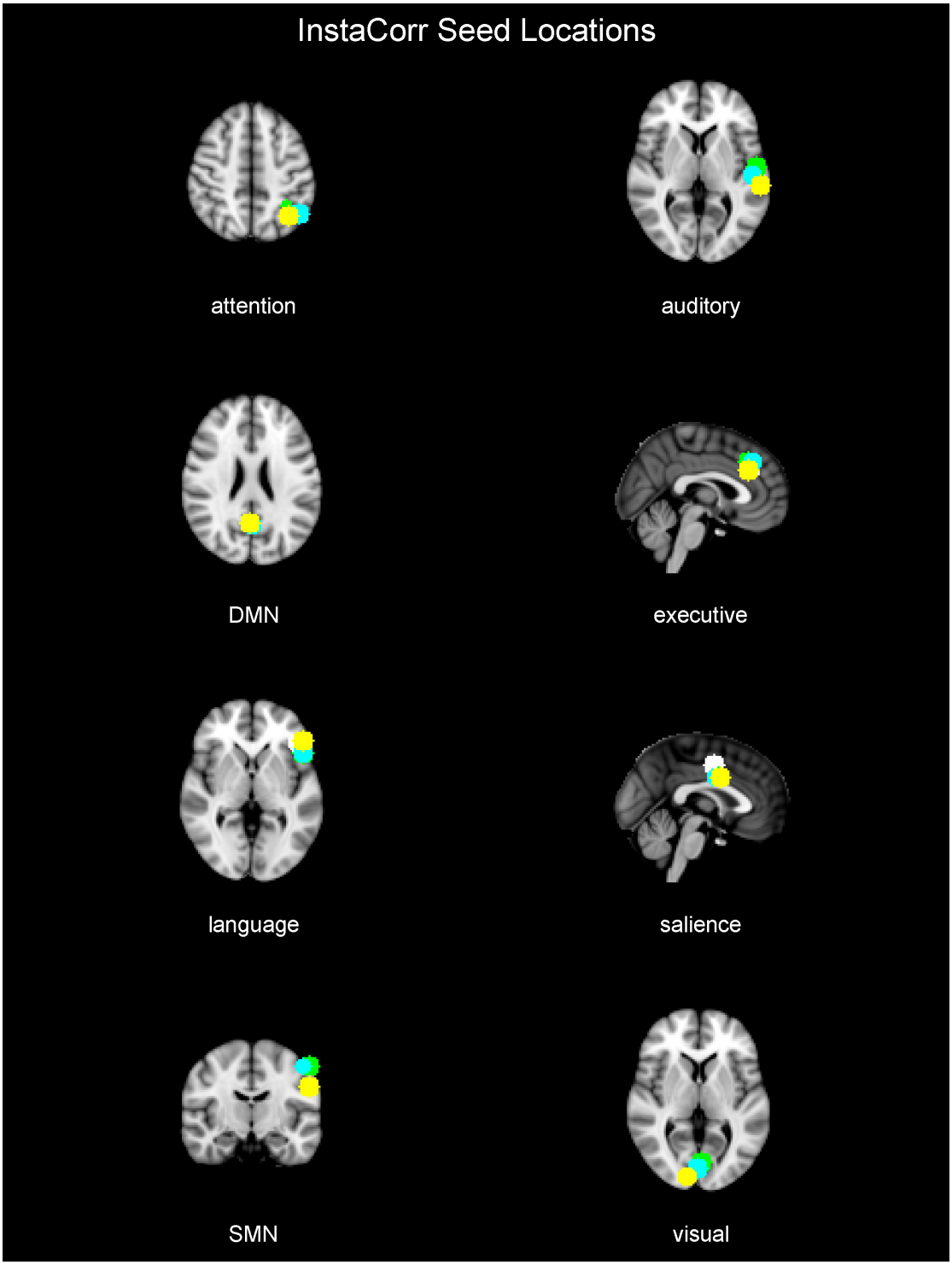

Figure 3.3: seed locations used for functional connectivity analyses

The seed locations for each network were taken from Talairach coordinates in AFNI and translated into 10-mm sphere masks in MNI space (1 sphere for each network per participant, i.e., 80 spheres in total). Each color represents a different seed for an individual participant. Only 2–3 different seed locations were required for each network, as the same seed coordinates could be used for some participants.

RESULTS

Individual seed locations

The functional connectivity networks identified in the participants are summarised in **Figure 3.4**. In each participant, we could identify the 7 canonical networks described in the literature, as well as a putative language network. The seed locations required to derive these networks exhibited a high degree of conformity, with the same location often used in several participants (**Figure 3.3**). However, fine-tuning of the seed location was of benefit in selected instances to establish a network configuration resembling that described in the literature. In general, the auditory and attention networks were the most difficult to identify.

Summary Networks

The qualitative assessments of each functional connectivity network in each participant are summarised in **Table 3.3**. All participants had at least 2 networks that showed an alteration, and each network was altered in at least 1 participant, except for the language network, which was normal in all participants. The default mode network (DMN) was altered in all patients. The next most commonly altered network was the executive control network, which was altered in 4 patients. Tumour location was closely related to determine which networks were affected. For example, tumours involving the superior parietal lobule (in Participants 1 and 2) affected the DMN and executive control network; tumors involving the occipital lobes (in Participants 2 and 3) affected the visual and DMN; and tumors that involved the anterior parietal region (in Participants 4 and 5) affected the SMN, DMN, and executive control network (**Figure 3.4**).

Dynamic Alterations

One advantage of our cohort having tumors in approximately the same area was that we could look for patterns of alterations in our identified functional connectivity networks. Our whole-brain functional connectivity analysis suggested that in this cohort of participants with right temporo-parieto-occipital tumours, the DMN was most commonly altered from its normal topology (**Figure 3.4**). Patterns appeared to represent local displacement (i.e., in Participant 4), novel topological area recruitment in combination with a reduction in the typical network architecture (in Participants 2

and 3), or an absence of a region typically associated with the network (in Participants 1 and 5). Interestingly, more posteriorly located tumors appeared to result in new network areas, whereas the more anteriorly located tumors reduced network volume, but further data will be required to quantify these changes.

Participant	#001	#002	#003	#004	#005
Tumour	parietal	parieto-occipital	occipital	fronto-parietal	temporo-parietal
Attention	Δ	↓	✓	✓	✓
Auditory	✓	✓	✓	✓	Δ
DMN	Δ	⟁	⟁	↓	Δ
Executive	↓	↓	✓	↓/Δ	↓
Language	✓	✓	✓	✓	✓
Salience	✓	✓	✓	Δ	✓
SMN	✓	✓	✓	Δ	Δ
Visual	✓	Δ	⟁	✓	✓

Table 3.3: seed connectivity networks summary

✓ = normal

↓ = reduced in area i.e. area missing

Δ = locally shifted i.e. due to mass effect

⟁ = reduced connectivity with new topological area i.e. asymmetrical

✖ = typical network pattern not found

DMN = default mode network, SMN = sensori-motor network

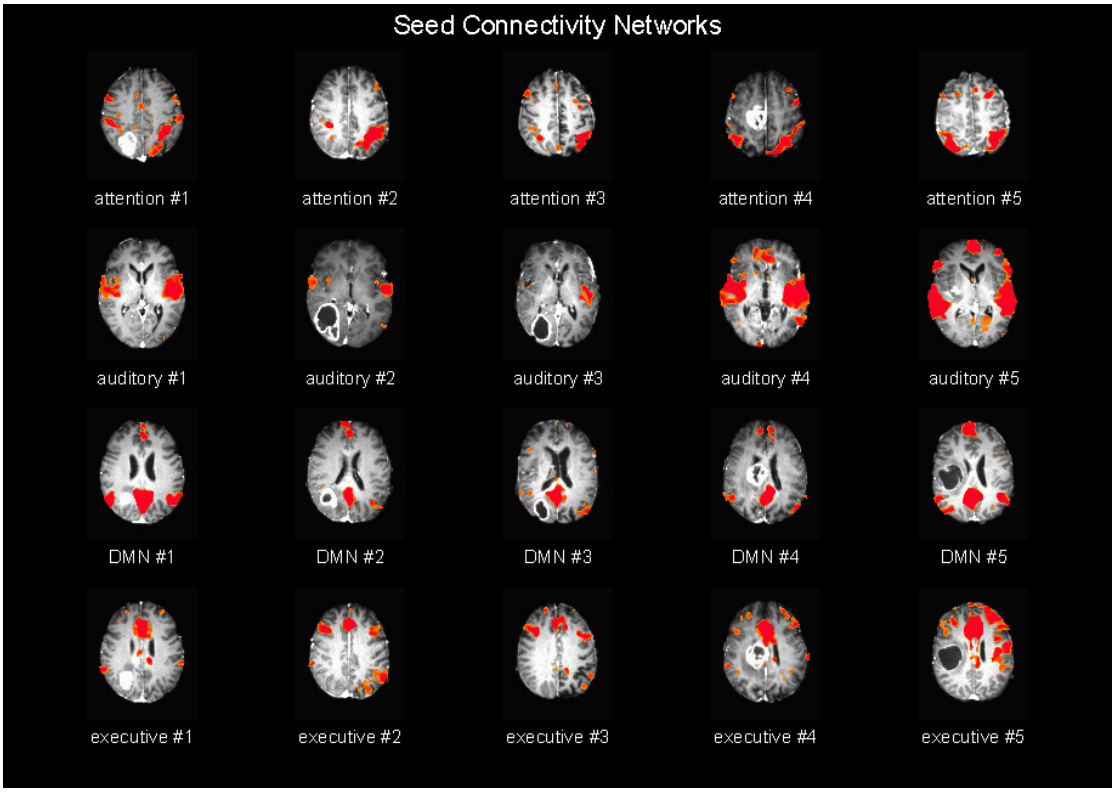

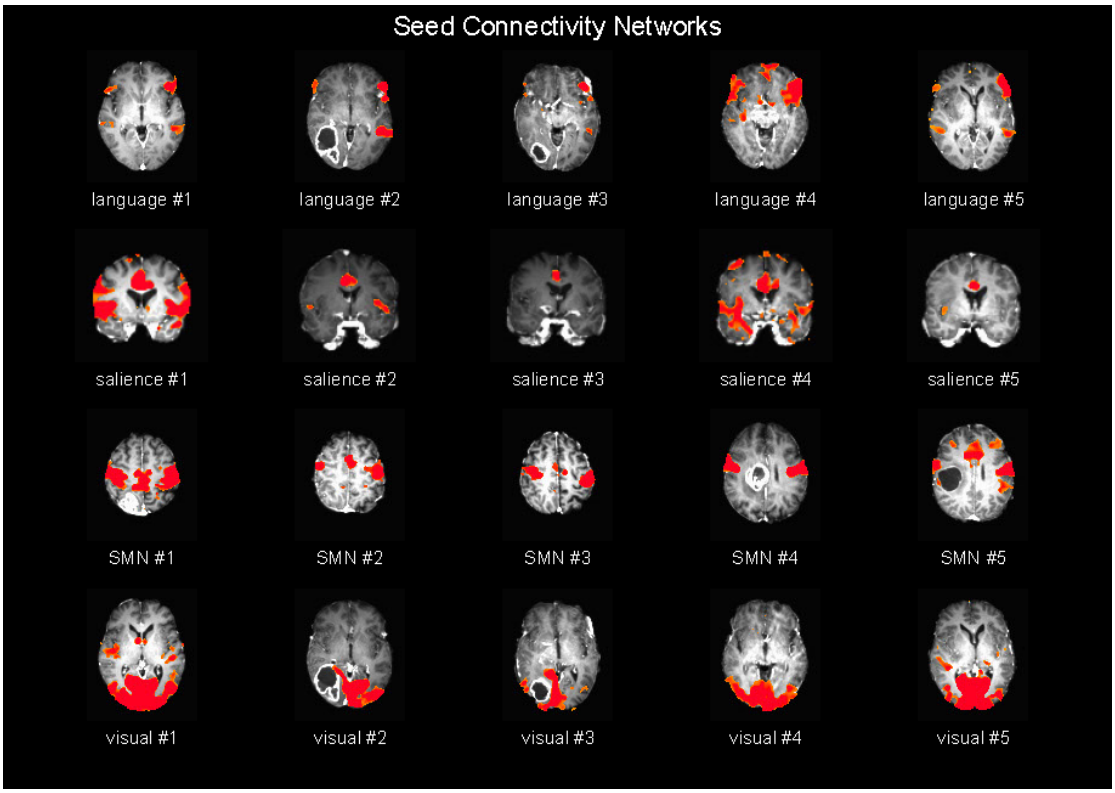

Figure 3.4: individual participant resting state networks

Resting-state networks in each study participant. Rows represent specific networks across participants, and columns represent individual participant network constellations (e.g., column 3 is always participant number 3). Putative plastic

changes can be readily observed in the DMN but also in some other networks. In Participants 1 and 5, a notable reduction in the DMN is present in 1 hemisphere. In Participants 2 and 3, there is a reduction in DMN in the lateral parietal component with a new frontal area of activation. In Participant 4, the medial component of the DMN appears to be physically displaced rather than reduced in area, given that it is the same general size but mainly moved forward and is located immediately adjacent to the tumor.

DISCUSSION

The most commonly described resting-state networks are able to be identified in a clinical cohort of study participants with right parietal glioblastoma. In addition, implementation of a refined preprocessing pipeline helped to resolve important resting state fMRI challenges specific to neuro-oncology patients, including brain extraction, registration to standard space, de-noising, and seed-selection at an individual participant level. Lastly, putative patterns of network plasticity, particularly involving the DMN, were able to be tentatively proposed.

Previous neurosurgical studies involving resting state fMRI have typically focused on the SMN, used a variety of techniques often yielding results that robustly correlate with the SMN mapped with cortical stimulation, and set in place early methodological achievements (Bottger et al, 2011; Harris et al, 2013; Kokkonen et al, 2009; Liu et al, 2009; Manglore et al, 2013; Mitchell et al, 2013; Quigley et al, 2001; Rosazza et al, 2014; Sair et al, 2015; Zhang et al, 2009). A key advancement of the present study was the identification of the full complement of functional connectivity networks. This advance was possible because of robust improvements in signal to noise achievable with ME-ICA pre-statistical processing and the flexibility of seed selection available with InstaCorr. Having the full complement of functional connectivity networks available for preoperative planning is a significant step toward facilitating individually tailored surgery that maximises resection while minimising functional deficits.

Inference of the function associated with individual functional connectivity networks is based on their topologically distinct nature (i.e., the SMN is adjacent to the central

sulcus, and the auditory network is centered on Heschl's gyrus). However, for those networks not centered on primary cortices, the cognitive and functional relevance may be less clear (**Table 3.1**). Moreover, when in the presence of a focal brain lesion a network is not found in its normal configuration, the question of whether this abnormality is a dynamic plastic change or indicates genuine functional impairment is more complex. Defining what a functional connectivity network is and what its dynamic alterations represent will require longitudinal imaging (pre- and post-surgery or during follow-up), correlation with neuropsychological outcomes, and use of multi-modality monitoring (such as cortical stimulation, electroencephalography, magnetoencephalography, or other imaging modalities).

To develop our qualitative description of network changes into formal quantitative testing, robust statistical methods are required, along with suitable control network. Resting state data in large populations of healthy participants is now freely available (e.g. at www.humanconnectome.org), but statistical testing may be more complicated. Valid inference of seed-connectivity networks is not normally expected because of difficulties with calculating degrees of freedom; therefore, most studies use an arbitrary threshold for R of approximately 0.5 (Kundu et al, 2013). With ME-ICA, multi-echo independent component regression can ensure valid inference. This technique takes the number of de-noised independent components as the degrees of freedom in the data and allows thresholding at a nominal p value (e.g., $p < 0.05$) based on z-scores or on more stringent comparisons involving a false-discovery rate. Studies in healthy participants have demonstrated robust connectivity networks with this method (Kundu et al, 2013), but these findings were unable to be replicated because of the de-noising process resulting in fewer surviving components and less representative networks. Nevertheless, we were able to use a correlation threshold of $R = 0.6$, which is larger than that typically applied (Kundu et al, 2013). A larger sample including participants with homogeneous disease would allow group analysis and effective multi-echo independent component regression.

Once network function can be inferred, one needs also to understand the significance of alterations in a network's topology. For example, one scenario involves a network perturbation that might be expected to normalise with removal of a lesion and active rehabilitation of the patient, in turn correlating with clear neuropsychological

improvement. However, robust testing of network changes may be challenging with seed-based connectivity methods because of the aforementioned issues. Ultimately, the role of SCA may be to rapidly estimate qualitative networks at the single subject level for clinical practice, with the aim of observing perturbed or displaced networks that one may wish to avoid at surgery (see discussion below). Complex analyses aiming to model plasticity or predict cognitive changes from expanded extra-lesional resections may require sophisticated methods more suited to a research setting (Beckman & Smith, 2004; Beckman, DeLuca, Devlin, & Smith, 2005; Smith et al, 2009; Smith et al, 2013b).

The rapidity and ease of use of the method presented here suggest it could be adopted in clinical practice, perhaps even with surface renditions integrated into neuronavigation software. This would also have the advantage of including a wider range of tumour histologies and locations that will be necessary to validate the applicability of our new resting state fMRI analysis method to the more diverse range of scenarios encountered in clinical practice. However, the aforementioned development required for improving our understanding of the neurocognitive basis of functional connectivity networks and the necessary improvements to statistical methods all suggest that a cautious approach should be adopted. For example, if the method reveals a functional connectivity network to be in close proximity to a tumor or the planned resection extent, counseling of the patient about the potential functional risks and goals of surgery could be warranted, possibly incorporating further monitoring (including awake craniotomy and cortical stimulation or other neurophysiological methods). In units that use cortical stimulation routinely (Duffau et al, 2003, Sanai, Mirzadeh, & Berger, 2008) or when extended resections are performed (Lus, Angelini, de Schotten, Mandonnet, & Duffau, 2011), the functional connectivity networks identified could be used to guide the selection of tasks chosen for intraoperative testing to increase the specificity and efficiency of the assessments at surgery. The key message is that functional connectivity network analysis should be an additive component to preoperative surgical planning.

Seed-based functional connectivity methods are part of a larger repertoire of techniques available with resting state fMRI. A similar method is independent component analysis, which also constructs distinct topological networks (some – but

not all – of which are similar to those found in SCA). However, in a data-driven manner, independent component analysis is advantageous, as it offers higher dimensionality and robust statistical testing, but at the cost of being potentially more complex to perform; in addition, independent component analysis also results in networks that can be harder to relate to cognitive function (Beckmann et al, 2005; Beckmann & Smith, 2004; Smith et al, 2009; 2011). Another avenue afforded by resting state fMRI is complex network analysis by graph theory (Bullmore & Sporns, 2009; Sporns 2010; 2012), which may also be performed with other methods, including PET, electroencephalography, magnetoencephalography, and diffusion imaging (Hagmann et al, 2007; 2008). Graph theory analysis creates an abstract representation of the brain akin to that of a social network. The analysis then focuses on the properties of the graphical representation, its global or local efficiency, linkage of highly connected regions (known as a "hubs") to the overall network architecture, and so on (van den Heuvel & Sporns, 2011; 2013). A significant advantage of graph theory is its potential to model lesions and their effects on general network function (Achard, Salvador, Whitcher, Suckling, & Bullmore, 2006; Alstott, Breakspear, Hagmann, CAmmoun, & Sporns, 2009). Lastly, resting state fMRI also enables the study of fractal dynamics, measured for example with the Hurst exponent (Wink, Bullmore, Barnes, Bernard, & Suckling, 2008), which is a marker of brain complexity and potential for information processing (Bullmore et al, 2009). In summary, resting state fMRI, along with the various analysis methods to which it is allied, has the opportunity to address questions about functional brain mapping within neurosurgery.

CONCLUSIONS

Resting state fMRI offers an efficient method for whole-brain mapping of multiple functional connectivity networks in neuro-oncology patients before surgery. Advancements to the image processing pipeline have made resting state fMRI feasible for use in clinical practice and for further research, particularly in longitudinal studies invoking multi-modality imaging and neuropsychological assessments. Further investigations of these techniques may reveal their potential for helping to predict cognitive deficits, increasing the extent of resection in a safe manner, and optimising rehabilitation strategies.

CHAPTER 4: BRAIN MAPPING WITH THE FUNCTIONAL CONNECTOME

The next section is based on the results from the following publication:

Hart MG, Price SJ, Suckling J. Pre-operative brain mapping with the functional connectome. British Journal of Neurosurgery 2016;30(5):506-17
doi: 10.1080/02688697.2016.1208809.

The following results were also the subject for the essay that one the Sir Hugh Cairns Prize of the Society of British Neurological Surgeons (SBNS) in 2016, and has been presented in abstract form at the SBNS spring meeting (2016) and Congress of Neurosurgeons annual meeting (2015).

PRECIS

In the following chapter the validation of resting state network analysis in brain tumours from the previous chapter is complimented by the application of higher order modelling, namely applying functional connectomics analysis. The original pilot dataset of 5 participants with right parietal based tumours is again used and the pre-statistical processing of the data is the same. The aim here is to assess the potential of functional connectome mapping in neurosurgery and serve as a lead in to more complex analysis of the effects of brain tumours in the final chapter on brain tumours.

INTRODUCTION

Neurosurgery requires an understanding of functional anatomy in order to make surgery safe and effective. Hence unsurprisingly neurosurgery has made significant contributions to brain mapping using multiple modalities over many years (Greenblatt, Dagi, & Epstein, 1997; Penfield & Rasmussen, 1950). One of the goals of this endeavour is to accurately predict the functional consequences of lesions (either endogenous or surgically induced) both immediately following surgery and in the long-term (that is, accounting for plasticity induced recovery). This ‘virtual brain’ will require incorporation of localisation and network-based approaches to neuroanatomy, and, in doing so, will model brain function in a holistic manner. In

other words, brain function is considered as a whole and not limited to one region or network. However, this goal has hitherto proven elusive. Solving the joint problems of modeling brain function predictively would allow one to better plan surgery with regards to timing, extent of resection, and expected recovery.

The development of the connectome, or 'wiring diagram' of the brain, offers the potential to answer these questions (Fornito, Zalesky, & Breakspear, 2013; Smith et al, 2013; Sporns, Tononi, Kotter, 2005; Sporns, 2011; Sporns, 2012). Here the brain is viewed as a constellation of nodes that are connected via edges (Hart, Ypma, Romero-Garcia, Price, & Suckling, 2005). Connectome analysis has revealed the brain – where nodes are circumscribed brain regions and edges the degree of synchronisation of endogenous signals (also known as functional connectivity) – to be organised as a 'small world' whereby it parsimoniously balances local specialisation with distributed connectivity and short-cuts between regions (Watts & Strogatz, 1998; Achard, Salvador, Whitcher, Suckling, & Bullmore, 2006; Bullmore & Sporns, 2009). In this manner, the brain network shares its small world properties (and others) with a wide variety of other complex networks including social networks, transportation routes, and the World Wide Web (Newman, 2010). The importance of the connectome paradigm in neuroscience research is epitomised by the $40 million Human Connectome Project, which the National Institutes of Health (NIH) has identified as one of the three 'grand challenges' for neuroscience research (NIH Blueprint, 2016).

Connectome analysis is attractive to neurosurgeons not only for the principle of mapping brain connectivity but also for allowing intuitive modeling of lesions and plasticity. For example, one can remove parts of a network (for example, friends or friendships in a social network) and identify changes in network properties (such as social cohesiveness or rumour propagation) to gain an understanding of the effects at both a local and global level. One can then investigate mechanisms of putative plasticity using models such as connection re-wiring, alternative routes for information flow, or re-activation of redundant pathways (Fornito, Zalesky, & Breakspear, 2015; Stam, 2014).

To begin to understand the applicability of connectome analysis to neurosurgery, and its potential to answer useful clinical questions concerning functional brain mapping,

MRI data depicting blood oxygenation level dependent (BOLD) contrast were acquired pre-operatively from patients with a brain tumour. Using this dataset connectome analysis was undertaken with the following objectives:

1. Derive the connectomes of individual patients with brain tumours;
2. Measure the key features of the connectome and how they compare with those previously described in healthy volunteers;
3. Visualise the connectome in an intuitive and surgically relevant manner;
4. Appraise the applicability of connectome analysis to presurgical planning;

METHODS

Parcellation

To form a connectome (**Figure 4.1**), pre-processed resting-state fMRI data were parcellated into an anatomical template of 116 regions (Tzourio-Mazoyer, 2002) (45 regions for each cerebral hemisphere and 26 for the cerebellum). BOLD time series were averaged over the extent of the parcel, and constituted a node in the subsequent network representation.

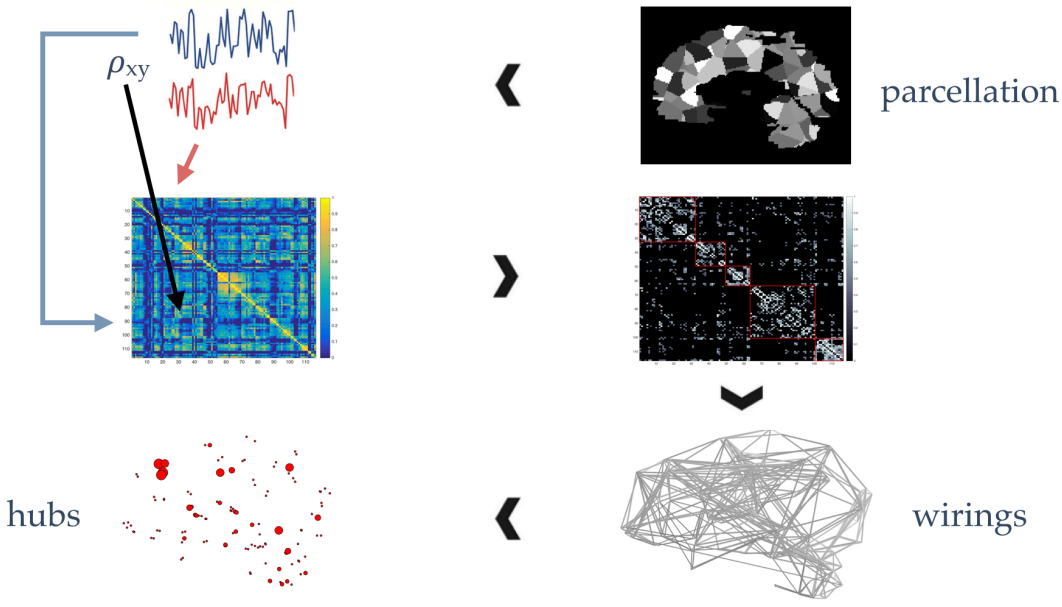

Figure 4.1: connectome construction

Methods for performing a connectome analysis using resting-state fMRI data as an example, but similar methods can be applied to data acquired from DTI or EEG/MEG. Initially a template is chosen to divide the brain into different regions (known as parcels) that form the network nodes. These nodes are used to form the rows and columns of a matrix. Entries of the matrix represent edges between each of the nodes and are formed by recording a measure of statistical dependency (such the Pearson correlation co-efficient) between the resting-state fMRI time series of each node. This correlation matrix can then be thresholded and binarised to form an adjacency matrix, although weighted and fully connected matrices (without thresholding) are also possible. Finally, the co-ordinates of each parcel are used to display the node location onto a surface reconstruction of the brain, with edges representing functional connections.

Wavelet filtering

A wavelet-based decomposition of the time series was performed to account for frequency-dependent heterogeneity in brain connectivity [Bullmore et al, 2003; Bullmore et al, 2004]. Wavelet correlation matrices were formed by applying the maximal overlap discrete wavelet transform (MODWT) to the time series from each parcel. This resulted in a set of five wavelet scales (i.e. frequency bands, scale 1.0.2–0.1 Hz, scale 2.0.1–0.05 Hz, scale 3.0.05–0.03 Hz, scale 4.0.03–0.01 Hz, and scale 5.0.01–0.006 Hz), at each of which, Pearson's correlation, r_{ij}, was calculated between all possible connections between parcels i and j. Wavelet scales 4 and 5 were not able to produce a matrix of the required mean degree at any threshold and were, therefore, not studied further.

Thresholding

At each wavelet scale, the network was thresholded; that is, connections were kept if the probability, p, of r_{ij} was greater than the threshold R, $p(r_{ij}>R)$(Achard, Salvador, Whitcher, Suckling, & Bullmore, 2006). As a result, a graphical representation was formed where connections between parcels were either present or absent; in other words, a binary network representation of the connectome. To allow for estimation of small world properties, the mean degree (i.e. mean number of connections associated with a parcel) was chosen to be equal to the log number of parcels: knet.2*log(n), following which we defined R as the value that resulted in a fixed number of

edges.n*knet, while controlling for multiple statistical testing by adjusting the probabilistic threshold with the false discovery rate (FDR): $p(r_{ij}>R)< \alpha FDR = 0.05$. This method of thresholding naturally leads to sparse networks that include only a proportion of all potential connections (Achard & Bullmore, 2007).

Graph theory analysis

Network analysis was performed in Matlab [MATLAB 2015a, The MathWorks, Inc., Natick, MA] with the Brain Connectivity Toolbox [http://www.brain-connectivity-toolbox.net] and the R statistical package [R Development Core Team, 2008] with the Brainwaver library (version 1.6) (Brainwaver, 2016). Specific graph theory measures and their definitions are given in **Table 4.1**.

Measure	**Definition**
Centrality	How critical a given node's features are to the overall network.
Clustering (co-efficient)	Number of neighbors of a node that are also neighbors of each other (e.g. shared friends in a social network). A measure of network segregation.
Degree	The number of connections of a node.
Efficiency	The inverse of path length (which accounts for disconnected nodes and weights more towards short edges). Can be local (based on a nodes community) or global.
Clustering co-efficient, γ	The clustering co-efficient expressed as a ratio of that from a corresponding random network ("normalized clustering co-efficient").
Giant component	Largest connected cluster of nodes in a network.
Hub	Nodes that form a key component of the overall network structure e.g. they have high degree, high centrality, or short path length to other nodes.
Information centrality	Percentage change in global efficiency due to removal of a single node.
Path Length, λ	The path length of the network expressed as a ratio of that from a corresponding random network ("normalized path length").
Path length	The number of discrete steps between nodes that are required to complete a journey from one node to another. A measure of network integration.
Percolation threshold	Critical point in the fragmentation process (i.e. removal of nodes) when the giant component disappears i.e. the network undergoes a phase transition from connected to disconnected state.
Random error	Removing nodes at random and measuring the change in network properties (e.g. size of the giant component or efficiency).
Resilience	The ability of a network to recovery from removal of specific components (nodes or edges). A network that is highly resilient will demonstrate little change in its graph theory measures after removing node(s) or edges(s). This definition is similar to robustness but implies a dynamic reparative process such as plasticity.
Robustness	The ability of a network to maintain its typical graph theory characteristics after removal of specific node(s) or edge(s) i.e. a network that is robust will tend not to change much after removal of specific components.
Small world, δ	A measure of simultaneous clustering (network segregation) and short path

	length (network integration) formed by network short-cuts. Typically defined as $\gamma/\lambda > 1$.
Targeted attack	Removing nodes based on a ranking of network features (e.g. degree, centrality, or clustering).

Table 4.1: definitions of network measures

Connectome analysis allows the application of measures from graph theory. These include the node degree, defined as the number of connections of each node (i.e. parcel). The clustering coefficient, a measure of network segregation or local specialisation, is defined as the ratio of neighbours of a node that are also neighbours of each other (and, therefore, form a triangle or local clique) over all possible neighbour connections. Path length, which measures network integration or information flow, is the number of steps (or edges) required to move from one node to another. Both the clustering co-efficient and the path length can be compared with the same measures from a randomised network (see below for creation of randomised networks) where they are given the names γ and λ, respectively. A small world network displays higher clustering but similar path length than a randomized network, and the small world parameter, $\sigma = \frac{\gamma}{\lambda}$, will be greater than one.

How a network changes after removal of individual node(s) or edges(s) is known as network robustness or resilience. A more robust network is one where removal of a node or edge does not lead to a significant change in graph theory measures (typically the size of the 'giant' component, path length, or global efficiency) (Achard, Salvador, Whitcher, Suckling, & Bullmore, 2006; Alstott et al, 2009; Kaiser et al, 2007). Robustness can be assessed by either removing nodes in a random manner, or by targeting nodes based on some characteristic such as clustering or path length, known respectively as random error and targeted attack (Latora & Marchiori, 2001). Information centrality per node is similar to robustness but defined as the change in global efficiency after removal of a single node (Latora & Marchiori, 2007).

Network comparisons

Group analysis was performed to allow robust estimation of overall network measures. This was possible given the overlap in lesion locations and, therefore, in the parcels that were adjacent to the tumour. Group networks were formed by averaging r_{ij} for each edge at each wavelet scale separately. Network comparisons

were based on simulated randomized networks, generated, and configured to match the number of nodes, mean degree, and degree distribution of the brain networks, and simulated scale-free networks of the same number of nodes and edges but with a power law degree distribution. Comparisons between each of these network models were performed with Akaike Information Criteria (AIC) [Akaike, 1974].

Visualization

Brain networks were displayed with the BrainNet viewer (Xia, Want, & He, 2013) [http://www.nitric.org/projects/bnv/] and Circos (Krzywinski et al, 2009) on an individual participant basis to highlight the potential application of the analysis to pre-operative brain mapping.

RESULTS

Key characteristics of functional brain networks

Small world features were identified over a range of wavelet scales for group average networks (**Table 4.2**). Compared with simulated random graphs, brain networks had comparable path lengths but markedly increased clustering, accounting for the associated small world features. Wavelet scale 2 (frequency band 0.5–0.10 Hz) was chosen for further analysis having the highest small world score (d.1.65, **Figure 4.2**).

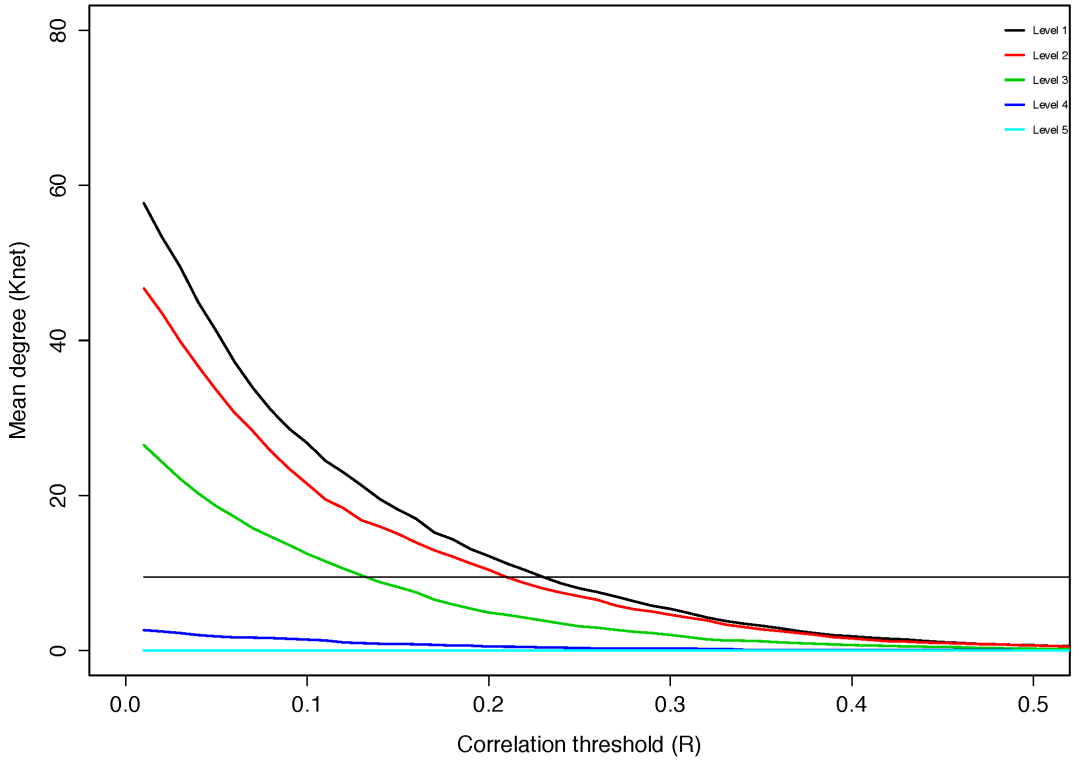

Figure 4.2: effects of thresholding on network degree

Increasing the cutoff of the correlation threshold results in a reduction in the number of edges that survive thresholding in the resulting matrix. The straight black line represents the minimum mean degree for small world networks (n*log(n) = 9.5). The point of intersection of the wavelet scale degree with this line is used as the threshold to form the binary network used for further analysis. Wavelet scales 4 and 5 were not able to produce a matrix of the required mean degree at any threshold and were therefore not studied further.

Scale	Hz	r	R	L_{net}	C_{net}	λ	γ	δ
1	0.10 – 0.20	0.28	0.23	3.53	0.54	1.50	1.83	1.22
2	0.05 – 0.10	0.35	0.21	2.72	0.56	1.17	1.94	1.65
3	0.03 – 0.05	0.41	0.13	2.99	0.61	1.29	1.96	1.51

Table 4.2: Small world features for group networks per wavelet scale

Increasing wavelet scale reflects decreasing time series frequency. Wavelet scales 4 and 5 are not shown because they did not produce the necessary mean degree to enable formation of small world networks (see **Figure 4.2**). r = mean correlation of the scale; R = correlation threshold to form the adjacency matrix; L_{net} = mean path length; C_{net} = mean clustering co-efficient; λ = ratio of path length to that of a corresponding random network ; γ = ratio of clustering co-efficient to that of a corresponding random network; δ = small world measure ($\delta = \gamma / \lambda$).

Anatomical brain networks

The anatomical network for a single participant at wavelet scale 2 is displayed in **Figure 4.3**. Thresholding resulted in a sparse group average functional network of 551 edges, or around 8% of all possible edges. While this brain network tended to form a giant component, it did not include all nodes due to the removal of low weight edges during thresholding and the inclusion of small parcels with limited signal-to-noise in their associated time series. Structures outside the giant component included subcortical structures such as the caudate nucleus and putamen which instead tended to form isolated connections to their contralateral homolog. We identified regions of high local connectivity (clustering) in the supplementary motor area and middle cingulate while regions with short path lengths to other regions were found in precuneus and superior frontal gyrus for example (**Table 4.3**). Simultaneous local clustering and efficient long distance connectivity (or short cuts between clusters) are the core characteristics of small world organization. Therefore, the connectome effectively carries the brain mapping concepts of functional localisation and network connectivity.

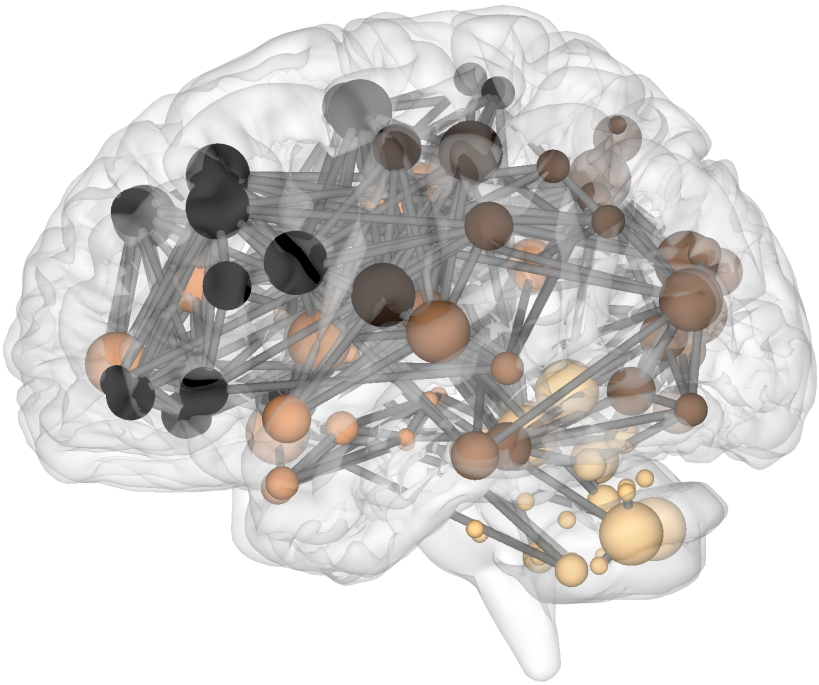

Figure 4.3: the connectome in glioblastoma

A sagittal view of an individual patient connectome at wavelet scale 2. Nodes are coloured according to their anatomical module (e.g. frontal, central, parietal, etc) and their size is proportional to their degree. Connections (or edges) are presented in grey and represent the binary entries of the adjacency matrix. Locations are based on the co-ordinates of their original parcels and projected onto a surface reconstruction in MNI152 space.

Side	Parcel abbreviation	Degree	Clustering	Path length	Information Centrality
l	MCIN	31	0.51	2.15	-3.43
l	PQ	31	0.35	1.94	-3.59
r	F1	30	0.41	1.99	-3.26
r	MCIN	28	0.53	2.23	-3.09
r	F2	28	0.51	2.18	-3.10
l	SMA	27	0.62	2.25	-3.01
l	T1	26	0.55	2.45	-2.84
r	T1	26	0.58	2.45	-2.81
r	PQ	25	0.38	2.11	-3.34
l	SMG	24	0.66	2.32	-2.85
l	F2	24	0.46	2.13	-4.44
l	PRE	23	0.68	2.29	-2.82
l	F3OP	23	0.69	2.40	-2.74
r	SMA	23	0.72	2.39	-2.76
r	F3T	22	0.61	2.37	-2.79
l	F1	22	0.49	2.09	-2.96
l	POST	22	0.69	2.25	-2.83
r	POST	22	0.61	2.24	-2.97
r	F3OP	21	0.78	2.38	-2.72
r	SMG	21	0.66	2.32	-2.77
l	IN	20	0.64	2.54	-2.62
l	V1	20	0.46	2.24	-2.86
l	RO	19	0.77	2.59	-2.55
r	PRE	19	0.73	2.30	-2.70
r	F1M	19	0.39	2.29	-3.00
l	O2	19	0.51	2.37	-2.78
l	F3O	18	0.53	2.43	-2.63
l	T2	18	0.56	2.32	-2.74
l	F1M	17	0.38	2.34	-2.80
l	LING	17	0.47	2.24	-3.40
r	RO	15	0.72	2.64	-3.94
l	PCL	15	0.81	2.49	-2.52
l	Q	14	0.67	2.31	-2.59
r	Q	14	0.69	2.52	-2.44
l	O3	14	0.66	2.41	-2.52
r	T2	14	0.44	2.37	-2.87
r	LING	13	0.74	2.49	-2.42
l	P2	13	0.51	2.43	-2.50
r	IN	12	0.62	2.85	-2.29
l	PCIN	12	0.56	2.43	-2.51
r	V1	12	0.82	2.54	-2.38
r	O3	12	0.73	2.64	-2.31
l	P1	11	0.56	2.44	-2.47

r	P2	11	0.64	2.52	-2.41
r	CVCU	10	0.44	2.37	-4.03
l	O1	10	0.53	2.91	-3.51
r	FUSI	10	0.38	2.83	-3.76
r	PCL	10	1.00	2.74	-2.25
l	F3T	9	0.86	2.68	-2.28
l	AG	9	0.64	2.57	-2.32
r	AG	9	0.69	2.61	-2.31
l	T1P	9	0.42	2.89	-2.42
l	ACIN	8	0.46	2.85	-2.21
r	ACIN	7	0.52	2.89	-2.15
r	O2	7	0.86	2.84	-2.08
l	HES	7	0.95	2.97	-2.09
r	CHS	6	0.27	3.46	-2.16
r	F1MO	6	0.67	3.10	-1.95
l	FUSI	6	0.67	2.89	-2.03
r	P1	6	0.67	2.84	-2.06
r	T1P	6	0.40	3.25	-1.94
l	CHCU	6	0.40	3.05	-3.21
l	CHS	6	0.27	2.93	-2.64
r	CVD	5	0.40	3.07	-3.15
r	F3O	5	0.50	3.00	-2.01
r	GR	5	0.30	3.13	-2.21
l	F1MO	4	0.50	3.20	-1.85
r	CAU	4	0.33	1.33	-0.50
r	T2P	4	0.33	3.25	-1.84
r	CHCU	4	0.33	3.13	-3.06
r	F2O	3	0.67	3.94	-1.45
r	PCIN	3	1.00	2.87	-1.98
l	HIP	3	0.67	1.25	-0.20
l	PHIP	3	0.33	1.25	-0.28
r	PHIP	3	0.67	1.25	-0.20
l	F1O	3	0.67	3.94	-1.45
r	F1O	3	0.33	4.05	-1.51
l	PUT	3	0.33	1.67	-0.36
l	THA	3	0.33	1.67	-0.36
l	F2O	3	0.33	3.05	-2.44
l	CHSS	3	0.00	3.83	-2.58
r	CHSS	3	0.00	4.36	-3.17
l	GR	2	0.00	4.09	-1.40
r	HIP	2	1.00	1.75	-0.16
r	O1	2	1.00	3.75	-1.53
l	CAU	2	1.00	1.83	-0.22
r	PUT	2	1.00	1.83	-0.22
l	T2P	2	1.00	3.79	-1.54

r	CHIS	2	0.00	5.32	-1.94
l	CHG	1	-1.00	1.00	-0.06
r	CHG	1	-1.00	6.31	-0.89
l	CHB	1	-1.00	1.00	-0.06
r	CVT	1	-1.00	4.06	-1.34
l	AMYG	1	-1.00	2.00	-0.13
l	PAL	1	-1.00	2.50	-0.17
r	THA	1	-1.00	2.50	-0.17
r	HES	1	-1.00	3.63	-1.57
l	T3	1	-1.00	3.90	-1.44
r	T3	1	-1.00	3.82	-1.46
l	CHIS	1	-1.00	4.82	-1.14
l	CHCL	1	-1.00	4.03	-1.36
r	CHCL	1	-1.00	4.11	-1.32
r	CHB	0	-1.00	-1.00	0.00
l	CHT	0	-1.00	-1.00	0.00
r	CHT	0	-1.00	-1.00	0.00
l	CHF	0	-1.00	-1.00	0.00
r	CHF	0	-1.00	-1.00	0.00
l	CVL	0	-1.00	-1.00	0.00
l	CVCL	0	-1.00	-1.00	0.00
r	CVP	0	-1.00	-1.00	0.00
l	CVU	0	-1.00	-1.00	0.00
l	CVN	0	-1.00	-1.00	0.00
l	OC	0	-1.00	-1.00	0.00
r	OC	0	-1.00	-1.00	0.00
r	AMYG	0	-1.00	-1.00	0.00
r	PAL	0	-1.00	-1.00	0.00

Table 4.3: complete network measures

Network measures are shown for all parcels in order of descending degree. Note that for the last parcels where the degree is the lowest the parcel can be outside of the main giant component of the network making clustering and path length values inaccurate. Parcel abbreviations are the same as in **Figure 4.7**. Regions are ranked in order of decreasing degree.

Defining network 'hubs'

The susceptibility of the brain network to injury is analytically dependent on the degree distribution. The degree distribution of our empirical group averaged functional brain network demonstrated a heavy tailed distribution that best fit an exponentially truncated power law (**Figure 4.4**). This degree distribution defines the

existence of hubs as those nodes with disproportionately high connectivity, but form a minority of all nodes in the network (**Table 4.3**).

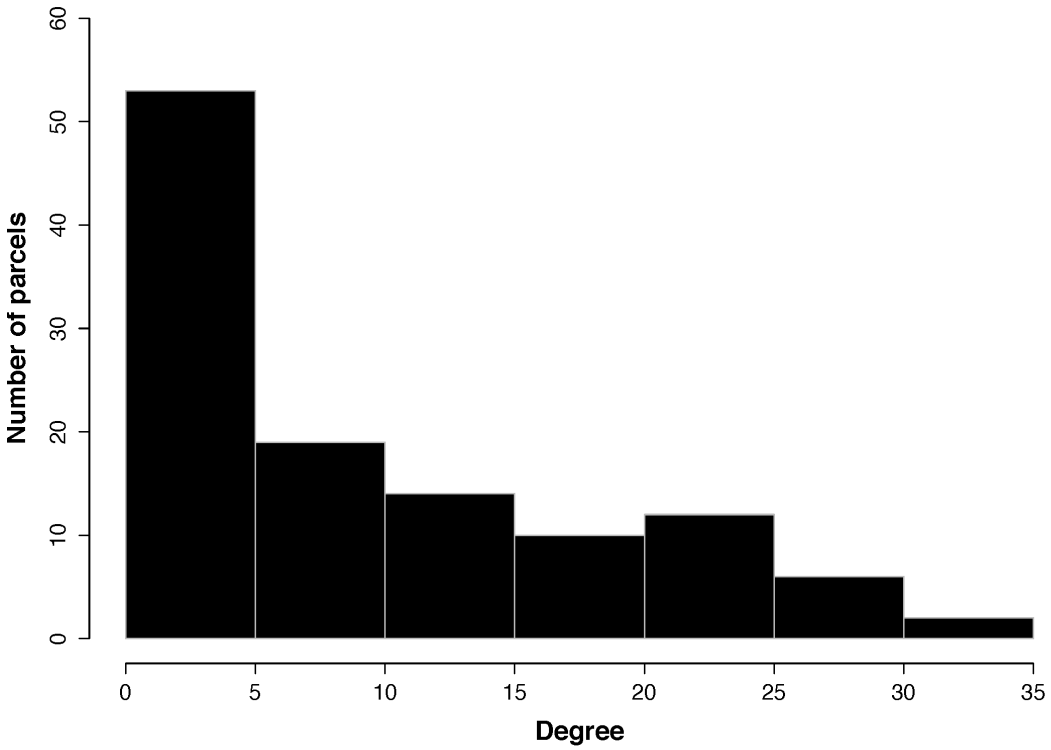

Figure 4.4A: degree distribution

A: the histogram for the group network node degrees. The majority of nodes are of low degree (<5) while the maximum degree extends above 30 (although few nodes have this degree).

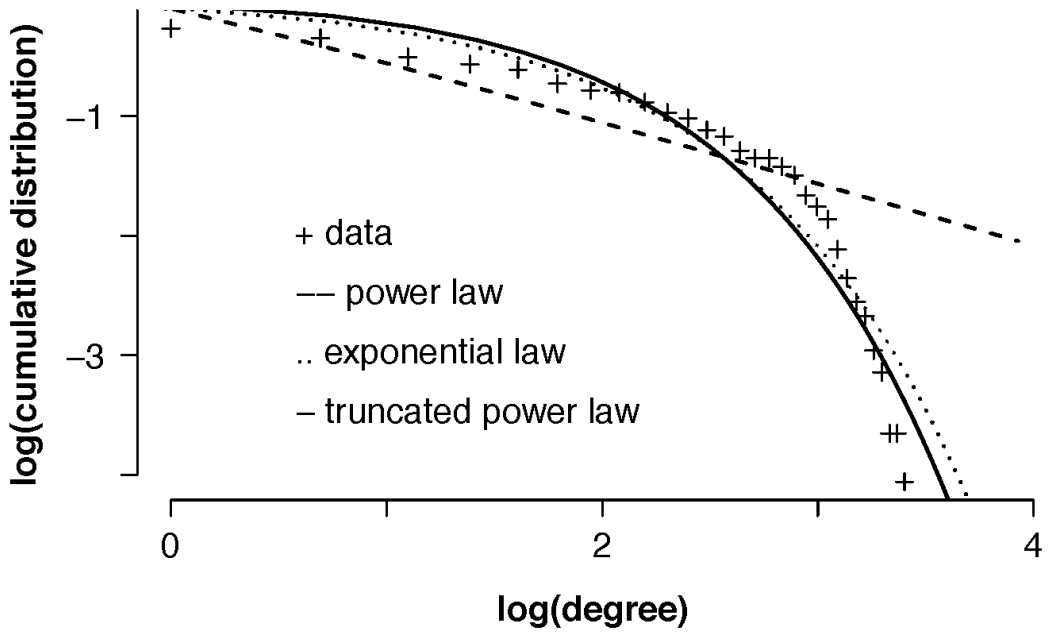

Figure 4.4B: degree distribution

B: the group network degree distribution is compared to that from simulated networks with either an exponential, power law, or exponentially truncated power law degree distribution. The best fit determined using Akaike Information Criteria was with the exponentially truncated power law degree distribution.

Mapping robustness to injury

The existence of hubs suggests random removal of nodes will have minimal effect on the overall topology as most nodes are of low connectivity, whereas focused removal of hubs will more likely have a significant effect on topology. Random node removal found our group averaged functional brain network to be as robust as both simulated randomized and scale-free networks (**Figure 4.5**). In this manner, the brain is remarkably tolerant to small areas of injury that occur at random. In comparison, targeted attack breaks down the brain network earlier, with the brain network demonstrating intermediate vulnerability between the scale-free and random networks, which is consistent with specific nodes being highly vulnerable to injury and acting as 'weak links' in the network. Information centrality can subsequently be generalized to determine the effects on the network of removing each node on overall network efficiency (**Table 4.3**). Information centrality identifies a core of highly vulnerable nodes which partially, but not fully, overlap those based on other measures of centrality or are otherwise defined as network hubs, but with more clinically intuitive inference (**Figure 4.6**). If one were to use this information for pre-surgical planning, one could purposefully sacrifice selected nodes whose loss would be predicted to have less effect overall network efficiency (and, therefore, by extrapolation on higher cognitive features such as intelligence). Furthermore, nodes that have a disproportionately large role in overall network efficiency could be avoided.

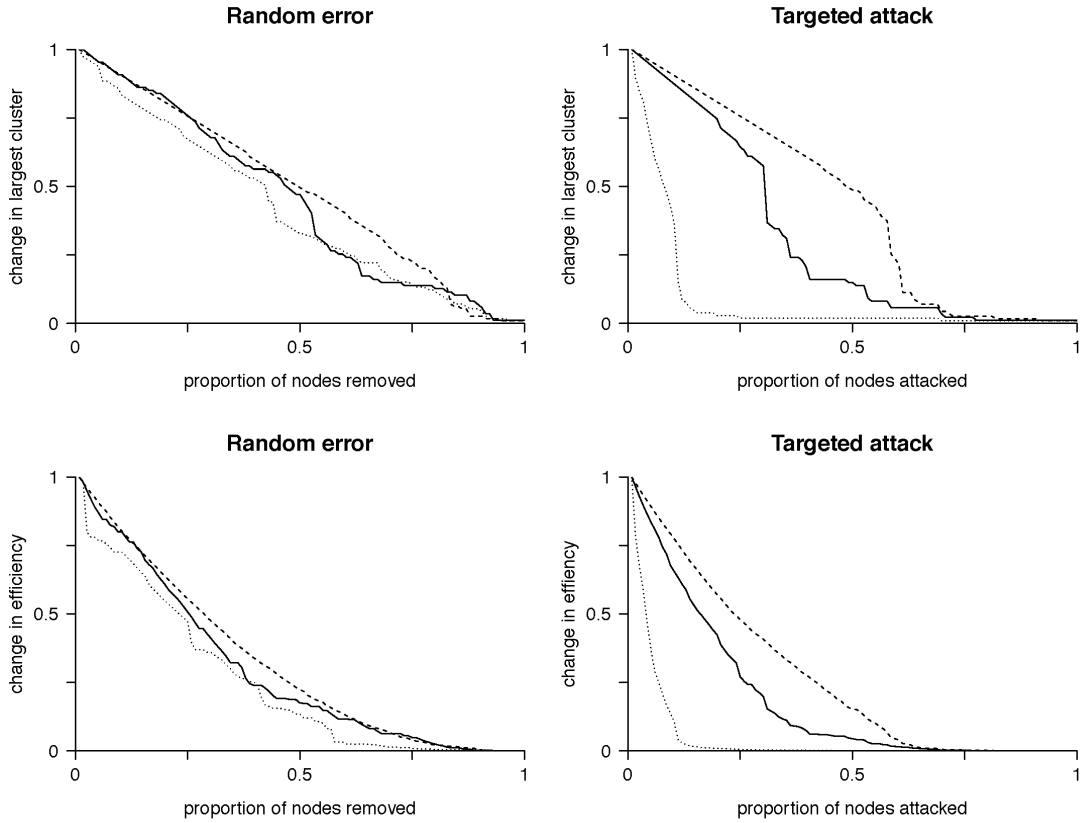

Figure 4.5: random error and targeted attack

The change in the size of the network giant component (top row) or efficiency (bottom row) due to either random error (left column) or targeted attack based on degree centrality (right column). Changes are relative to the values for the intact network. All networks are approximately equally affected by random error. However, targeted attack reveals vulnerability of the scale free network, while the brain network is of intermediate vulnerability between the scale-free and random networks. Horizontal axis values are the proportion of nodes removed and vertical axis values are scaled to maximum. Solid line = brain networks, dotted line = simulated scale-free networks, dashed line = simulated random networks

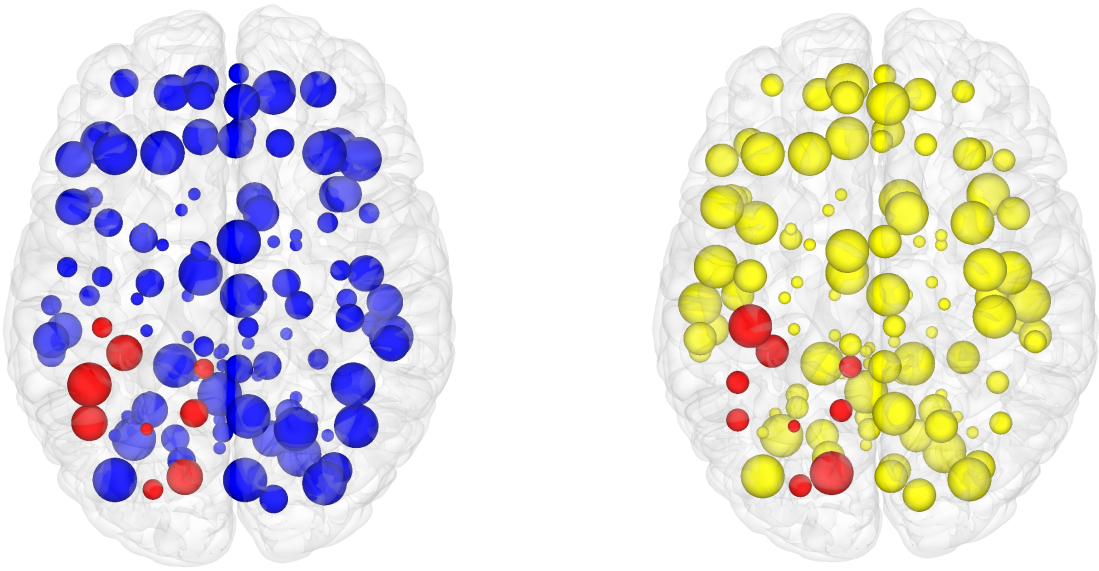

Figure 4.6: brain mapping with graph theory network measures

Axial view of node features displayed in cortical surface reconstructions. Node size is proportional to clustering co-efficient (nodes in blue, left); node size is proportional to information centrality (nodes in yellow, right). In both figures those nodes that are spatially adjacent to the tumor are highlighted in red. Network edges are removed to focus on the node features. If one were to use this information for pre-surgical planning, purposefully sacrificing selected smaller nodes to allow an extended surgical resection could be seen as having a minimal effect on overall network efficiency (and therefore by extrapolation on higher cognitive features such as intelligence). However, inadvertently affecting too many of larger nodes would be expected to have a disproportionate effect on overall network efficiency, and therefore should be avoided.

Network effects of tumours

One can use a network approach to visualise the connectivity that is either lost, or is at risk of being lost due to real (rather than simulated) lesions (**Figure 4.7**). Compared with the contra-lateral hemisphere, brain tumours produced clear and consistent effects at an individual subject level including reduced connectivity at intra-lobar, intra-hemispheric, and inter-hemispheric scales.

Another perspective to view these data is as the 'connections at risk' by removing a specific region adjacent to the tumour, for example, if one wished to include a

resection margin around the lesion (**Figure 4.7**, red edges). In each participant, the effects of an extended tumour resection were not only local but also included long-range connections both within and between hemispheres. Therefore, to fully understand the effects of surgery on brain function, one must use an approach that considers the connectivity of the brain in its entirety.

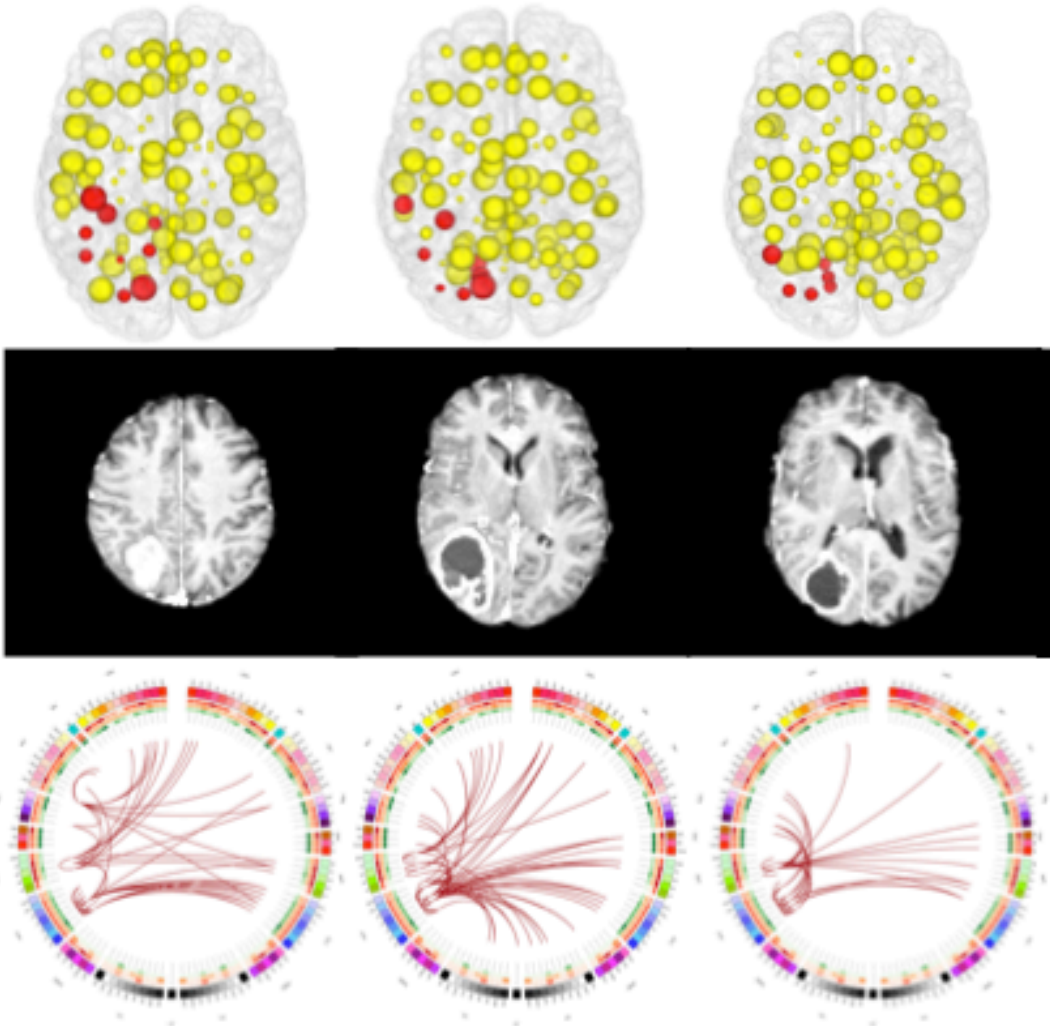

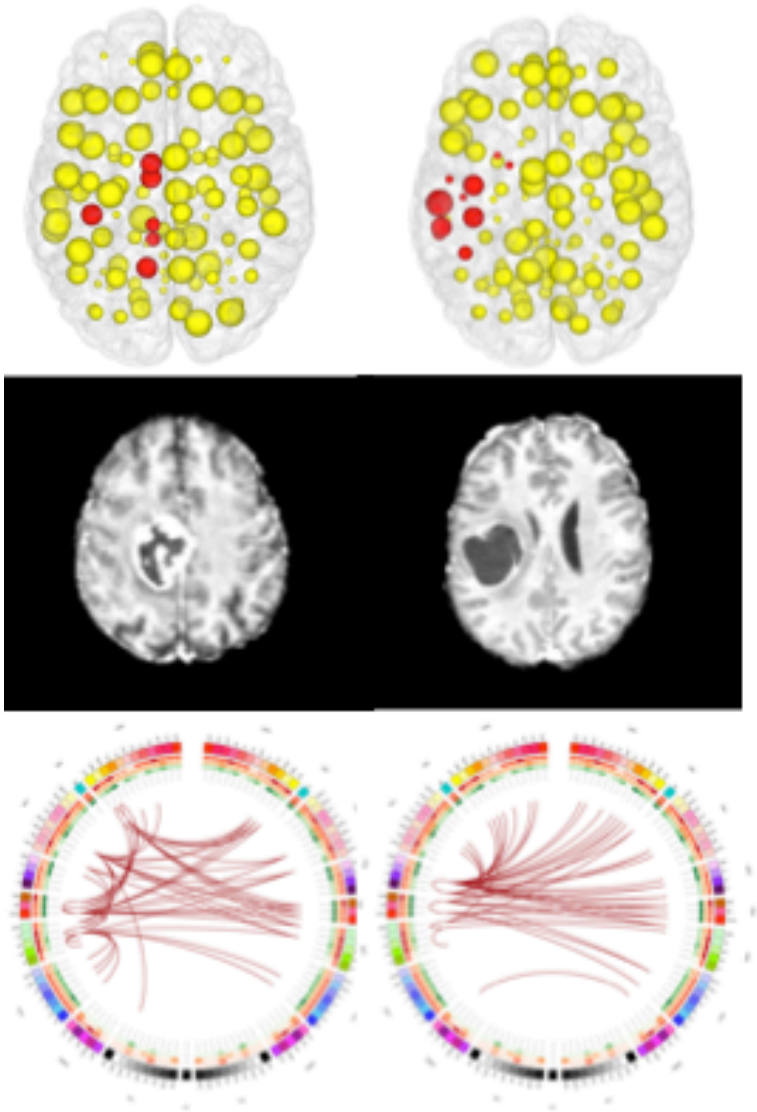

Figure 4.7: connections at risk

Combined connections at risk visualisation at the individual participant level. Columns represent individual participants. The centre row represents structural images with slices chosen to highlight the lesion character and location. The top row describes node robustness (as per **figure 4.6**). The bottom row includes circular representations of brain functional connectivity data (individual patient data, wavelet scale 2). Images are in radiological projection (image left = right hemisphere) with superior aspect of the image representing anterior brain (akin to an axial view). The sides are symmetrical representations of individual lobes (and parcels within) in their anterior-posterior co-ordinates. Inner circular heatmaps represent degree, clustering, and information centrality (outside to inside) per parcel. Lines representing intra-lobe

connections are outside with inter-lobe connections in the centre. On the right the nodes closest to the tumour are highlighted in red, while on the left the homologous nodes from the contralateral hemisphere are shown for comparison. The tumor was associated with reduced connectivity at intra-lobar, intra-hemispheric and inter-hemispheric levels. These effects were clear and consistent at the individual participant level. If one were to use this for tumour planning, then the connections in red would represent those that could be affected by extending the resection outside of the contrast enhancing margin, and would then become ‘connections at risk’.

Parcel codes (alphabetical): ACIN = anterior cingulate, AG = angular gyrus, AMYG = amygdala, CAU = caudate, CHB = biventricular, CHCL = central lobule, CHCU = culmen, CHF = floculus, CHG = gracilis, CHIS = inferior semilunar, CVL = lingual, CHS = simplex, CHSS = superior semilunar, CHT = tonsil, CV = vermis, F1M = superior medial frontal, F1MO = superior frontal medial orbital, F2 = middle frontal, F20 = middle orbital, F30 = inferior frontal pars orbitalis, F3OP = inferior frontal pars opercularis, F3T = inferior frontal pars triangularis, FUSI = fusiform, GR = gyrus recturs, HES = Heschl gyrus, HIP = hippocampus, IFG = inferior frontal gyrus, IN = insula, LING = lingual, MCIN = middle cingulate, O1 = inferior occipital, O2 = middle occipital, O3 = superior occipital, OC = olfactory cortex, P1 = superior parietal lobule, P2 = inferior parietal lobule, PAL = lentiform nucleus, PCIN = posterior cingulate, PCL = paracentral lobule, PHIP = parahippocampal gyrus, POST = post-central, PRE = precentral, PQ = precuneus, PUT = putamen, Q = cuneus, RO = rolandic operculum, SMA = supplementary motor area, SMG = supramarginal gyrus, T1 = superior temporal, T1P = temporal pole, T2 = middle temporal, T2P = middle temporal pole, T3 = inferior temporal, THA = thalamus, V1 = calcarine,

DISCUSSION

We present the first comprehensive analysis of the functional connectome in patients with brain tumours. Key achievements were validating the methodology behind connectome construction and identifying the core network features that have previously been identified in healthy controls. Functional brain networks were simultaneously locally clustered, but highly efficient with effective short cuts that formed a quintessential small world (Watts & Strogatz, 1998; Bullmore & Sporns, 2009). We also expanded on the technical aspects of network analysis to include measures specifically relevant to neurosurgery, such as information centrality (Latora & Marchiori, 2007). Finally, we demonstrated the relevance of network analysis to neurosurgery, including brain mapping of specific network features, understanding the effects of lesions, and visualising the data in an intuitive yet principled manner (Margulie, Botter, Watanabe, & Gorgolewski, 2013).

Mapping hubs (and indeed other graph theory-related measures such as efficiency and path length) creates a new vocabulary to use for functional brain mapping. This can be used for pre-surgical planning to preserve nodes that are critically important to the network composition while tolerating the removal of other nodes that may have less effect on the network. Furthermore, the potential long-range connectivity that is at risk from resection of the tumour can be isolated, characterised, and preserved. This method could be expanded to model virtual lesions on control networks and comparing them with empirical networks to identify putative plasticity. The ability to model real lesions and potential plasticity are key requirements for any future 'virtual brain'.

Current brain-mapping techniques (e.g. cortical stimulation and task-based functional MRI) are immensely useful, particularly at mapping local function or individual networks (Bello et al, 2007; Bello et al, 2008; De Benedictis, Moritz-Gasser, & Duffau, 2010; Duffau, 2011; Duffau, 2015), but are usually constrained to identifying a focus of maximal activation for a specific function that is in turn deemed most relevant to the proposed surgical outcome. Theories of functional neuroanatomy that have been applied to these methods have been those of localisation or regional specialisation (e.g. primary cortex function) and brain circuit connectivity (e.g. the

Wernicke–Geschwind-Lichtheim language circuit). Connectome analysis naturally balances these theories of functional localisation and network connectivity in a small world framework (and other related concepts) (Deco, Tononi, Boly, & Kringelbach, 2015) and can, therefore, be viewed as complimentary to these established models.

One of the key requirements for the connectome to gain acceptance in the neurosurgical domain is to confirm the relationship of graph theory measures to neuro-cognitive outcome (Castellanos, Di Martino, Craddock, Meta, & Milham, 2013). Connectome analysis is a relatively recent field; therefore, most of the data on neuro-cognitive outcomes is in healthy controls. The efficiency of a network is related to general intelligence quotient (van den Heuvel, Stam, Kahr, & Pol, 2009; Li et al, 2009), while the extent of small world features is negatively correlated with the performance of a task and higher education (Micheloyannis et al, 2006), suggesting that the degree of small worldness functions as a rheostat depending on the perceived complexity of the task. Preliminary work on patients with low grade glioma have found a small worldness and efficiency are related to cognitive deficits and intelligence in participants with frontal lobe tumours (Xu et al, 2013; Huang et al, 2014). Overall it appears that the basic measures of connectome analysis are related to core neuro-cognitive measures in healthy controls and potentially in patients with tumours too, although the data is currently somewhat limited. A novel approach to improving the cognitive relevance of connectome analysis would be to use a parcellation based on resting-state state fMRI networks that have been shown to correspond to task-based functional activations in a hierarchical clustering model (Smith et al, 2009; Smith et al, 2013). Therefore, the resulting network would be the interplay of different functional components, allowing more intuitive inference of network links and their pathophysiology.

While our cohort is of sufficient size to demonstrate the core network features and provide a proof of principle with our methods, these data could be improved upon by including a larger cohort with a variety of lesion locations and pathologies. Longitudinal imaging with neuro-cognitive outcome data will aid not only in validating the consistency of network metrics but also in identifying dynamic network changes that could be related to either plasticity or decompensation depending on the direction of cognitive effect (Kelly & Castellanos, 2014; Duffau, 2014). Practically

this process should be reasonably straightforward and achievable with minimal infrastructural investment. Most modern MRI scanners can acquire resting state fMRI data, the sequences themselves last less than 10 min, while neurocognitive assessment is readily being viewed as standard practice for many types of neurosurgical procedures both at presentation and during follow-up (Papagno et al, 2012; Fernandez-Coello et al, 2013). Successfully integrating these research protocols into routine clinical practice will be critical to establishing connectome analysis in neurosurgery as well as in developing high quality datasets.

Another aspect that could be developed further is the technical methodology behind connectome construction and analysis. For constructing the first connectomes in participants with real lesions, we wished to concentrate on the least complicated and most established methods of network construction, such as binary thresholded networks based on anatomical parcellations (Achard, Salvador, Whitcher, Suckling, & Bullmore, 2006; De Vico Fellani, Richiardi, Chavez, & Achard, 2014). This was to allow our methods to be valid and understandable yet not to distract from our key message, which was what a connectome analysis could bring to neurosurgery. Now we have established the key features and challenges of connectome analysis in a neurosurgical population, there is now a foundation with which to base further development of our methods. Improvements could be by applying more refined parcellation templates (Craddock et al, 2013; Zalesky et al, 2010), exploring alternative measures of statistical dependency between nodes (such as partial correlation or mutual information) (Zalesky et al, 2012), preserving edge weights, and obviating thresholding to create fully connected graphs (Simas & Rocha, 2015).

Finally, the field of network dynamics, or how information flows over the network, is a largely untapped avenue to explore (Gonzalez-Castillo & Bandettini, 2015; Misic et al, 2015). Network approaches (known as cascading failures) have been successfully applied to studying blackout propagation in power networks (Motter & Lai, 2002) and traffic jams (Huang, Vodenska, Havlin, & Stanley, 2013; Daqing, Yinan, Rui, & Havlin, 2014). Similar approaches could be applied in the brain to study seizure propagation and model the effects of cortical stimulation. This latter approach would view cortical stimulation as local overload leading to a network ‘blackout’, which not only allows the creation of an analytical model but also allows extrapolation of local

effects to a network level. To use an analogy with a power grid network, cortical stimulation could be looked upon as overloading certain links, which then results in information overload throughout the network and subsequent functional shut down. Such a solution may resolve the discrepancy in why function appears to be so variable between individuals (Sanai, Mirzadeh, & Berger, 2008). Refinement of this model offers a unique opportunity to pre-operatively predict the likely sites for positive stimulation, thereby marrying old and new techniques of brain mapping to result in improvements in patient care.

CONCLUSIONS

We present the principles underlying a connectome analysis of functional brain data in patients with brain tumours and demonstrate how analytically principled methods can be used to explore the key features of these networks. With these initial results, we hope to have demonstrated the potential of connectome analysis to addressing important questions in functional neuroanatomy. Understanding how the brain copes with and responds to lesions from a network perspective may bring us one step closer to developing a working 'virtual brain' to plan surgery in a way that is not only safer but also allows more extensive surgical resection.

CHAPTER 5: NETWORK HUB PLASTICITY DUE TO FOCAL BRAIN TUMOURS

This work was presented in poster form at the Cambridge Neuroscience Seminar, and as an oral presentation at the British Neurosurgery Research Group meeting, both in March 2016.

PRECIS

With the premises underlying resting state networks and graph theory analysis in patients with brain tumours having been established in chapters 4 and 5, this chapter moves on to testing specific hypotheses regarding the effects of focal brain tumours. Firstly, while graph theory allows intuitive modelling of focal lesions at a matrix level, the accuracy of this approach compared with empirical lesions is not known. Moreover, graph theory approaches to lesioning are traditionally static in that they do not encompass the potential effects of plasticity or diaschisis (long-range disconnectivity). Finally, the effects of lesions on putative network hub re-organisation are of interest given their proposed role in cognitive function and the growing clinical recognition of subtle higher order cognitive deficits.

Furthermore, this chapter takes the opportunity to develop the methods of graph theory analysis. Previous chapters had used binary and thresholded graphs based on anatomical templates that allowed establishment of the principles and validity of network approaches in brain tumours. In this chapter, weighted and fully connected networks are constructed at high dimensionality then analysed with a comprehensive range of weighted network measures. Additionally, the cohort is expanded from 5 to 11 participants. Overall these features allow a more sophisticated and nuanced analysis with the confidence in knowing that the fundamentals principles are valid.

Finally, this chapter introduces a healthy adolescent development dataset that forms the control group. This same cohort is also the subject of the final two results chapters in this thesis, where adolescent development is used to address specific hypotheses on network plasticity and robustness, thereby linking the pathological and healthy development datasets that constitute this thesis.

INTRODUCTION

Neurosurgery can be considered as the operative management of focal lesions, not just specifically tumours, but also including epileptogenic foci, traumatic injuries, and cerebral haemorrhage from a range of aetiologies. Mapping brain function has traditionally interested neurosurgeons because it constrains what one can do surgically; if a lesions is in brain deemed to be eloquent, it is often considered un-resectable. Better understanding the effects of focal brain lesions could allow individually tailored surgical management that facilitates more effective operative resection while safely preserving function.

Analysis of the effects of focal lesions has a long tradition of providing insight into brain function (Rorden & Karnath, 2004), which has been complimented by high-resolution neuro-imaging (Bates et al., 2006). Traditionally the effects of focal brain lesions have been considered at the local level i.e. the resultant phenotype is due to injury or related functional impairment of the involved or immediately adjacent brain. However this approach is limited in its ability to account for dynamic changes, individual variability, and neurocognitive processes that require distributed rather than discrete processing.

Network based analysis of lesion effects offers a complimentary approach to understanding system-wide functional disturbance. Removal of nodes or links in a connectivity matrix is an intuitive process that has previously been applied to create synthetic lesions. This can be done for either individual nodes, whereby it is known as delta centrality (Latora & Marchiari, 2003), or synchronously for multiple entries or rows/columns in a matrix, potentially designed to correspond to an *in vivo* lesion. Previous studies using this approach have identified regions of the brain that are more vulnerable to the effects of lesions, typically involving the default mode network and higher association cortex (Alstott, Breakspear, Hagmann, Cammoun, & Sporns, 2009). Notably these locations were outside the primary cortices, the quintessential eloquent brain, and related more to areas of higher cognitive function.

A weakness of the traditional network approach to creating synthetic lesions is that the effects are static: that is, once the matrix entries are removed, no dynamics or

plasticity in the network is simulated. This is important as profound phenotypic improvement is often observed clinically. For example, injury to the supplementary motor area often recovers in a characteristic spatial and temporal manner essentially completely (Vassal et al, 2016). At second surgery, re-organisation of awake brain stimulation sites away from areas previously identified as eloquent has been identified (Duffau et al, 2010). Furthermore stimulation of adjacent eloquent cortex through chronically implanted subdural grids can allow redistribution of such sites away from the tumour (Rivera-Rivera et al, 2016). If it were possible to identify this plasticity potential *pre hoc* it could be harnessed to allow safe resection of regions that were initially believed to be eloquent, but subsequently had significant potential for recovery due to plasticity. Therefore in this model, resectability would not just be governed by eloquence, but by plasticity potential too.

Connectomics has shown potential sensitivity to dynamic changes underlying putative plasticity mechanisms. Furthermore, connectomics offers a window into eloquence of higher cognitive function, or cognitive eloquence. Network hubs, determined through graph theory centrality measures, have been identified as key components in overall network function (Crossley et al, 2014; Sporns, Kotter, Tononi, 2007). Hubs are common foci for disease, display characteristic late development patterns, and facilitate integration of information for higher cognitive function. These features suggest that network hubs may not only play a vital role in maintaining higher cognitive function, but may underlie potential plasticity involved in recovery of deficits too.

This chapter addresses the accuracy of creating lesions in graphs from healthy brain networks. To do this, a cohort of individuals with *in vivo* brain tumours will be compared with a cohort of otherwise healthy individuals that have synthetic lesions. These data will be used to answer the following objectives and hypotheses:

1. Create *in silico* models of *in vivo* brain tumours by making synthetic lesions in brain networks of otherwise healthy individuals;
2. Compare the graph theory properties of networks with empirical and corresponding synthetic lesions;
3. Identify potential plasticity in relation to empirical lesions not captured by synthetic lesions, particularly relating to network hubs;

4. Determine the driving mechanisms underlying plasticity phenomena in terms of graph theory measures.

METHODS

Data comprised the full cohort (n=11) of the MALTINGS study with control data from the oldest 20 participants (10 female) in the NSPN UChange study (age 22-25 cohort). Participant demographics, study design, imaging parameters, and pre-statistical processing are described in **chapter 2**. Detailed methods specific to this chapter are described below. A summary of the analysis pipeline is presented in **figure 5.1**.

Parcellation

A whole brain (cortex, subcortical and cerebellum) 116 region anatomical network (Tzourio-Mazoyer et al, 2002) was sub-divided in a random manner to 251 discrete parcels of approximately equivalent volume (Zalesky et al, 2011). The standard space template was subsequently registered to functional space for time series extraction (**figure 2.2**).

Connectome formation

Wavelet correlation based connectivity matrices were formed as in **chapter 4**.

Hub definition

To reduce the number of comparisons a specific set of network measures were chosen to be of interest *pre-hoc*. The following centrality measures were used to define hubs: strength; betweenness centrality; within-module degree z-score centrality; between-module participation co-efficient; and eigenvector centrality. Additionally a consensus hub index was created by generating the sum total of hub scores for each node across all centrality measures (i.e. the maximum score was 5 if a node was in the top 10% of individual centrality measures). Group hubs were defined by averaging the overall hub scores across subjects. Definitions of all network measures are presented in **chapter 2.3.2**.

Synthetic lesions

For each participant, parcels overlapping a hand drawn brain tumour mask were used to zero-out the matrix entries for the corresponding parcels (nodes) in the average healthy participant connectivity matrix e.g. a tumour involving the precuneus required all connections for that parcel / node in the average healthy participant matrix were set to zero. This was repeated for each individual tumour resulting in 11 synthetically lesioned control matrices.

Statistical comparisons

Hubs were defined as the top 10% of all nodes for each specific measure, and a consensus hub was one that was in the top 10% for more than two or more measures (maximum 4). For each participant, the hubs for the empirical brain networks were compared with those from the synthetically lesioned network. Hubs were subsequently classified as: new hubs, defined as those present in the empirical but not the synthetic network; absent hubs, defined as present in the synthetic but not the empirical network; and concordant hubs, defined as those present in both the synthetic and empirical networks. For each hub category, the mean network measures for the hub nodes were extracted from the empirical and synthetic networks, and the values subtracted from each other to give the difference in hub network measures between the two network categories. Therefore each participant contributed one degree of freedom for each network measure. Comparisons between subjects were performed with a two-sided paired t-test. All statistics were corrected for multiple comparisons using the Bonferroni method to control for family wise error.

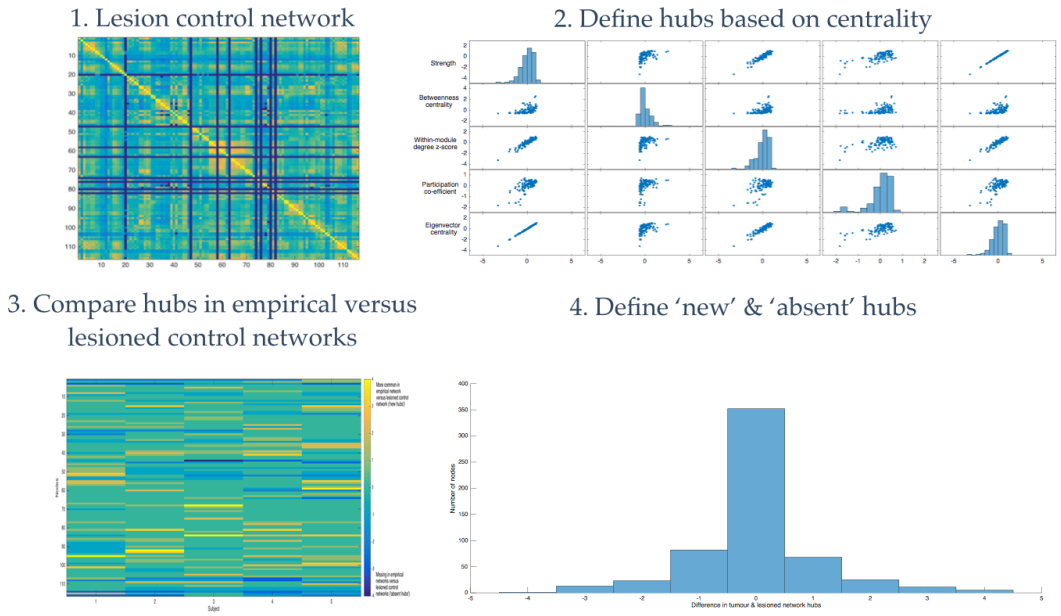

Figure 5.1: synthetic lesions analysis pipeline

Firstly the nodes that overlap the empirical tumour are removed from the control network to create a synthetic lesion. This matrix will now be of size N nodes minus the number of nodes removed. Next hubs are identified based on a series of centrality measures. Each participant then has two vectors of hub scores for the empirical and corresponding synthetically lesioned control network which can be subtracted from each other. The rows are summed across participants producing a positive score if a node is a hub in the empirical network but not in the synthetic network, a negative score if a node is a hub in the synthetic but not the empirical network, or a score of zero if the two networks agree.

RESULTS

1. Empirical and synthetic lesion network measures

The distributions of nodal network measures and their relationships between each other are displayed in **figure 5.2**. Notably each measure is appropriately normalised, and also there are significant positive correlations between many network measures, particularly strength and other related measures (e.g. degree, clustering co-efficient, local efficiency, and closeness centrality). Predictably degree centrality shows little variance in a fully connected network (all nodes have a degree of N nodes), while within-module degree z-score and between-module participation co-efficient are mutually exclusive and therefore anti-correlated with each other. Overall empirical and control networks appear to show broadly consistent patterns and distributions of measures.

A

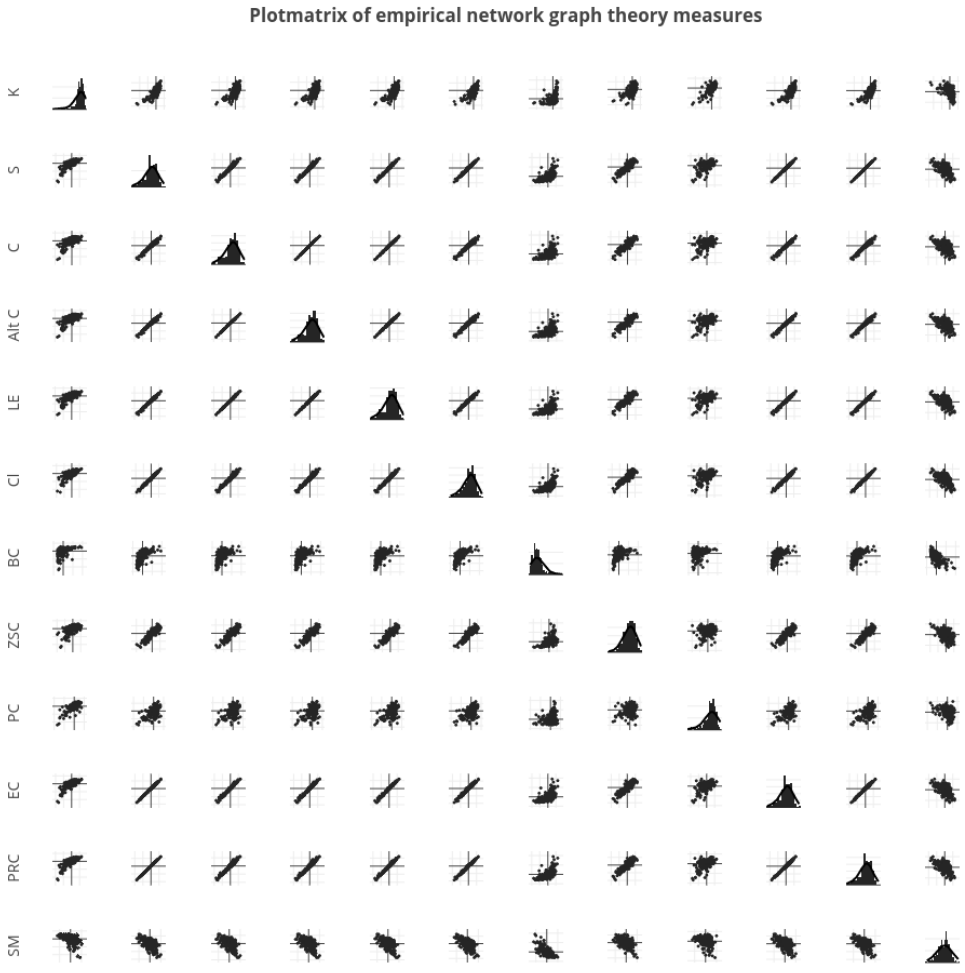

B

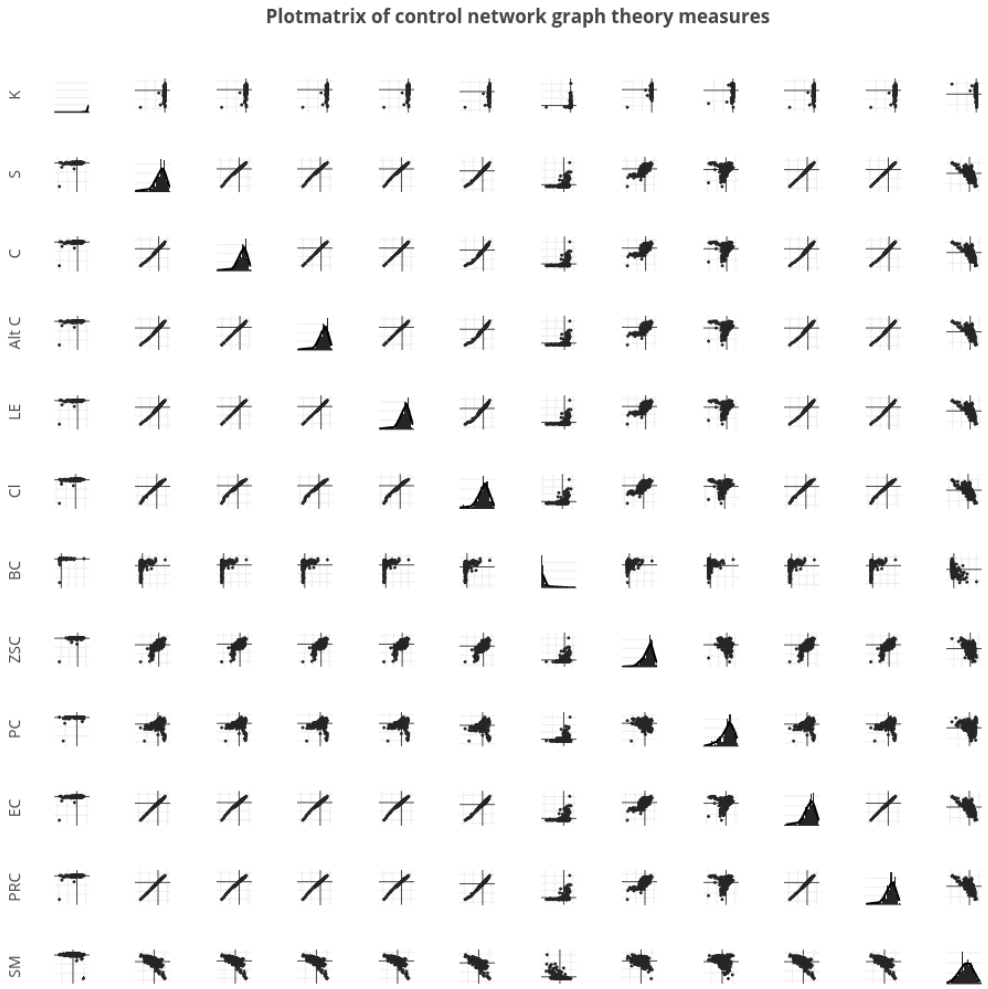

Figure 5.2: network measures for (A) empirical and (B) control networks

A plotmatrix of graph theory measures for the empirical (A) and synthetic (B) lesion networks. Entries on the positive diagonal comprise the histograms for each network measure (which were previously normalised to 0 mean and unit standard deviation). Off diagonal entries reflect the correlation between network measures per node. Abbreviations are: K, degree; S, strength; Alt C, normalised clustering; LE, local efficiency; Cl, closeness centrality; BC, betweenness centrality; ZSC within-module degree z-score centrality; PC, between-module participation co-efficient; EC, eigenvector centrality; PRC, pagerank centrality; and SM, semi-metricity.

2. Network hub measures

Following on from analysing the full set of network measures, a specific set of centrality measures were identified *pre-hoc* in the methods (**figure 5.3**). These measures are of intrinsic relevance to network architecture and have intuitive meanings in terms of their centrality properties. Furthermore they have reduced dependence between each other and therefore constitute a smaller set of measures with which to correct for multiple comparisons in subsequent analyses (i.e. 5 instead of 12 measures).

A

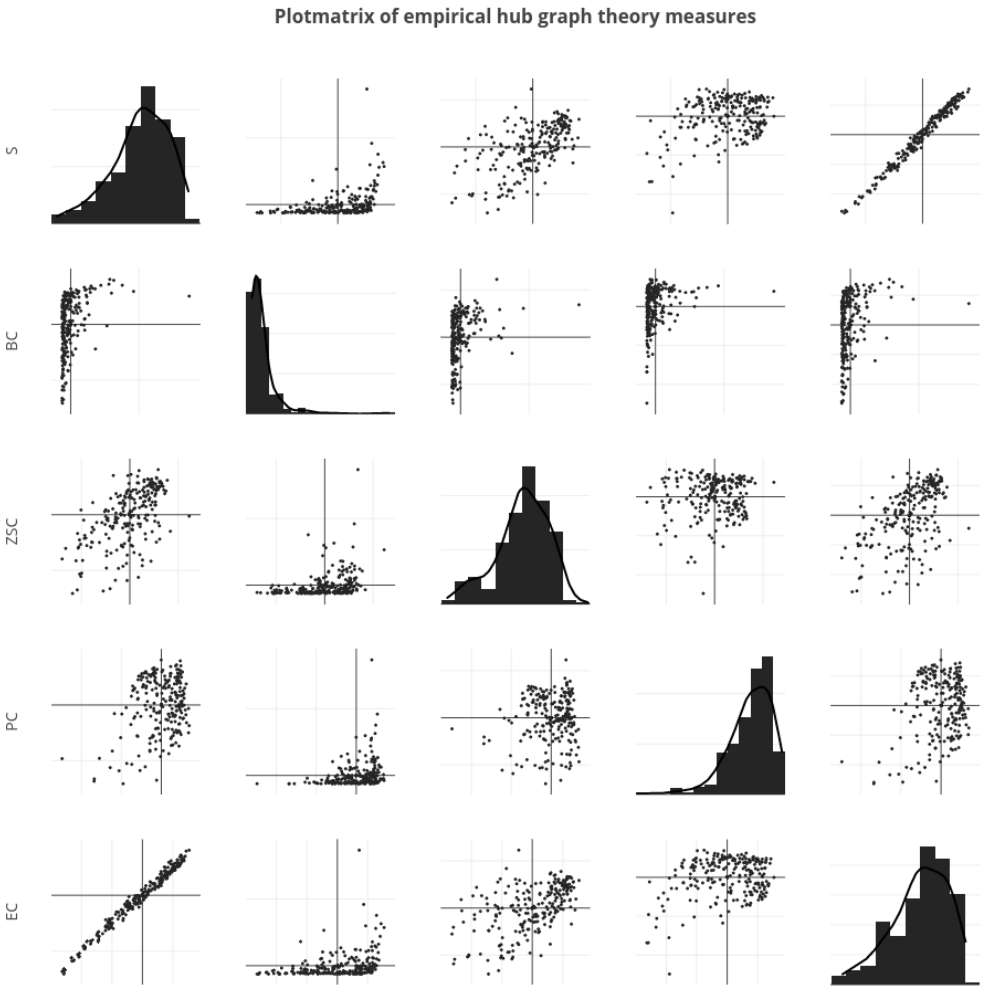

B

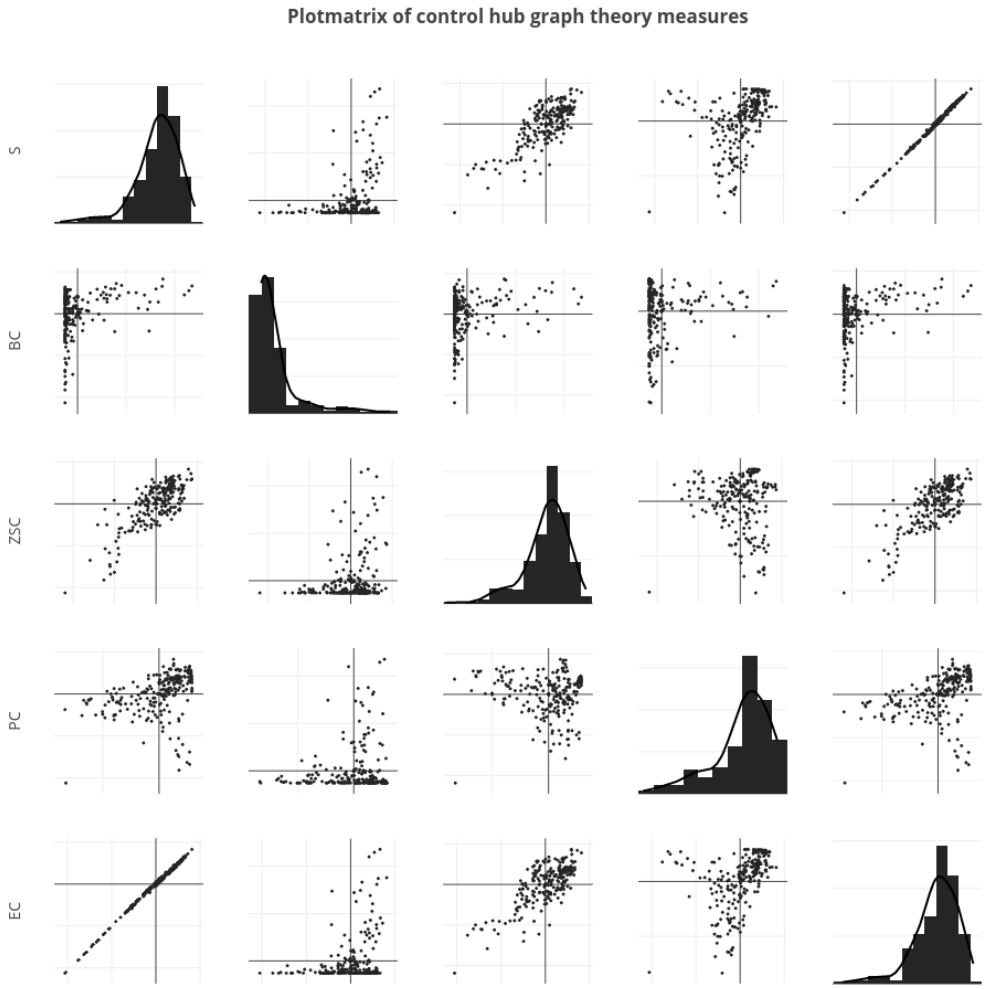

Figure 5.3: network hub measures for (A) empirical and (B) control networks
A subgraph analysis of figure 5.2 of only centrality measures specified *pre-hoc*. Abbreviations are as in figure 5.2.

3. Network hub topology

The topological locations of hubs defined on either individual or consensus centrality measures are displayed in **figure 5.4**. Each network centrality measure identifies hubs in brain regions defined as association cortex, involved with higher cognitive function, and consistent with previously reported to be sites for network hubs. Typical regions included the precuneus, posterior cingulate, lateral frontal and parietal

regions. Additionally these data also identified numerous subcortical and cerebellar network hubs. These latter locations have been less commonly noted to be hub locations in the literature, partly because surface reconstruction methods (e.g. FreeSurfer) are best described in the cortex (which is a common part of parcellation), and partly because of difficulties with diffusion imaging tractography in the infratentorial compartment (a common step involved in structural connectomes).

Additionally, it is clear that there is a degree of concordance with network hubs identified across centrality measures. For example, the hub locations based on strength and eigenvector centrality show a degree of overlap, while those based on within-module degree z-score and between-module participation co-efficient rarely overlap. This is reflected in the overall hub plots (**figure 5.4A**), where many nodes are noted to be a hub on multiple centrality measures, and a minority are specific to a single centrality measure.

A

B

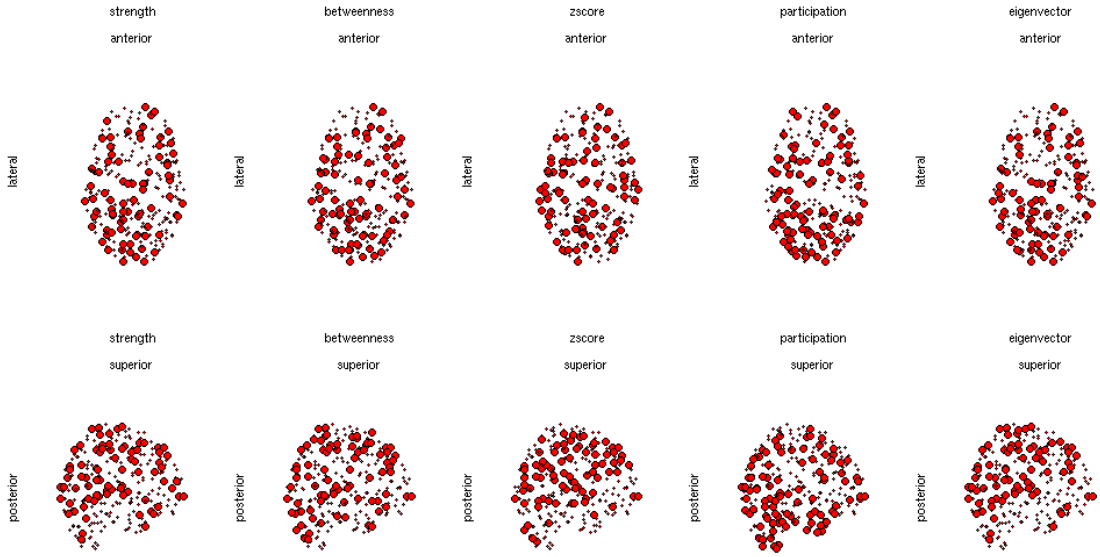

Figure 5.4: empirical hub topology

A: overall hubs

Hubs are defined on a concordance of centrality features. Given that within-module degree z-score and between-module participation co-efficient are effectively mutually exclusive, the maximum any one node can score is 4 out of 5. These scores are then averaged across all subjects; node size therefore reflects those nodes most likely to be a network hub across all participants in the cohort.

B: individual metrics

Hubs are defined on one of five individual centrality measures (node strength, betweenness centrality, within-module degree z-score, participation co-efficient, and eigenvector centrality). Size reflects the consistency of a node to be in the top 10% of each measure across participants i.e. the larger nodes are more likely to be a hub in the cohort as a whole.

4. Hub classification

Comparison of hubs in empirical and synthetic lesions allows hubs to be classified as either new, absent, or consistent (**figure 5.5**). Nodes were ranked according to their classifications across all participants, producing a cumulative ranking of a nodes likelihood of being in any one category. A significant proportion of nodes were accurately predicted (48 out of 256 nodes) and classified as consistent hubs. Furthermore the majority of nodes were only misclassified in at most two participants (172 out of 256 nodes).

Hubs that were found in the empirical data that weren't predicted from the synthetic lesions were classified as new hubs (136 out of 256 nodes). Overall new hubs tended to be individual rather than consistent across participants. Almost a quarter of all nodes were a new hub in at least one participant (61 of 256), but the most prevalent new hub nodes were only present in 5 out of 11 participants and these nodes constituted <2% of all nodes (5 out of 256).

In contrast absent hubs were less common (72 out of 256 nodes) but revealed a core of nodes that were consistent across participants rather than individuals. In total 34 nodes were consistently absent in at least 5 participants and approximately 2% were consistently absent in at least 9 of 11 participants.

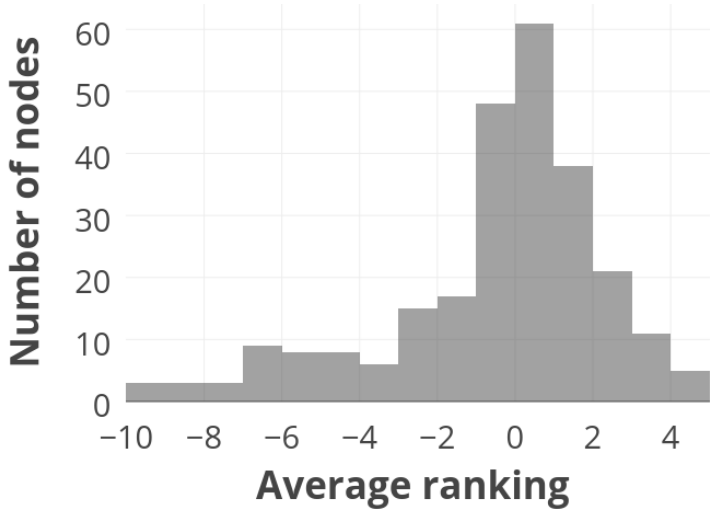

Figure 5.5: hub classifications

Numbers of nodes and the prevalence that they were a hub or not in the empirical versus synthetic lesion data. Values less than zero reflect absent hubs, and greater than zero as new hubs. A higher absolute value reflects consistency across participants (maximum n=11). Most nodes were comparable between the two networks but the tail of the distribution reflects a core of nodes that were consistently present as absent hubs across participants, whereas new hubs were more variable across participants.

Overall these data suggest that while synthetic lesions are accurate at modelling empirical data to an extent, there is significant hub plasticity in terms of new and absent hubs. In general new hubs tended to be highly individual, with few nodes consistently appearing as new hubs across participants, most likely reflecting the variability in participant demographics (e.g. tumour location, age, and presence of neurological deficits). However, while absent hubs were less common, they tended to be more consistent across participants. This suggests that the brain has a core of hubs that it chooses to 'lose' in response to a lesion, but in turn the hubs it chooses to 'gain' are more individual (**figure 5.6**). A further observation is that missing hubs tended to involved posterior and midline structures closely related to the default mode, whereas new hubs tended to form in the contralateral areas homologous to the cortex involved by the tumour. This is consistent with previous work in this thesis on seed connectivity networks (**chapter 3**), suggesting that plasticity or variance was greatest in the default mode network.

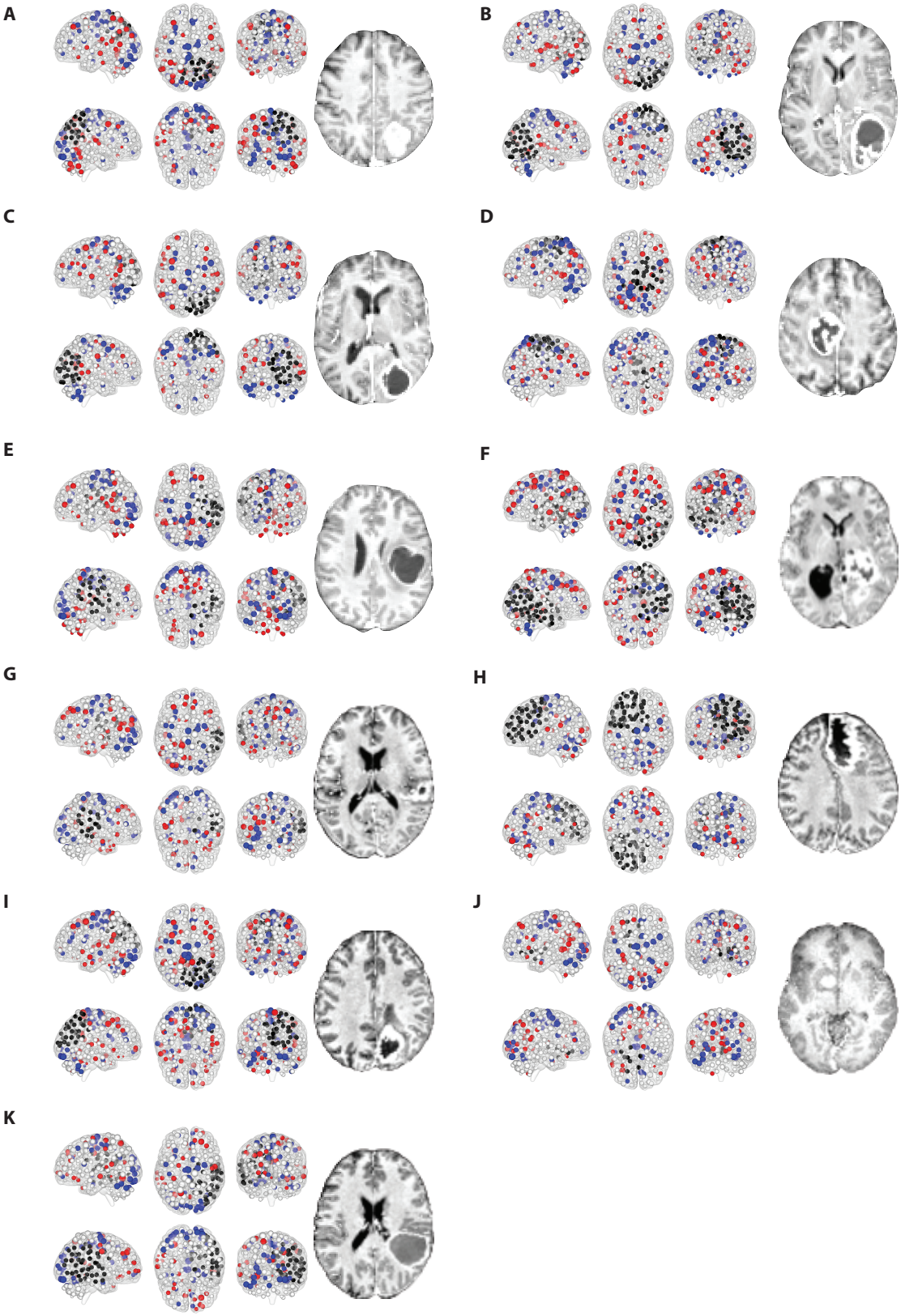
A
B
C
D
E
F
G
H
I
J
K

Figure 5.6: Individual Hub Categories

Each sub-figure A – L represents an individual participant and their respective functional connectome. Opposite each connectome is the corresponding structural image in MNI space, highlighting the tumour character and localisation, to aid interpretation of the connectome visualisation. Nodes are coloured according to those overlapping the tumour (black), new hubs (red), absent hubs (blue), and consistent hubs (white). Sizes reflect node strength in the unit interval. All categories are defined on the corresponding synthetically lesioned network for that individual.

5. Hub category features

Finally, the features that were driving the apparent changes in hub classification were identified with graph theory measures (**figure 5.7 & 5.8 and table 5.1**). New hubs tended to score higher on the majority of measures but this was only statistically significant for betweenness centrality when corrected for multiple comparisons. In contrast semi-metricity was lower in new hubs i.e. nodes involved more indirect connections. Both new and absent hubs involved longer distance connections than consistent hubs. Overall synthetic lesions tend to identify shorter connection hubs, with absent hubs constituting the least 'hub-like' nodes with the lower centrality values (particularly between-module participation co-efficient), and new hubs constituting 'super hubs' with the highest overall values, particularly on measures of communicability and integration such as betweenness centrality and semi-metricity.

	New	Consistent	Absent
Distance	**77.31***	59.68	**78.44§**
Strength	0.58	0.09	-0.27
Clustering	0.48	-0.08	-0.20
Normalised clustering	0.48	-0.07	-0.20
Local efficiency	0.54	0.01	-0.22
Closeness	0.61	0.02	-0.30
Betweenness	**1.12***	-0.20	-0.82
Z-score	0.55	-0.06	-0.45
Participation co-efficient	0.55	0.13	**-0.51§**
Eigenvector	0.54	0.04	-0.25
Pagerank	0.69	0.10	-0.27
Semi-metricity	**-0.72***	0.26	0.44

Table 5.1: Hub Classification Features

Hub classification is defined at the individual level based on consensus hub features. Values are the difference between the same nodes in the empirical and synthetic lesion networks. Distance is mean in mm. *significant differences between new and consistent hubs. §significant differences between absent and consistent hubs. All statistics are after Bonferroni correction for multiple comparisons (i.e. <0.05/12 = 0.004).

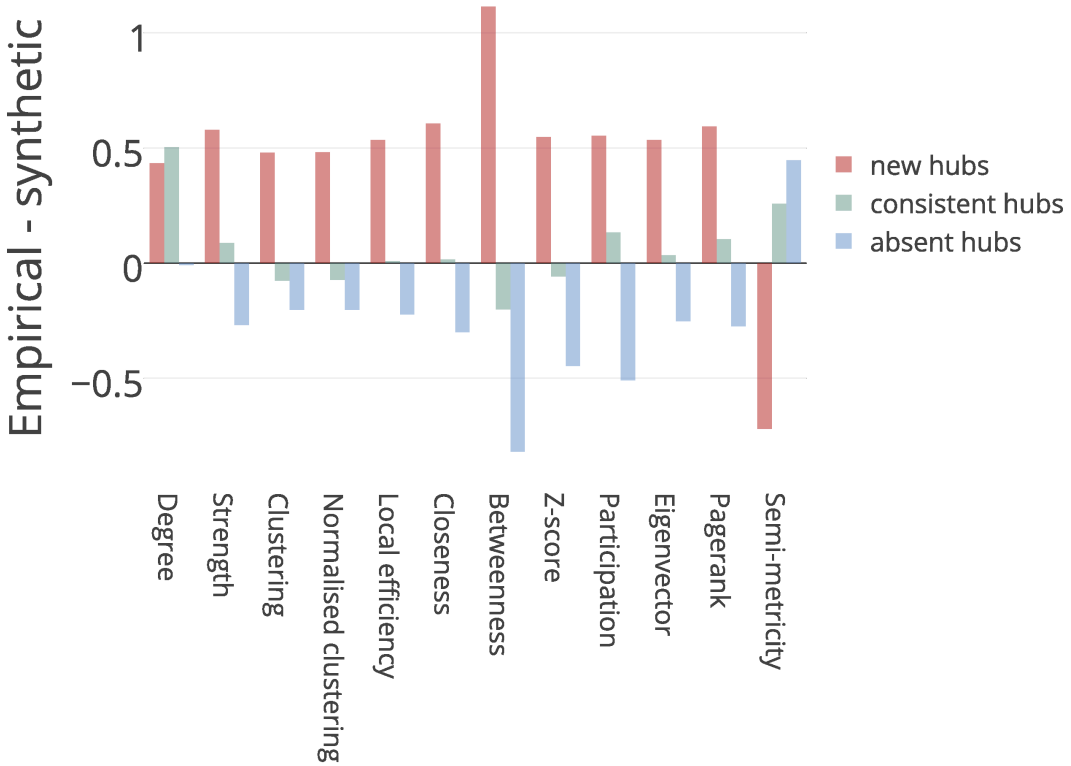

Figure 5.7: Hub Classification Features

Graph theory measures versus hub categories. For each measure the hubs were classified and measures extracted at an individual level, then compared as a difference to those from the corresponding synthetic lesion, before these differences were compared at a group level. Positive values imply higher values in empirical versus empirical networks, while the converse is true for negative values. Data are based on **table 5.1**.

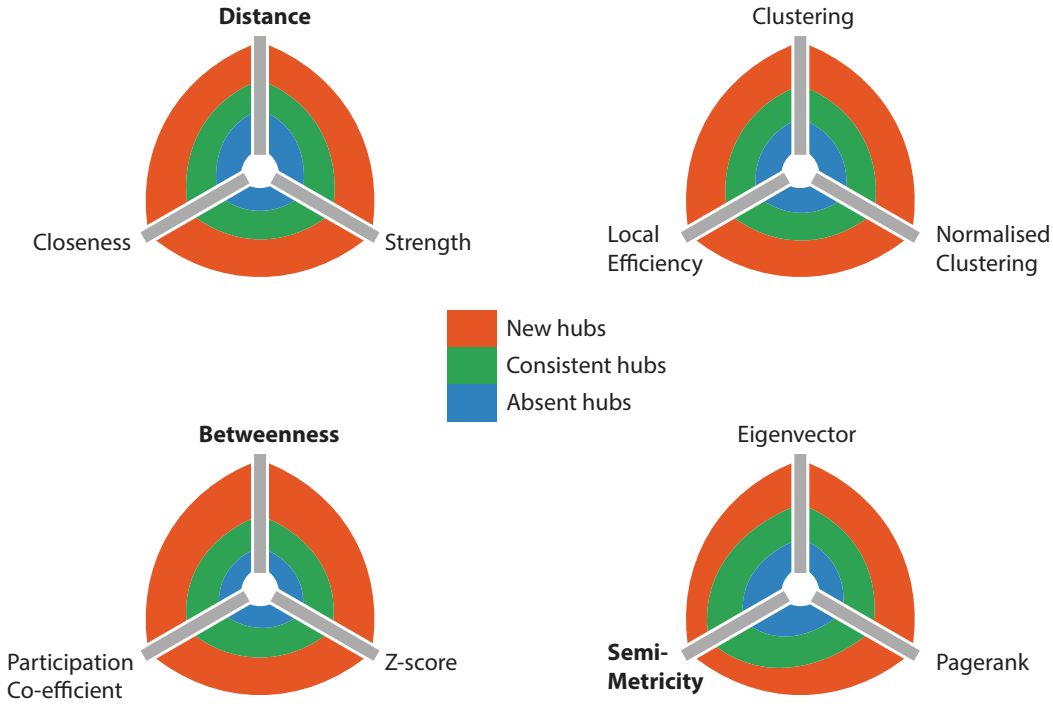

Figure 5.8: nest of hives / stacked bar plots of hub category features

Hive plots are a technique for visualising ratios in a consistent and principled manner, thereby facilitating multiple comparisons (in this example 12 measures and 3 categories = 36 comparisons). Data are from **table 5.1**. The main statistically significant features are: increased distance for new and absent hubs versus consistent hubs; higher betweenness centrality for new hubs versus consistent hubs; lower participation co-efficient for absent hubs versus consistent hubs; and lower semi-metric percentage for new hubs versus consistent hubs. Bold headings represent measures with significant differences between hub categories. Overall both new and absent hubs had longer distance connections than consistent hubs, while new hubs had higher betweenness centrality and lower semi-metricity than consistent hubs.

DISCUSSION

In summary, these data have found that while the classical graph theory approach to creating synthetic lesions in connectivity matrices generated from healthy control participants offers some consistency with data from empirical lesions, there are important differences, particularly in hub dynamics. Focal lesions appear to induce the formation of new hubs at the cost of selectively down regulating a core of already established hubs. Furthermore, the balancing of these hub ratings preferentially selects those involved in long-range connectivity and network integration, while those that are lost are costly in terms of distance but serve less of a role in network communication. While decisions on these new hubs tend to be formed at the individual level, those involving missing hubs tend to be more consistent. Finally, while new hubs involve the homologous regions in the contralateral hemisphere, missing hubs are based in the posterior parieto-occipital regions, in a pattern that overlaps topologically with the default mode network. Overall these data are consistent with a dynamic rather than static response to the presence of focal lesions.

Previously, attempts at modelling the effects of focal lesions with graph theory had been performed using virtual computationally-based lesions i.e. not based on any corresponding clinical lesions (Alstott, Breakspear, Hagmann, Cammoun, & Sporns, 2009). This analysis develops the field through the use of empirical data to create realistic approximations of *in vivo* lesions. Furthermore, previous interpretations of the effects of focal lesions had assumed the effects to be static; that is, once a lesion is created, the network does not change further (Van Horn et al, 2012). This is inconsistent with clinical observation of functional recovery after focal lesions from a variety of causes (e.g. stroke (Price, Seghier, & Leff, 2010), traumatic brain injury (Fagerholm, Hellyer, Scott, Leech & Sharp, 2015), and neoplasia (Duffau, 2014)). Typically patients show an improvement over weeks to months (occasionally earlier), but there are also instances of patients deteriorating too (either early or late), suggesting complex network level effects such as diaschasis. One can now propose network hub plasticity as a proxy for these clinically observed dynamics.

Finally, while the data presented here has some important differences from previous lesioning studies, they are consistent with a broader movement in graph theory

analysis that focuses on the key role of network hubs in health and disease (Achard et al, 2012; Bassett & Bullmore, 2009; van den Heuvel & Sporns, 2013). Myriad psychiatric and medical diseases are starting to be defined by their effects on networks, and hubs in particular appear to a major site of disease activity (Crossley et al, 2013). These findings suggested a particular class of hubs that is high cost (in terms of Euclidean distance of connections) and involved with overall network communicability.

An advantage of this present study is the inclusion of a dataset that is consistent in pathology yet shows a degree of variability in location. Furthermore, the data processing strategy took advantage of contemporary technological advances such as ANTs and ICA, which have been shown to demonstrate superior sensitivity and improved robustness to noise than previous techniques (Smith et al, 2013; Tustison et al, 2014). Additionally, the graph theory analysis took advantage of weighted measures and fully connected networks; methods for binarising and thresholding networks (the respective antonyms) are not universally agreed upon and both reflect an additional pre-processing step that distances one from the original data. Therefore the current analysis is not only less complicated but remains closer to the data and should therefore be more robust to the specific analysis code, without compromising sensitivity to detecting the actual signal of putative plasticity-related changes.

In terms of analysis methodology, further research is needed in defining statistical dependencies in functional connectivity data, with early work suggesting regularised regression methods may be useful (Varoquaux et al, 2010). Optimal parcellation strategies, and how to appraise their effectiveness, are also clearly needed. Parcellation based on multi-modal data potentially offers improved consistency and functional delineation (Glasser et al, 2016), while ICA based parcellations offer attractions for individually based parcellations (Smith et al, 2011). Analysis of neuroimaging data with focal lesions presents numerous challenges beyond that involved with the analysis of healthy participants. While the pre-processing strategies implemented in this review are physically principled and have an evidence base suggesting they offer advantages compared with more traditional methods, there remains the possibility that differences in dealing with artefacts due to the brain lesions are contributing to the results instead of underlying neurobiological signal.

However, an earlier study with elementary analysis methods revealed findings consistent with those in this present report (Hart, Price & Suckling, unpublished data), suggesting that the findings are robust to the specific analysis code and are reproducible in an expanded cohort.

Improvements to the current study potentially include expanding the analysis methods to a broader range of participants, for example those involving tumours with different histological characteristics. For example, patients with low grade gliomas are believed to demonstrate greater plasticity than those with high grade tumours (Duffau, 2014), and therefore may constitute a more dynamic population with which to study plasticity. Including different tumour locations as well as histologies will allow one to determine whether the effects observed are replicable and generalizable, or specific to only certain sub-classes.

To develop this work further longitudinal data could be acquired which would allow within-subject comparisons and mediate any issues with collecting sufficiently similar control data for statistical comparisons. For example, the control data in this current study are significantly younger than those in the empirical data population. A further advantage of longitudinal data would be the ability to determine predictors of plasticity, and identify plasticity trajectories for individual participants that may show greater or lesser degrees of recovery. If one were to expand this to data pre and post-surgery one could in turn use hub plasticity to plan neurosurgical resection of the tumour in a safer and more effective manner (**chapter 8**).

A further and necessary expansion of this work would be to include neuro-cognitive outcomes in synchrony with neuro-imaging. This is important to serve as a 'ground-truth' for any putative network plasticity effects; currently, while hub dynamics are apparent, their clinical significance is uncertain. Most likely hub dynamics reflect an adaptive response by the brain to a lesion given that often the focal effects of a tumour are less than expected given the size of the lesion. However the converse is also possible, in that the plasticity response may be maladaptive (Giza & Prins, 2006; Fornito, Zalesky, & Bullmore, 2014). Furthermore, alterations in network architecture may be advantageous in one respect, such as restoring or maintaining function, but maladaptive in another respect, such as by inducing seizure propagation. Indeed there

is evidence in low grade gliomas that the greatest degree of plasticity is associated with a higher likelihood of seizures (Duffau, 2014). In order to link slower time scale plasticity effects with the faster dynamics associated with seizure phenomenae it will be necessary to combine MRI with high temporal resolution neurophysiological data (e.g. electrocorticography, EEG or MEG).

CONCLUSION

This study is the first to present a comparison on real versus synthetic lesions using graph theory analysis of the functional connectome. In doing so important dynamics in hub locations were identified that suggest significant global functional plasticity is occurring in response to the presence of focal brain tumours. Furthermore, this work also allows insight into the drivers of these plasticity changes suggest important cost-utility decisions the brain is making in order to adapt to a lesion.

These conclusions represent a novel and valuable contribution to a potential virtual brain model, where one is able to mimic the *in vivo* clinical effects of focal brain lesions *in silico*. Ultimately such a virtual brain could be used by neurosurgeons to plan their surgery to account for plasticity and long-range network connectivity underlying higher cognitive function, thereby allowing more extensive surgery with the former (and by inference improved oncological outcomes) while balancing this with preserved or even improved function for the patient. Overall this work is an example of how a clinical observation and be tested as a hypothesis using graph theory that can then be used to understand the neuroscience underlying the observed clinical phenomenae.

CHAPTER 6: DEVELOPMENTAL DYNAMICS IN RESTING STATE NETWORKS DURING ADOLESCENCE

Parts of this work were presented as an abstract, both orally and in poster format, at the Resting State Brain Connectivity conference (Vienna, September 2016).

Distinct gender and age related changes in the functional connectome during development from adolescence to adulthood.

M.G. Hart[1,2], E. Bullmore[1], R. Dolan[3], I. Goodyer[1], P. Jones[1], J. Suckling[1]

[1]Department of Psychiatry, University of Cambridge, UK, [2]Department of Neurosurgery, Addenbrooke's hospital, Cambridge, UK, [3]Wellcome Trust Centre for Neuroimaging, University College London, London, UK

PRECIS

This chapter develops the previous work on the global effects of focal lesions by using evidence from studies of healthy development to create enhanced models of network plasticity and robustness. Here, healthy development is treated as a proxy for brain repair and plasticity. Under this hypothesis mechanisms of brain repair or plasticity after injury are believed to utilise the same original mechanisms of network formation that were used to form the pre-lesional network architecture. Therefore by understanding the macroscopic signal changes related to underlying adolescent development one could apply these as contrasts to study plasticity in empirical lesions. However in order to understand the process of healthy development better it is first necessary to clarify where, when and in whom putative development dynamics in functional connectivity are occurring.

INTRODUCTION

Adolescence can be defined as the transitional epoch between childhood and adulthood (Ernst, Torrisi, Balderston, Grillon, & Hale, 2015). Healthy development during this period is characterised by significant changes in multiple domains. Cognitive processes improve including working memory, task execution speed, and the ability to inhibit actions. Emotional behaviour is characterised by peaks in lability

of affect and risk taking behaviour that subsequently decline in adulthood. Finally, psychiatric pathology can also become manifest including anxiety and depression (di Martino et al, 2015). While significant brain development has already occurred prior to adolescence, clearly non-trivial features are still emerging. Such a protracted course of brain development is specific to humans and potentially underlies many of the unique phenotypic traits distinctive of our species.

Brain development is also relevant to neurosurgery where it could be viewed as a model of neural dynamics. Such neural dynamics could function as a proxy for brain repair after injury; that is, when the brain is injured, it recovers from this state using the same or similar neurobiological processes as it did to form its functional architecture originally, thereby sharing mechanistic resources. Typically such dynamics seen in neurosurgery are viewed as brain plasticity. Therefore understanding the mechanisms involved in healthy dynamics may well allow one to quantify the potential for plasticity after injury, or manipulate the underlying processes using invasive (e.g. deep brain stimulation) or non-invasive (e.g. transcranial magnetic stimulation) means.

Synaptic refinement – the selective removal of neuronal connections – is the prototypical neurodevelopmental process active during adolescence and is therefore intimately involved in developmental plasticity (Luo & O'Leary, 2005). Hebbian learning is believed to play a key role, with those synapses that activate together becoming stronger and therefore 'connected', whereas those synapses that do not activate together are deactivated or 'lost' (Hebb, 1942). At a microstructural level synaptic plasticity and strengthening is reflected in changes in inducible ionotropic glutamate receptors on dendritic spines (Nishiyama & Yasuda, 2015). Long term potentiation and depression, microstructural homologues of Hebbian learning, are mediated in part through either selective increase or decrease respectively in a specific subset of the receptor family known as *N*-methyl-*D*-aspartate (NMDA) receptors (Henley & Wilkinson, 2016). Stabilisation of dendritic spines is medicated via interactions with extracellular matrix components including cadherin-catenin complexes (Bian et al, 2015). Competitive interactions of dendritic spines with such complexes drive the stabilisation or elimination of spines through stabilisation of synapses. Finally, myelination is also active during adolescence and likely plays a

role in development during this period too, in combination with synaptic refinement (Dennis & Thompson, 2013). Myelination typically begins in the 3rd trimester *in utero* and progresses in a caudo-rostral and posterior-anterior manner. However, the effects are not specific to adolescence and the majority of myelination occurs within the first two years of life.

Neuroimaging has allowed unique insights into the structural and functional mechanisms involved in late childhood and adolescent brain development; notably many studies combine these two developmental periods to allow a more extended age range to capture non-linear trajectories in maturation. At a structural level, grey matter volume demonstrates an inverted quadratic developmental trajectory with region specific features while white matter follows a linear increase in volume (Giedd & Rapoport, 2010; Dennis & Thompson, 2013). Both grey and white matter trajectories demonstrate gender differences with earlier maturation typically occurring in girls compared with boys.

Investigations in adolescence utilising resting state functional MRI can be grouped into those using graph theoretical approaches or resting state networks (RSN); the former represents a higher order analysis while the latter is closer to the underlying data and will be focused on here. Most of these studies have focused on descriptive analyses of the number and characteristics of RSNs in specific age bands, summarised in the subsequent section. In a large study of 168 participants 21 RSNs were identified (Littow et al, 2010). A subsequent study comparing RSNs in 11-13 year olds (18 participants) and young adults (29 participants) focused on 14 RSNs (Jolles et al, 2011). A smaller study (18 participants) identified 14 RSNs but in a younger age range of 5-8 years old (de Bie et al, 2014). More recently a large study of 113 participants aged 7-18 years old focused on 8 RSNs (Sole-Padulles et al, 2016). Finally the largest study included 536 participants aged 6-10 years old and identified 25 RSNs and also quantified their reliability with repeated subsampling (Muetzel et al, 2016). Overall these studies provide consistent evidence for the formation of a core backbone of RSNs prior to and during adolescence, while the derived RSNs are already sensitive to reflecting distinct age and gender related changes.

This present investigation seeks to characterise the developmental dynamics in functional connectivity networks in the adolescence period. To do this a model-free data-driven approach was selected to maximise the potential yield of the data and prevent the selection of a particular model constraining the results to one specific feature or region. These analysis features are particularly attractive to investigating adolescent development whereby the exact mechanisms are still incompletely understood and it is necessary to consider dynamics at the whole brain level. Additional benefits are the potential for robust de-noising at multiple analysis levels (individual subject and group level) and the availability of canonical networks in the literature to allow comparisons outwith this specific dataset. It was hypothesised that not only would these RSNs be present, but that they would reflect those seen in adults. Furthermore these networks would show distinct gender, age, and age-gender interaction effects reflecting the external phenotypic differences observed in terms of cognitive, emotional, and social behaviours.

METHODS

Data comprised the NSPN UChange study. Participant demographics, study design, imaging parameters, and pre-statistical processing are described in **section 2.2.** Detailed methods specific to this chapter are described below.

Independent Component Analysis (ICA)

Dimensionality was set manually to 50 networks to represent large, robust networks, based on similar analyses in the literature. Additionally, automatic dimensionality estimation was performed with a Laplace approximation to the Bayesian evidence of the model order.

Network analysis

Between network connectivity was computed with Pearson product-moment correlations for concordance with previous studies in the literature. However, Pearson correlations are susceptible to the influence of indirect connections. Therefore, regression with L2-regularisation (ridge or Tikhonov regression) was also used to more specifically focus on direct connections.

Statistics

Statistical analysis was performed using a cross-subject GLM with inference using FSL's randomise permutation-testing tool (Winkler et al, 2014). Data and models were demeaned temporally before fitting. A total of 10,000 permutations were performed with threshold-free cluster-enhancement (Smith & Nichols, 2012). For between network testing, a one-group t-test on the original network links was also used to threshold at a t-statistic of 10 prior to permutation testing. All p values were subsequently corrected for family wise error with additional Bonferroni correction for the number of ICA network comparisons.

RESULTS

1. Group ICA: 50 Networks

Manually selecting a dimensionality of 50 ICA networks (**Table 6.1**) produced 34 good (BOLD-related) and 16 bad (noise-related) components (**Figure 6.1**). Bad components tended to both poor spatial and temporal characteristics (13); few were rejected on the basis of their spatial (2) or temporal (1) features individually. Removal of noise-related components resulted in a clear 1/f power spectra with the majority of the signal power being due to low frequencies (**Figure 6.2**).

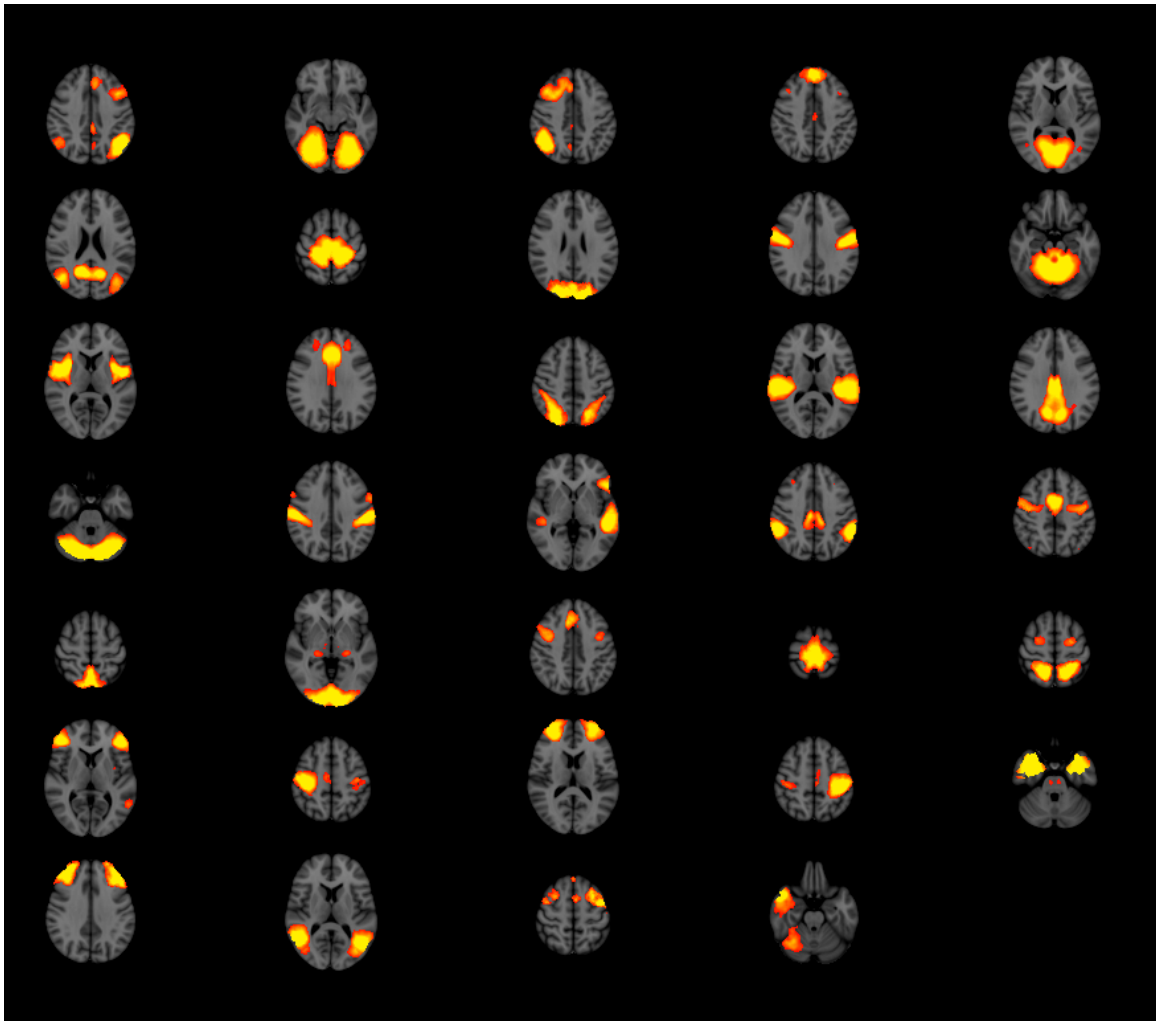

Figure 6.1: BOLD and noise-related ICA components

A: Good nodes

Nodes (34) with both spatial and temporal (1/f) features consistent with BOLD contrast are demonstrated above. These include (from left to right and top to bottom): left fronto-temporal-parietal; right DVS; medial prefrontal; medial visual; limbic / lateral parietal; midline sensorimotor; posterior occipital; lateral sensorimotor; superior cerebellum; insula; anterior cingulate; posterior attention; auditory; precuneus; posterior cerebellum; lateral sensory; language; DMN; superior SMA; superior midline parietal; posterior occipital; salience; superior sensorimotor; superior parietal lobule; bilateral anterior midline frontal; right sensorimotor; frontal pole; left sensorimotor; hippocampi bilaterally; bilateral anterior frontal; posterior temporal-occipital; midline SMA; superior parietal; superior temporal / cerebellum.

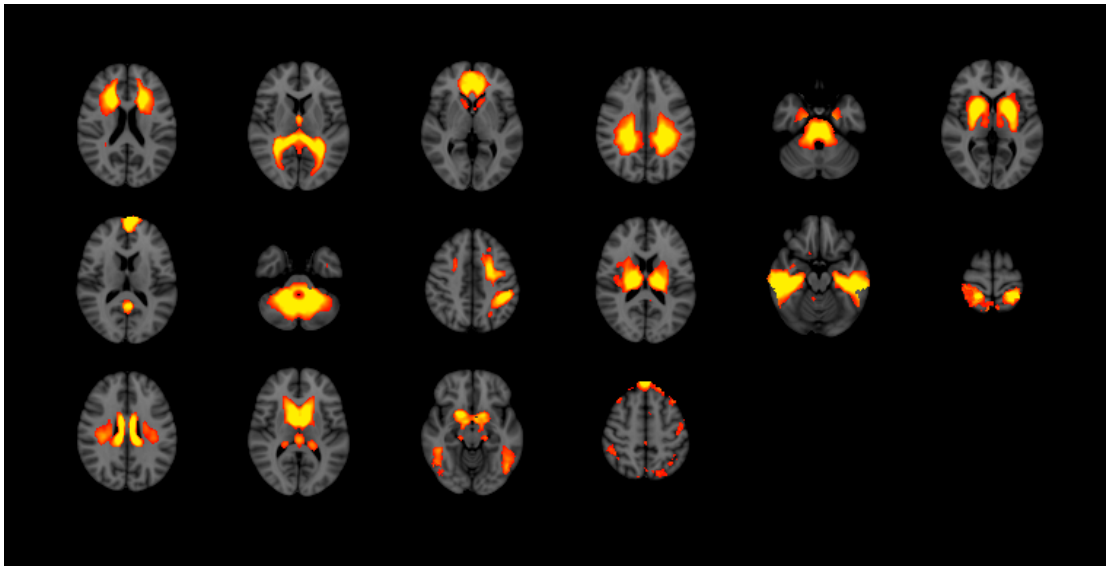

Figure 6.1: BOLD and noise-related ICA components

B: Bad nodes

Examples of 16 nodes with spatial and / or temporal features suggestive of being related to noise rather than BOLD contrast. These include (from left to right and top to bottom): anterior white matter; posterior basal cisterns; inferior midline frontal; posterior white matter; pons / midbrain; basal ganglia; frontal pole / posterior cingulate; middle cerebellar peduncle; left lateral white matter; internal capsule; inferior temporal; superior parietal; corpus callosum; ventricles; hypothalamus / fusiform gyrus; head motion.

DVS = dorsal visual stream, DMN = default mode network, SMA = supplementary motor area

ICA Network	Description	Canonical network cross correlation	Laterality	Centre of gravity Co-ordinates	Category
1	Fronto-temporal-parietal	#4 | 0.25 #5 | 0.11 #10 | 0.49	Left > Right	-0.387744 -18.306891 18.047615	BOLD
2	Lateral visual	#1 | 0.23 #2 | 0.19 #3 | 0.51	Bilateral	0.066198 -18.854692 17.549550	BOLD
3	Right DVS	#4 | 0.14 #7 | 0.11 #9 | 0.47	Right	0.610441 -17.993857 18.137943	BOLD
4	Medial prefrontal	N/A	Midline	0.015472	BOLD

				-17.683953 18.050626	
5	Medial visual	#1 | 0.77	Bilateral	0.036377 -18.629974 17.888391	BOLD
6	Limbic / lateral parietal	#4 | 0.35 #6 | 0.46	Midline	-0.016169 -18.633976 17.870287	BOLD
7	Sensorimotor	N/A	Bilateral	0.119246 -18.209502 18.599546	BOLD
8	Frontal white matter	#2 | 0.11 #7 | 0.12 #8 | 0.2	Bilateral	-0.017888 -17.531722 17.934017	Noise
9	Posterior occipital	#1 | 0.21 #3 | 0.25 #8 | 0.13	Bilateral	-0.094856 -18.719049 17.990901	BOLD
10	Posterior basal cisterns	N/A	Bilateral	-0.083591 -18.429945 17.739018	Noise
11	Sensorimotor	#6 | 0.11 #7 | 0.14	Midline	0.008163 -17.973113 18.107651	BOLD
12	Inferior frontal	#12 | 0.17 #8 | 0.44	Midline	0.017254 -17.390909 17.717524	Noise
13	Superior cerebellum	#1 | 0.15 #3 | 0.18 #5 | 0.32	Midline	-0.158370 -18.591967 17.319513	BOLD
14	Insula	#6 | 0.16 #7 | 0.32 #9 | 0.11	Bilateral	0.314850 -18.004674 17.810634	BOLD
15	Posterior white matter	#4 | 0.12 #6 | 0.13	Bilateral	0.070066 -18.407490 18.105323	BOLD
16	Anterior cingulate	#6 | 0.2 #8 | 0.44	Midline	-0.175403 -17.517486 18.004473	BOLD
17	Posterior attention	#3 | 0.31 #9 | 0.11 #10 | 0.2	Bilateral	0.222665 -18.851753 18.239491	BOLD
18	Auditory	#6 | 0.16 #7 | 0.52	Bilateral	-0.114518 -18.267478 17.700657	BOLD
19	Precuneus	#1 | 0.11 #4 | 0.56 #6 | 0.13 #8 | 0.22 #10 | 0.13	Midline	0.054114 -18.806205 18.189768	BOLD
20	Posterior cerebellum	#3 | 0.16 #5 | 0.16	Bilateral	-0.153348 -18.978697	BOLD

				17.199853	
21	Lateral sensory	#3 | 0.21 #6 | 0.31 #7 | 0.15 #10 | 0.15	Bilateral	0.030414 -18.151548 18.067722	BOLD
22	Language	#3 | 0.12 #4 | 0.16 #7 | 0.25 #10 | 0.18	Left	-1.056624 -18.036460 17.661706	BOLD
23	DMN	#1 | 0.11 #7 | 0.19 #8 | 0.12 #9 | 0.32 #10 | 0.14	Bilateral	0.121549 -18.385719 18.146050	BOLD
24	Superior SMA	#1 | 0.13 #5 | 0.17 #6 | 0.26 #7 | 0.16 #8 | 0.12	Bilateral	-0.114056 -18.156404 18.139805	BOLD
25	Superior midline parietal	N/A	Midline	-0.003467 -18.380025 18.065867	BOLD
26	Pons / midbrain	#5 | 0.18	Midline	0.020977 -18.067613 17.605879	Noise
27	Posterior occipital	#1 | 0.18 #2 | 0.66	Midline	-0.016215 -18.615644 17.831629	BOLD
28	Basal ganglia	#7 | 0.22 #8 | 0.2	Bilateral	-0.096859 -17.712160 17.769854	Noise
29	Salience	#7 | 0.1 #8 | 0.17 #9 | 0.18	Bilateral	0.551592 -17.474362 17.978173	BOLD
30	Superior sensorimotor	N/A	Midline	-0.045908 -18.138040 18.124812	BOLD
31	Superior parietal lobule	#3 | 0.11 #6 | 0.2	Bilateral	0.083841 -18.284066 18.243948	BOLD
32	Frontal pole / posterior cingulate	#4 | 0.3 #5 | 0.12 #6 | 0.13 #8 | 0.1	Midline	0.138594 -17.757660 17.876922	Noise
33	Middle cerebellar peduncle	#5 | 0.47	Midline	0.001379 -18.434343 17.323930	Noise
34	Anterior midline frontal	#4 | 0.17 #7 | 0.21 #8 | 0.1 #10 | 0.32	Bilateral	-0.302400 -17.567432 17.767172	BOLD
35	Left lateral white	#6 | 0.22	Left	-0.672391	Noise

	matter	#9 | 0.1 #10 | 0.3		-18.047898 18.157000	
36	Right sensorimotor	#6 | 0.34	Right	0.543469 -18.100429 18.223498	BOLD
37	Frontal pole	#8 | 0.25	Midline	0.038272 -17.509060 17.858830	BOLD
38	Left sensorimotor	#4 | 0.13 #6 | 0.27	Left	-0.585003 -18.181350 18.211228	BOLD
39	Internal capsule	#2 | 0.11 #7 | 0.18	Bilateral	0.136831 -18.108123 17.801455	Noise
40	Hippocampi	N/A	Bilateral	0.057187 -17.875575 17.520330	Bold
41	Inferior temporal	N/A	Bilateral	0.067614 -18.036356 17.640990	Noise
42	Anterior frontal	#8 | 0.19	Bilateral	0.050149 -17.639074 18.181843	BOLD
43	Posterior temporal occipital	#3 | 0.36 #4 | 0.2 #7 | 0.11	Bilateral	0.093549 -18.887677 17.883360	BOLD
44	Superior SMA	#8 | 0.1	Midline	0.044784 -18.018768 18.316488	BOLD
45	Superior parietal	N/A	Bilateral	0.024405 -18.162938 18.303156	Noise
46	Corpus callosum	#6 | 0.2	Bilateral	0.055797 -17.925335 18.061570	Noise
47	Ventricles	#8 | 0.18	Bilateral	-0.002877 -17.954201 17.943486	Noise
48	Superior temporal / cerebellum	#3 | 0.14 #7 | 0.2 #9 | 0.18	Right	1.341446 -18.209971 17.570345	BOLD
49	Hypothalamus / Fusiform gyrus	#3 | 0.13	Bilateral	0.092924 -18.259705 17.527044	Noise
50	Head motion	N/A	Bilateral	0.028392 -17.809208 18.222047	Noise

Table 6.1: ICA network characteristics

Characteristics of the 50 group-average ICA networks. Canonical networks refer to those previously defined in **Figure 2.6**. Co-ordinates are those based on the space defined by the MNI152 template. Features represent a binary categorisation of whether the ICA network represents BOLD contrast or noise, defined on spatial and temporal (1/f) properties. DVS = dorsal visual stream, DMN = default mode network, SMA = supplementary motor area.

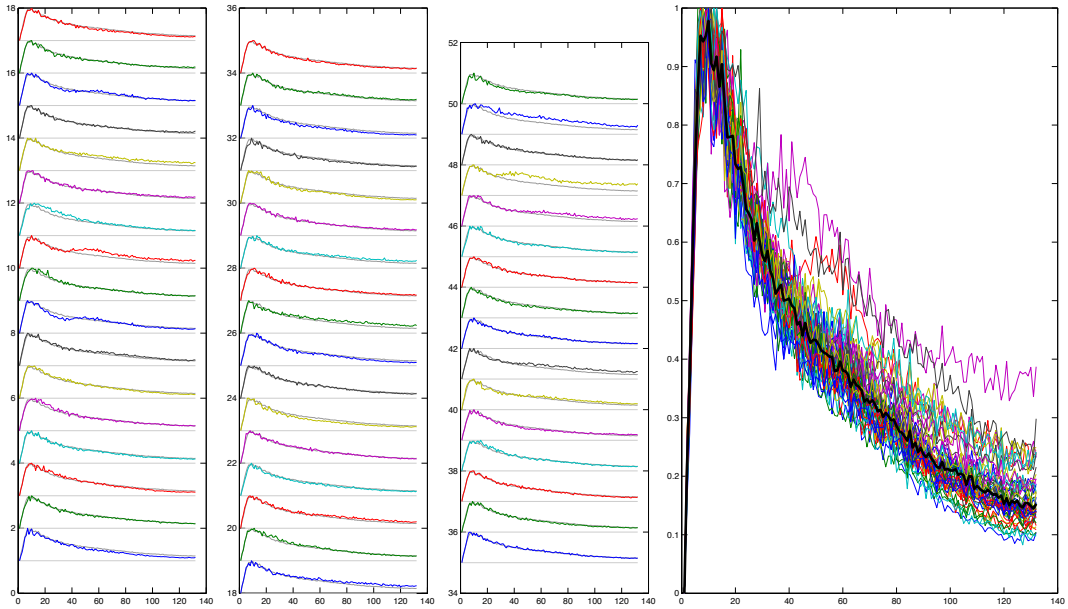

Figure 6.2: power spectra of ICA networks

A: Original power spectra of all components. While there is a clear group trend for a 1/f power spectra selected components did not fit this model well (e.g. components 7, 9, 40, 45 46, & 48)

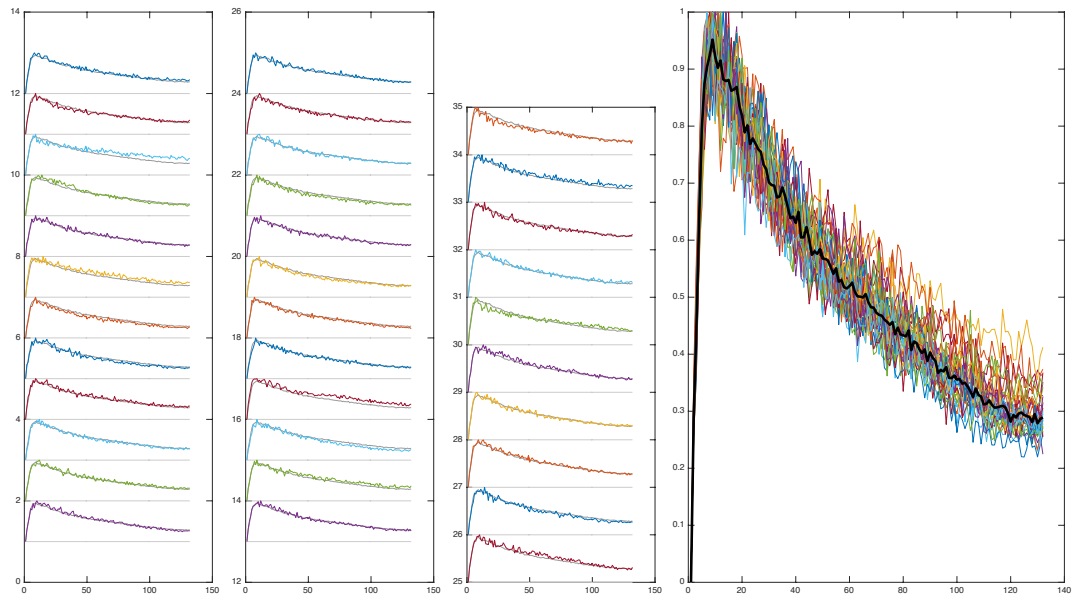

Figure 6.2: power spectra of ICA networks

B: Regression of components with either a poor 1/f power spectra or spatial features or both resulted in a more consistent overall power spectra with the majority of signal power arising from low frequencies.

2. Group ICA: 230 Networks

Automatic dimensionality estimation (**Figure 6.3**) resulted in 230 ICA networks of which 167 were classified as good and 63 as bad. Cross correlation with canonical networks revealed a hierarchical organisation with each canonical network reflected by multiple smaller networks (**Figure 6.4**).

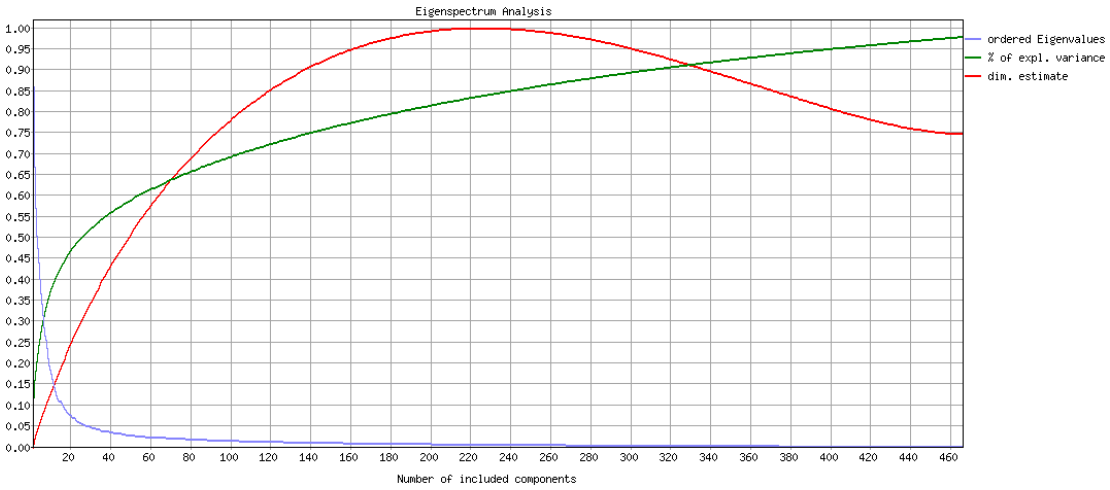

Figure 6.3: automatic dimensionality estimation of ICA

With increased dimensionality (dependent variable) the percentage of variance explained increases however the ordered Eigenvalues has a sharp drop off reflecting increased fitting to noise rather than signal. The dimensionality estimate is fit using a Laplacian approximation to the Bayesian probability of the model order.

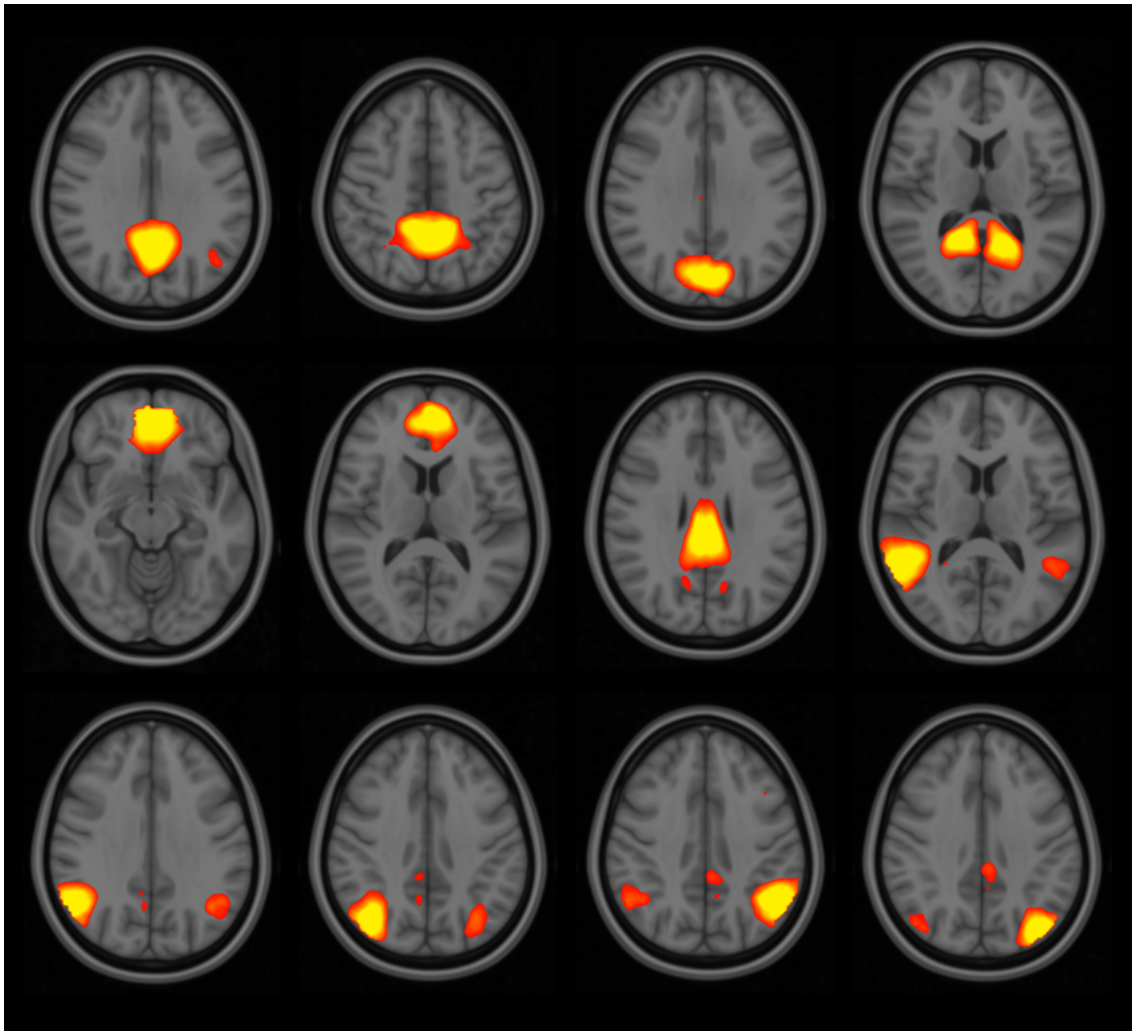

Figure 6.4: hierarchical network organisation at higher ICA dimensionality
Cross correlation of 230 ICA networks with a canonical default mode network template revealed 12 sub-components with most correlations between 0.11 - 0.26. The lower average correlations reflected the small spacial distribution of each ICA network which was therefore only contributing to part of the template. Here we see the typical default mode organisation is split into specific sub-components comprising the superior parietal lobule, cingulate isthmus and precuneus, medial anterior frontal lobs, middle and posterior cingulate gyrus, and separate left and right lateral parietal components involving the supramarginal and angular gyrus.

3. Within network functional connectivity dynamics

Age, gender, and age-gender interaction effects were present within ICA networks (**Table 6.2**) at 50 dimensions. Gender related changes were present while controlling for age (**Figure 6.5**). Higher connectivity within ICA networks in females than males was present in postero-medial parieto-occipital cortices, extending into the cingulate isthmus and precuneus. A smaller cluster was present in the superior posterior putamen on the right. Overall these clusters involve primary visual cortex, higher order association parietal cortex, and subcortical structures. Higher connectivity in males than in females involved multiple smaller and scattered clusters predominantly involving the right hemisphere posteriorly. These clusters included the ventral-lateral and posterior thalamus, putamen, insula, and superior parietal lobule laterally and posteriorly.

Age related changes were present while controlling for gender (**Figure 6.6**). A single cluster that increased in connectivity with age was present in the pulvinar of the thalamus bilaterally extending into the left medial thalamus. Multiple smaller clusters decreased in connectivity with age involving the right isthmus of the cingulate gyrus extending into the precuneus and posterior parahippocampal gyrus, right anterior insula, and right posterior thalamus.

Age-gender interaction effects were present (**Figure 6.7**). Increased connectivity with age in females and decreased connectivity with age in males was present in the medial occipital lobes bilaterally and right precuneus. Increased connectivity with age in males and decreased connectivity with age in females was present in a single small cluster involving the left sensorimotor cortex superiorly.

The higher dimensionality ICA network formed with automatic dimensionality estimation did not result in any statistically significant within network changes.

Contrast	ICA network	Location of cluster	Co-ordinates of cluster	P-value
Male > Female	4	Left medial visual		0.001
	8	Right occipital		0.01
	16	Right superior parietal		0.02
	20	Right insula		0.006
	27	Posterior precuneus		0.002
	39	Cerebellar nuclei		0.03
Female > Male	14	Right superior parietal lobule		0.02
	16	Right lateral parietal		0.003
	17	SMA & medial visual		0.01
	30	Left fusiform		0.02
	37	Right inferior frontal		0.02
Increase with age	15	Medial thalamus		0.02
Decrease with age	28	Right pulvinar		0.01
	30	Right precuneus		0.02
	37	Right occipital		0.01
	47	Right fusiform		0.008
Male > Female with age	8	Right caudate / left precuneus		0.004
	22	Left fusiform / right occipital		0.008
	28	Right lateral parietal		0.04
	47	Left medial occipital		0.03
Female > Male with age	20	Left motor		0.01
	1	Right inferior occipital		0.04

Table 6.2: within network functional connectivity dynamics

ICA networks correspond to those in **Table 6.1**. Co-ordinates are those based in the space defined by the MNI152 template brain. P values are corrected for family wise error and subsequently Bonferroni corrected for the number of BOLD related components tested (0.05 / 34 = 0.002)

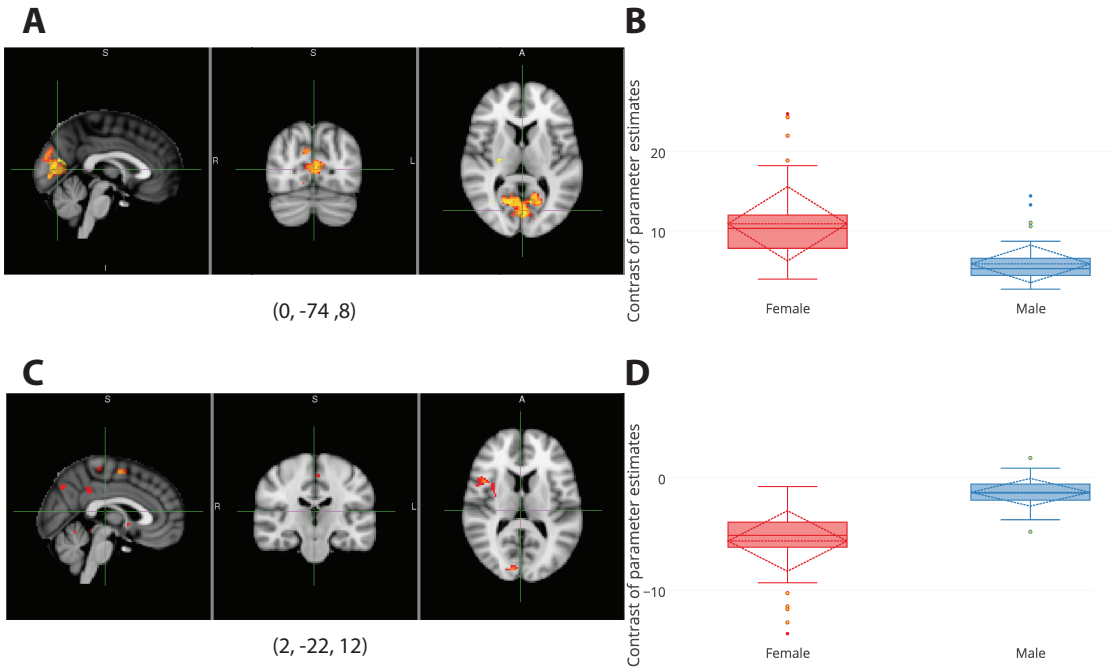

Figure 6.5: gender related within network functional connectivity dynamics

A: Within network connectivity greater in females than males. Changes are combined from 6 ICA networks. B: Box plots of parameter (beta) estimates A. C: Within network connectivity greater in males than females. Changes are combined from 4 ICA networks. D: Box plots of parameters estimates from C. Co-ordinates are mm in MNI space.

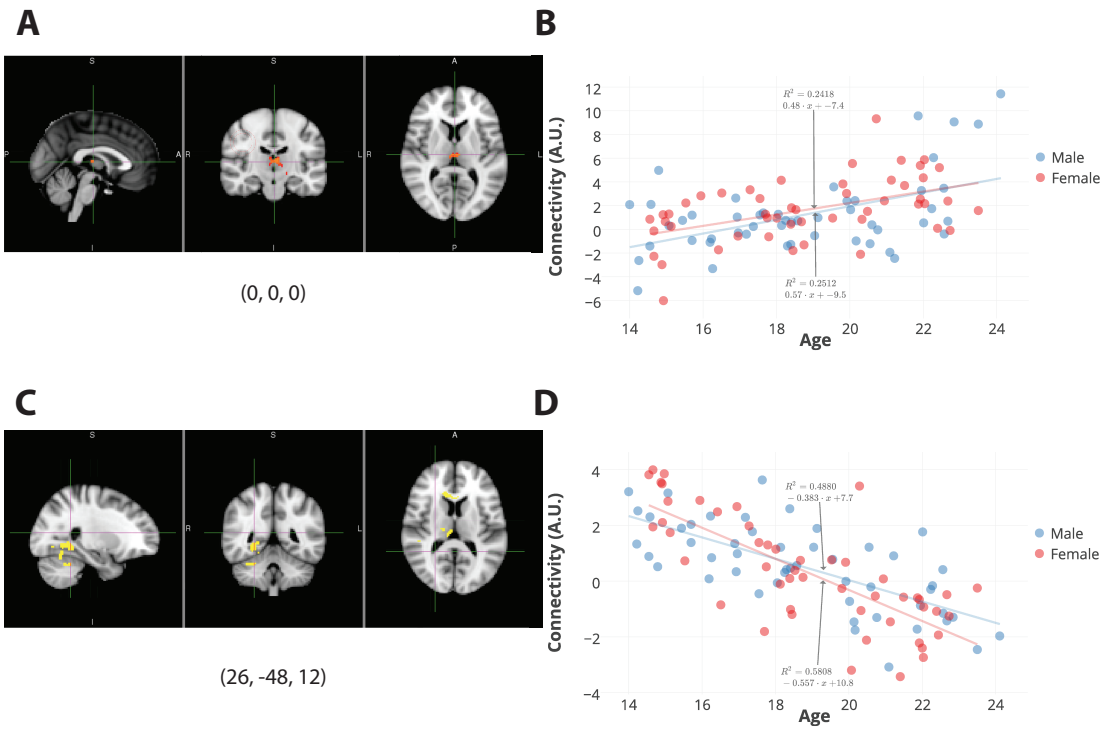

Figure 6.6: age related within network functional connectivity dynamics

A: within network connectivity increase with age while controlling for gender. B: corresponding parameter (beta) estimates for A (R^2=0.24). C: within network connectivity decreases with age while controlling for gender. D: corresponding parameter (beta) estimates for C (R^2=0.49).

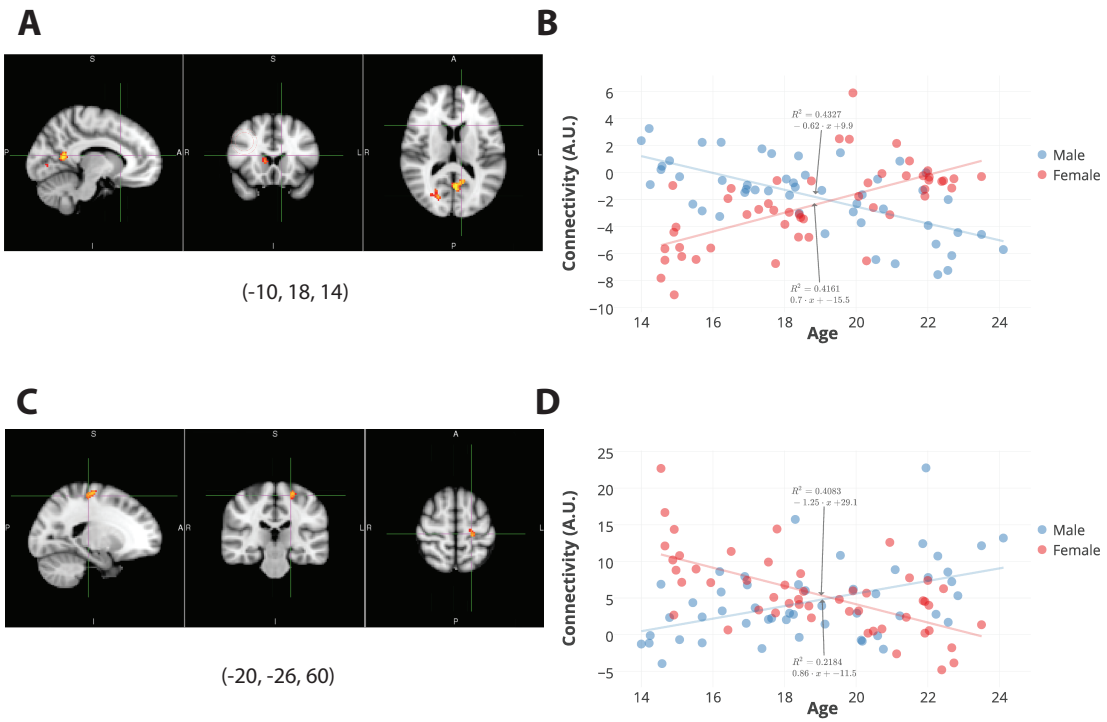

Figure 6.7: age-gender interaction related within network functional connectivity dynamics

A: within network age-gender interaction effects, with decreased connectivity in males and increased connectivity in females. B: corresponding parameter (beta) estimates for A (R^2=0.43 males, R^2=0.41 females). C: within network age-gender interaction effects, with increased connectivity in males and decreased connectivity in females. D: corresponding parameter (beta) estimates for D (R^2=0.41 males, R^2=0.22 females).

3. Between network functional connectivity dynamics

Connectivity between networks was computed using full correlation and L2-regularised partial correlation at a dimensionality of 50 (**Figure 6.8**). Hierarchical clustering revealed the individual ICA networks to be related to each other within higher functional domains (**Figure 6.9**). For example, individual ICA networks related to the default mode network were part of the same functional hierarchy, as were individual ICA networks related to visual networks.

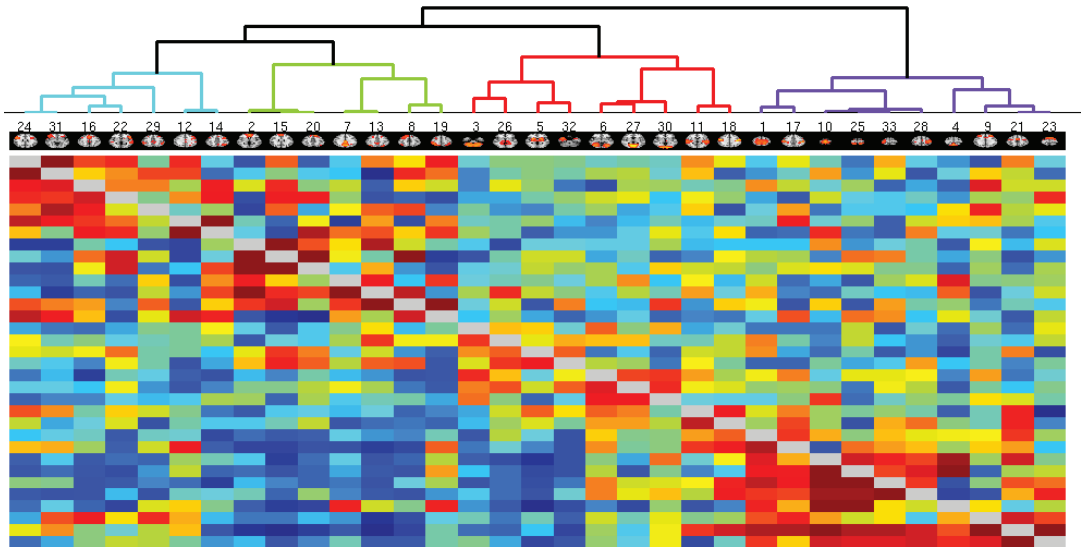

Figure 6.4.8: ICA based functional connectivity network

Connectivity matrix for links between ICA networks. Below the diagonal are Pearson correlations while above the diagonal are L2-regularised (Tikhonov or ridge regression) values (rho = 0.1) both after R-to-Z conversion. Note the later has a generally sparser matrix than the former. Above the matrix are individual ICA network images numbered according to **table 6.1** and arranged according to a hierarchical clustering algorithm (**section 2.2**) before being displayed in a dendrogram.

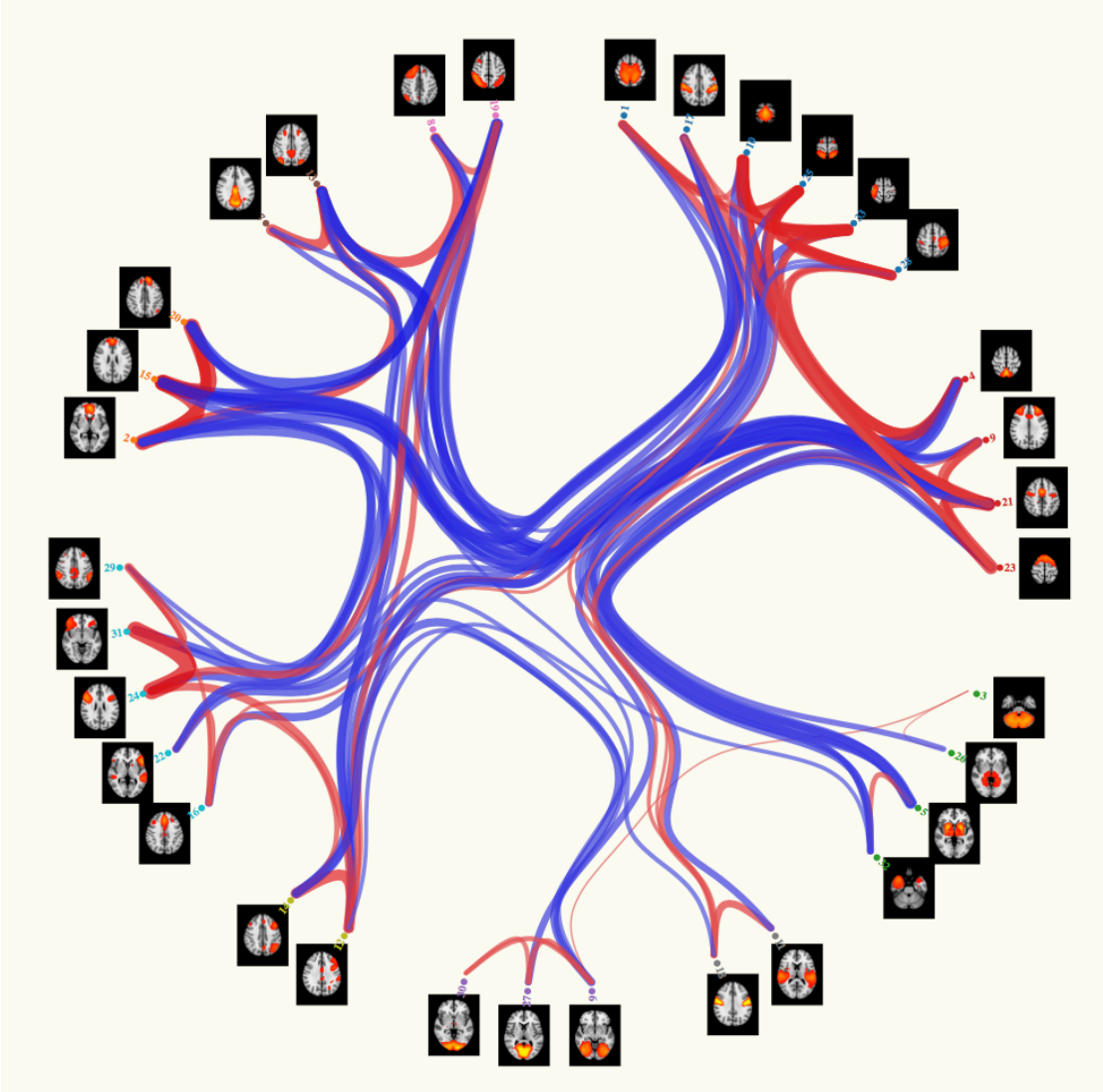

Figure 6.9: hierarchical functional connectivity network architecture

Circular representation of the connectivity matrix in **figure 6.8**. Images on the circumference correspond to individual ICA networks from **table 6.1**. ICA networks are arranged in clusters corresponding to the dendrogram levels. Links between individual ICA networks corresponding to Pearson correlations (after R-to-Z transform): thickness corresponds to connectivity strength and colour to direction (red = positive, blue = negative).

Age, gender, and age-gender interaction effects were present between ICA networks (**Table 6.3**) at 50 dimensions. Gender related changes were present while controlling for age (**Figure 6.10**). Females had higher connectivity between a predominantly left sided lateral fronto-parietal network and a bilateral prefrontal network (**Figure 6.10 A & B**). Males had higher connectivity between a cerebellar network extending into the middle cerebellar peduncles and a superior sensorimotor network, both of which were symmetrical (**Figure 6.10 C & D**). Age related changes were present with increased connectivity with age (while controlling for gender) between a superior sensorimotor network and a right superior lateral sensorimotor network (**Figure 6.10 E & F**). A reduction in connectivity with age was present between a predominantly left sided fronto-parietal network and a primary visual cortex network (**Figure 6.10 G & H**). Finally age and gender interaction effects were present (**Figure 6.10 I & J**). Connectivity between a predominantly left sided lateral fronto-parietal network and a right sided superior lateral sensorimotor network decreased with age in males but increased with age in females.

Table 6.3: between network changes – summary of findings

Contrast	Networks	Mean connectivity	P-value
Females > Males	31 & 1	-3.9373	0.01
Males > Females	24 & 10	0.3656	0.03
Increase with age	27 & 7	3.2301	0.05
Decrease with age	5 & 1	-1.004	0.03
Female increase with age / male decrease with age	27 & 1	2.5053	0.01

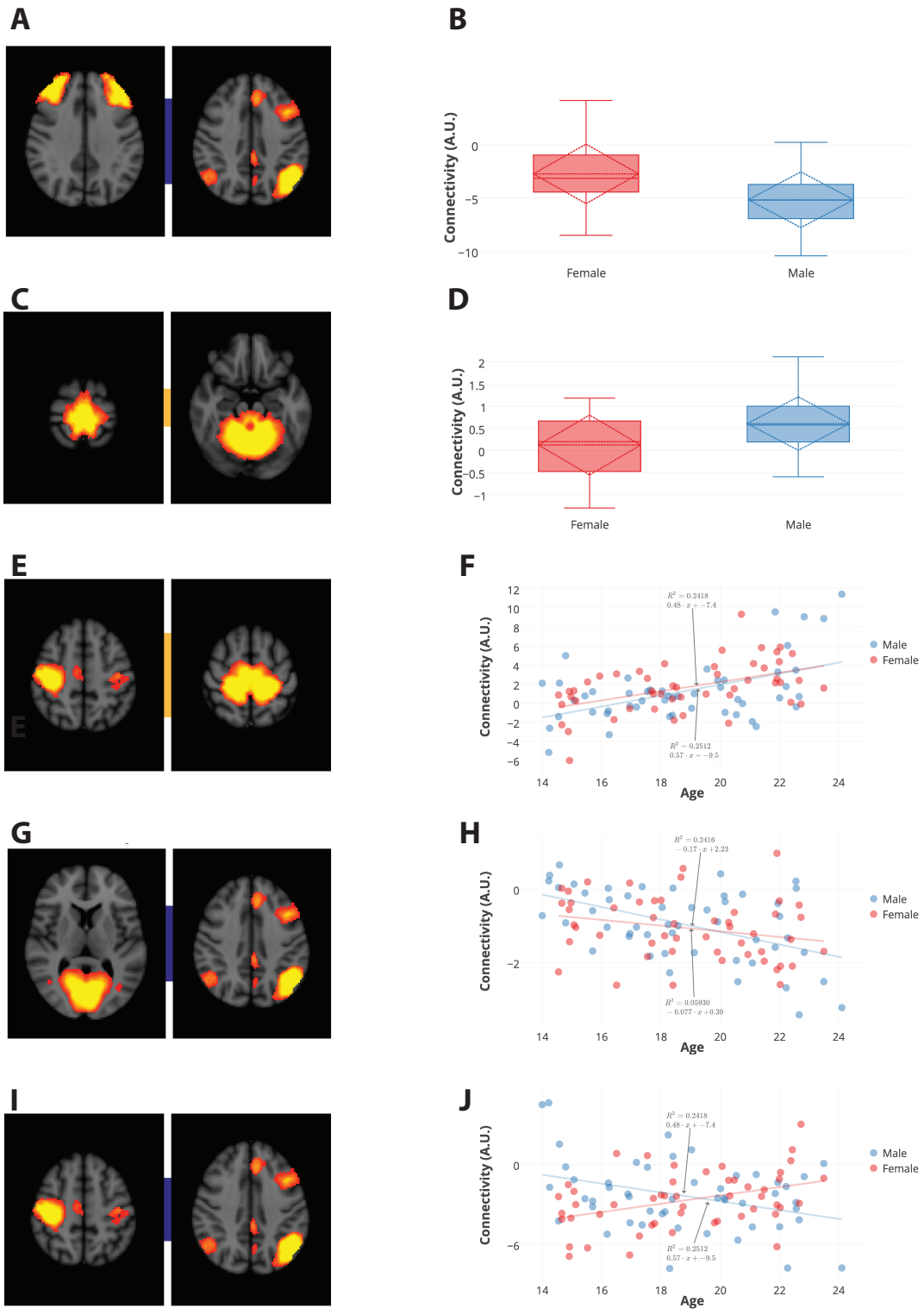

Figure 6.10: between network changes in adolescence

A & B: increased connectivity in females compared with males

C & D: increased connectivity in males compared with females

E & F: increased connectivity with age (R^2=0.24 males, R^2=0.25 females).

G & H: decreased connectivity with age (R^2=0.24 males, R^2=0.06 females).

I & J: age gender interaction effects (R^2=0.24 males, R^2=0.25 females).
On the left side of the figure each image corresponds to a single slice of the involved ICA network and the coloured bar between them reflects the mean network connectivity (size) and sign (colour). On the right, boxplots represent mean and standard deviations with additional diamond boxes reflecting medians and interquartile ranges.

DISCUSSION

In summary, discrete yet diverse changes were found in functional connectivity within RSNs related to gender and age during adolescence. These effects were spread over multiple ICA networks but typically involved the precuneus, isthmus of the cingulate gyrus, thalamus, and insula. Between network effects were also present and again involved complex changes related to gender, age, and age-gender interactions. These changes focused on only a selection of possible network combinations consistently involving a large left sided fronto-parietal network incorporating higher association cortices, and primary cortex networks involving the visual and sensorimotor regions including the cerebellum. Both within and between network changes were only seen at a low dimensionality analysis; automatic dimensionality estimation resulted in almost five times more networks, none of which demonstrated any changes related to gender or age in adolescence.

Synaptic refinement, otherwise known as pruning, is the predominant biological process occurring in this age range, together with on-going myelination. These neurodevelopmental processes are presumed to underlie the changes in functional connectivity seen in this present study. However, a link between actions at a synaptic level and functional connectivity changes is problematic due to the differences in resolution (nanometer to millimetre), timescale of activity (millisecond to low frequency 0.01-0.1 Hz oscillations), and underlying biological mechanisms driving the signal (long term potentiation and depression versus resting state BOLD contrast). Identifying an imaging proxy for these underlying biological processes will require higher order modelling such as graph theoretical analysis of complex brain networks.

Structural connectome data is believed to reflect direct axonal trajectories between regions and has found a general strengthening between hub regions during adolescence (Whitaker et al, 2016). Direct connectivity in functional connectome networks is more difficult to quantify due to indirect and non-anatomical (i.e. connectivity outside a recognised major white matter tract) paths between regions. In general, information flow within complex networks remains an open question; the most common means of quantifying communication involves calculation of the shortest geodesic path, but this relies on accurate computation of the statistical dependencies and conversion to distances in the first instance, and there is sparse evidence that this is actually the route chosen for any individual neural interaction. Consequently models of information diffusion (Misic et al, 2015) and indirect paths (Simas & Amaral, 2015) have gained traction and may prove to be more realistic models of network interactions. Resolving these issues with network communicability will allow the development of more realistic models of dynamics in these processes that may more accurately reflect synaptic strengthening or extinction.

Compared with previous studies using resting state networks in adolescent cohorts the changes identified here are consistent. Studies involving larger participant numbers, a broader age range, or fewer RSNs have tended to find more age related effects (Muetzel et al, 2016). Smaller studies and those with higher dimensionality RSNs tended to find smaller or less consistent changes (Jolles et al, 2011; Sole-Padules et al, 2016). In general, both the functional connectivity changes identified here and in the literature tended to be spatially discrete; that is, the majority of the grey matter was not found to be undergoing change. However the spatial extent of changes do not necessarily reflect their functional significance; it is quite conceivable that smaller focal changes in functional connectivity may achieve greater phenotypic effects than more extensive changes which may reflect an epiphenomenon such as myelination or cortical thickness maturation. Furthermore one would not necessarily expect the changes to be spatially extensive given that many higher order cognitive processes are already well established before or during early adolescence. Rather, one could argue for a more discrete re-tuning, such as in the dual systems model of protracted fronto-parietal activity and overactive subcortical activity (Duijenvoorde et al, 2015). This latter model would also be consistent with a ‘last in/first out’ theory of cortical maturation, whereby the brain network mature in a pyramidal trajectory, with the last

to mature also being the earliest to be affected in dementia (Douaud et al, 2015). These results are consistent with this focal but specific developmental emphasis.

The implications of these findings are important for subsequent group analyses; for example, analysing even a relatively narrow age range of between 14 and 24 years is likely to incorporate significant within group heterogeneity. Furthermore, there is evidence for distinct gender related dynamics during adolescence, suggesting that each sex should be analysed separately rather than together in a group. Dynamics in functional connectivity are not restricted to the higher association cortices typically thought to be undergoing the greatest changes during adolescence. This study has identified significant changes that are still occurring on primary cortices related to vision and sensorimotor function, subcortical nuclei including the thalamus, and the cerebellum. The latter is particularly significant as structural (grey matter and white matter) analyses do not often include the cerebellum because of technical difficulties related to segmentation on T1 images or motion with diffusion based imaging. Therefore, resting state fMRI is the sequence of choice for incorporating cerebellar dynamics during development.

Strengths of this study include firstly the large and balanced dataset involving 100 healthy participants evenly matched for age and gender. Data driven methods allowed a freedom from hypothesis constraint and maximise the ability of the data to reveal the underlying signal in an unbiased manner. A further benefit of these methods is their methodological robustness and strong underlying basis in statistical principles, suggesting that any identified changes are likely to be genuine rather than artefact related to unprincipled data processing. With this in mind it is notable that few studies have utilised these methods in full despite them forming a clear analysis pipeline (Bos et al, 2014; Filipini et al, 2009), and those that have commented upon the conservative nature of the changes found. Finally, a future benefit of this analysis is that the functional connectivity network can be used for a subsequent graph theory analysis whereby not only is the parcellation template customised to the group but also individualised for each participant. It is helpful that automatic dimensionality estimation and higher dimensionality parcellations are robust to any within group effects (such as during adolescence), which is advantageous for graph theory whereby

one wishes to focus on complex network topology rather than on the features of individual nodes or links.

Studying adolescence with neuroimaging requires careful attention to study design in order to draw reliable inferences. For example, cross-sectional or cohort designs only allow inference about inter-individual variability and not intra-individual developmental trajectories, which can only be characterised with longitudinal studies (Vijayakumar et al, 2016). Furthermore if the age range is large it is likely that variability within the cohort exceeds any age related effects (Schaie, 1994). Longitudinal study designs can obviate some of these difficulties but such studies are more costly and difficult to run (Mills & Tamnes, 2014). Relating dynamics to only age or gender and their interactions also misses out several drivers of functional connectivity dynamics. For example, endocrine effects including pituitary hormones have known effects on mood, cognition, and emotional lability, and are therefore likely to be affecting functional connectivity networks both temporally and to varying degrees between genders (Sisk & Zehr, 2005). Furthermore, the time of onset of puberty and consequent hormonal changes involved is another confound when using chronological age as a dependent variable (Satterthwaite et al, 2014). Onset of menstruation has historically been used to mark the onset of puberty in females and is known to be highly variable; in males however there is no such proxy available. Non-invasive hormonal profiling, for example through saliva samples, may allow a means of correcting for endocrine effects (Netherton et al, 2004).

In the future the natural way to develop these findings would be to perform a graph theory analysis on the resultant functional connectivity network. This could allow the application and development of network measures to capture synaptic refinement and myelination. For example, the indirect paths of a network could be used as a marker for synaptic refinement; as the majority of synapses are eliminated in preference to strengthening a minority of direct connections, the number of indirect connections would be hypothesised to increase. Therefore even if a node is originally weakly connected to all other nodes, strengthening a few connections may actually shorten the indirect paths involved i.e. the indirect path become ‘faster’ than direct paths. Consequently the proportion of indirect paths of a given node could serve as a marker for its stage of synaptic refinement, with more available direct paths suggesting higher

potential for plasticity and subsequent synaptic refinement. Applications semi-metric topology has shown promise in capturing direct and indirect paths (Simas & Amaral, 2015); this may represent a promising avenue for understanding network communicability and the effects of synaptic refinement.

CONCLUSIONS

Development in the adolescence to adult period is characterised by discrete but diverse age and gender related effects. Distinct gender related profiles in this developmental period are apparent with a propensity towards increased between-network connectivity in females than males. Observed effects are apparent not just in higher association cortices but also involve primary cortices, subcortical nuclei, and the cerebellum. Modelling synaptic refinement (for example with graph theory and semi-metricity) using these specific regions as pre-existing hypothesised regions of dynamic changes could reveal mechanisms applicable to brain repair and plasticity in later life.

CHAPTER 7: NETWORK TOPOLOGY AND ROBUSTNESS DURING ADOLESCENCE

Parts of this work were presented in poster format at the Society for Neuroscience meeting in San Diego, November 2016:

Age-dependent response to simulated brain injury in the functional connectome
M.G. Hart[1,2], E. Bullmore[1], R. Dolan[3], I. Goodyer[1], P. Jones[1], J. Suckling[1]

[1]Department of Psychiatry, University of Cambridge, UK, [2]Department of Neurosurgery, Addenbrooke's hospital, Cambridge, UK, [3]Wellcome Trust Centre for Neuroimaging, University College London, London, UK

PRECIS

In this final results chapter adolescent development is used to study how complex network topology affects the brain's response to injury. Specifically, the focus is on network robustness; that is, how a network can maintain its function upon injury. This also allows us to address a long-stand hypothesis in developmental biology on how the response to brain injury changes with age.

To do this a combined graph theory and percolation analysis is performed. Compared to previous chapters, the network analysis complexity is expanded to include the high dimensionality ICA based parcellation from **chapter 6** and negatively weighted graph theory measures. The overall aim is to relate the response to simulated brain injury with the underlying network topology.

This work will conclude the thesis by bringing together models of network resilience (**chapter 6**) and robustness elucidated from adolescent development to compliment the study of empirical brain lesions in neurosurgery (**chapters 3 & 4**).

INTRODUCTION

Clinicians have historically recognised that the brain's response to injury is critically dependent on age (Kennard, 1936, 1940; Dennis, 2010). That is, for any given injury, a younger patient would be expected to be initially functionally less impaired, and recover better, than an older patient with a similar injury. An extreme example of this hypothesis is how seemingly trivial brain injuries in elderly patients often have far-reaching consequences such as long-term hospitalisation, permanent cognitive dysfunction, and increased requirements for community support upon discharge. Despite the prevalence of this belief and its commonness in day-to-day clinical practice (Hart & Faust, 1988; Webb et al, 1996), there is very little scientific basis to explain the underlying neurobiological mechanisms involved. Understanding the mechanisms behind this variance in the brain's potential response to injury could allow one to better plan rehabilitation, improve supportive services to allow more effective integration into a community environment, and tailor acute therapies such as neurosurgical interventions to those most likely to benefit.

Historically, the field of age-related response to brain injury has enjoyed considerable academic interest. During the 1970s, driven in part by effective animal models and a dynamic scientific dialogue, the field was highly active (Dennis, 2010). This era is epitomised by the Kenard principle, which states that developmental recovery from injury is maximal during childhood then declines through adolescence (**Figure 5.1**). Intriguingly Margaret Kennard (1899-1975), the eponym of the theory, never stated such a simple relationship. Indeed she believed quite the opposite was true, with her considerable contributions to the field suggesting the response to brain injury was conditional on a number of variables, of which age was but one. Nevertheless, the eponym stood, possibly due to attempts to undermine her considerable contributions to the field that were often performed decades earlier (Dennis, 2010). Somewhat disappointingly however this fruitful field of research became less active over the coming decades despite never succeeding in creating a unified model to describe the clinical and scientific data (possibly related to a decline in appetite for using animal models).

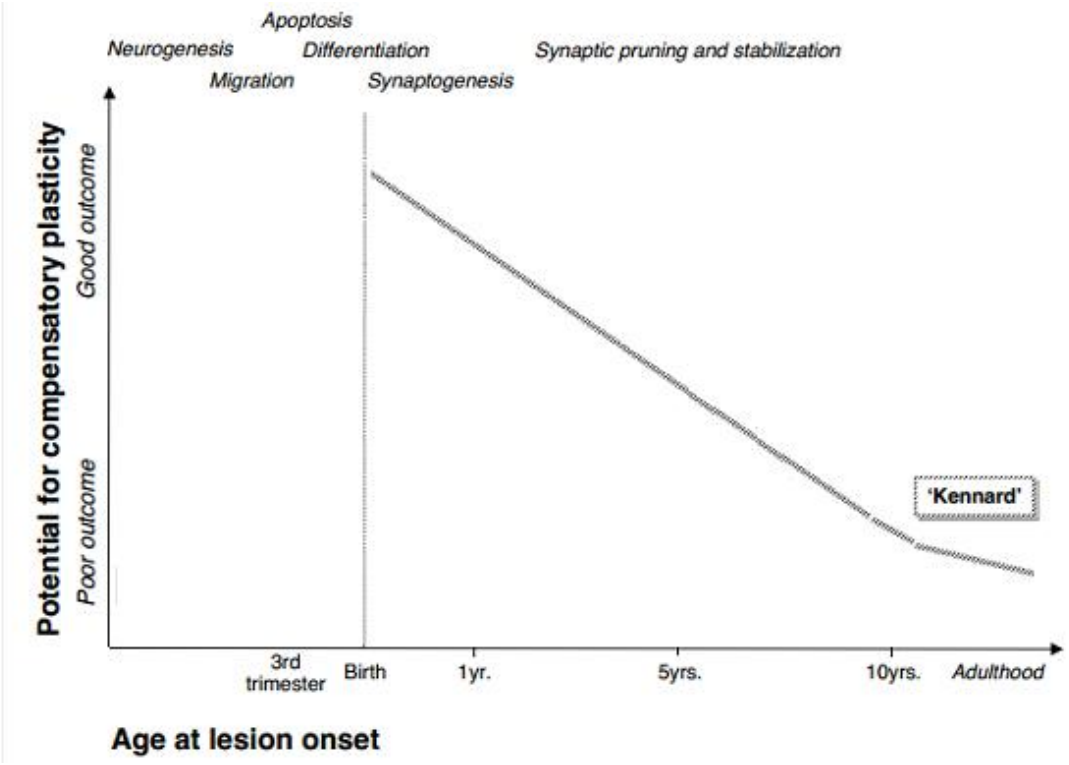

Figure 8.1: The Kenard Principle for neurorecovery

The relationship of the potential for brain recovery after injury plotted against age at onset of injury; the Kenard principle hypothesises that there is a negative linear relationship between the age and potential for a good outcome. The key developmental processes active at each age are highlighted above; the Kenard principle is believed to specifically relate to adolescent brain injury during which synaptic pruning and stabilisation are the main active developmental processes, although a degree of late myelination is probably also active. Adapted from: https://commons.wikimedia.org/wiki/File:Kennard_Principle.jpg

Comparative research in clinical populations has produced inconsistent findings. Typically studies group together a diverse range of brain injuries in order to allow sufficient numbers in each age group to allow meaningful comparisons. One recent study using a wide age range of participants between neonatal period and early adulthood suggested an inverse quadratic relationship between age and response to injury, with the extremes of age having the most severe consequences while the intervening period including adolescence was more benign (Anderson et al, 2009).

Increasingly studies have started to look at longer-term data, albeit at a retrospective level. These studies, usually performed in cohorts that have sustained serious illness or brain injuries in childhood, have consistently demonstrated that long-term cognitive sequelae are more common than previously appreciated, and that deficits are often not recognised without specific testing (Kesler, Gugel, Huston-Warren, & Watson, 2016; Yuan et al, 2014). These findings open up the possibility that previous studies suggesting good outcomes after early brain injury lack sensitivity to detecting late cognitive dysfunction, and are therefore over-estimating potential recovery.

These discordant clinical findings have led to two distinct hypotheses on the vulnerability of the developing brain. On the one hand there is the developmental plasticity hypothesis defined by the Kenard principle that states age at injury onset is inversely related to the probability of recovery, the inference being that younger people have a greater potential for plasticity. Studies consistent with this hypothesis focus on early brain injury and language (Ballantyne et al, 2008; Heywood & Canavan, 1987; Smith & Sugar, 1976; Taylor & Alden, 1997), including left hemispherectomy for epilepsy (Dennis & Whitaker, 1976). On the other hand there is the early vulnerability hypothesis defined by Hebb, whereby the younger brain is more susceptible to injury (Hebb, 1949). Studies consistent with this approach have focused on global rather than focal brain injury and more extensive age ranges of participants (Anderson & Moore, 1995; Anderson et al, 2004, 2005; Gronwall et al, 1997; Taylor et al, 2002). A notable confounding factor with all of these studies is the variability in brain injuries that occur with time. That is, injuries that are common in infancy (e.g. developmental and ischaemic, both usually bilateral and involving subcortical structures) are different in their nature, extent and location than those that occur in later childhood and into adolescence (e.g. neoplasia and traumatic brain injury, both typically focal and hemispheric).

Network science and graph theory offer an attractive analytical approach to reinvigorating interest in this uncompleted and clinically relevant field of research. In particular, network models offer tractable analytical solutions to modelling *in silico* brain injury, often drawing on a diverse range of influences including statistical

physics and random graphs (**chapter 1**). The response of the brain to injury can be defined in a number of ways, including initial robustness to injury; resilience or potential for recovery; and redundancy or capacity of the remaining brain to compensate for the loss of function due damage elsewhere (akin to the concept of cognitive reserve).

Typically network science applies percolation theory to study brain robustness, whereby upon removal of network elements there is a transition in some global network property. Removal of nodes can be done in a random manner (known as random error) or by targeting some nodes based on a measure of their centrality (focused attack). A key finding from early percolation studies of complex networks demonstrated a link between scale-free architecture and the emergence of hubs with increased robustness to random error but vulnerability to focused attack (Barabasi & Albert, 1999). Conceptually one can imagine how in a scale-free network with hubs, random error is most likely to select a low-degree node with little impact on the network of its removal, while focused removal of hubs would be expected to have a disproportionate effect on the network and hence vulnerability to focused attack (this is also where the term 'weak links' originated).

Previous studies using network percolation to understanding brain injury have agreed in general that the brain's network architecture is remarkably robust to injury. However, despite elegantly describing the relationship between degree distribution, network architecture, and simulated brain injury, these studies gave little information behind the driving forces behind the changes. In particular, it is unclear whether the brain's robust design is a goal of its maturational processes, or a consequence of some other developmental process, such as the emergence of hubs and the rich-club phenomena. Also the dynamics of the changes have not been described; that is, while it is known that the brain is robust to injury, it is not known whether this evolves with time and over development, or whether robustness is a universal feature of brain networks, independent of its development.

Development, as well as potentially affecting the network architecture and thereby robustness, may also define network resilience or recovery from injury. Key developmental processes at a microstructural level that are occurring during this

period are myelination and synaptic refinement. Conceptually the brain at onset of adolescence is viewed as being completely but weakly connected, while over the coming years the majority of these connections are simply removed or refined, while those that activate in unison are strengthening, akin to Hebbian learning. At a macroscopic network level these dynamics are reflected as: increased long-range as opposed to short-range connectivity with resultant improvements in network integration; transformation from mainly local, short-range and anatomical connectivity to long-range functional connectivity; and an increasingly modular organisation with modules becoming more connected within themselves but more segregated from each other. Hubs are believed to play a critical role in healthy adult brain networks and perhaps unsurprisingly their rise during adolescence is a key feature believed to underpin higher cognitive development (Baker et al, 2015; Grayson et al, 2014; Hwang et al, 2013; Whitaker et al, 2016). Specifically, hubs are a key location for structural and genetic changes, and become more strongly connected within each other, forming the so-called rich-club architecture. A challenge for the field is to relate these microstructural and macrostructural changes. In particular, it would be attractive to know what connections are still available, what is the potential for recovery, and how one can see the conditions required to predict Hebbian learning and synaptic strengthening.

One potential avenue to link micro and macroscopic changes is semi-metric graph theory analysis (Simas & Rocha, 2015). This is based on the premise that the most functional link between any two given nodes may not be the direct link but rather an indirect path (**section 2.3**). Semi-metricity refers to the ratio of these direct to indirect connections, with a higher proportion of indirect connections reducing the semi-metric percentage. In terms of development, one could imagine how synaptic refinement would reduce the number of direct connections to other nodes, and hence increasing the indirect connections (and therefore node semi-metricity). Therefore high semi-metric percentages would serve as a proxy for immaturity in synaptic refinement (most connections are indirect), and potentially a biomarker for the number of synapses available (and therefore plasticity). Alternatively, if in early adolescence most connections are direct but weak and the link-strength distribution is heterogenous, it could be that indirect connections are more prevalent. In this case

increased synaptic refinement may not change overall graph semi-metricity percentages but the indirect paths would get shorter.

This current work focuses on developmental dynamics of *in silico* brain injury. In particular, a goal was to test the Kenard principle and whether the consequences of brain injury were related to age at onset. A further goal was to determine how the underlying network architecture related to robustness. Specifically, prior studies identifying emergence of hubs, modules and rich-clubs in development (Baker et al, 2015; Gu et al, 2015) would imply the brain develops more weak links and a greater vulnerability to focused attack but with improved robustness to random error. These aims can be summarised by the following hypotheses:

1. What are the graph theory markers of healthy brain development over adolescence, and do they reflect an emerging hub-based or rich-club architecture?
2. Is there an alteration in the brains response to injury during adolescence development?
3. Are there dynamics in the spatial location of vulnerable areas, otherwise known as weak links, in the network?
4. Finally, can synaptic refinement and plasticity be reflected at a macroscopic level through the analysis of network paths and semi-metricity, as a proxy for network resilience?

METHODS

The study population consisted of the full NSPN interim cohort described in **section 2.1**. Study design, participant demographics, MRI sequence parameters, image pre-statistical processing, and initial network construction are described in **section 2.2**. Specific analysis features specific to this chapter are presented below, including details on network construction, network percolation, and statistical testing. An overview of the imaging and network analysis methods is presented in **figure 7.2**.

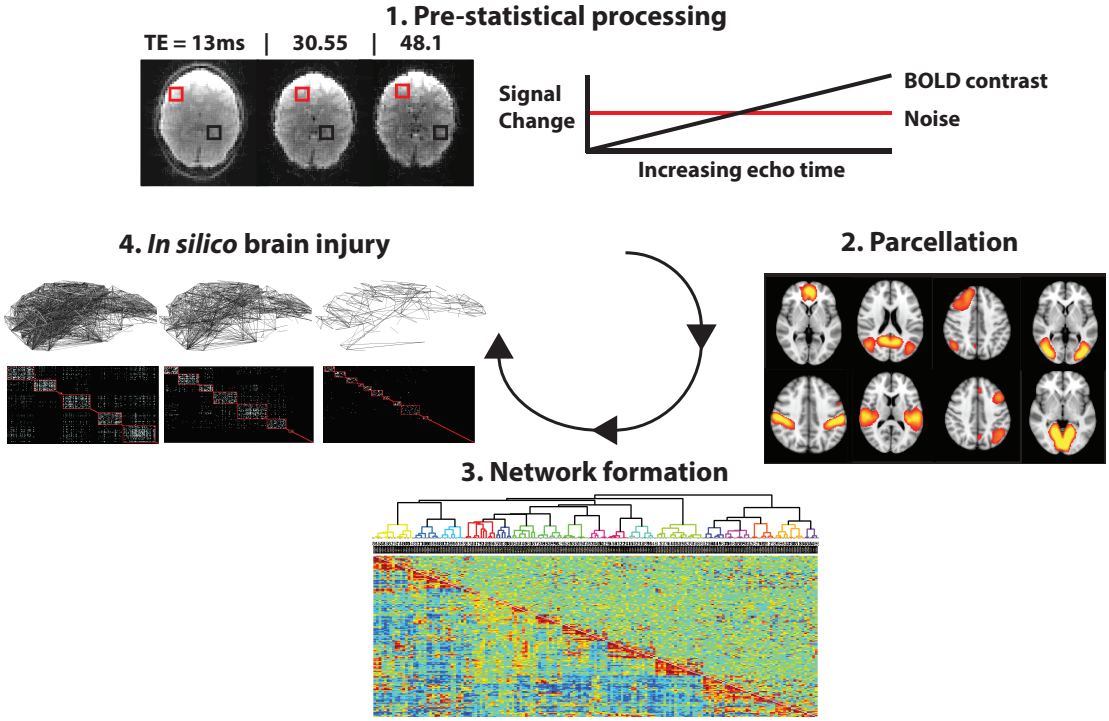

Figure 7.2: overview of specific methods used for network robustness analysis

Resting state functional MRI data was processed and de-noised using multi-echo independent component analysis (MEICA). Subsequently a group ICA was performed with automatic dimensionality estimation of 230. Connectivity matrices were subsequently formed by computing the statistical dependencies (Pearson product moment correlations) between pairs of ICA networks for all possible pairs. Finally percolation of the individual ICA-based connectivity matrices was performed for each node either individually (resulting in delta centrality measures or percentage changes in global measures from baseline before and after node removal) or sequentially, through targeting nodes either randomly or in a manner focused on properties of the individual nodes.

Network construction & parcellation

Node construction was based on an ICA-based parcellation used in **chapter 6** using individual representations (calculated through dual regression) of group ICA networks. That is, each node was an individual subject's representation of a group ICA 'network'. This allowed testing of the template for stability of changes across development both within and between nodes. Consequently, if any changes were identified in the response to brain injury, one could be confident that these were

specifically due to network architecture rather than changes within the template itself. A 230-dimensional parcellation selected using the Laplace approximation to the Bayesian evidence of the model order (Beckmann & Smith, 2004; Minka, 2000). The high dimensionality of the ICA decomposition allowed sufficient resolution to capture complex network topology, minimised the spatial extent of parcels, and often reduced spatial 'splitting' of individual parcels, all of which are recognised compromises when implementing ICA-based parcellation. A final advantage of using an ICA template was that it allowed a parcellation unique to each study participant and to the complete cohort, which was important given the ages and age-range involved and putative development changes believed to be occurring.

For each subject, the 230-node time series were fed into network modelling, creating a 230x230 node matrix of connectivity estimates. Network matrixes were calculated using full correlation (normalised covariances); other connectivity measures were too computationally burdensome to implement in the repeated manner required for percolation analysis.

Focal lesioning

Individual node vulnerability was performed by removing each node (and all of its connections) from the network, then calculating the percentage change of selected global graph theory measures. In addition to removal of the node in question its original time series was also regressed to minimise its residual influence on the subsequent network. Historically delta centrality has been used in the context of changes in global efficiency, where it is known as delta efficiency. In addition, the following weighted global topology measures were used as well: assortativity; transitivity; and modularity "Q" score (for negative measures). This method allows one to detect weak spots, analogous to the Achilles heel of the network, that cause disproportionate effects on network topology upon their individual removal.

Cumulative lesioning

Global network robustness was tested by node removal (also known as site percolation), which involved removing a node and calculating global network measures then repeating this process sequentially over all nodes in the network. Focussed attack involves targeting nodes for removal in order of specific graph theory

measures designed to capture centrality, which in this study were: nodal strength; clustering; closeness centrality, betweenness centrality; within-module degree z-score; between-module participation co-efficient; eigenvector centrality; and semi-metric percentage. Additionally, a cumulative hub score was calculated whereby each node scored a point for being in the top ten for each of the above centrality measures: those nodes that then had the highest cumulative score across measures were defined as hubs upon which the attack was focused. When multiple nodes had equivalent rank their order of removal was decided randomly.

Random error involved selecting the sequence order for nodes to be removed in a randomised manner. For this study 25 separate random number sequences, all generated from a standard seed point using the Mersenne Twister, to aid repeatability. These vectors for node removal order were tested across all subjects, resulting in the same 25 random error sequences for each subject. Results were then averaged across all 25 randomisations.

Historically changes in the giant component have been used to model percolation with focused attack and random error (Albert & Barabasi, 2001). In this approach there is a criticality or phase transition where the network goes from connected to disconnected (**Figure 7.3**). In random graph theory, this phase transition and the features required for its prediction (specifically a mean degree of 1), has been well characterised (Erdos & Reny, 1959). However, in the case of fully connected connectomes with *NxN* edges, this phase transition only occurs after greater than 99% of the edges have been removed (**Figure 7.4**). This limited the potential to demonstrate any changes between groups, as well as the potential relevance of any changes at the far end of the spectrum. Therefore for both focussed attack and random error global graph theory outcome measures were the same as for individual lesioning. Changes in measures were computed as percentage changes compared to baseline to account for changes in individual measures across the study cohort.

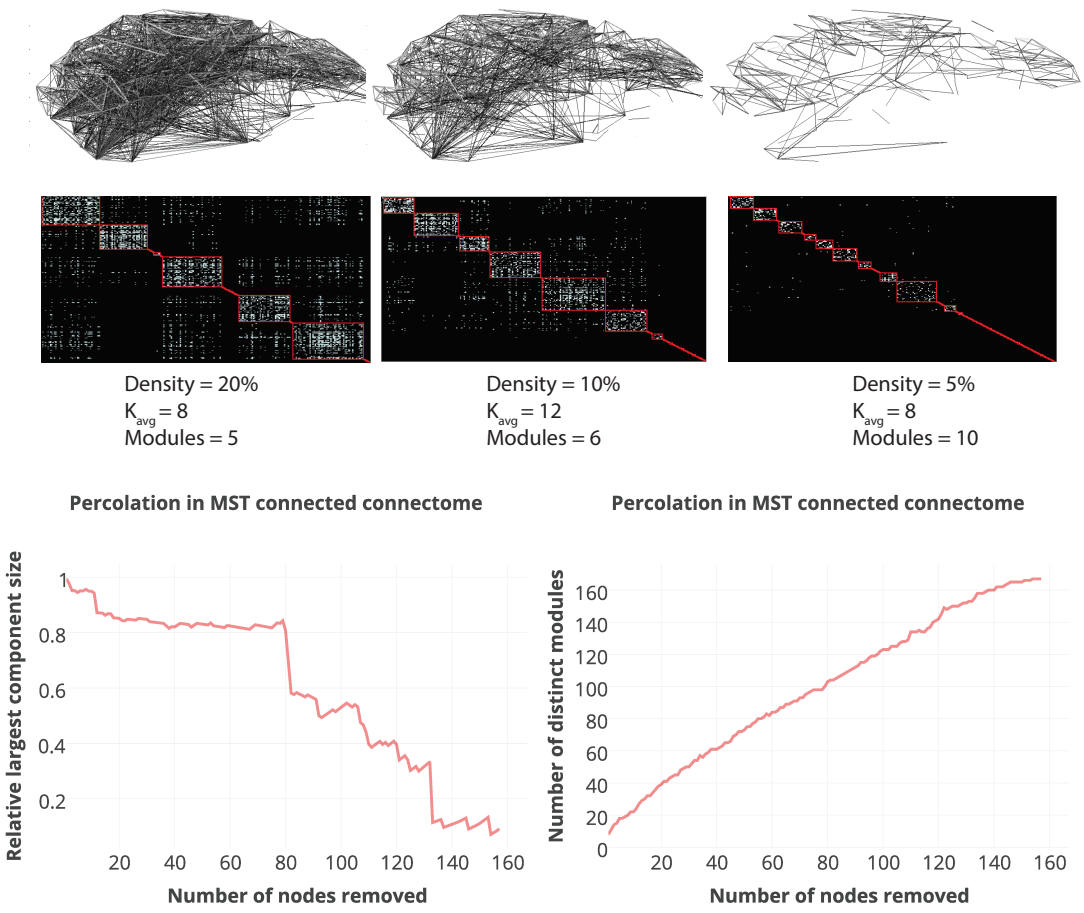

Figure 7.3: methodology for percolation theory analysis of connectome data

Connectomes are gradually reduced in density through random removal of connections (edges). This results in a gradual increase in the number of modules as isolated components are counted separately. In a network that is originally sparsely connected, disconnectivity is prevented by the use of minimum spanning trees (MST). When these networks are percolated, the giant component demonstrates an early transition to disconnectivity, followed by subsequent larger step-wise decreases at approximately 50% and 90% disconnectivity.

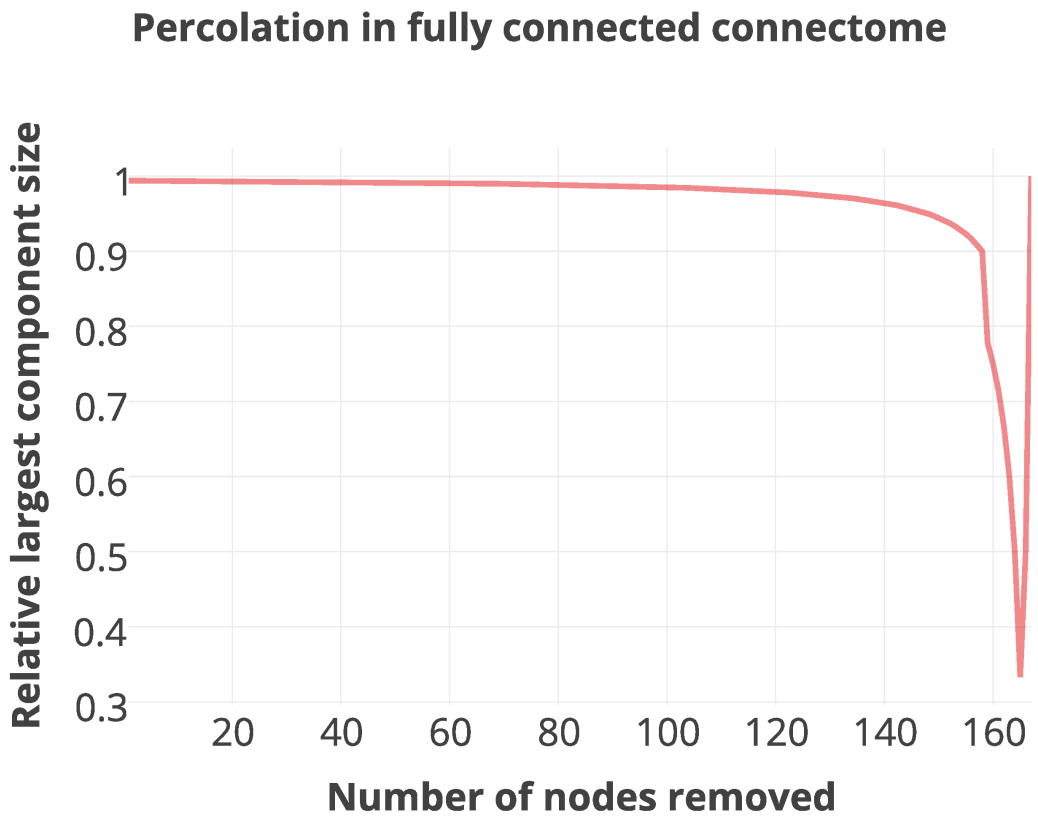

Figure 7.4: giant component changes in fully connected networks

In a fully connected network a significant change in the giant component is only apparent when over 95% of nodes have been removed. Relative size is the number of nodes in the giant component versus all possible number of nodes remaining in the network, hence the large increase for the final node.

Statistical analysis

Between subject statistical comparisons were performed by computing the area under the curve for each measure. A linear model was used for comparisons with age and gender as covariates including their interaction effects together with permutation testing (10000 permutations). All comparisons were computed for the false discovery rate (FDR) rather than family-wise error given that the number of comparisons per family was proportionate to the number of nodes and somewhat less than when performing comparisons at the edge level, where the number of comparisons would be *NxN*. Significance was defined as $p<0.05$ after correction for the FDR.

RESULTS

1. General topological properties

Global graph theory measures include small world architecture, defined in **section 2.3**. In this analysis of fully connected (i.e. unthresholded) networks, there was a propensity to a lattice-like rather than small world or randomised network architecture (**Table 7.1**). This is in contrast to other network analyses that use thresholded connectivity matrices; in this instance typically a Humphries small world score would be approximately 1.5 (**section 7.2**). This variation is consistent with predictions that generating appropriate lattice and random comparison networks is more limited when networks are non-sparse i.e. there is less variability with which to randomly generate different null models.

Humphries	Latora	Telesford
1.04 (+/- 0.01)	0.67 (+/- 0.04)	0.61 (+/- 0.03)

Table 7.1: Small world network properties

Definitions of the different means of characterising small world properties are given in **chapter 2**. Values are mean (standard deviation). A Humphries score of ~1 and Latora and Telesford scores of <1 are consistent with a lattice like topology.

Analysis of network cost and its relationship to global graph theory measures revealed the most of the variation to be occurring when networks were sparse i.e. at low cost (**Figure 5.5.5**). Typically the most dramatic changes were seen at very low cost (<5% connection density) for measures relating to network distances (closeness and betweenness), a reflection of network disconnection. However, changes in most global graph theory measures were still occurring even at 40% cost. Increasing network cost results in measures that are more stable and therefore any changes in values are less likely to be an effect of a particular threshold.

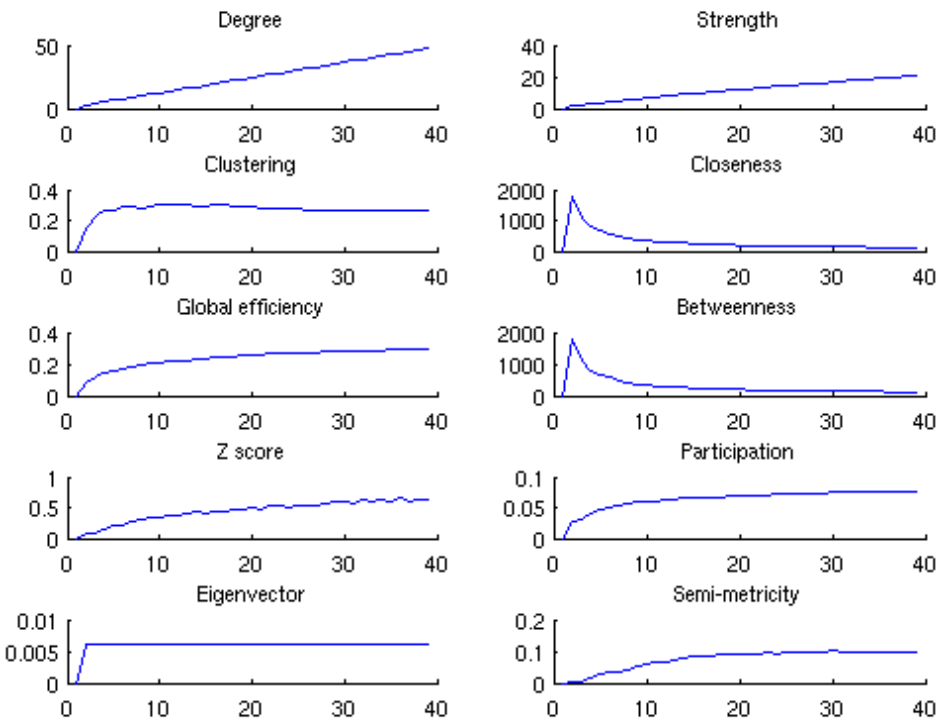

Figure 7.5: global graph theory measures and network cost

Changes in 10 global network properties (weighted, non-negatively weighted) with network cost. Only a single group average connectivity network was tested. As cost increases there is initially an increase for most measures, most dramatically for those that involve distance measurements that are adversely affected by network disconnectivity, but these measures then reduce as the network becomes increasingly connected. Subsequently most measures showed slower increases except degree and overall strength, while centrality measures such as betweenness and closeness peak early and then decline as more paths are added.

2. Global graph theory measures

The only global graph theory measure that demonstrated changes with gender, age, or their interaction was modularity (weighted and signed), which demonstrated an overall increase with age (**Figure 7.6**). All other global graph theory measures (small worldness, mean strength, transitivity, assortativity, and semi-metricity) did not show any effects for any of the contrasts tested (gender, age, and age-gender interactions).

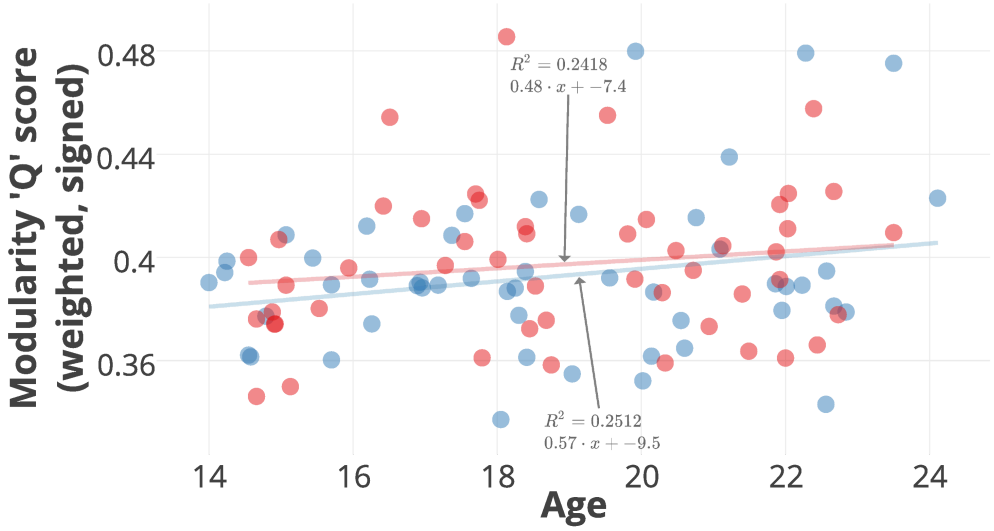

Figure 7.6: global modularity changes with age

Modularity was calculated with weighted and signed (negative value) networks. An increase in Q score reflects higher modularity.

3. Nodal graph theory measures

Statistical properties for the full set of nodal graph theory measures are shown in **Table 7.2**. Only eigenvector centrality demonstrated a significant number of nodal outlier values (10%). All measures were suitably normalised to approximately zero mean and unit standard deviation. Correlations between network measures are shown in **Figure 7.7**. This demonstrates that many network measures are significantly correlated with each other, and therefore analysis of the full set of graph theory measures incorporates a degree of redundancy. A subset of measures was chosen for further analysis in order to minimise this degree of inter-measure correlation. Graph theory measures were chosen on the basis of being of either of fundamental interest to graph topology (strength), the focus of significant attention in the existing literature (within module degree z-score, participation co-efficient, betweenness centrality), or potentially relevant to the underlying processes of adolescent development (semi-metricity as a proxy for synaptic refinement).

	Strength	Clustering	Local efficiency	Eigenvector	Within module degree Z-score	Participation coefficienct	Betweenness	Closeness	Semi-metricity
Mean	0	0	0	0	0	0	0	0	0
SD	0.84	1	0.83	1	0.79	0.58	0.54	0.84	0.88
Median	-0.07	0.07	-0.09	-0.11	-0.04	0.05	-0.10	-0.06	0.06
Range	3.66	13.07	3.85	9.17	3.62	2.81	2.51	4.09	3.76
Q_1	-0.56	0.02	-0.44	-0.11	-0.69	-0.35	-0.45	-0.55	-0.61
Q_2	-0.07	0.07	-0.09	-0.11	-0.04	0.05	-0.10	-0.06	0.06
Q_3	0.58	0.14	0.57	-0.11	0.50	0.37	0.30	0.55	0.65
SID	0.57	0.06	0.50	0	0.60	0.36	0.38	0.55	0.63
Outliers	0	1	0	10	0	0	2	0	0

Table 7.2: mean network measures statistical properties

SD = standard deviation, Q_1 = 1st quartile, Q_2 = 2nd quartile, Q_3 = 3rd quartile, SID = semi-interquartile deviation. Outliers are defined as values greater than 2 SD from the mean.

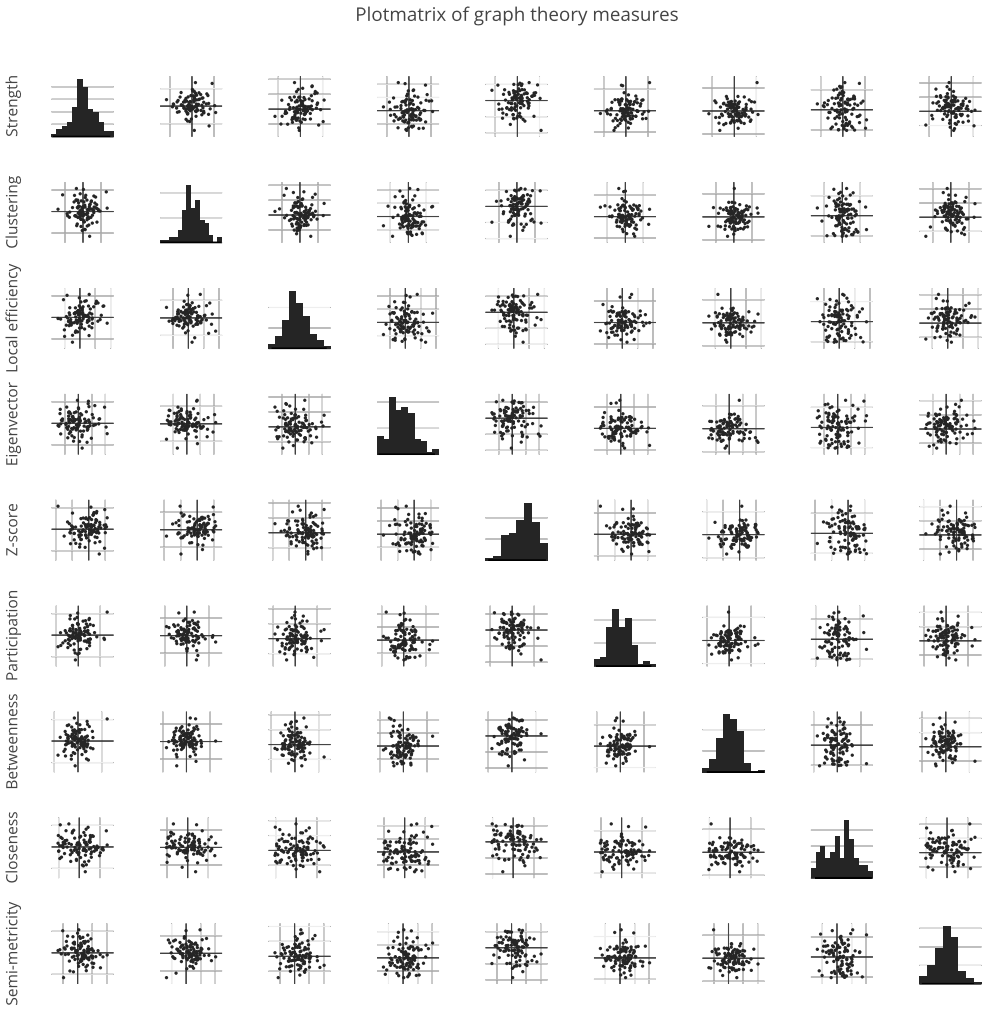

Figure 7.7: plotmatrix of nodal graph theory measures

Nodal graph theory measures are mean centred and normalised to unit standard deviation. Main diagonal elements are histograms

In contrast to global graph theory measures, nodal graph theory measures did demonstrate significant changes for all contrasts, albeit in a limited proportion of all total nodes (**Table 7.3**). Semi-metricity showed the highest number of nodes with significant changes identified for all contrasts tested. The next most sensitive measure was participation co-efficient, which showed changes across all contrasts, but fewer than semi-metricity.

	Strength	**Within modular degree Z-score**	**Participation coefficient**	**Betweenness**	**Semi-metricity**
Male > Female		37			159
Female > Male	167	38	28		13 24 156
Age increase	20 84	3 20	3		23
Age decrease		60		73	136 149
Male:age > Female:age	104 109	104 111		101	8 44 74 107
Female:age > Male:age	31	152		73 86	87

Table 7.3: nodal network measure changes

Contrasts are along the left axis and nodal graph theory measures along the top. Table entries refer to the nodes (ICA networks) where there were significant changes.\

4. Focused attack

Focused attack refers to the removal of individual nodes cumulatively until all nodes are eliminated, while targeting removal at those nodes believed to be most central to the network. Focused attack was performed targeting nodes based on centrality measures individually (strength, betweenness, within-module degree z-score, participation co-efficient, eigenvector centrality, or semi-metricity) or by taking cumulative centrality measures (nodes were more central if they consistently scored highly across a range of centrality measures). Outcome measures included those of global network architecture including global efficiency, transitivity, assortativity, and modularity. No significant changes were seen for any of the 10 focussed attacks for any of the 4 outcome measures (**Figure 7.8**).

5. Random error

Random error is similar to focused attack in that nodes are removed individually and sequentially until the network is completely absent, but in this case the targeting of nodes is done randomly. Outcome measures were otherwise as described for focused attack.

An age related increase in robustness to module breakdown upon random node removal (random error) was identified (**Figure 7.8**). Modularity is defined as the ability of a network to be split into distinct modules; a lower score therefore represents a less modular network. Typically as a network becomes more disconnected its modularity score increase as more modules can be formed from its disconnected components. With age this increase in modularity upon node removal was less apparent, suggesting networks were becoming less fragmented, and that they were able to maintain their original modularity for longer in the face of random error.

In contrast, the assortativity of a network upon random error increased with node removal, but this increase declined with age. Assortativity reflects the degree to which similar nodes connect to each other (i.e. hubs-to-hubs and peripheral-to-peripheral nodes), otherwise known as node homophily. An increase in assortativity upon random error suggests that most connections are heterophilic i.e. hub to peripheral. However a neutral response of assortativity suggests balanced homophilic and heterophilic connections i.e. hub-to-hub and hub-to-peripheral nodes, as in a rich-

club. Therefore the observation that the increased assortativity response to random error declines with age is evidence for a transition from initially hub-to-peripheral network to rich-club network architecture.

No significant change in other measures – including global efficiency and transitivity – were found with age, nor were any changes found related to gender, or age-gender interaction effects with any network measures.

6. Individual node lesioning & delta measures

Complex networks are predicted to have 'weak links', whereby the removal of certain node leads to a disproportionate effect on overall network function; this can be tested analytically with delta centrality measures. Overall the average delta centrality did not change with age or gender (**Figure 7.9**) suggesting that networks were not generally changing their overall distribution of weak links i.e. it wasn't a general feature for one group to have proportionately large delta centrality measures. However, within a given network, specific individual nodes did demonstrate gender, age, and interaction effects, although likely other nodal graph theory measures these changes were distributed across the minority of total nodes in the network (**Table 7.4** and **Figure 7.10**). Changes were most readily apparent when global efficiency or transitivity were used as outcome measures; assortativity or semi-metricity did not demonstrate any changes associated with the contrasts tested.

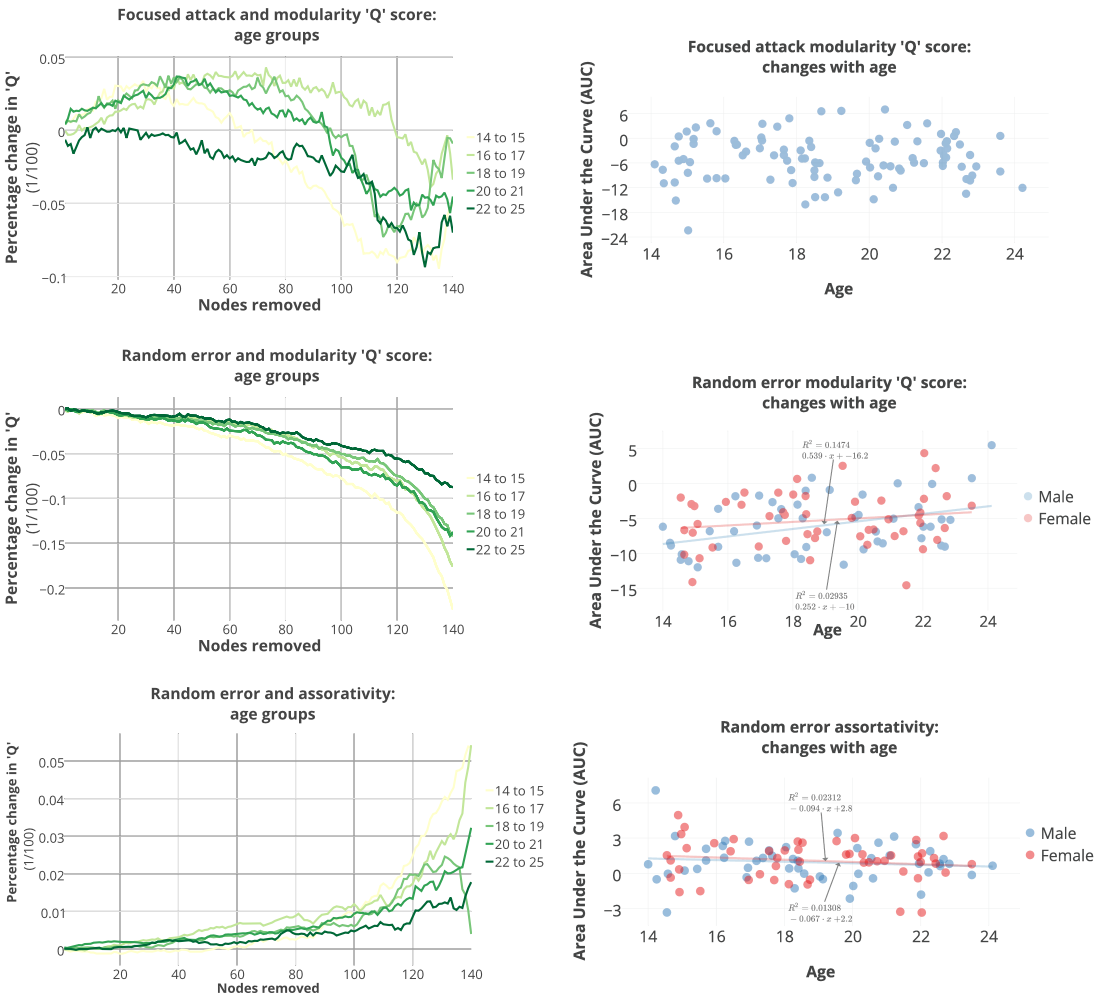

Figure 7.8: percolation theory analysis results

Focused attack, based on any one of 10 centrality measures, did not result in consistent changes for any of the 4 outcome measure across age groups, and consequently when analysing the area under the curve (AUC) per subject did not demonstrate any well fitted trend. In contrast for random error there was a consistent effect in modularity with the greatest change in the youngest group and the smallest change in the oldest group. Negative values reflect a percentage increase in modularity compared to the within-subject baseline. This time when the AUC was analysed as a feature of age there was a clear linear relationship with age (i.e. the area under the curve became less negative). Assortativity showed the opposite trend to modularity in random error. In this instance the assortativity decreased with node removal (reflected by the positive values), and this increase was most marked in the youngest age group and least apparent in the oldest age group. When the AUC was analysed there was a clear linear relationship towards increased robustness with age.

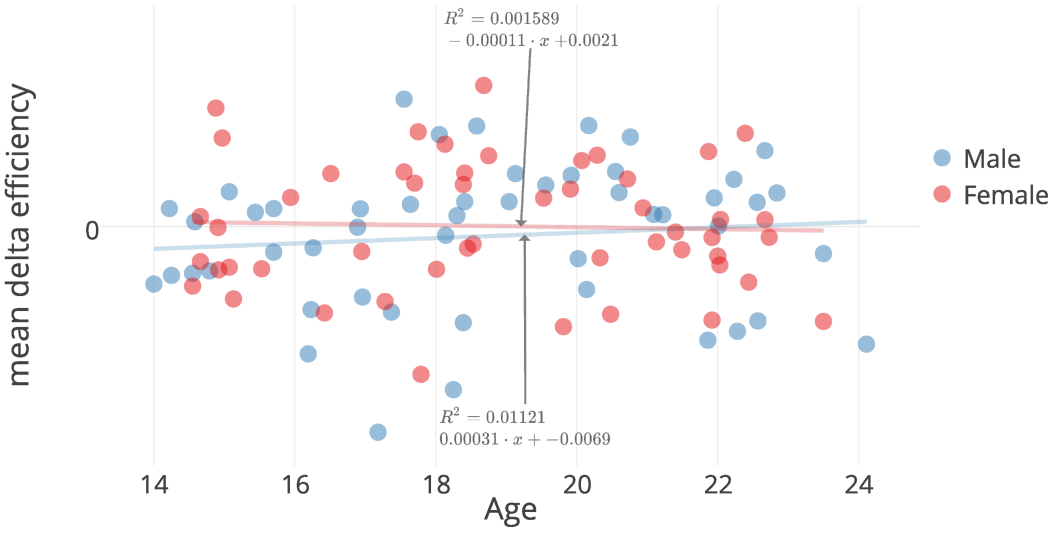

Figure 7.9: mean delta centrality with age

The average delta centrality of any node within a network did not change with age or gender or their interactions.

	Delta efficiency	**Delta transitivity**
Male > Female	48	50
Female > Male	118	-
Age increase	86	20, 21, 52, 86, 88, 112, 128, 153
Age decrease	4	-
Male:age > Female:age	-	29
Female:age > Male:age	19	-

Table 7.4: significant results for delta centrality measures

Contrasts are shown on the left axis, delta centrality measures across the top. Only delta efficiency (global efficiency) and delta transitivity are shown; delta assortativity and delta semi-metricity did not show any significant changes. Table entries refer to the ICA network nodes displaying the changes.

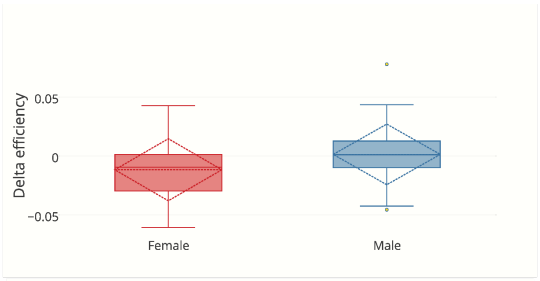
Delta efficiency
0.05
0
−0.05
Female
Male

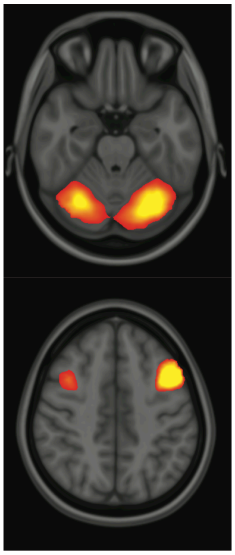

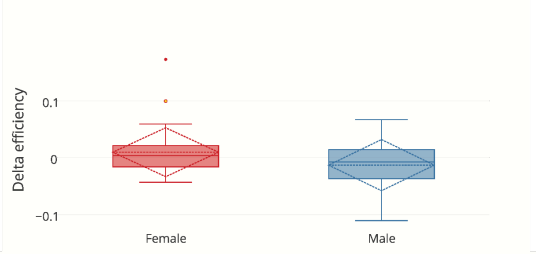
Delta efficiency
0.1
0
−0.1
Female
Male

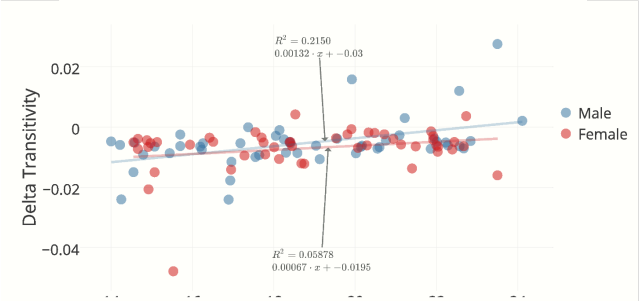
$R^2 = 0.2150$
$0.00132 \cdot x + -0.03$
$R^2 = 0.05878$
$0.00067 \cdot x + -0.0195$
Delta Transitivity
0.02
0
−0.02
−0.04
Male
Female

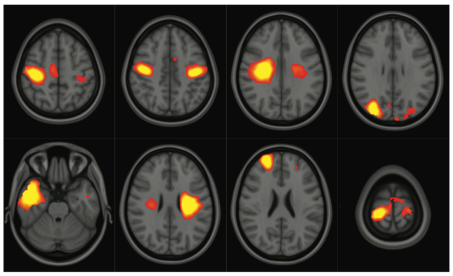

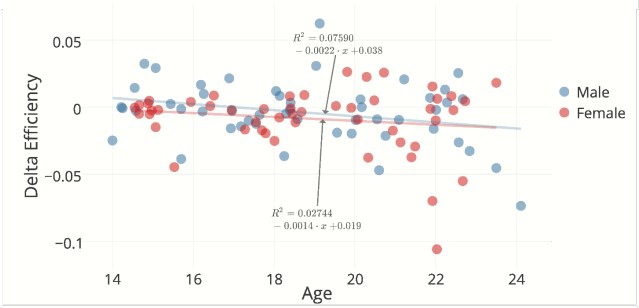
$R^2 = 0.07590$
$-0.0022 \cdot x + 0.038$
$R^2 = 0.02744$
$-0.0014 \cdot x + 0.019$
Delta Efficiency
0.05
0
−0.05
−0.1
14
16
18
20
22
24
Age
Male
Female

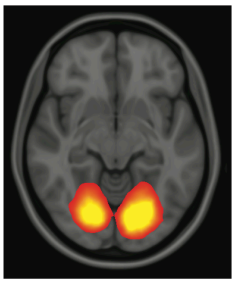

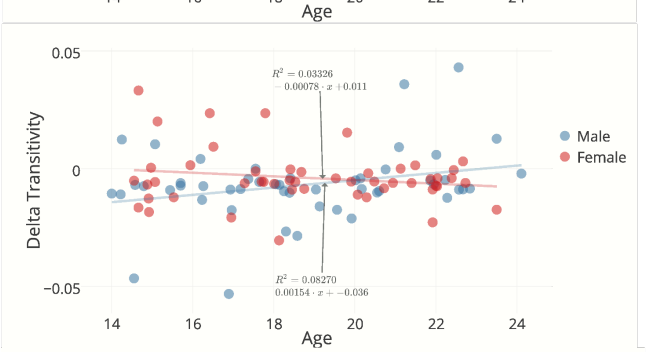
$R^2 = 0.03326$
$-0.00078 \cdot x + 0.011$
$R^2 = 0.08270$
$0.00154 \cdot x + -0.036$
Delta Transitivity
0.05
0
−0.05
14
16
18
20
22
24
Age
Male
Female

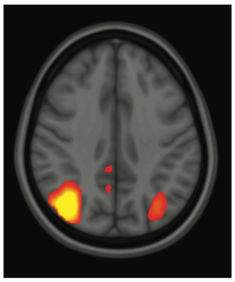

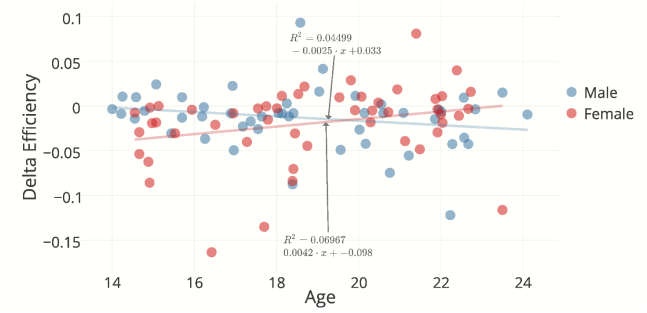
$R^2 = 0.04499$
$-0.0025 \cdot x + 0.033$
$R^2 = 0.06967$
$0.0042 \cdot x + -0.098$
Delta Efficiency
0.1
0.05
0
−0.05
−0.1
−0.15
14
16
18
20
22
24
Age
Male
Female

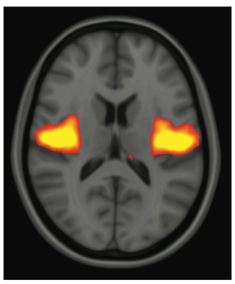

Figure 7.10: focal lesioning and delta centrality measures

Negative values refer to the percentage change in centrality lost upon node removal for either transitivity or global efficiency i.e. a more negative value implies more of the measure in question is lost on node removal and therefore that the node has higher delta centrality. A bilateral cerebellar hemisphere network is more vulnerable in females than males. A predominantly left sided lateral frontal network is more vulnerable in males than females. A reduction in delta transitivity was seen with age in eight predominantly higher association networks. An increase in delta efficiency with age was seen in an association visual network. Finally a lateral sensorimotor and predominantly right sided lateral parietal network showed interaction effects with age and gender. Notably nodes demonstrating changes in delta centrality tended to involve higher association rather than primary cortices.

A key feature of delta centrality analysis was the disproportionate number of nodes that became more robust with age i.e. their removal was more detrimental in younger rather than older participants. When the core structure of this hub network cluster was analysed the overall positive strength between these nodes increased with age, while their was no change in their negative strength (**figure 7.11**). Overall this suggests that this individual clique is becoming more connected within its self. This observation therefore explains the reduced effect on transitivity for removal of an individual node; if all the hub nodes are well connected within each other, removal of a single node will have a less deleterious effect than if connectivity was lower. Furthermore, this highly connected core serves to limit the effects of sequentially removing many hubs, as the positive assortativity within this network serves to protect the remaining nodes.

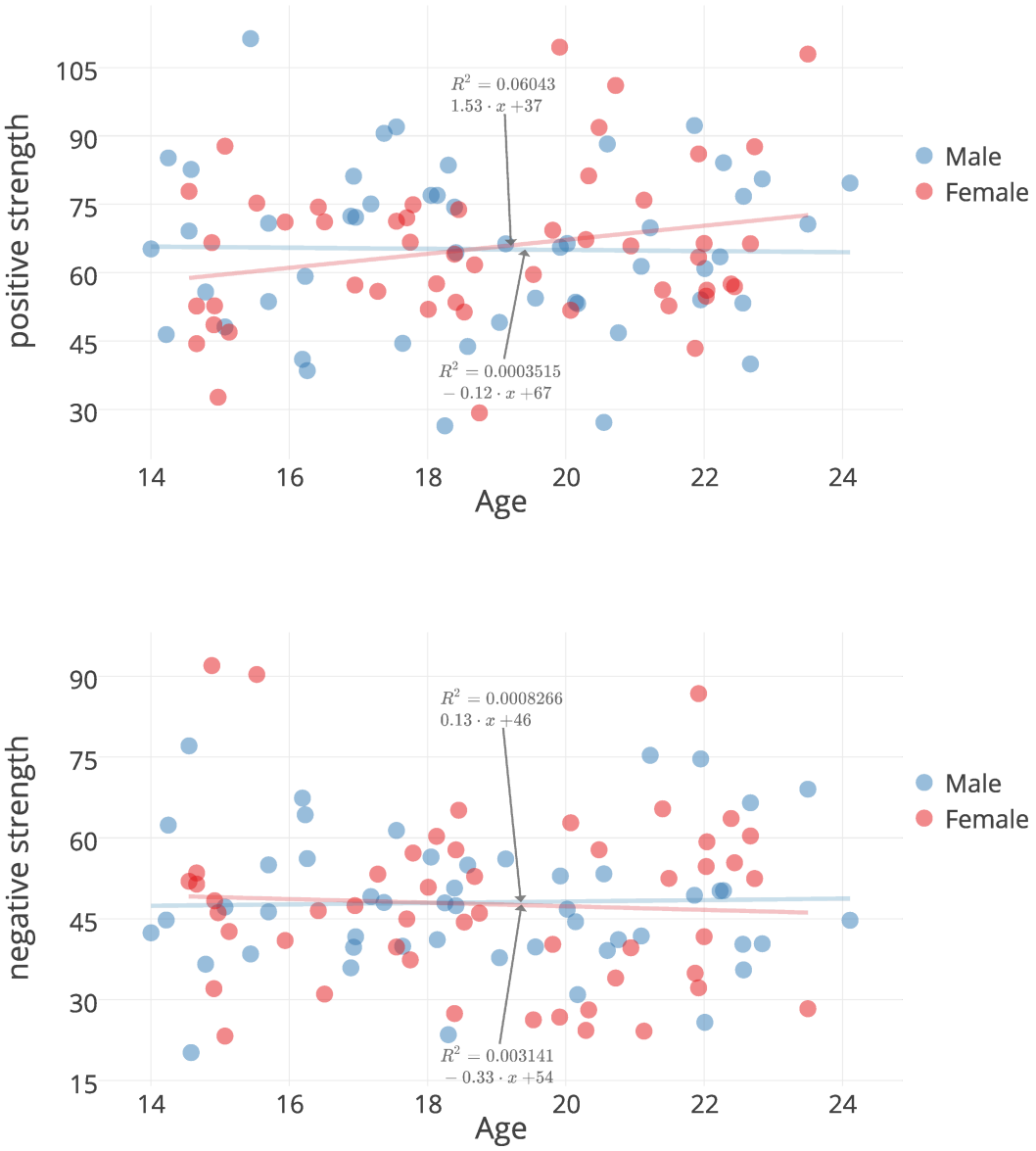

Figure 7.11: between delta centrality hub strength with age

Changes in total strength between delta centrality hubs: linear increase in positive strength (top) and stable negative strength (bottom).

DISCUSSION

In summary, brain networks demonstrated stable global graph theory properties throughout adolescence, but featured specific local nodal changes both with age and gender, particularly for semi-metric connectivity. During adolescence networks became more robust to random error. Specifically, younger participant's networks became fragmented and lost hub-to-peripheral connections. However in older participants formation of hubs and a rich-club architecture ameliorated these effects. Despite these changes in random error there was no corresponding effect in response to focused attack. Single node lesioning identified numerous 'weak links' within the network that demonstrated diverse changes with gender, age, and their interactions. Notably, there was a core of higher association cortex nodes that become increasingly robust with age. Finally, the connectivity within this clique of delta centrality hubs increased, providing a link between focal and cumulative lesioning effects, and proving how brain networks are able to increase robustness to random error without compromising vulnerability to focused attack through increased hub-to-hub connectivity.

Classically focused attack and random error have been seen as corollaries of each other. That is, increased robustness to one must lead to increased vulnerability to the other. Hub development is believed to be a key feature of adolescent brain development as demonstrated in connectomes based on structural covariance (Whitaker et al, 2016), diffusion imaging based tractography (Baker et al, 2015), and functional connectivity (Grayson et al, 2014; Hwang et al, 2013). In this scenario, one would expect that the resultant networks would demonstrate increased resistance to random error but with increased vulnerability to focused attack. Conversely, in our analysis there is an increased robustness to random error but without increased vulnerability to focused attack. Formation of rich-club architecture enables protection against focused attack without compromising response to random-error: assortativity and delta centrality effects are therefore a by-product of rich-club architecture.

In terms of the main theories on the vulnerability of the developing brain, these current findings are supportive of the early vulnerability hypothesis, in that brain

robustness increased with age. However, the results of chapter 6 and the current graph theory analysis also indicate that significant functional connectivity changes occur during adolescence, potentially related to underlying synaptic refinement. If the extent to which synaptic pruning has occurred then functions as a proxy for brain plasticity, this is consistent with both early vulnerability and plasticity being present.

Compared with animal models, the traditional method for brain injury research, connectomics has many advantages. For example, it allows studying the effects of varying injury extent, location, and timing. Non-invasive brain imaging also lends itself to studying large cohorts of healthy human participants and repeating this imaging over time. Network analysis is already a multi-disciplinary field and studying brain injury lends itself to including techniques from statistical physics such as percolation theory; this creates a fertile niche for new ideas adopting the strengths and ideas from this diverse range of backgrounds. Finally, this study is also a prime example of how to integrate networks based research into neuroscience by taking a well described theory and approaching it from a new perspective, thereby advocating the benefits of a new approach while grounding its findings in those of previous established research.

In contrast one could argue that network percolation is not an entirely realistic model of *in vivo* brain injury. A counter argument is that it is designed to act as a tool for studying network architecture and complex topological features primarily, and only secondarily serve as a model of brain injury. Further improvements to this study would be to include a variety of participants with both healthy and pathological development to capture how variance in development can affect brain robustness. Inclusion of longitudinal imaging would also have been advantageous to allow inference on individual trajectories rather than only differences across a single cohort.

In the future there are many avenues one could pursue to expand upon this work. The most pertinent would be to include potential plasticity after brain injury to model the overall response to brain injury. Current models of percolation assume a static injury and do not include any potential repair mechanisms. Previous results in **chapter 5.4** have identified sites and characteristics of functional connectivity dynamics across development. Also promising are the dynamics in semi-metric topology identified in

this graph theory analysis. Both functional connectivity and semi-metric topology are potentially more abstracted to models of synaptic refinement and strengthening of residual connections. To include either of these measures as biomarkers of plasticity potential will require understanding what features can predict whether dynamics in functional connectivity will occur. A promising avenue to expand on these dynamics would be to study the longitudinal effects of empirical lesions and determine the predictive markers of these functional connectivity and semi-metricity related biomarkers of synaptic plasticity.

Another potential avenue to explore would be more realistic modelling of brain lesions. For example, node removal could be focused on clinically meaningful patterns of cumulative brain injury, such as spreading patterns of dementia in Alzheimer's disease or the evolution of chronic traumatic encephalopathy, both of which involve a characteristic array of regions in their evolution. Furthermore, the assumption that zeroing the effects of a node in a matrix is a realistic model of its injury in real life could be tested. It was already shown earlier in this thesis (**section 5.3**) that while this matrix-zeroing approach holds a degree of validity for focal lesions, it fails to capture all the resultant dynamics associated with empirical lesions, for example those potentially due to plasticity. One could therefore reduce node connectivity in a continuous (linear or non-linear) manner, or impair node connectivity by adding in white noise to the underlying BOLD time series (Tononi, Sporns, Edelman, 1999), while determining changes in the resultant network architecture.

Finally, current research in complex networks has focused on models of optimal percolation and improving network robustness. Identifying the most efficient or optimal manner in which to fragment a network is a non-deterministic polynomial-time (NP) hard problem i.e. all possible combinations of node removal would have to be tested and there is no suitable algorithm in which to shorten this process (Kovacs & Barabasi, 2015). However by mapping the integrity of a tree-like random network to an inverse percolation problem a set of optimal percolation nodes were identified (Morone & Makse, 2015). Intriguingly these nodes were not necessarily the most central in the network but also included a critical set of more peripheral nodes that are connected to other high degree nodes, which together are known the collective

influencers of the network. A consequence of this is that a new concept of centrality is defined not just the number of direct links but also by the other nodes it is connected to. This may offer a link between network robustness, node distances, and direct and indirect connections identified through semi-metric analysis. Furthermore, it may allow a more effective process of focused attack, and thereby increase sensitivity to identifying age related changes in robustness.

CONCLUSION

Adolescent development results in more robust network architecture, particularly to random error. Focal weak spots of the network are re-organised with higher association cortices becoming less vulnerable. A core of delta centrality hubs become increasingly connected together, forming a putative rich-club architecture, which allows increasing robustness to random error without compromising vulnerability to focused attack. In conclusion, these data provide evidence for the theory of early vulnerability rather than that of enhanced plasticity.

CHAPTER 8: DISCUSSION

'Science never solves a problem without creating 10 more'

George Bernard Shaw [1856-1950]

SUMMARY

Functional connectivity networks in neuro-oncology

Functional connectivity networks are readily apparent in patients with brain tumours using resting state functional MRI. The full complement of canonical resting state networks reported in healthy participants are able to be identified with subtle yet significant refinements to standard image processing pipelines to account for artefacts related to the presence of a brain tumour. Seed connectivity analysis also allowed one to speculate on putative patterns of network plasticity. Default mode network topological alterations appear to be universally prevalent, while alterations in other networks are more individual and based on the lesion location. This work serves as a proof of concept the BOLD contrast time series from resting state functional MRI provides comparable signal properties to that found in healthy participants and that the elementary principles for analysing the signal are valid.

Brain mapping with the functional connectome in neurosurgery

Establishing the fundamental properties of resting state functional MRI in patients with brain tumours enables more abstract and higher level analyses to be performed with the functional connectome. Again, important validation of the underlying features of functional connectomes was performed by comparison with data from healthy participants, supporting subsequent analyses. Viewing the brain as a complex network was found to offer significant potential in neurosurgery, particularly in mapping specific network features, understanding the effects of focal brain lesions, and for visualising the data in an intuitive yet principled and surgically relevant manner. Furthermore, it was possible to identify potential signatures of node robustness and connections at risk that could be used to plan surgery at an individual patient level. This work serves as an important lead in to more sophisticated connectome-based analysis and testing of specific hypotheses, such as the effects of brain lesions on brain dynamics and hub plasticity.

Synthetic versus empirical lesions and network hub plasticity

Earlier analyses had identified the potential of connectomics to identify the effects of focal brain lesions and also to create synthetic lesions that might, for example, correspond to an extended resection of an existing tumour. In order to progress this idea it was necessary to validate the underlying principles of creating lesions in connectivity matrices and identify potential biomarkers of plasticity *in vivo*. While it was found that classical graph theory approaches to creating synthetic lesions in connectivity matrices generated from healthy control participants, there are important differences particular with regard to hub dynamics. Focal lesions induced the formation of new hubs at the cost of selectively down regulating a core of previously established hubs. The balancing of these hub categories involved selecting those involved in long-range connectivity and network integration at the cost of those that are also expensive in terms of distance but sub-serve less of a role in overall network integration. Decisions regarding new hubs tended to be formed at an individual level, while absent hubs tended to involve a consistent core of nodes. Furthermore, while new hubs involved homologous regions in the contralateral hemisphere, missing hubs were based in the posterior parieto-occipital regions, in a pattern that overlaped with the default mode network. Overall these data are consistent with a dynamic rather than a static response to the presence of focal lesions.

Developmental dynamics in resting state networks during adolescence

Clinical observations had identified the important contributions of plasticity in the response to focal brain lesions. In order to understand the effects of and mechanisms underlying neural plasticity, adolescent development was used as a model to study network dynamics. Here it was hypothesised that adolescent development could serve as a proxy for brain repair, whereby the mechanisms the brain used to repair itself when injured were the same or similar to those used to form its original phenotype in the first instance. Specifically, synaptic refinement, the main developmental process active during adolescence, was also a significant factor in brain repair, whereby the number of available synapses reflected the potential for alternative routes of communication after injury. The work in this chapter confirmed that functional connectivity was sensitive to developmental dynamics during adolescence, albeit in a localised and discrete manner. Furthermore, said developmental dynamics demonstrated distinct gender specific and age-gender interactions. These findings

have important implications for subsequent studies investigating group level effects, suggesting that future cohorts need to be gender homogenous and encompass narrow age brackets. Alternatively, individual trajectories or classifications may be more appropriate, for example by using longitudinal data or machine learning techniques.

Evolution of the effects of brain injury with age

Adolescent development was also used to determine the relationship between complex network features and the brain's response to injury. Firstly, it was first necessary to characterise the graph theory dynamics occurring during this epoch. During adolescence hub-based and rich club architecture was found to develop, consistent with previous studies, but additionally markers of available network paths could be discerned through analysis of semi-metric graph topology.

Adolescent development results in more robust network architecture, particularly to random removal of nodes and edges. Focal weak spots of the network are re-organised with higher association cortices becoming less vulnerable. A core of delta centrality hubs become increasingly connected together, forming a putative rich-club architecture, which allows increasing robustness to random error without compromising vulnerability to focused attack. In conclusion, these data provide evidence for the theory of early vulnerability rather than that of enhanced plasticity.

Summary

Overall the data presented in this thesis supports the validity and interest in applying complex network analysis of the functional connectome to neurosurgery. Hypotheses regarding global effects of lesions, network hub plasticity, and modelling the sequelae of surgery can all be addressed in an intuitive and principled manner. Taken together, the results presented herein on the effects of focal lesions highlight the individual, global, and dynamic effects of focal lesions, with consequently important implications in how one interprets historical works on functional localisation.

Adolescent development is presented as a fertile ground for understanding principles involved in plasticity and network robustness. Both functional connectivity and graph theory measures demonstrate sensitivity to developmental dynamics, but in a discrete and gender specific manner. During adolescence, the brain improves its robustness,

thereby linking the development of complex network topology and the response to brain injury. When these findings from adolescent development are interpreted in a neurosurgical context, it is apparent that to understand the focal effects need to be interpreted in the context of the brains robustness to injury, and resilience to repair itself.

Our ability to understand network level effects is now at a level where we can attempt to test mapping of higher cognitive functions in neurosurgery, such as in the follow-up project CAESAR. Ultimately this work may form part of a virtual brain – whereby one can perform *in silico* surgery accounting for individual connectivity, robustness, and resilience - with the aim of making surgery not only more effective, but safer for the patient.

LIMITATIONS

"Nothing in neurobiology makes sense except in the light of behavior."
Gordon Shepherd [1933-]

Neuro-cognitive baseline

A significant limitation in both the neurosurgery and adolescent development cohorts was the lack of neuropsychological data to compare the MRI data. With the neurosurgery data, originally the MALTINGS study (from which the original pilot data was derived) was designed as a diffusion imaging based investigation into tumour invasiveness, and functional imaging was not part of the protocol. Subsequently the development of resting state functional MRI data was seen to be of interest, and a pilot study was formed using redundant scanning time at the end of the original sequence acquisition. The aims for this dataset were determine what data quality was available, understanding the necessary image processing steps involved, and explore the potential practical applications of the findings. The results could then be used for subsequent funding applications, and this strategy was proven to be successful with the consequent CAESAR project.

With regard to the adolescent development dataset extensive efforts were made at acquiring multi-modal data including genetic, behavioural, and neuropsychological data. However with this ambition came significant logistical demands for analysis in terms of time, finances, and personnel. While high quality behavioral data will undoubtedly transpire at a later data, unfortunately at the time of writing hopes of incorporating these data are premature. When these data do become available, it will be helpful to identify the neuropsychological correlates of functional connectivity dynamics presented in this work, particularly regarding gender specific changes. However an alternative perspective could be that analysing the neuroimaging data in isolation is superior, particularly when combined with the data driven approach utilised in this thesis, as it potentially reduces any biases and limitations in the analysis driven by known neuropsychological changes. With regard to the brain injury model, the neuropsychological data is somewhat less relevant, given that the analysis is predominantly computational and theoretical in nature. Nevertheless the underlying complex network topology changes that are affecting the dynamics in brain

robustness may be also be involved in neuropsychological development during adolescence.

Longitudinal data

Cross-sectional or cohort designs, such as those in the studies included in this thesis, only allow inference about inter-individual variability. To identify intra-individual developmental trajectories longitudinal studies are required. Furthermore if the age range is large it is likely that variability within the cohort exceeds any age related effects. Longitudinal study designs can obviate some of these difficulties but such studies are more costly and logistically complex to run. However, the recent commencement by the NIH of a longitudinal study of adolescent development looks set to address these limitations in study design.

In terms of neurosurgery, longitudinal study designs offer several advantages. Firstly they allow intra-individual comparisons, obviating the need for matched control participants. Secondly, as all comparisons are intra-individual, artifacts in image processing due to variability in tumour location for example are less problematic. Finally, one can study time dependent changes, such as how the brain recovers after surgery or deteriorates after radiotherapy. Longitudinal studies in neurosurgery are potentially more complex than in adolescence, given that participants may be undergoing additional medical therapies, demonstrating signs of illness from their disease that impact their ability to adhere to a follow-up protocol, and potentially have to travel further to imaging resources than studies of healthy participants due to the extensive catchment areas of tertiary referral hospitals.

Premises underling functional MRI

Non-invasive, tomographic, *in-vivo* functional neuroimaging began with the discovery of Blood Oxygenation-Level Dependent (BOLD) endogenous contrast (Ogawa et al., 1992) where neuronal activity produces local blood oxygenation changes detectable by magnetic resonance imaging (MRI). The cognitive neuroscience community was an early adopter of this technology with a burgeoning in discoveries that certain brain functions are localised to anatomical regions, previously only surmised through lesioning or electrophysiological studies (Varela, Lachaux, &

Rodriguez, 2001), with significant contributions from neurosurgery (Greeblatt, Dagi, & Epstein, 1997).

Despite the interest and findings, vocal detractors have attempted to highlight perceived shortcomings of functional MRI, both task based and resting state. Possibly the most common limitation presented is that BOLD contrast itself is not a direct marker of neural activity. While it is true that the origins of BOLD contrast and cerebrovascular blood-oxygen coupling are incompletely understood, numerous lines of convergent evidence from human and non-human mammalian studies have shown the correspondence between neuronal activity and BOLD contrast. Currently one of the more accepted theories is that BOLD contrast is related to the input and intracortical processing of a given area, and is driven by changes in the medium-calibre venules and veins.

Another common misconception about functional MRI in general is its inability to demonstrate causal relationships. However, while this may be true in certain instances, it is in general more a feature of experimental design. Studies that manipulate participants perception or behaviour, or that use interventions such as TMS, are designed to demonstrate causal relationships. Perhaps a more accurate portrayal then would be that neuroimaging provides causal information without necessarily causal certainty.

Further limitations are the lack of SI units in measurements, poor temporal and spatial resolution, and the predominance of noise in the underlying data. Despite all of these limitations however, findings have transpired to be highly replicable and non-trivially explained.

FUTURE WORK: CONNECTOMICS AND ELECTRICAL STIMULATION FOR AUGMENTING RESECTION (CAESAR) STUDY

The following work is based on a successful grant application to The Brain Tumour Charity and as a subsequent application for post-doctoral funding led by Dr Rafael Romero-Garcia.

INTRODUCTION

Over 5000 people die every year in the UK from brain tumours; the most common cause of death from cancer in children and adults younger than 40 years old. In the UK, around 20% of patients undergoing surgery for a brain tumour will be alive 5 years later, although for around a third it may also lead to cognitive problems, and a reduction in quality of life. Current clinical practice is based on maximal resection but this is only worthwhile if function can be maintained. More recent studies have focused on extending the margin surrounding the tumour that is removed to delay the neoplastic transformation of normal tissue in this region. Maximising the resection whilst minimising harm is complicated by the difficulty in determining the tumour margin and limitations in mapping the function of apparently normal brain tissue surrounding the tumour.

The aim of the CAESAR project is to incorporate the recently established frameworks of brain connectomics to pre-operatively improve functional mapping, and therefore better predict post-operative rehabilitation (http://www.mrmikehart.com/caesar.html). The CAESAR project is funded by The Brain Tumour Charity to collect advanced Magnetic Resonance Images (MRI) prior to surgery, post-operatively, and during follow-up (3 and 12 months, n=18, 72 scans in total). This new MRI protocol includes: (i) resting state functional MRI (fMRI), measuring brain activity through changes in blood oxygenation; (ii) Diffusion Kurtosis Imaging (DKI), mapping the water diffusion to determine white matter alignment; (iii) quantitative structural imaging, tracking of changes to brain morphology. These three MRI modalities will be used to generate structural and functional connectome maps in each of the four scanning sessions. A further proposal for the CAESAR project is to combine advanced magnetic resonance images, and structural and functional connectivity analysis with a neuro-navigation system that orientates the physician during the

surgery, in a proof-of-concept system for real-time estimation of the potential risk of resection at any location (**figure 8.1**). Predictions generated by the system will be tested against actual clinical outcomes during a 3 and 12 months follow-up.

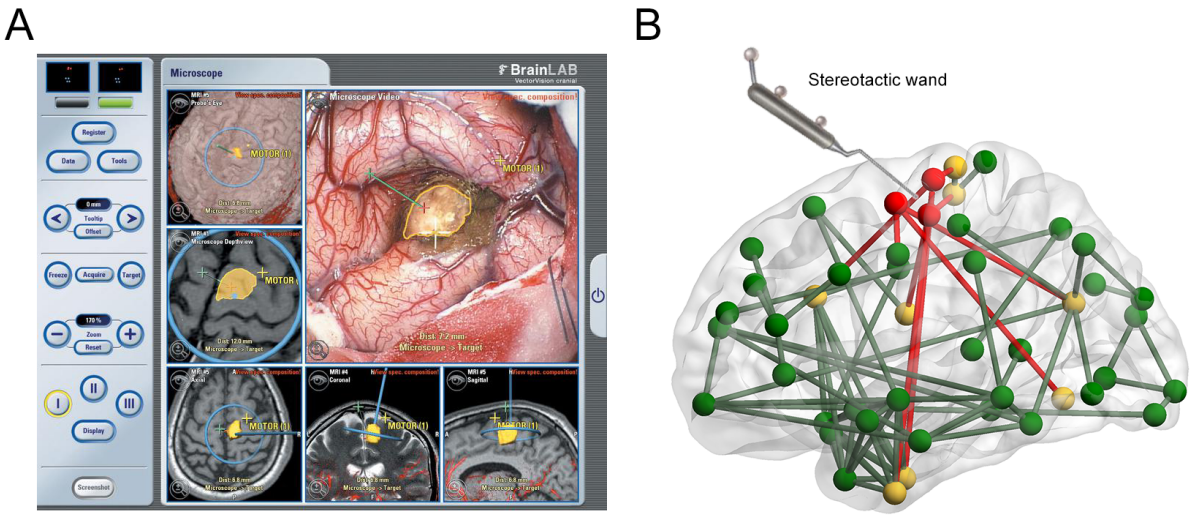

Figure 8.1. The neuro-navigation system currently used in clinical practice matches the position of a stereotactic wand on the patient's cortical surface with its position on the MRI (A). Schematic representation of the combination of neuro-navigation system with the connectomic framework proposed (B); Spheres denote brain regions while edges represent structural or functional connections between regions. Brain regions located in the tumour area are represented in red, regions connected to a tumour are shown in orange and regions not connected to the tumour are illustrated in green.

HYPOTHESES

1. Executive function and other higher order cognitive processes involve distributed neural circuits rather than focal, eloquent regions
2. Patients with low grade gliomas often exhibit a range of higher cognitive function deficits related not just to tumour location, but also to a complex interaction between pre-operative cognitive reserve and adaptive neural plasticity
3. Connectomics can provide quantitative information on networks related to higher-order cognition of individual patients that can influence resection margins, and thus improve recovery and cognitive outcomes.

AIMS

The overall aim is to improve planning for surgical resection of tumours, reducing use of electrical stimulation during surgery (therefore reducing risks associated with stimulation such as seizures), and permitting more radical resections with less functional impairment. Additional aims include a better understand how brain networks relate to cognitive function, and how cognitive function post-surgery relates to the resected brain regions:

1. The use of connectomics to map high-order cognitive functions in patients with DLGG.
2. Integrate preoperative MRI data with the neuro-navigation system used during awake stimulation to obtain accurate functional mapping of the brain for surgeons.
3. The use of MRI scans before surgery to assist with intraoperative functional mapping and provide basis for interpretation of post-operative changes.
4. The use of follow-up MRI scans to monitor recovery longitudinally, which in turn will be key to understanding plasticity pre-operatively.
5. Create connectome-based biomarkers for patient stratification that can predict rehabilitation outcomes.

OUTCOMES

1. A surgical feedback system that can present in real time connectomic data to surgeons in a clear and informative manner
2. Optimum connectomic models based on pre-operative data for predicting the recovery rates and cognitive outcomes following surgical resection.
3. Biomarkers based on connectomic features can support patient stratification for tailored treatment and rehabilitation.
4. A clinical trial design of the surgical feedback system that addresses safety and ethical considerations

NEURONAVIGATION INTERFACE

Connectomes generated from individual MRI data will instantaneously model the effect on cognitive function of a virtual lesion corresponding to the putative resected tissue (**figure 8.1B**). The predictive modelling will first be evaluated on post-operative MRI and neuropsychological assessment to determine the impact of tumour resection on brain function and its recovery; for example, did resected regions of high connectivity lead to greater reductions in specific cognitive functions? Do resected margins including brain circuits with high redundancy lead to faster and fuller recovery?

Individual or combined network metrics such as: (i) betweenness centrality, quantifying the relevance of the node as a relay station for information flowing; (ii) nodal robustness, measuring the effect of nodal removal in network efficiency; and (iii) nodal redundancy, estimating the number of alternative paths between regions; will help estimate how neural activity is transmitted across brain areas affected by the tumour in the context of percolation theory. Thus, by matching the preoperative MRI with the location of the stereotactic wand in the neuronavigation system used during surgery, we plan to estimate connectome disruption in the exact location of the potential resection margin. We consequently hypothesise that potential resilience of the brain function and patient cognitive outcome can be predicted by connectome measures derived from pre-operative MRI.

Brain shift refers to the movement of the brain from its original position during registration upon opening the dura, releasing CSF, and during resection of the lesion with resultant reduction in neuronavigation accuracy. Overall this is an unsolved problem in neurosurgery due to the complex and non-linear relationships between the interacting variables described above. In general three broad approaches can be defined. One seeks to update the registration intra-operatively, either by repeating imaging (for example intra-operative MRI or ultrasound) or using localised surface based registration (for example sulcal and gyral landmarks intra-operatively to a surface reconstruction). However the optimal method of registering the intra-operative tumour resection cavity is still not defined, plus there are significant time and cost burdens. Another approach is to model the predicted effects of CSF release and resection progression on the brain structure using approaches from structural

engineering, however this again is at best only theoretical in nature due to the complex and interacting variables, as well as the lack of any true gold standard with which to train such a model upon. Finally one can seek to minimise the dependence on registration, for example using pre-operative planning to define broad regions (for example, a particular margin in one direction) of interest to either avoid or resect intra-operatively, or use imaging in combination with a method that acquires data intra-operatively (for example, awake brain stimulation or electrocorticography).

DISCUSSION

During the execution of the project we'll evaluate whether connectomics can contribute reliable information about the potential for patient recovery. We'll focus on those questions that are particularly relevant for the design of further trials, such as:

(i) Robustness of connectomic metrics in the context of recovery prediction and stratification of rehabilitation

(ii) Susceptibility of both structural and functional connectome analysis for false positive and false negative results

(iii) Necessary sample size to achieve enough statistical power for determining the accuracy of the proposed models

(iv) Most appropriate way to present the information during the surgery without disrupting the attention of the surgeons

Resulting conncetome-based plasticity models could be used to help inform patients on what to expect during surgery in terms of task performance, their potential post-operative functional impairment, and plan for rehabilitation if necessary.

Finally, an assessment will be undertaken of the feasibility of future interventional studies and the viability of implementing the feedback system into the clinical routine. This will include investigations on how best to visually present feedback to the surgeons, what educational programme is required for surgeons to exploit connectomics and its functional implications, how stratification can help to create alternative rehabilitation pathways**,** and what ethical issues are raised by augmenting surgery with advice generated autonomously from neuroimaging. By the end of the project we expect to have generated accurate and generalizable plasticity model based

on connectomic analysis of preoperative MRI for predicting recovery performance that can be validated in a further randomized clinical trial.

REFERENCES

Achard, S., & Bullmore, E. (2007). Efficiency and cost of economical brain functional networks. *PLoS Computational Biology*, *3*(2), e17. http://doi.org/10.1371/journal.pcbi.0030017

Achard, S., Delon-Martin, C., Vértes, P. E., Renard, F., Schenck, M., Schneider, F., et al. (2012). Hubs of brain functional networks are radically reorganized in comatose patients. *Proceedings of the National Academy of Sciences of the United States of America*, *109*(50), 20608–20613. http://doi.org/10.1073/pnas.1208933109

Achard, S., Salvador, R., Whitcher, B., Suckling, J., & Bullmore, E. (2006). A Resilient, Low-Frequency, Small-World Human Brain Functional Network with Highly Connected Association Cortical Hubs. *Journal of Neuroscience*, *26*(1), 63–72. http://doi.org/10.1523/JNEUROSCI.3874-05.2006

Akaite, H. (1974). A new look at the statistical model identification. *IEEE Transactions on Automatic Control*, *19*(6), 716–723.

Albert, R., & Barabasi, A.-L. (2002). Statistical mechanics of complex networks. *Reviews of Modern Physics*, *74*(1), 47–97.

Albert, R., Jeong, H., & Barabási, A. L. (1999). Diameter of the World-Wide Web. Nature.

Alstott, J., Breakspear, M., Hagmann, P., Cammoun, L., & Sporns, O. (2009). Modeling the Impact of Lesions in the Human Brain. *PLoS Computational Biology*, *5*(6), e1000408. http://doi.org/10.1371/journal.pcbi.1000408

Amaral, L. A. N., Scala, A., Barthelemy, M., & Stanley, H. E. (2000). Classes of small-world networks. *Proceedings of the National Academy of Sciences*, *97*(21), 11149–11152. http://doi.org/10.1073/pnas.200327197

Anderson, V. A., Morse, S. A., Catroppa, C., Haritou, F., & Rosenfeld, J. V. (2004). Thirty month outcome from early childhood head injury: a prospective analysis of neurobehavioural recovery. *Brain: a Journal of Neurology*, *127*(Pt 12), 2608–2620. http://doi.org/10.1093/brain/awh320

Anderson, V., & Moore, C. (1995). Age at injury as a predictor of outcome following pediatric head injury: A longitudinal perspective. *Child Neuropsychology*, *1*(3), 187–202. http://doi.org/10.1080/09297049508400224

Anderson, V., Catroppa, C., Morse, S., Haritou, F., & Rosenfeld, J. (2005). Functional plasticity or vulnerability after early brain injury? *Pediatrics*, *116*(6), 1374–1382. http://doi.org/10.1542/peds.2004-1728

Anderson, V., Spencer-Smith, M., Leventer, R., Coleman, L., Anderson, P., Williams, J., et al. (2009). Childhood brain insult: can age at insult help us predict outcome? *Brain: a Journal of Neurology*, *132*(Pt 1), 45–56. http://doi.org/10.1093/brain/awn293

Avants, B. B., Tustison, N., & Johnson, H. (n.d.). Advanced normalization tools (ANTS) 2009. *Insight J*

Baker, S. T. E., Lubman, D. I., Yucel, M., Allen, N. B., Whittle, S., Fulcher, B. D., et al. (2015). Developmental Changes in Brain Network Hub Connectivity in Late Adolescence. *Journal of Neuroscience*, *35*(24), 9078–9087. http://doi.org/10.1523/JNEUROSCI.5043-14.2015

Ballantyne, A. O., Spilkin, A. M., Hesselink, J., & Trauner, D. A. (2008). Plasticity in the developing brain: intellectual, language and academic functions in children with ischaemic perinatal stroke. *Brain: a Journal of Neurology*, *131*(Pt 11), 2975–2985. http://doi.org/10.1093/brain/awn176

Barabási, A. L., & Albert, R. (1999). Emergence of scaling in random networks. *Science*, *286*, 509–512. http://doi.org/10.1126/science.286.5439.509

Barabási, A.-L. (2016). Network Science (1st ed.). Cambridge: Cambridge University Press.

Bartolomei, F., Bosma, I., Klein, M., Baayen, J. C., Reijneveld, J. C., Postma, T. J., Heimans, J. J., van Dijk, B. W., de Munck, J. C., de Jongh, A., Cover, K. S., & Stam, C. J. (2006a). Disturbed functional connectivity in brain tumour patients: evaluation by graph analysis of synchronization matrices. *Clinical Neurophysiology : Official Journal of the International Federation of Clinical Neurophysiology*, *117*(9), 2039–2049. http://doi.org/10.1016/j.clinph.2006.05.018

Bartolomei, F., Bosma, I., Klein, M., Baayen, J. C., Reijneveld, J. C., Postma, T. J., Heimans, J. J., van Dijk, B. W., de Munck, J. C., de Jongh, A., Cover, K. S., & Stam, C. J. (2006b). How do brain tumors alter functional connectivity? A magnetoencephalography study. *Annals of Neurology*, *59*(1), 128–138. http://doi.org/10.1002/ana.20710

Bassett, D. S., & Bullmore, E. (2006). Small-World Brain Networks. *The Neuroscientist*, *12*(6), 512–523. http://doi.org/10.1177/1073858406293182

Bassett, D. S., Bullmore, E. T., Meyer-Lindenberg, A., Apud, J. A., Weinberger, D. R., & Coppola, R. (2009). Cognitive fitness of cost-efficient brain functional networks. *Proceedings of the National Academy of Sciences of the United States of America*, *106*(28), 11747–11752. http://doi.org/10.1073/pnas.0903641106

Bates, E., Wilson, S. M., Saygin, A. P., Dick, F., Sereno, M. I., Knight, R. T., & Dronkers, N. F. (2003). Voxel-based lesion-symptom mapping. *Nature Neuroscience*, *6*(5), 448–450. http://doi.org/10.1038/nn1050

Beckmann, C. F., & Smith, S. M. (2004). Probabilistic independent component analysis for functional magnetic resonance imaging. *IEEE Transactions on Medical Imaging*, *23*(2), 137–152. http://doi.org/10.1109/TMI.2003.822821

Beckmann, C. F., DeLuca, M., Devlin, J. T., & Smith, S. M. (2005). Investigations into resting-state connectivity using independent component analysis. *Philosophical Transactions of the Royal Society of London. Series B, Biological Sciences*, *360*(1457), 1001–1013. http://doi.org/10.1098/rstb.2005.1634

Beckmann, C. F., DeLuca, M., Devlin, J. T., & Smith, S. M. (n.d.). Investigations into Resting-state Connectivity using Independent Component Analysis. *FMRIB Technical Report TR05CB1*, 1–16.

Beckmann, C. F., Mackay, C. E., Filippini, N., & Smith, S. M. (2009). Group comparison of resting-state FMRI data using multi-subject ICA and dual regression. *NeuroImage*, *47*, S148. http://doi.org/10.1016/S1053-8119(09)71511-3

Bello, L., Gallucci, M., Fava, M., Carrabba, G., Giussani, C., Acerbi, F., et al. (2007). Intraoperative subcortical language tract mapping guides surgical removal of gliomas involving speech areas. *Neurosurgery*, *60*(1), 67–82. http://doi.org/10.1227/01.NEU.0000249206.58601.DE

Bello, L., Gambini, A., Castellano, A., Carrabba, G., Acerbi, F., Fava, E., et al. (2008). Motor and language DTI Fiber Tracking combined with intraoperative subcortical mapping for surgical removal of gliomas. *NeuroImage*, *39*(1), 369–382. http://doi.org/10.1016/j.neuroimage.2007.08.031

Biswal, B., Yetkin, F. Z., Haughton, V. M., & Hyde, J. S. (1995). Functional connectivity in the motor cortex of resting human brain using echo-planar MRI. *Magnetic Resonance in Medicine*, *34*(4), 537–541.

Bonacich, P. (1972). Technique for analyzing overlapping memberships. *Sociological Methodology*, *4*, 176–185. http://doi.org/10.2307/270732

Bosma, I., Douw, L., Bartolomei, F., Heimans, J. J., van Dijk, B. W., Postma, T. J., et al. (2008). Synchronized brain activity and neurocognitive function in patients with low-grade glioma: a magnetoencephalography study. *Neuro-Oncology*, *10*(5), 734–744. http://doi.org/10.1215/15228517-2008-034

Bosma, I., Reijneveld, J. C., Klein, M., Douw, L., van Dijk, B. W., Heimans, J. J., & Stam, C. J. (2009). Disturbed functional brain networks and neurocognitive function in low-grade glioma patients: a graph theoretical analysis of resting-state MEG. *Nonlinear Biomedical Physics*, *3*(1), 9. http://doi.org/10.1186/1753-4631-3-9

Böttger, J., Margulies, D. S., Horn, P., Thomale, U. W., Podlipsky, I., Shapira-Lichter, I., et al. (2011). A software tool for interactive exploration of intrinsic functional connectivity opens new perspectives for brain surgery. *Acta Neurochirurgica*, *153*(8), 1561–1572. http://doi.org/10.1007/s00701-011-0985-6

Bullmore, E. (2012). The future of functional MRI in clinical medicine. *NeuroImage*, *62*(2), 1267–1271. http://doi.org/10.1016/j.neuroimage.2012.01.026

Bullmore, E., & Sporns, O. (2009). Complex brain networks: graph theoretical analysis of structural and functional systems. *Nature Reviews Neuroscience*, *10*(3), 186–198. http://doi.org/10.1038/nrn2575

Bullmore, E., & Sporns, O. (2012). The economy of brain network organization. *Nature Reviews Neuroscience*. http://doi.org/10.1038/nrn3214

Bullmore, E., Barnes, A., Bassett, D. S., Fornito, A., Kitzbichler, M., Meunier, D., & Suckling, J. (2009). Generic aspects of complexity in brain imaging data and other biological systems. *NeuroImage*, *47*(3), 1125–1134. http://doi.org/10.1016/j.neuroimage.2009.05.032

Bullmore, E., Fadili, J., Breakspear, M., Salvador, R., Suckling, J., & Brammer, M. (2003). Wavelets and statistical analysis of functional magnetic resonance images of the human brain. *Statistical Methods in Medical Research*, *12*(5), 375–399. http://doi.org/10.1191/0962280203sm339ra

Bullmore, E., Fadili, J., Maxim, V., Şendur, L., Whitcher, B., Suckling, J., et al. (2004). Wavelets and functional magnetic resonance imaging of the human brain. *NeuroImage*, *23*, S234–S249. http://doi.org/10.1016/j.neuroimage.2004.07.012

Cabral, J., Hugues, E., Kringelbach, M. L., & Deco, G. (2012). Modeling the outcome of structural disconnection on resting-state functional connectivity. *NeuroImage*, *62*(3), 1342–1353. http://doi.org/10.1016/j.neuroimage.2012.06.007

Callaway, D. S., Newman, M., Strogatz, S. H., & Watts, D. J. (2000). Network robustness and fragility: Percolation on random graphs. *Physical Review Letters*, *85*(25), 5468–5471. http://doi.org/10.1103/PhysRevLett.85.5468

Castellanos, F. X., Di Martino, A., Craddock, R. C., Mehta, A. D., & Milham, M. P. (2013). Clinical applications of the functional connectome. *NeuroImage*, *80*, 527–540. http://doi.org/10.1016/j.neuroimage.2013.04.083

Catani, M. (2005). The rises and falls of disconnection syndromes. *Brain: a Journal of Neurology*, *128*(10), 2224–2239. http://doi.org/10.1093/brain/awh622

Krzywinski, M. I., Schein, J. E., Birol, I., Connors, J., Gascoyne, R., Horsman, D., Jones, S. J., Marra, M. A. Circos: An information aesthetic for comparative genomics. Genome Res. Published in Advance June 18, 2009, doi:10.1101/gr.092759.109

Cox, R. W. (1996). AFNI: software for analysis and visualization of functional magnetic resonance neuroimages. *Computers and Biomedical Research, an International Journal*, *29*(3), 162–173.

Cox, R. W. (2012). AFNI: what a long strange trip it's been. *NeuroImage*, *62*(2), 743–747. http://doi.org/10.1016/j.neuroimage.2011.08.056

Craddock, R. C., Jbabdi, S., Yan, C.-G., Vogelstein, J. T., Castellanos, F. X., Di Martino, A., et al. (2013). Imaging human connectomes at the macroscale. *Nature Methods*, *10*(6), 524–539. http://doi.org/10.1038/nmeth.2482

Crossley, N. A., Mechelli, A., Scott, J., Carletti, F., Fox, P. T., McGuire, P., & Bullmore, E. T. (2014). The hubs of the human connectome are generally implicated in the anatomy of brain disorders. *Brain: a Journal of Neurology*, *137*(Pt 8), 2382–2395. http://doi.org/10.1093/brain/awu132

Csányi, G., & Kertész, J. (1995). Scaling behaviour in discrete traffic models. *Journal of Physics a: Mathematical and General*, *28*(16), L427–L432. http://doi.org/10.1088/0305-4470/28/16/002

Damoiseaux, J. S., & Greicius, M. D. (2009). Greater than the sum of its parts: a review of studies combining structural connectivity and resting-state functional connectivity. *Brain Structure and Function*, *213*(6), 525–533. http://doi.org/10.1007/s00429-009-0208-6

Daqing, L., Yinan, J., Rui, K., & Havlin, S. (2014). Spatial correlation analysis of cascading failures: congestions and blackouts. *Scientific Reports*, *4*, 5381. http://doi.org/10.1038/srep05381

Das, S. R., Avants, B. B., Grossman, M., & Gee, J. C. (2009). Registration based cortical thickness measurement. *NeuroImage*, *45*(3), 867–879. http://doi.org/10.1016/j.neuroimage.2008.12.016

De Benedictis, A., Moritz-Gasser, S., & Duffau, H. (2010). Awake Mapping Optimizes the Extent of Resection for Low-Grade Gliomas in Eloquent Areas. *Neurosurgery*, *66*(6), 1074–1084. http://doi.org/10.1227/01.NEU.0000369514.74284.78

De Vico Fallani, F., Richiardi, J., Chavez, M., & Achard, S. (2014). Graph analysis of functional brain networks: practical issues in translational neuroscience. *Philosophical Transactions of the Royal Society of London. Series B, Biological Sciences*, *369*(1653), 20130521–20130521. http://doi.org/10.1098/rstb.2013.0521

Deco, G., Tononi, G., Boly, M., & Kringelbach, M. L. (2015). Rethinking segregation and integration: contributions of whole-brain modelling. *Nature Reviews Neuroscience*, *16*(7), 430–439. http://doi.org/10.1038/nrn3963

Dennis, E. L., & Thompson, P. M. (2013). Mapping connectivity in the developing brain. *International Journal of Developmental Neuroscience : the Official Journal of the International Society for Developmental Neuroscience*, *31*(7), 525–542. http://doi.org/10.1016/j.ijdevneu.2013.05.007

Dennis, M. (2010). Margaret Kennard (1899-1975): not a "principle" of brain plasticity but a founding mother of developmental neuropsychology. *Cortex; a journal devoted to the study of the nervous system and behavior* (Vol. 46, pp. 1043–1059). http://doi.org/10.1016/j.cortex.2009.10.008

Dennis, M., & Whitaker, H. A. (1976). Language acquisition following hemidecortication: linguistic superiority of the left over the right hemisphere. *Brain and Language*, *3*(3), 404–433. http://doi.org/10.1016/0093-934X(76)90036-5

Di, X. (2012). Metabolic brain covariant networks as revealed by FDG-PET with reference to resting-state fMRI networks. *Brain: a Journal of Neurology*. http://doi.org/10.1089/brain.2012.0086

Dosenbach, N. U. F., Nardos, B., Cohen, A. L., Fair, D. A., Power, J. D., Church, J. A., et al. (2010). Prediction of individual brain maturity using fMRI. *Science*, *329*(5997), 1358–1361. http://doi.org/10.1126/science.1194144

Douw, L., Baayen, H., Bosma, I., Klein, M., Vandertop, P., Heimans, J., et al. (2008). Treatment-related changes in functional connectivity in brain tumor patients: A

magnetoencephalography study. *Experimental Neurology*, *212*(2), 285–290. http://doi.org/10.1016/j.expneurol.2008.03.013

Duffau, H. (2011). Brain Mapping. (H. Duffau, Ed.). Vienna: Springer Science & Business Media. http://doi.org/10.1007/978-3-7091-0723-2

Duffau, H. (2012). A new concept of diffuse (low-grade) glioma surgery. In *Advances and Technical Standards in Neurosurgery* (Vol. 38, pp. 3–27). Vienna: Springer Vienna. http://doi.org/10.1007/978-3-7091-0676-1_1

Duffau, H. (2014a). Diffuse low-grade gliomas and neuroplasticity. *Diagnostic and Interventional Imaging*, 1–11. http://doi.org/10.1016/j.diii.2014.08.001

Duffau, H. (2014b). The huge plastic potential of adult brain and the role of connectomics: New insights provided by serial mappings in glioma surgery. *Cortex*, *58*(C), 325–337. http://doi.org/10.1016/j.cortex.2013.08.005

Duffau, H. (2015). Stimulation mapping of white matter tracts to study brain functional connectivity. *Nature Reviews Neurology*, *11*(5), 255–265. http://doi.org/10.1038/nrneurol.2015.51

Duffau, H., Capelle, L., Denvil, D., Sichez, N., Gatignol, P., Taillandier, L., et al. (2003). Usefulness of intraoperative electrical subcortical mapping during surgery for low-grade gliomas located within eloquent brain regions: functional results in a consecutive series of 103 patients. *Journal of Neurosurgery*, *98*(4), 764–778. http://doi.org/10.3171/jns.2003.98.4.0764

Erdös, P., & Rényi, A. (1959). On random graphs, I. *Publicationes Mathematicae (Debrecen)*, *6*, 290–297. http://doi.org/10.1234/12345678

Fagerholm, E. D., Hellyer, P. J., Scott, G., Leech, R., & Sharp, D. J. (2015). Disconnection of network hubs and cognitive impairment after traumatic brain injury. *Brain: a Journal of Neurology*, *138*(6), 1696–1709. http://doi.org/10.1093/brain/awv075

Fair, D. A., Dosenbach, N. U. F., Church, J. A., Cohen, A. L., Brahmbhatt, S., Miezin, F. M., et al. (2007). Development of distinct control networks through segregation and integration. *Proceedings of the National Academy of Sciences*, *104*(33), 13507–13512. http://doi.org/10.1073/pnas.0705843104

Fernández Coello, A., Moritz-Gasser, S., Martino, J., Martinoni, M., Matsuda, R., & Duffau, H. (2013). Selection of intraoperative tasks for awake mapping based on relationships between tumor location and functional networks. *Journal of Neurosurgery*, *119*(6), 1380–1394. http://doi.org/10.3171/2013.6.JNS122470

Filippini, N., MacIntosh, B. J., Hough, M. G., Goodwin, G. M., Frisoni, G. B., Smith, S. M., et al. (2009). Distinct patterns of brain activity in young carriers of the APOE-ε4 allele. *Proceedings of the National Academy of Sciences*, *106*(17), 7209–7214. http://doi.org/10.1073/pnas.0811879106

Finger, S. (2001). Origins of neuroscience: a history of explorations into brain function (1st ed.). Oxford.

Fornito, A., Zalesky, A., & Breakspear, M. (2013). Graph analysis of the human connectome: Promise, progress, and pitfalls. *NeuroImage*, *80*, 426–444. http://doi.org/10.1016/j.neuroimage.2013.04.087

Fornito, A., Zalesky, A., & Breakspear, M. (2015). The connectomics of brain disorders. *Nature Reviews Neuroscience*, *16*(3), 159–172. http://doi.org/10.1038/nrn3901

Fox, M. D., & Raichle, M. E. (2007). Spontaneous fluctuations in brain activity observed with functional magnetic resonance imaging. *Nature Reviews Neuroscience*, *8*(9), 700–711. http://doi.org/10.1038/nrn2201

Freeman, L. C. (1978). Centrality in social networks conceptual clarification. *Social Networks*, *1*(3), 215–239. http://doi.org/10.1016/0378-8733(78)90021-7

Friston, K. J. (1994). Functional and effective connectivity in neuroimaging: a synthesis. *Human Brain Mapping*, *2*, 56–78. http://doi.org/10.1002/hbm.460020403/full

Giza, C. C., & Prins, M. L. (2006). Is being plastic fantastic? Mechanisms of altered plasticity after developmental traumatic brain injury. *Developmental Neuroscience*, *28*(4-5), 364–379. http://doi.org/10.1159/000094163

Glasser, M. F., Coalson, T. S., Robinson, E. C., Hacker, C. D., Harwell, J., Yacoub, E., et al. (2016). A multi-modal parcellation of human cerebral cortex. *Nature*, *536*(7615), 171–178. http://doi.org/10.1038/nature18933

Gonzalez-Castillo, J., & Bandettini, P. A. (2015). What Cascade Spreading Models Can Teach Us about the Brain. *Neuron*, *86*(6), 1327–1329. http://doi.org/10.1016/j.neuron.2015.06.006

Grayson, D. S., Ray, S., Carpenter, S., Iyer, S., Dias, T. G. C., Stevens, C., et al. (2014). Structural and functional rich club organization of the brain in children and adults. *PLoS ONE*, *9*(2), e88297. http://doi.org/10.1371/journal.pone.0088297

Greve, D. N., & Fischl, B. (2009). Accurate and robust brain image alignment using

boundary-based registration. *NeuroImage*, *48*(1), 63–72. http://doi.org/10.1016/j.neuroimage.2009.06.060

Greenblatt S. H., Dagi T. F., Epstein M. H. (eds). (1997). A history of neurosurgery: in its scientific and professional contexts.

Griffanti, L., Salimi-Khorshidi, G., Beckmann, C. F., Auerbach, E. J., Douaud, G., Sexton, C. E., et al. (2014). ICA-based artefact removal and accelerated fMRI acquisition for improved resting state network imaging. *NeuroImage*, *95*(C), 232–247. http://doi.org/10.1016/j.neuroimage.2014.03.034

Gronwall, D., Wrightson, P., McGinn, V., & McGinn, V. (1997). Effect of mild head injury during the preschool years. *Journal of the International Neuropsychological Society*, *3*(6), 592–597.

Gu, S., Satterthwaite, T. D., Medaglia, J. D., Yang, M., Gur, R. E., Gur, R. C., & Bassett, D. S. (2015). Emergence of system roles in normative neurodevelopment. *Proceedings of the National Academy of Sciences of the United States of America*, *112*(44), 13681–13686. http://doi.org/10.1073/pnas.1502829112

Guggisberg, A. G., Honma, S. M., Findlay, A. M., Dalal, S. S., Kirsch, H. E., Berger, M. S., & Nagarajan, S. S. (2008). Mapping functional connectivity in patients with brain lesions. *Annals of Neurology*, *63*(2), 193–203. http://doi.org/10.1002/ana.21224

Guimera, R., & Amaral, L. I. S. A. N. (2005). Functional cartography of complex metabolic networks. *Nature*, *433*(7028), 895–900. http://doi.org/10.1038/nature03288

Hagmann, P., Cammoun, L., Gigandet, X., Meuli, R., Honey, C. J., Van J Wedeen, & Sporns, O. (2008). Mapping the Structural Core of Human Cerebral Cortex. *PLoS Biology*, *6*(7), e159. http://doi.org/10.1371/journal.pbio.0060159

Hagmann, P., Kurant, M., Gigandet, X., Thiran, P., Wedeen, V. J., Meuli, R., & Thiran, J.-P. (2007). Mapping Human Whole-Brain Structural Networks with Diffusion MRI. *PLoS ONE*, *2*(7), e597. http://doi.org/10.1371/journal.pone.0000597

Harris, R. J., Bookheimer, S. Y., Cloughesy, T. F., Kim, H. J., Pope, W. B., Lai, A., et al. (2013). Altered functional connectivity of the default mode network in diffuse gliomas measured with pseudo-resting state fMRI. *Journal of Neuro-Oncology*, *116*(2), 373–379. http://doi.org/10.1007/s11060-013-1304-2

Hart, K. J., & Faust, D. (1988). Prediction of the effects of mild head injury: A

message about the Kennard Principle. *Journal of Clinical Psychology*, *44*(5), 780–782. http://doi.org/10.1002/1097-4679(198809)44:5<780::AID-JCLP2270440519>3.0.CO;2-1

Hart, M. G., Ypma, R. J. F., Romero-Garcia, R., Price, S. J., & Suckling, J. (2016). Graph theory analysis of complex brain networks: new concepts in brain mapping applied to neurosurgery. *Journal of Neurosurgery*, *124*(6), 1665–1678. http://doi.org/10.3171/2015.4.JNS142683

He, Y., Chen, Z. J., & Evans, A. C. (2007). Small-World Anatomical Networks in the Human Brain Revealed by Cortical Thickness from MRI. *Cerebral Cortex*, *17*(10), 2407–2419. http://doi.org/10.1093/cercor/bhl149

Heywood, C., & Canavan, A. (1987). "Developmental neuropsychological correlates of language." *Language development and disorders: Clinics in developmental medicine (no.101-102)* (pp. 146–158). London: MacKeith/Blackwell.

Huang, Q., Zhang, R., Hu, X., Ding, S., Qian, J., Lei, T., et al. (2014). Disturbed small-world networks and neurocognitive function in frontal lobe low-grade glioma patients. *PLoS ONE*, *9*(4), e94095. http://doi.org/10.1371/journal.pone.0094095

Huang, X., Vodenska, I., Havlin, S., & Stanley, H. E. (2013). Cascading Failures in Bi-partite Graphs: Model for Systemic Risk Propagation. *Scientific Reports*, *3*. http://doi.org/10.1038/srep01219

Hutchings, F., Han, C. E., Keller, S. S., Weber, B., Taylor, P. N., & Kaiser, M. (2015). Predicting Surgery Targets in Temporal Lobe Epilepsy through Structural Connectome Based Simulations. *PLoS Computational Biology*, *11*(12), e1004642. http://doi.org/10.1371/journal.pcbi.1004642

Hwang, K., Hallquist, M. N., & Luna, B. (2013). The development of hub architecture in the human functional brain network. *Cerebral Cortex*, *23*(10), 2380–2393. http://doi.org/10.1093/cercor/bhs227

Hyvarinen, A. (1999). Fast and robust fixed-point algorithms for independent component analysis. *Neural Networks, IEEE Transactions on*, *10*(3), 626–634. http://doi.org/10.1109/72.761722

Irimia, A., Chambers, M. C., Torgerson, C. M., & Van Horn, J. D. (2012a). Circular representation of human cortical networks for subject and population-level connectomic visualization. *NeuroImage*, *60*(2), 1340–1351. http://doi.org/10.1016/j.neuroimage.2012.01.107

Irimia, A., Chambers, M. C., Torgerson, C. M., Filippou, M., Hovda, D. A., Alger, J. R., et al. (2012b). Patient-Tailored Connectomics Visualization for the Assessment of White Matter Atrophy in Traumatic Brain Injury. *Frontiers in Neurology*, *3*. http://doi.org/10.3389/fneur.2012.00010

Ius, T., Angelini, E., de Schotten, M. T., Mandonnet, E., & Duffau, H. (2011). Evidence for potentials and limitations of brain plasticity using an atlas of functional resectability of WHO grade II gliomas: Towards a "minimal common brain." *NeuroImage*, *56*(3), 992–1000. http://doi.org/10.1016/j.neuroimage.2011.03.022

Jenkinson, M., & Smith, S. (2001). A global optimisation method for robust affine registration of brain images. *Medical Image Analysis*, *5*(2), 143–156.

Jenkinson, M., Bannister, P., Brady, M., & Smith, S. (2002). Improved optimization for the robust and accurate linear registration and motion correction of brain images. *NeuroImage*, *17*(2), 825–841.

Kaiser, M. (2011). A tutorial in connectome analysis: Topological and spatial features of brain networks. *NeuroImage*, *57*(3), 892–907. http://doi.org/10.1016/j.neuroimage.2011.05.025

Kaiser, M., Martin, R., Andras, P., & Young, M. P. (2007). Simulation of robustness against lesions of cortical networks. *European Journal of Neuroscience*, *25*(10), 3185–3192. http://doi.org/10.1111/j.1460-9568.2007.05574.x

Kelly, C., & Castellanos, F. X. (2014). Strengthening Connections: Functional Connectivity and Brain Plasticity. *Neuropsychology Review*, *24*(1), 63–76. http://doi.org/10.1007/s11065-014-9252-y

Kennard, M. A. (1936). Age and other factors in motor recovery from precentral lesions in monkeys. *American Journal of Physiology*.

Kennard, M. A. (1940). Relation of age to motor impairment in man and in subhuman primates. *Archives of Neurology & Psychiatry*, *44*(2), 377–397. http://doi.org/10.1001/archneurpsyc.1940.02280080137008

Kesler, S. R., Gugel, M., Huston-Warren, E., & Watson, C. (2016). Atypical Structural Connectome Organization and Cognitive Impairment in Young Survivors of Acute Lymphoblastic Leukemia. *Brain Connectivity*, *6*(4), 273–282. http://doi.org/10.1089/brain.2015.0409

Khundrakpam, B. S., Lewis, J. D., Zhao, L., Chouinard-Decorte, F., & Evans, A. C. (2016). Brain connectivity in normally developing children and adolescents.

NeuroImage, *134*, 192–203. http://doi.org/10.1016/j.neuroimage.2016.03.062

Kokkonen, S.-M., Nikkinen, J., Remes, J., Kantola, J., Starck, T., Haapea, M., et al. (2009). Preoperative localization of the sensorimotor area using independent component analysis of resting-state fMRI. *Magnetic Resonance Imaging*, *27*(6), 733–740. http://doi.org/10.1016/j.mri.2008.11.002

Kovács, I. A., & Barabási, A.-L. (2015). Network science: Destruction perfected. *Nature*, *524*(7563), 38–39. http://doi.org/10.1038/524038a

Kundu, P., Brenowitz, N. D., Voon, V., Worbe, Y., Vértes, P. E., Inati, S. J., et al. (2013). Integrated strategy for improving functional connectivity mapping using multiecho fMRI. *Proceedings of the National Academy of Sciences of the United States of America*, *110*(40), 16187–16192. http://doi.org/10.1073/pnas.1301725110

Kundu, P., Santin, M. D., Bandettini, P. A., Bullmore, E. T., & Petiet, A. (2014). Differentiating BOLD and non-BOLD signals in fMRI time series from anesthetized rats using multi-echo EPI at 11.7 T. *NeuroImage*, *102 Pt 2*, 861–874. http://doi.org/10.1016/j.neuroimage.2014.07.025

Latora, V., & Marchiori, M. (2001). Efficient behavior of small-world networks. *Physical Review Letters*, *87*(19), 198701. http://doi.org/10.1103/PhysRevLett.87.198701

Latora, V., & Marchiori, M. (2007). A measure of centrality based on network efficiency. *New Journal of Physics*, *9*(6), 188–188. http://doi.org/10.1088/1367-2630/9/6/188

Lee, M. H., Smyser, C. D., & Shimony, J. S. (2013). Resting-State fMRI: A Review of Methods and Clinical Applications. *American Journal of Neuroradiology*, *34*(10), 1866–1872. http://doi.org/10.3174/ajnr.A3263

Lenroot, R. K., & Giedd, J. N. (2006). Brain development in children and adolescents: Insights from anatomical magnetic resonance imaging. *Neuroscience & Biobehavioral Reviews*, *30*(6), 718–729. http://doi.org/10.1016/j.neubiorev.2006.06.001

Li, Y., Liu, Y., Li, J., Qin, W., Li, K., Yu, C., & Jiang, T. (2009). Brain anatomical network and intelligence. *PLoS Computational Biology*, *5*(5), e1000395. http://doi.org/10.1371/journal.pcbi.1000395

Liu, H., Buckner, R. L., Talukdar, T., Tanaka, N., Madsen, J. R., & Stufflebeam, S. M. (2009). Task-free presurgical mapping using functional magnetic resonance

imaging intrinsic activity. *Journal of Neurosurgery*, *111*(4), 746–754. http://doi.org/10.3171/2008.10.jns08846

Louis, D. N., Ohgaki, H., Wiestler, O. D., Cavenee, W. K., Burger, P. C., Jouvet, A., et al. (2007). The 2007 WHO Classification of Tumours of the Central Nervous System. *Acta Neuropathologica*, *114*(2), 97–109. http://doi.org/10.1007/s00401-007-0243-4

Lutkenhoff, E. S., Rosenberg, M., Chiang, J., Zhang, K., Pickard, J. D., Owen, A. M., & Monti, M. M. (2014). Optimized brain extraction for pathological brains (optiBET). *PLoS ONE*, *9*(12), e115551. http://doi.org/10.1371/journal.pone.0115551

Lutti, A., Hutton, C., Finsterbusch, J., Helms, G., & Weiskopf, N. (2010). Optimization and validation of methods for mapping of the radiofrequency transmit field at 3T. *Magnetic Resonance in Medicine*, *64*(1), 229–238. http://doi.org/10.1002/mrm.22421

Manglore, S., Bharath, R. D., Panda, R., George, L., Thamodharan, A., & Gupta, A. K. (2013). Utility of resting fMRI and connectivity in patients with brain tumor. *Neurology India*, *61*(2), 144–151. http://doi.org/10.4103/0028-3886.111120

Margulies, D. S., Böttger, J., Watanabe, A., & Gorgolewski, K. J. (2013). Visualizing the human connectome. *NeuroImage*, *80*, 445–461. http://doi.org/10.1016/j.neuroimage.2013.04.111

Margulies, D. S., Vincent, J. L., Kelly, C., Lohmann, G., Uddin, L. Q., Biswal, B. B., et al. (2009). Precuneus shares intrinsic functional architecture in humans and monkeys. *Proceedings of the National Academy of Sciences of the United States of America*, *106*(47), 20069–20074. http://doi.org/10.1073/pnas.0905314106

McGirt, M. J., Mukherjee, D., Chaichana, K. L., Than, K. D., Weingart, J. D., & Quinones-Hinojosa, A. (2009). Association of surgically acquired motor and language deficits on overall survival after resection of glioblastoma multiforme. *Neurosurgery*, *65*(3), 463–470. http://doi.org/10.1227/01.NEU.0000349763.42238.E9

McGonigle, J., Malizia, A. L., & Mirehdi, M. (2011). Visualising functional connectivity in fMRI using hierarchical edge bundles (pp. 1–1). Presented at the th annual meeting of the organization for Human Brain Mapping.

Mesulam, M. (2005). Imaging connectivity in the human cerebral cortex: The next frontier? *Annals of Neurology*, *57*(1), 5–7. http://doi.org/10.1002/ana.20368

Micheloyannis, S., Pachou, E., Stam, C. J., Vourkas, M., Erimaki, S., & Tsirka, V. (2006). Using graph theoretical analysis of multi channel EEG to evaluate the neural efficiency hypothesis. *Neuroscience Letters*, *402*(3), 273–277. http://doi.org/10.1016/j.neulet.2006.04.006

Minka, T. P. (2000). *Automatic choice of dimensionality for PCA*. *M.I.T. Media Laboratory Perceptual Computing Section Technical Report No. 514* (pp. 1–16).

Mišić, B., Betzel, R. F., Nematzadeh, A., Goñi, J., Griffa, A., Hagmann, P., et al. (2015). Cooperative and Competitive Spreading Dynamics on the Human Connectome. *Neuron*, *86*(6), 1518–1529. http://doi.org/10.1016/j.neuron.2015.05.035

Mitchell, T. J., Hacker, C. D., Breshears, J. D., & Szrama, N. P. (2013). A Novel Data-Driven Approach to Preoperative Mapping of Functional Cortex Using Resting-State Functional Magnetic Resonance Imaging. *Neurosurgery*. http://doi.org/10.1227/NEU.0000000000000141

Morone, F., & Makse, H. A. (2015). Influence maximization in complex networks through optimal percolation. *Nature*, *524*(7563), 65–68. http://doi.org/10.1038/nature14604

Motter, A. E., & Lai, Y.-C. (2002). Cascade-based attacks on complex networks. *Physical Review E*, *66*(6 Pt 2), 065102.

Newman, M. (2004). Fast algorithm for detecting community structure in networks. *Physical Review E*, *69*(6), 066133. http://doi.org/10.1103/PhysRevE.69.066133

Newman, Mark. (2010). Networks: An Introduction. OUP Oxford.

NIH Blueprint: http://www.neuroscienceblueprint.nih.gov/connectome/. (n.d.). NIH Blueprint: http://www.neuroscienceblueprint.nih.gov/connectome/. Retrieved from http://www.neuroscienceblueprint.nih.gov/connectome/

Oh S. W., Harris J. A., Ng L., Winslow B., Cain N., et al. A mesoscale connectome of the mouse brain. (2014). Nature 10;508(7495):207-214. doi 10:1038/nature13186

Papagno, C., Casarotti, A., Comi, A., Gallucci, M., Riva, M., & Bello, L. (2012). Measuring clinical outcomes in neuro-oncology. A battery to evaluate low-grade gliomas (LGG). *Journal of Neuro-Oncology*, *108*(2), 269–275. http://doi.org/10.1007/s11060-012-0824-5

Penfield, W., & Rasmussen, T. (1950). The cerebral cortex of man. New York: Macmillan.

Preibisch, C., & Deichmann, R. (2009). Influence of RF spoiling on the stability and

accuracy of T1 mapping based on spoiled FLASH with varying flip angles. *Magnetic Resonance in Medicine*, *61*(1), 125–135. http://doi.org/10.1002/mrm.21776

Price, C. J., Seghier, M. L., & Leff, A. P. (2010). Predicting language outcome and recovery after stroke: the PLORAS system. *Nature Reviews Neurology*, *6*(4), 202–210. http://doi.org/10.1038/nrneurol.2010.15

Quigley, M., Cordes, D., Wendt, G., Turski, P., Moritz, C., Haughton, V., & Meyerand, M. E. (2001). Effect of focal and nonfocal cerebral lesions on functional connectivity studied with MR imaging. *American Journal of Neuroradiology*, *22*(2), 294–300.

Raichle, M. E. (2011). The restless brain. *Brain Connectivity*, *1*(1), 3–12. http://doi.org/10.1089/brain.2011.0019

Raichle, M. E., & Mintun, M. A. (2006). Brain work and brain imaging. *Annu Rev Neurosci*, *29*(1), 449–476. http://doi.org/10.1146/annurev.neuro.29.051605.112819

Rivera-Rivera, P. A., Rios-Lago, M., Sanchez-Casarrubios, S., Salazar, O., Yus, M., González-Hidalgo, M., et al. (2016). Cortical plasticity catalyzed by prehabilitation enables extensive resection of brain tumors in eloquent areas. *Journal of Neurosurgery*, 1–11. http://doi.org/10.3171/2016.2.JNS152485

Rorden, C., & Karnath, H. O. (2004). Using human brain lesions to infer function: a relic from a past era in the fMRI age? *Nature Reviews Neuroscience*, *5*(10), 812–819. http://doi.org/10.1038/nrn1521

Rosazza, C., Aquino, D., D'Incerti, L., Cordella, R., Andronache, A., Zacà, D., et al. (2014). Preoperative Mapping of the Sensorimotor Cortex: Comparative Assessment of Task-Based and Resting-State fMRI. *PLoS ONE*, *9*(6), e98860–19. http://doi.org/10.1371/journal.pone.0098860

Rubinov, M., & Sporns, O. (2010). Complex network measures of brain connectivity: Uses and interpretations. *NeuroImage*, *52*(3), 1059–1069. http://doi.org/10.1016/j.neuroimage.2009.10.003

Rubinov, M., Ympa, R-Y., Watson, C., Bullmore, E. T. (2015). Wiring cost and topological participation of the mouse brain connectome. Proceedings of the National Academy of Sciences of the United States of America 112(32):10032-10037, doi: 10.1073/pnas.1420315112

Sair, H. I., Yahyavi-Firouz-Abadi, N., Calhoun, V. D., Airan, R. D., Agarwal, S.,

Intrapiromkul, J., et al. (2015). Presurgical brain mapping of the language network in patients with brain tumors using resting-state fMRI: Comparison with task fMRI. *Human Brain Mapping*. http://doi.org/10.1002/hbm.23075

Salimi-Khorshidi, G., Douaud, G., Beckmann, C. F., Glasser, M. F., Griffanti, L., & Smith, S. M. (2014). Automatic denoising of functional MRI data: combining independent component analysis and hierarchical fusion of classifiers. *NeuroImage*, *90*, 449–468. http://doi.org/10.1016/j.neuroimage.2013.11.046

Salvador, R., Suckling, J., Schwarzbauer, C., & Bullmore, E. (2005). Undirected graphs of frequency-dependent functional connectivity in whole brain networks. *Philosophical Transactions of the Royal Society of London. Series B, Biological Sciences*, *360*(1457), 937–946. http://doi.org/10.1098/rstb.2005.1645

Sanabria-Diaz, G., Martínez-Montes, E., & Melie-Garcia, L. (2013). Glucose Metabolism during Resting State Reveals Abnormal Brain Networks Organization in the Alzheimer's Disease and Mild Cognitive Impairment. *PLoS ONE*, *8*(7), e68860. http://doi.org/10.1371/journal.pone.0068860

Sanai, N., Mirzadeh, Z., & Berger, M. S. (2008). Functional outcome after language mapping for glioma resection. *The New England Journal of Medicine*, *358*(1), 18–27. http://doi.org/10.1056/NEJMoa067819

Shimony, J. S., Zhang, D., Johnston, J. M., Fox, M. D., Roy, A., & Leuthardt, E. C. (2009). Resting-state spontaneous fluctuations in brain activity: a new paradigm for presurgical planning using fMRI. *Academic Radiology*, *16*(5), 578–583. http://doi.org/10.1016/j.acra.2009.02.001

Simas, T. (2012, May 4). *Stochastic models and transitivity in complex networks*. (L. M. Rocha, Ed.).

Simas, T., & Rocha, L. M. (2015). Distance closures on complex networks. *Network Science*, 1–42. http://doi.org/10.1017/nws.2015.11

Simas, T., Chattopadhyay, S., Hagan, C., Kundu, P., Patel, A., Holt, R., et al. (2015). Semi-Metric Topology of the Human Connectome: Sensitivity and Specificity to Autism and Major Depressive Disorder. *PLoS ONE*, *10*(8), e0136388. http://doi.org/10.1371/journal.pone.0136388

Smith, A., & Sugar, O. (1975). Development of above normal language and intelligence 21 years after left hemispherectomy. *Neurology*, *25*(9), 813–813. http://doi.org/10.1212/WNL.25.9.813

Smith, S. M. (2012). The future of FMRI connectivity. *NeuroImage*, *62*(2), 1257–

1266. http://doi.org/10.1016/j.neuroimage.2012.01.022

Smith, S. M., Beckmann, C. F., Andersson, J., Auerbach, E. J., Bijsterbosch, J., Douaud, G., et al. (2013a). Resting-state fMRI in the Human Connectome Project. *NeuroImage*, *80*(C), 144–168. http://doi.org/10.1016/j.neuroimage.2013.05.039

Smith, S. M., Fox, P. T., Miller, K. L., Glahn, D. C., Fox, P. M., Mackay, C. E., et al. (2009). Correspondence of the brain's functional architecture during activation and rest. *Proceedings of the National Academy of Sciences*, *106*(31), 13040–13045. http://doi.org/10.1073/pnas.0905267106

Smith, S. M., Miller, K. L., Salimi-Khorshidi, G., Webster, M., Beckmann, C. F., Nichols, T. E., et al. (2011). Network modelling methods for FMRI. *NeuroImage*, *54*(2), 875–891. http://doi.org/10.1016/j.neuroimage.2010.08.063

Smith, S. M., Vidaurre, D., Beckmann, C. F., Glasser, M. F., Jenkinson, M., Miller, K. L., et al. (2013b). Functional connectomics from resting-state fMRI. *Trends in Cognitive Sciences*, *17*(12), 666–682. http://doi.org/10.1016/j.tics.2013.09.016

Achard, S. (2012). Brainwaver: Basic wavelet analysis of multivariate time series with a visualisation and parametrisation using graph theory. R package version 1.6. http://CRAN.R-project.org/package=brainwaver

Sporns, O (ed). (2012). Discovering the Human Connectome. USA, MIT Press.

Sporns, O (ed). (2010). Networks of the Brain. MIT Press.

Sporns, O., Chialvo, D., Kaiser, M., & Hilgetag, C. (2004). Organization, development and function of complex brain networks. *Trends in Cognitive Sciences*, *8*(9), 418–425. http://doi.org/10.1016/j.tics.2004.07.008

Sporns, O., Honey, C. J., & Kötter, R. (2007). Identification and classification of hubs in brain networks. *PLoS ONE*, *2*(10), e1049. http://doi.org/10.1371/journal.pone.0001049

Sporns, O., Tononi, G., & Kötter, R. (2005). The Human Connectome: A Structural Description of the Human Brain. *PLoS Computational Biology*, *1*(4), e42. http://doi.org/10.1371/journal.pcbi.0010042

Stam, C. J. (2004). Functional connectivity patterns of human magnetoencephalographic recordings: a “small-world” network? *Neuroscience Letters*, *355*(1-2), 25–28. http://doi.org/10.1016/j.neulet.2003.10.063

Stam, C. J. (2014). Modern network science of neurological disorders. *Nature Reviews Neurology*, *15*(10), 683–695. http://doi.org/10.1038/nrn3801

Stam, C. J., Jones, B. F., Nolte, G., Breakspear, M., & Scheltens, P. (2007). Small-world networks and functional connectivity in Alzheimer's disease. *Cerebral Cortex*, *17*(1), 92–99. http://doi.org/10.1093/cercor/bhj127

Stummer, W., Meinel, T., Ewelt, C., Martus, P., Jakobs, O., Felsberg, J., & Reifenberger, G. (2012). Prospective cohort study of radiotherapy with concomitant and adjuvant temozolomide chemotherapy for glioblastoma patients with no or minimal residual enhancing tumor load after surgery. *Journal of Neuro-Oncology*, *108*(1), 89–97. http://doi.org/10.1007/s11060-012-0798-3

Stummer, W., Pichlmeier, U., Meinel, T., Wiestler, O. D., Zanella, F., & Reulen, H.-J. (2006). Fluorescence-guided surgery with 5-aminolevulinic acid for resection of malignant glioma: a randomised controlled multicentre phase III trial. *The Lancet Oncology*, *7*(5), 392–401. http://doi.org/10.1016/S1470-2045(06)70665-9

Taylor, H. G., & Alden, J. (1997). Age-related differences in outcomes following childhood brain insults: an introduction and overview. *Journal of the International Neuropsychological Society : JINS*, *3*(6), 555–567.

Taylor, H. G., Yeates, K. O., Wade, S. L., Drotar, D., Stancin, T., & Minich, N. (2002). A prospective study of short- and long-term outcomes after traumatic brain injury in children: behavior and achievement. *Neuropsychology*, *16*(1), 15–27.

Tononi, G., Sporns, O., & Edelman, G. M. (1999). Measures of degeneracy and redundancy in biological networks. *Proceedings of the National Academy of Sciences*, *96*(6), 3257–3262.

Tustison, N. J., Avants, B. B., & Cook, P. A. (2013). The ANTs cortical thickness processing pipeline. *Proceeds of SPIE*, *8672*, 86720K–2. http://doi.org/10.1117/12.2007128

Tustison, N. J., Cook, P. A., Klein, A., Song, G., Das, S. R., Duda, J. T., et al. (2014). Large-scale evaluation of ANTs and FreeSurfer cortical thickness measurements. *NeuroImage*, *99*, 166–179. http://doi.org/10.1016/j.neuroimage.2014.05.044

Tzourio-Mazoyer, N., Landeau, B., Papathanassiou, D., Crivello, F., Etard, O., Delcroix, N., et al. (2002). Automated Anatomical Labeling of Activations in SPM Using a Macroscopic Anatomical Parcellation of the MNI MRI Single-Subject Brain. *NeuroImage*, *15*(1), 273–289. http://doi.org/10.1006/nimg.2001.0978

van den Heuvel, M. P., & Pol, H. E. H. (2010). Exploring the brain network: A review

on resting-state fMRI functional connectivity. *European Neuropsychopharmacology*, *20*(8), 519–534. http://doi.org/10.1016/j.euroneuro.2010.03.008

van den Heuvel, M. P., & Sporns, O. (2011). Rich-club organization of the human connectome. *The Journal of Neuroscience : the Official Journal of the Society for Neuroscience*, *31*(44), 15775–15786. http://doi.org/10.1523/JNEUROSCI.3539-11.2011

van den Heuvel, M. P., & Sporns, O. (2013). Network hubs in the human brain. *Trends in Cognitive Sciences*, *17*(12), 683–696. http://doi.org/10.1016/j.tics.2013.09.012

van den Heuvel, M. P., Stam, C. J., Kahn, R. S., & Hulshoff Pol, H. E. (2009). Efficiency of functional brain networks and intellectual performance. *Journal of Neuroscience*, *29*(23), 7619–7624. http://doi.org/10.1523/JNEUROSCI.1443-09.2009

Van Horn, J. D., Irimia, A., Torgerson, C. M., Chambers, M. C., Kikinis, R., & Toga, A. W. (2012). Mapping Connectivity Damage in the Case of Phineas Gage. *PLoS ONE*, *7*(5), e37454. http://doi.org/10.1371/journal.pone.0037454

Varoquaux, G., Gramfort, A., & Poline, J. B. (2010). Brain covariance selection: better individual functional connectivity models using population prior. *Advances in Neural …*, *23*, 1–9.

Vassal, M., Charroud, C., Deverdun, J., Le Bars, E., Molino, F., Bonnetblanc, F., et al. (2016). Recovery of functional connectivity of the sensorimotor network after surgery for diffuse low-grade gliomas involving the supplementary motor area. *Journal of Neurosurgery*, 1–10. http://doi.org/10.3171/2016.4.JNS152484

Vértes, P. E., Alexander-Bloch, A., & Bullmore, E. T. (2014). Generative models of rich clubs in Hebbian neuronal networks and large-scale human brain networks. *Philosophical Transactions of the Royal Society of London. Series B, Biological Sciences*, *369*(1653), 20130531–20130531. http://doi.org/10.1098/rstb.2013.0531

Wang, J., Zuo, X., & He, Y. (2010). Graph-based network analysis of resting-state functional MRI. *Frontiers in Systems Neuroscience*, *4*. http://doi.org/10.3389/fnsys.2010.00016

Watts, D. J., & Strogatz, S. H. (1998). Collective dynamics of “small-world” networks., *393*(6684), 440–442. http://doi.org/10.1038/30918

Webb, C., Rose, F. D., Johnson, D. A., & Attree, E. A. (1996). Age and recovery

from brain injury: clinical opinions and experimental evidence. *Brain Injury*, *10*(4), 303–310. http://doi.org/10.1080/026990596124476

Weiskopf, N., Suckling, J., Williams, G., Correia, M. M., Inkster, B., Tait, R., et al. (2013). Quantitative multi-parameter mapping of R1, PD(*), MT, and R2(*) at 3T: a multi-center validation. *Frontiers in Neuroscience*, *7*, 95. http://doi.org/10.3389/fnins.2013.00095

Wen, P. Y., Macdonald, D. R., Reardon, D. A., Cloughesy, T. F., Sorensen, A. G., Galanis, E., et al. (2010). Updated response assessment criteria for high-grade gliomas: response assessment in neuro-oncology working group. *Journal of Clinical Oncology : Official Journal of the American Society of Clinical Oncology*, *28*(11), 1963–1972. http://doi.org/10.1200/JCO.2009.26.3541

Whitaker, K. J., Vértes, P. E., Romero-Garcia, R., Váša, F., Moutoussis, M., Prabhu, G., et al. (2016). Adolescence is associated with genomically patterned consolidation of the hubs of the human brain connectome. *Proceedings of the National Academy of Sciences of the United States of America*, *113*(32), 9105–9110. http://doi.org/10.1073/pnas.1601745113

Wink, A.-M., Bullmore, E., Barnes, A., Bernard, F., & Suckling, J. (2008). Monofractal and multifractal dynamics of low frequency endogenous brain oscillations in functional MRI. *Human Brain Mapping*, *29*(7), 791–801. http://doi.org/10.1002/hbm.20593

Xia, M., Wang, J., & He, Y. (2013). BrainNet Viewer: A Network Visualization Tool for Human Brain Connectomics. *PLoS ONE*, *8*(7). http://doi.org/10.1371/journal.pone.0068910

Xu, H., Ding, S., Hu, X., Yang, K., Xiao, C., Zou, Y., et al. (2013). Reduced efficiency of functional brain network underlying intellectual decline in patients with low-grade glioma. *Neuroscience Letters*, *543*, 27–31. http://doi.org/10.1016/j.neulet.2013.02.062

Young, M. P. (1992). Objective analysis of the topological organization of the primate cortical visual system. *Nature*, *358*, 152–155.

Yuan, W., Wade, S. L., & Babcock, L. (2014). Structural connectivity abnormality in children with acute mild traumatic brain injury using graph theoretical analysis. *Human Brain Mapping*, n/a–n/a. http://doi.org/10.1002/hbm.22664

Zalesky, A., Fornito, A., & Bullmore, E. (2012). On the use of correlation as a measure of network connectivity. *NeuroImage*, *60*(4), 2096–2106.

http://doi.org/10.1016/j.neuroimage.2012.02.001

Zalesky, A., Fornito, A., Harding, I. H., Cocchi, L., Yücel, M., Pantelis, C., & Bullmore, E. T. (2010). Whole-brain anatomical networks: Does the choice of nodes matter? *NeuroImage*, *50*(3), 970–983. http://doi.org/10.1016/j.neuroimage.2009.12.027

Zhang, D., & Raichle, M. E. (2010). Disease and the brain's dark energy. *Nature Reviews Neurology*, *6*(1), 15–28. http://doi.org/10.1038/nrneurol.2009.198

Zhang, D., Johnston, J. M., Fox, M. D., Leuthardt, E. C., Grubb, R. L., Chicoine, M. R., et al. (2009). Preoperative sensorimotor mapping in brain tumor patients using spontaneous fluctuations in neuronal activity imaged with functional magnetic resonance imaging. *Neurosurgery*, *65*, ons226–ons236. http://doi.org/10.1227/01.NEU.0000350868.95634.CA